Green Energy and Technology

Avinash Kumar Agarwal
Rashmi Avinash Agarwal
Tarun Gupta
Bhola Ram Gurjar *Editors*

Biofuels

Technology, Challenges and Prospects

Springer

Green Energy and Technology

More information about this series at http://www.springer.com/series/8059

Avinash Kumar Agarwal
Rashmi Avinash Agarwal
Tarun Gupta
Bhola Ram Gurjar
Editors

Biofuels

Technology, Challenges and Prospects

Springer

Editors
Avinash Kumar Agarwal
Department of Mechanical Engineering
Indian Institute of Technology Kanpur
Kanpur, Uttar Pradesh
India

Rashmi Avinash Agarwal
Department of Chemistry
Indian Institute of Technology Kanpur
Kanpur, Uttar Pradesh
India

Tarun Gupta
Department of Civil Engineering
Indian Institute of Technology Kanpur
Kanpur, Uttar Pradesh
India

Bhola Ram Gurjar
Department of Civil Engineering, Centre for Transportation Systems (CTRANS)
Indian Institute of Technology Roorkee
Roorkee, Uttarakhand
India

ISSN 1865-3529 ISSN 1865-3537 (electronic)
Green Energy and Technology
ISBN 978-981-10-3790-0 ISBN 978-981-10-3791-7 (eBook)
DOI 10.1007/978-981-10-3791-7

Library of Congress Control Number: 2017930135

Printed on acid-free paper

This Springer imprint is published by Springer Nature
The registered company is Springer Nature Singapore Pte Ltd.
The registered company address is: 152 Beach Road, #21-01/04 Gateway East, Singapore 189721, Singapore

Preface

Current energy scenario clearly suggests that oil and gas reserves are finite and will last only few more decades. Therefore, massive research efforts are underway globally for developing energy from resources with lower carbon footprint for sustainable development and environmental protection. In order to ensure energy security and to reduce impact of global and local pollution from fossil fuels, utilization of biofuels has been adopted as an immediate solution. Biofuels play an important role in the future scientific research portfolio, which will affect energy independence and energy security, revitalize rural infrastructure and shift energy landscape of the twenty-first century towards greater sustainability and towards low carbon-intensity. Discussing multidisciplinary research dimensions of bioenergy and its potential for replacing fossil fuels in coming decades, this monograph provides a roadmap for understanding broad sweep of technological, sociological, and energy policy issues that intermingle and intertwine. Biotechnology and especially synthetic biology can play a key role in promoting sustainable production and use of bioenergy through development of next-generation biofuels from locally available biomass feedstocks using advanced sunlight-to-biomass-to-bioenergy conversion processes. Socio-economic and environmental challenges need to be duly considered while designing these technological solutions. This monograph covers such advanced techniques for efficient production of biofuels from locally available raw biomaterials and their utilization in IC engines and power generating equipment.

An international workshop, 3rd ISEES Workshop on "Sustainable Energy, Environment & Safety with Railway Centric Theme", was held at Research Designs and Standards Organisation (RDSO), Lucknow, India from December 21 to 23, 2015 under the aegis of International Society for Energy, Environment and Sustainability (ISEES). This workshop provided a platform for discussions between eminent scientists and engineers from various countries including India, USA, South Korea, Thailand, and Austria. In this workshop, eminent speakers presented their views related to different aspects of biofuels, and alternative energy resource for sustainable development and cleaner environment. This research monograph is based on the topics covered at the workshop, and brings together a wealth

of knowledge from renowned experts on the latest developments in selected technology domains with a focus on fundamentals, applications, and advanced teaching pedagogy. Main areas covered in this monograph are biofuels and their advantages, advanced biofuel production techniques and their utilization in various sectors such as transportation and power generation. This monograph also includes methodologies of increasing biofuel yield from different resources. Research on using biofuel blended with conventional fossil fuels for power generation is also presented. In addition, novel technology developments in biofuel production from microalgae are also discussed.

The editors would like to express their sincere gratitude to the authors for submitting their work in a timely manner and revising it appropriately at a short notice. We would like express our special thanks to Dr. Bhaskar Thallada, Dr. S. Venkata Mohan, Prof. Ashok Pandey, Prof. Atul Dhar, Prof. Santanu De, Prof. V.S. Moholkar, Prof. Dhananjay Srivastava, and Akhilendra Pratap Singh, who reviewed various chapters of this monograph and provided their valuable suggestions to improve the draft manuscripts. We acknowledge the support received from various funding agencies and organizations for the successful conduct of the ISEES workshop, where these monographs germinated. These include Science and Engineering Research Board, Department of Science and Technology, Government of India (Special thanks to Dr. Sanjay Bajpai); RITES Ltd, India (Special thanks to Sh. Pradeep Gupta); Office of Naval Research Global, Singapore (Special thanks to Dr. Ramesh Kolar); TSI, India (Special thanks to Dr. Deepak Sharma); Caterpiller India; AVL India; Dynomerk Controls, India (Special thanks to Sh. Kishore Raut); CEI Softwares, India; ESi Group, Pune; BHEL India; and Bosch India.

This monograph is intended for researchers, practitioners of engineering and technology, and we hope that the monograph would be of great interest to the professionals involved in biofuels as well as students, government officials, decision makers, policy makers, and civil society organizations interested in renewable energy and more specifically to those working in biofuel production, optimization, and their utilization in IC engines. Its objective is to promote a better and more accurate understanding of the nature, production, challenges, technological status, and usage of biofuels from vegetable oils and algae and to provide an updated and reliable reference and guidebook on biofuels.

Kanpur, India — Avinash Kumar Agarwal
Kanpur, India — Rashmi Avinash Agarwal
Kanpur, India — Tarun Gupta
Roorkee, India — Bhola Ram Gurjar

Contents

About the Editors

Prof. Avinash Kumar Agarwal joined IIT Kanpur in 2001. He worked at ERC, University of Wisconsin, Madison, USA as a postdoctoral Fellow (1999–2001). His areas of interest include IC engines, combustion, alternative fuels, hydrogen, conventional fuels, lubricating oil tribology, optical diagnostics, laser ignition, HCCI, emission and particulate control, and large bore engines. He has published more than 200 peer-reviewed international journal and conference papers. He is associate editor of ASME Journal of Energy Resources Technology, and International Journal of Vehicle Systems Modelling and Testing. He has edited "Handbook of Combustion" (5 Volumes; 3168 pages), published by Wiley VCH, Germany. He is a Fellow of SAE (2012), Fellow of ASME (2013) and a Fellow of INAE (2015). He is the recipient of prestigious Shanti Swarup Bhatnagar Prize-2016 in Engineering Sciences.

Dr. Rashmi Avinash Agarwal is a senior researcher at IIT Kanpur. She completed her doctoral degree in Inorganic Chemistry from IIT Kanpur in 2014. She completed her M.Sc. in Organic Chemistry from Rajasthan University, Jaipur in 2002 and B.Sc. in Chemistry, from Kanoria College, Rajasthan University, Jaipur in 2000. She has expertise in coordination chemistry, coordination polymers, organic synthesis, inorganic synthesis, crystal structure determination, supramolecular chemistry, porous materials, topology, florescence, SC (single crystal)-to-SC

transformation, and synthesis of nanoparticles. Dr. Rashmi A. Agarwal has published over 20 research papers in leading international journals.

Prof. Tarun Gupta is a PK Kelkar Research Fellow at IIT Kanpur. He completed his Doctor of Science (2004) in Environmental Health from Harvard University, USA. He has been involved in teaching and research activities at IIT Kanpur since June 2006. He has published more than 80 international peer-reviewed journal papers and has filed three Indian patents. He has received numerous awards and recognitions such as NASI Scopus Young Scientist (2015), INSA Young Scientist (2011), INAE Young Engineer (2009), and IEI Young Engineer (2008). He has extensively worked on engine emissions and controls using development and testing of non-noble metal catalyst based DOC.

Dr. Bhola Ram Gurjar is Associate Professor and the Coordinator of the Environmental Engineering Group at IIT Roorkee. He holds a PhD in Environmental Risk Analysis from IIT Delhi. His present research interests include mega-cities, air pollution: environmental impact and risk assessment: atmospheric emissions and climate change; and integrated cross-disciplinary study of science and policy issues of the environment, health, energy, economy, technology, and infrastructure and resources particularly from the global change, sustainable development, and risk governance perspectives. Dr. Gurjar has (co) authored/(co)edited seven books and more than 100 publications. He has received prestigious Advanced Postdoctoral Research Fellowship of the Max Planck Society (Germany) (2002–2005) and UKIERI Grant. He is also co-recipient of the Nawab Zain Yar Jung Bhadur Memorial Medal (best research paper award) from Environmental Engineering Division of the Institution of Engineers (India) Kolkata, for the year 1995–1996.

Part I
General

Introduction to Biofuels

Avinash Kumar Agarwal, Rashmi Avinash Agarwal, Tarun Gupta and Bhola Ram Gurjar

Abstract Sustainable energy source and cleaner environment is the most important requirement for developing countries. In India, total primary energy consumption was ~0.5 BTOE in 2008, which is expected to rise up to ~1.2 BTOE by 2035. In such a scenario, biofuel utilization program seems to be a promising solution because biofuels are relatively cleaner and can be produced from indigenous resources available locally. However availability and continuous supply are the most challenging tasks for the countrywide implementation of biofuels program. In such a scenario, advanced techniques of biofuel production including bio-technology route seem to have significant potential for the energy security in future. This monograph covers practical aspects of biofuel production, utilisation, challenges and limitations and outlines the strengths and constraints of different biofuel production techniques.

Keywords Biofuels · Hydrothermal liquefaction · Microalgae · Biodiesel · Bioprocessing

Large quantities of low carbon fuels are required to meet increasing global energy demand and drive to achieve climate change goals. Electricity and hydrogen appear

A.K. Agarwal (✉)
Department of Mechanical Engineering, Indian Institute of Technology Kanpur, Kanpur 208016, Uttar Pradesh, India
e-mail: akag@iitk.ac.in

R.A. Agarwal
Department of Chemistry, Indian Institute of Technology Kanpur, Kanpur 208016, Uttar Pradesh, India

T. Gupta
Department of Civil Engineering, Indian Institute of Technology Kanpur, Kanpur 208016, Uttar Pradesh, India

B.R. Gurjar
Department of Civil Engineering, Indian Institute of Technology Roorkee, Roorkee 247667, Uttaranchal, India

A.K. Agarwal et al. (eds.), *Biofuels*, Green Energy and Technology,
DOI 10.1007/978-981-10-3791-7_1

to be potentially attractive fuels for light-duty vehicles, however these energy carriers may not be suitable for heavy-duty transport applications and for agricultural applications in rural areas. Therefore many alternatives transport fuels are being considered, which include natural gas, liquefied petroleum gas, hydrogen, unconventional fossil oils, electricity, Fischer-Tropsch liquids, ethers, alcohols, biodiesels, etc. Amongst these test fuels, biofuels are a promising solution because they can be produced directly from biomass

About the biofuels, Henry Ford predicted in 1925, "The fuel of the future is going to come from fruit like that sumac out by the road, or from apples, weeds, sawdust—almost anything. There is fuel in every bit of vegetable matter that can be fermented".

EPA report shows that use of renewable fuel results in 20% savings in GHG emissions, which can be further improved up to 60% if biofuels are produced from cellulosic biomass. Therefore several countries have adopted different measures to introduce biofuels, depending on their resource base. Two most common types of biofuels in use today are ethanol and biodiesel. Use of lower gasoline-alcohol blends in SI engine results in reduction in CO, HC and NO_x emissions, while producing almost similar torque output. Alcohol blends can also be used in CI engines as a supplementary fuel. The Green Paper of the European Commission proposed 20% substitution of conventional fossil fuels by alternative fuels in the road transport sector by the year 2020. Directive 2003/30/EC requires EU member states sets indicative targets for biofuel sales and the reference values were 2% biofuels penetration in petrol and diesel by 2005, increasing to 5.75% by 2010. Biofuel policy of Indian government targets 20% blending of biofuels, both bio-diesel and bio-ethanol by 2017. In 2010, India launched a National Ethanol Blending Programme, thus establishing a 5% mandatory ethanol blending in 20 states across the country. As rising crude oil prices and increasing energy requirements put huge burden on economy, continuation of blended transport fuels may offer some immediate relief. However alcohol availability remains a key challenge for this program's success. Conflict between energy and food security is yet another challenge for biofuels because most of the first generation biofuels are produced from food-crops. Therefore producing biofuels from agricultural waste (e.g. rice straw) using thermo-chemical process may be a sustainable option through recycling of waste. Second generation bioethanol can be produced by breakdown of cellulosic biomass in several steps including hydrolysis and finally fermentation to produce bioethanol. Presently researchers are focusing on third generation biofuels, which can be produced using bio-reactors for ethanol and transesterification for biodiesel. Research into production of liquid transportation fuels from micro-algae is also gaining importance throughout the world. These micro-organisms use solar energy to combine carbon dioxide with water and create biomass more efficiently and rapidly than terrestrial plants. Biofuels from microalgae are also attracting researchers due to their 'carbon neutral' nature because the carbon generated in the fuel combustion is almost neutralized by the CO_2 consumption during microalgae growth.

This monograph explores such key technologies, including biotechnology, bioprocessing, and thermo-chemical process, which show a sustainable future of biofuels. The future of biofuels from a broader perspective needs appropriate addressing of the economic, social, and environmental issues, which are critical for the sustainable development of bioenergy. This monograph contains 12 chapters, which include introduction of biofuels, optimization of biofuel production techniques, advanced techniques for biofuel production and biofuel utilization. These are as follows

- Introduction
- Sustainable production of chemicals and energy fuel precursors from lignocellulosic
- Microbial electrochemical platform: Biofactory with diverse applications
- Biomass-derived HMF oxidation with various oxidants
- Hydrothermal liquefaction of lignocellulosic biomass components: Effect of alkaline Catalyst
- Pretreatment strategies of lignocellulosic biomass towards ethanol yield: Case study of pine needles
- Ultrasound-assisted biodiesel synthesis: A mechanistic insight
- Thermo-chemical ethanol production from agricultural waste through polygeneration: Performance assessment through a case study
- Microalgae Based Biofuel: Challenges and opportunities
- Surrogates for biodiesel: Review and challenges
- Response surface methodology based multi-objective optimization of the performance-emission profile of a CI engine running on ethanol in blends with diesel
- Effect of alcohol blending on performance of kerosene fuelled four-stroke spark ignition genset

This monograph shows the optimization of ethanol production process using an efficient integrated multi-utility system called polygeneration, which is beneficial for the environment. This chapter presents the suitability of the process using thermodynamic, economic and environmental performance assessment. To improve biofuel production process, several novel techniques have been discussed in one chapter. Microbial catalyzed electro-chemical systems (MES) can be used for degradation of organic carbon present in the waste. This technique utilizes a biocatalyst and generates the reducing equivalents in the form of redox carriers.

Another chapter presents the role of individual biomass components (cellulose and lignin) on the production of hydrocarbons during hydrothermal liquefaction (HTL) of ligno-cellulose, which is composed of mainly three components, namely: cellulose, hemicellulose and lignin. Main focuss of this chapter is to promote the third generation biofuel production using microalgae. Microalgae can produce high oil yields compared to other terrestrial plants. Microalgae requires non-cultivable soil and waste water for cultivation, which reduces overall cost of production. Bioprocessing of lignocellulose using chemical catalysis is an impressive

methodology for biofuel synthesis. One chapter provides an account of value addition to biomass via chemical catalysis of cellulosic, hemicellulosic and lignin fractions towards product chemical's synthesis.

The climate change is presently an important element dictating energy use pattern and energy resource development. Biodiesel is considered "climate neutral" because all of carbon dioxide released during consumption is sequestered out of the atmosphere in advance during the crop growth in the previous crop-cycle. Biodiesel is an alternative to conventional diesel, and is made from renewable resources, such as non-edible vegetable oils, algae and animal fat. To optimize biodiesel production, exact physical mechanism of ultrasound-induced enhancement of biodiesel synthesis is also described in a chapter. Analysis of physical mechanism of ultrasound-assisted biodiesel synthesis is discussed, which provides links between physical and chemical effects of ultrasound and cavitation, and the basic chemistry of biodiesel synthesis.

For better utilization of biofuels, few experimental studies are also discussed in this monograph, in which the effect of ethanol-diesel blends on the engine performance and emission characteristics have been discussed. Researchers explored the potential of biodiesel to completely or partially replace mineral diesel in a CI engine. For better understanding of biodiesel combustion in CI engines, development of reaction kinetics to describe its oxidation using surrogates plays a crucial role. This monograph also includes a chapter on review of the existing studies wherein different surrogates for biodiesel are discussed at length.

Sustainable Production of Chemicals and Energy Fuel Precursors from Lignocellulosic Fractions

Bhumica Agarwal, Vivek Ahluwalia, Ashok Pandey, Rajender Singh Sangwan and Sasikumar Elumalai

Abstract From time immemorial, bioprocessing of lignocelluloses via chemical catalysis has been an impressive methodology of numerous value added commodities and energy fuel precursors (drop-in-fuel) synthesis. The most common technique for biomass fragmentation is catalytic hydrolysis using various acid catalysts covering inorganic or organic liquid acids as well as solid acids (heterogeneous). Most research in the past decade has been focused on cost-effective production of such biomass derived commodities with the aim of their commercialization. Till date, in order to improve final product yields and minimize production costs, various improvised production schemes have been developed like pretreatment methods for improved saccharification and displacement and/or reconstruction of recalcitrant biomass constituents, such as lignin to improve accessibility, employing multi-functional catalysts to promote single stage transformations, continuous extraction of desired product by use of specific solvents to improve product stability as well as to inhibit by-product formation, integration of physical processes for example microwave and ultrasonic irradiation resulting in decreased residence time, etc. With these technological advancements, researchers have overcome substantial limitations associated with lignocellulose transformation including mass-transfer hindrances and expensive downstream processing; as a result a wide array of commercially important chemicals and fuel precursors have been synthesised. The chapter provides an account of value addition to biomass via chemical catalysis of cellulosic, hemicellulosic and lignin fractions towards product chemicals synthesis.

Keywords Lignocellulose · Chemical catalysis · Biorefining · Fuel precursors · Value-added chemicals

B. Agarwal · V. Ahluwalia · A. Pandey · R.S. Sangwan · S. Elumalai (✉)
Center of Innovative and Applied Bioprocessing (CIAB),
Mohali 160071, Punjab, India
e-mail: sasikumar@ciab.res.in

A.K. Agarwal et al. (eds.), *Biofuels*, Green Energy and Technology,
DOI 10.1007/978-981-10-3791-7_2

1 Introduction

Till date, most of the worlds' energy requirements are met from one or the other form of conventional petroleum derived fossil fuels. Apart from its main application in the transportation sector and machinery energy resources, fossil reserves also play an important role in synthesis of industrial chemicals and solvents. However, regrettably, near depleting fossil reserves increases energy insecurity along with excessive greenhouse gas emissions (GHCs), evolved due to incombustible hydrocarbons. In order to tackle this fast energy crisis, worldwide many scientists have believed that biomass derived fuel chemicals (second generation cellulosic fuels) are the sustainable energy source to satisfy both energy replacement and net zero carbon emissions. With expectation, over the past few decades, biorefining of lignocellulose feedstock is attracting worldwide interest. According to the recent survey, global biomass production is estimated to be $1.7–2.0 \times 10^{11}$ tons per year [27]. Considering the current policy scenarios of India, its primary energy demand is postulated to double in the next two decades i.e., from 750 MTOE in 2011 to 1469 MTOE in 2030 [32]. Contrarily, India's biofuel production currently accounts for nearly 1% of global production, which estimates for approximately 127.7 billion litres. The major source of first-generation bio-ethanol in India remains molasses, a by-product of sugar industry. While for second generation biofuels, sugarcane bagasse and leaves, rice straw and husk and wheat straw accounts most of the agricultural residues (crop residues) generated in India [16].

Around world, the abundancy of lignocellulosic biomass is widely distributed as energy crops (e.g., switchgrass and short rotation woody crops), forestry residues (e.g., branches and unused trees), agricultural residues (e.g., straws and stover), and industrial residues (e.g., sawdust and brewers spent grains). In general, the inherent biomass comprises up to 75% carbohydrate sugars in the form of cellulose and hemicelluloses, and therefore, represents a store of abundant sugar polymers labile to be converted into specialty chemicals. Thus, making it an ideal feedstock for sustainably renewable energy applications [75]. In broad classification, lignocellulosic conversion methodologies are thermal, thermochemical and biochemical conversions, and in specific each method is employed for appropriate feedstock types and resulting specific end product yield. Although most of these technologies are at pre-commercial stage, production of bio-ethanol from biomass feedstocks is well established (biochemically) and fully commercialized. Industrial-scale synthesis of lactic acid via fermentation of glucose is also established on the market. Undoubtedly, the usefulness of biomass-based chemicals is realized in biorefineries (Fig. 1), where transformation of lignocellulosic feedstocks into value-added products is envisaged by sequential transformations of a set of biomass derivative molecules, the so-called platform molecules (or building blocks). The US Department of Energy (DOE) in 2004 identified top 12 building blocks as 1,4-diacids (succinic, fumaric and malic), 2,5-furan dicarboxylic acid, 3-hydroxy propionic acid, aspartic acid, glucaric acid, glutamic acid, itaconic acid, levulinic acid, 3-hydroxybutyrolactone, glycerol, sorbitol, and xylitol/arabinitol, which can

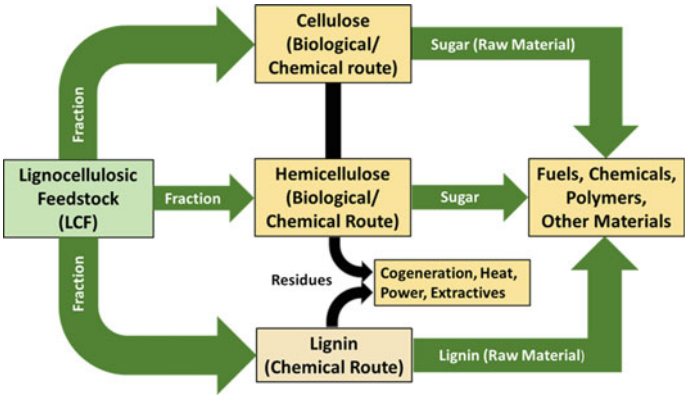

Fig. 1 Schematic illustration of concept of LCF based biorefinery for energy and product chemicals

be produced from biomass derived sugars via sequential chemical or biochemical processing steps [81]. Later, few other important platform molecules have been included in the list, such as fatty acids, fatty acid alky esters and triglycerides [21]. Thus, this chapter takes into account production strategies of few important platform molecules which could be chemically catalyzed and their potential applications as industrial chemicals and energy fuel precursors [88].

2 Lignocellulosic Biomass: Fraction and Its Structure

Inherently, lignocellulosic biomass is known as a polymeric material comprised predominantly of three biogenic polymers, namely cellulose (30–50% wt.), hemicellulose (20–30% wt.) and lignin (20–30% wt.) along with other trace components including organic and organic extractives (phenolic substituents) and ash (10–15% wt.). In understanding, the structural characteristics of lignocellulose are governed by composition and alignment of its polymeric constituents [63]. These polymers are clustered to form microfibrils, as depicted in Fig. 2, which mediate structural stability in the plant cell [69].

Typical lignocellulosic biomass is of recalcitrant nature to resist microbial degradation, which stems from the high crystallinity of cellulose, hydrophobicity of lignin, and encapsulation of cellulose by strong lignin–hemicellulose matrix. Based on the constituent representation, cellulose consists of only anhydrous glucose units imparting high crystallinity due to interlinked hydrogen bonding between same and adjacent cellulose chains, while hemicelluloses is a polymer of different sugar monomers and therefore, hemicellulose has a random, amorphous structure. Likewise, lignin is composed of complex, cross-linked, three-dimensional biopolymers with phenylpropane units imparting relative hydrophobic and

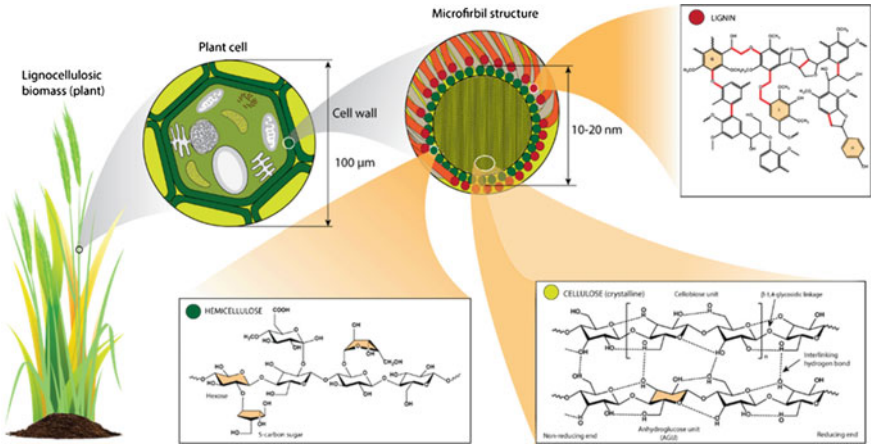

Fig. 2 Schematic representation of lignocellulose microfibril assembly consisting predominant biogenic polymer constituents [69]

aromatic properties. Adversely, the most difficult and energy-consuming step in the conversion of lignocellulosic biomass is the decomposition and degradation of cellulose structure due to its high crystallinity. The intrinsic molecular structure of cellulose is comprised of linearly connected β-D-anhydroglucopyranose units (AGUs), covalently linked through acetal functions (known as β-1,4-glycosidic linkages) between the equatorial hydroxyl groups of C4 and C1 carbon atoms [11] (Fig. 3).

Owing to the abundance of hydroxyl groups and oxygen atoms of AGUs, extensive networks of intra- and inter-molecular hydrogen bonds are formed, aligning cellulose fibrils together in a highly ordered fashion forming a crystalline

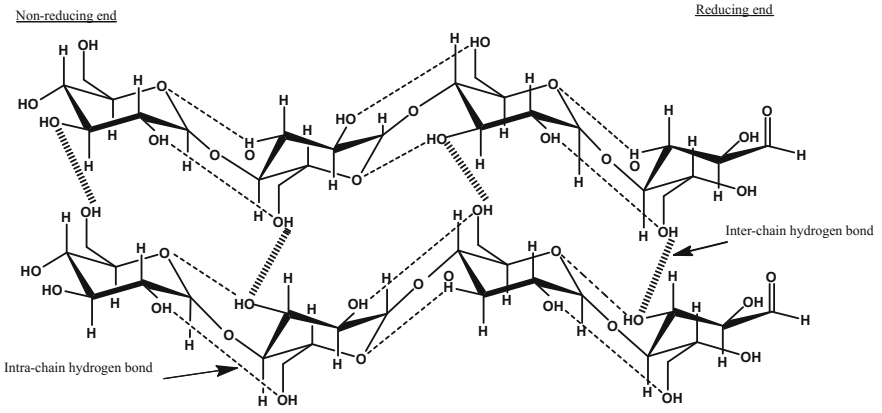

Fig. 3 Biomass cellulose alignment representing intra-and inter-linked hydrogen bonding [18]

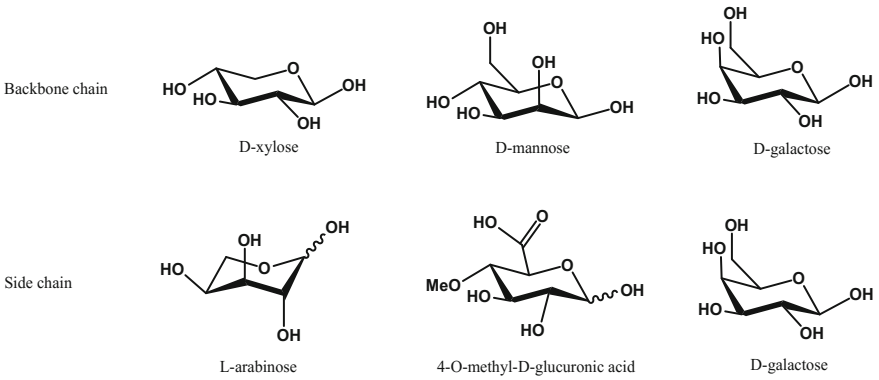

Fig. 4 Chemical structure of hemicellulose backbone monomers including C5- and C6-sugars as backbone and side chain molecules [3]

region, which is water insoluble and very resistant to chemical or enzymatic cleavage. Based on its crystalline structure, cellulose can be categorized into seven known allomorphic forms, denoted as cellulose I_{α}, I_{β}, II, II_{II}, III_{II}, IV_{I}, and IV_{II}.

Although cellulose I is the naturally occurring form (native cellulose), its crystal structure is thermodynamically less stable than that of cellulose II. Four other polymorphs of cellulose (II_{II}, III_{II}, IV_{I} and IV_{II}) are less commonly encountered and less relevant from commercial perspectives.

Unlike cellulose, hemicellulose has a random and amorphous structure, which is composed of several heteropolymers of different 5- and 6-carbon sugars or sugar acids including xylans (arabinoxylans and 4-O-methyl-glucuronoxylans), galactomannans, glucuronoxylans, arabinoxylans, glucomannans and xyloglucans (4- linked β-D-glucans with attached side chains) (Fig. 4).

These polysaccharides backbone usually consists of one repeating sugar unit linked through β-(1 → 4) with branch points (1 → 2), (1 → 3), and/or (1 → 6). In addition, it consists certain side groups, such as uronic acids and acetyl-and methyl-substituted groups [7].

Pectins, another group of polysaccharides made up of polycarboxylic acid, also account for minor fraction of carbohydrates in some plants. Pectins function together with hemicelluloses as a matrix component providing structural support to the cell walls. However, hemicellulose polymers have a low degree of polymerization (only 50–300 dp) as compared to cellulose. The predominant polysaccharide in hemicellulose is the glucuronoxylans, comprised of a xylan backbone of β-D-xylopyranose units linked through β (1 → 4) with acetyl groups at C-2 or C-3 of the xylose units [18]. Therefore, xylan is generally considered to be the simplest representation of a typical hemicellulose. It functions as the cellular glue which provides compressive strength to the plant tissue and the individual fibres, stiffness to the cell wall and resistance against insects and pathogens.

Similarly, lignin is a three-dimensional, highly cross-linked polymer composed of three types of phenylpropanoid units viz. trans-p-coumaryl, trans-coniferyl, and

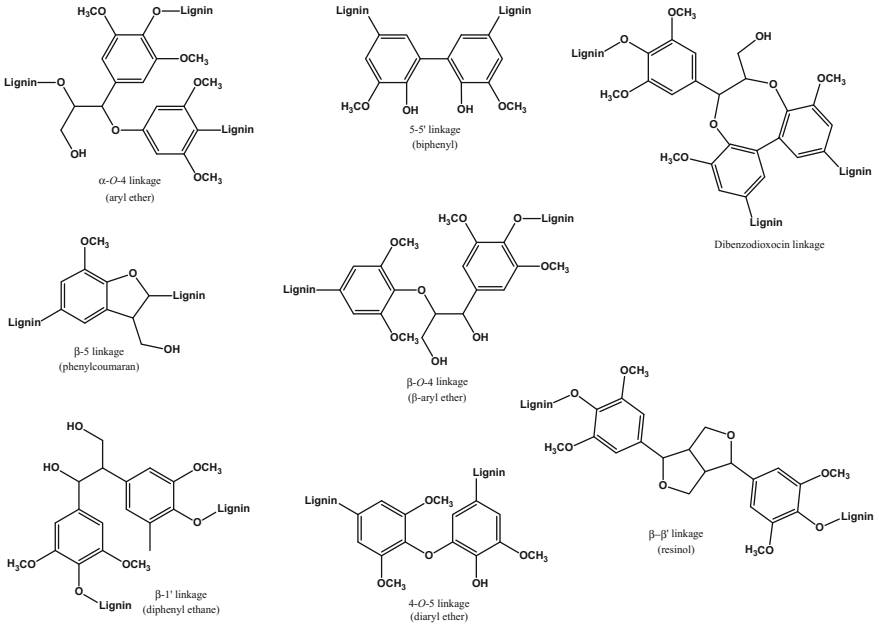

Fig. 5 Representation of major linkages present in biogenic lignin polymer [4]

trans-sinapyl alcohols formed by oxidative coupling, yielding a number of functional groups and linkages.

These precursors are aligned variedly to form three main type of lignin units in plants i.e., p-hydroxyphenyl-propane (H), syringylpropane (S) and guaiacylpropane (G) units. Within the lignin polymer, the phenylpropane units (S, G and H units) are bonded together by a set of linkages include β-O-4, α-O-4, 5-5′, β-5, β-1′, β-β′ and dibenzodioxcin linkages, as depicted in Fig. 5. The crosslinked, lyophilic nature of lignin makes it insoluble and stable in water and acts as the "cellular glue" that connects the polysaccharides, such as cellulose and hemicellulose together providing comprehensive strength to plant tissue. The most common linkage between the lignin monomer units is recognized as the β-O-4 linkage, accounting for 50–60% of total linkages. Lignin also consists of additional functional groups, such as hydroxyl, methoxyl, carboxyl and carbonyl, which play an important role during delignification and lignin fragmentation reactions [46].

3 Hydrolysis of Lignocellulose

Hydrolysis of cellulose commonly refers to breakdown of glucan polymer to its monomer units, is a pre-requisite step in utilization of lignocellulosic biomass and can be accomplished via acidic catalysis using most common mineral acids or

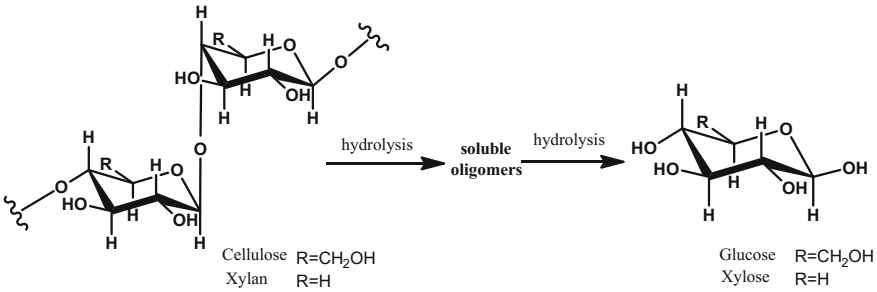

Fig. 6 Proposed reaction scheme of cellulose and hemicellulose hydrolysis [2]

biocatalyst (cellulase complex). Presumably, cellulase comprised of three major enzymes depending on their mode of action and end-product i.e., (i) endoglucanase attacks low crystallinity regions in the cellulose fibers, creating free chain-ends, (ii) exoglucanase or cellobiohydrolase hydrolyze the 1,4-glycocidyl linkages to form cellobiose, and (iii) β-glucosidase converts cello-oligosaccharides and dimers (cellobiose) into glucose residues. At the same time, breaking down of hemicellulose polymers into monomer mixtures consisting 5-and 6-carbon sugars) can be achieved via enzymatic reactions using enzyme cocktails include glucoronide, acetylesterase, xylanase, β-xylosidase, galactomannase and glucomannase [75]. Figure 6 depicts general reaction scheme for hydrolysis of cellulosic and hemicellulosic fraction of lignocellulosic biomass. These enzymes work synergistically to hydrolyse cellulose and hemicellulose. Enzymatic hydrolysis of lignocellulosic biomass is considered to be more effective than the use of acid catalysts owing to their highly specific action and operation at mild process conditions. In spite of these advantages, the use of enzymes in lignocellulosic hydrolysis is still limited due to several associated factors for example their relative instability at high temperature conditions, high costs of enzyme isolation and purification as well as difficult recovery and reusability. When considering the advantages offered by acidic catalysis, various aspects of chemically mediated hydrolysis are briefly discussed in the following sections.

The concept of utilization of lignocellulosic biomass, specifically carbohydrate based fuels and specialty chemicals rely heavily on availability of monomeric C5 and C6 sugars. It is well established that lignocellulose resist any changes in their structural integrity owing to its complexity. Therefore, the first and foremost step in the biorefineries is fragmentation of lignocellulose into its fractional components i.e., cellulose, hemicellulose and lignin. Often termed as pretreatment, the objective of this step is to disrupt the matrix structure to relieve lignin and decrease cellulose crystallinity, enabling enhanced chemical or enzyme accessibility to the cellulose during hydrolysis [56].

Though number of methods have evolved for lignocellulose pretreatment, intrinsic drawbacks, such as development of undesired byproducts, components loss and high processing cost have to be kept in mind while selecting appropriate

approach. For instance, pretreatment severity has to be sometimes reduced to reduce overall economic cost (normally accounts for about 30% of operating cost) as well as inhibitory degradation products. However, low severity factor corresponds to low sugar yields. Therefore, a balance has to be stroked out between various factors. Many different pretreatment methodologies viz. biological, physical, chemical and physico-chemical pretreatments have been employed during the last few decades. Since the chapter focus on chemical catalysis of lignocellulose biomass, pretreatment via chemical methods is discussed in the perspective of integration of pretreatment and production step with the aim of reducing overall production cost in future.

3.1 Homogeneous Hydrolysis Strategy

Mineral acid pretreatment is generally carried out with aim of hemicellulose solubilization and thereby, rendering cellulose more accessible for further processing [75]. A key advantage of acid pretreatment is that subsequent hydrolysis step could be sometimes over-stepped, as the acid itself hydrolyses the biomass to yield fermentable sugars by careful modulating reaction conditions. Most studies have employed strong acids like sulfuric, hydrochloric, nitric and phosphoric acids for biomass pretreatment with favored use of sulfuric acid, owing to being relatively less expensive than other acids and promising yield results [2]. Typically, both dilute (1–2% wt.) and concentrated (30–70% wt.) preparations of acid are evaluated for pretreatment; however, latter strategy is prone to intense formation of inhibitory compounds (poison to microbes), excessive corrosion problems and expensive product downstream. Nevertheless, literature cites that concentrated acid treatment (up to 50% wt.) causes apparent swelling of cellulose leading to the dissolution of cellulose to glucose, whereas dilute acid treatment offers the advantage of solubilizing hemicellulose, mainly xylan and subsequent conversion of solubilized hemicellulose to fermentable sugars depending upon reaction severity.

At the same time, organic acids such as fumaric, maleic and trifluoroacetic acid have emerged as hydrolyzing agents with comparable monosaccharide yields as sulfuric acid along with limited sugar degradation and corresponding furfural production [40, 52]. With time, various types of reactors have been developed and applied for large-scale acidic pretreatment of lignocellulosic materials such as percolation, plug flow, shrinking-bed and counter-current reactors [77]. Voluminous amount of literature is available on acidic pretreatment of lignocellulose biomass [10, 87] and it has been summarized that optimum conditions for the acid pretreatment are highly dependent on the purpose of pretreatment in terms of targeted sugars [49]. For instance, Saha and co-workers [71] achieved maximum carbohydrate content of 76% and 60% wt. from mild acid pretreated wheat straw and rice hull substrates, respectively, after enzyme saccharification and reported less or no formation of sugar degradation products (furfural and HMF) under typical reaction conditions (1.0% v/v H_2SO_4 at 121 °C for 1 h) [71]. Alternatively, several

other studies have proposed for addition of supplementary agents during acidic hydrolysis, in order to improve the direct conversion of cellulose into glucose. For example, Ragg and co-workers [62] employed HCl (6–7 M) supplemented with LiCl or $CaCl_2$ in aqueous phase for conversion of cellulose to glucose and yielded ~85% fermentable sugar release [62]. Later, in a similar fashion Cao and co-workers [5] employed ZnCl in a homogeneous cellulose pretreatment system followed by hydrolysis with dilute HCl, resulting in improved glucose yield (up to 91.5%) [5]. In modified study, Luterbacher and co-workers [50] evaluated the applicability of biphasic reaction system consisting aqueous (0.05% by wt. H_2SO_4) and organic (γ-valerolactone, a biomass derived green organic solvent) phase for the conversion of various cellulosic substrates to glucose and reported 70–90% conversion yield [50].

Likewise, studies have also been conducted on C5 sugar production from hemicellulosic fraction of lignocellulose via dilute acid hydrolysis. Herrera and co-workers [30] evaluated the production of xylose (16.2 g/L) which corresponded to 71.6% of theoretical yield from sorghum straw using 6% wt. HCl at 122 °C for 70 min [30]. Later, Rita and co-workers demonstrated further improved xylose yield (~74% wt.) from sugarcane bagasse using sulfuric acid (100 mg acid/g dm) under comparatively low severity conditions (130 °C for 10 min) [65]. In modified study, Zhang and co-workers [85] investigated combined dilute acid-catalyzed hydrolysis of palm oil empty fruit bunch by employing both dilute H_2SO_4 (0.5% w/v) and H_3PO_4 (0.2% w/v) to achieve 91.3% xylose yield. The apparent improved yields is mainly attributed to the synergistic action of acids under the modest reaction conditions (160 °C within 10 min) [85].

It is profound that typical alkaline pretreatments increase cellulose digestibility through fiber swelling and are known to be more effective for lignin solubilization, exhibiting minor cellulose and hemicellulose solubilization (less sugar loss) than acid or hydrothermal processes [6]. In perception, alkalis viz. sodium, potassium, calcium and ammonium hydroxides generally enables degradation of ester and glycosidic side chains, resulting in structural alterations of lignin, cellulose swelling and increase its internal surface area, partial decrystallization of cellulose, and partial solvation of hemicellulose [53]. In support, several early studies have revealed for the improved digestibility of lignocellulose (for example hardwood substrate) after pretreatment using NaOH yielded up to 55% wt. glucose, due to enhanced enzyme accessibility through recalcitrant lignin removal [41]. Similarly, numerous comparative studies have established for the better delignification capabilities of NaOH (up to 59% wt.) than sulfuric acid (31% wt.) while increasing its concentration from 0.05 to 0.2% g/g solids [19].

Alongside, studies have also demonstrated using weak base (for example CaOH) for biomass hydrolysis through removal of acetyl groups in hemicellulose and reducing steric hindrance, resulting in enhanced cellulose digestibility. Indeed, biomass pretreatment using lime offers the advantages of lower cost and less safety requirements compared to NaOH or KOH pretreatments, and easy recovery from hydrolysate by reaction with CO_2. Consequently, application of this approach has resulted in 89% wt. glucose recovery from leafstar rice straw [59]. Furthermore,

supplementation of oxidative reagents, for example O_2 or H_2O_2 to alkali during biomass pretreatment could improve cellulose and hemicellulose hydrolysis by favoring lignin removal and more importantly, decreased furfural and HMF formation [6]. Apparent studies have witnessed for no obvious furfural or HMF formation during alkaline peroxide pretreatment, which favors further microbial fermentation of sugars to ethanol [77]. Several other chemical pretreatment methods like ozonolysis, organosolv and wet oxidation have been practiced with considerably high delignification yields, however, these methods restricted for use in cellulose to bioethanol transformations, due to high expenses involved as well as subsequent enzymatic inhibition by chemical agents employed [58, 75, 86]. Table 1 summarizes few examples of lignocellulosic biomass processing for C5 and C6 sugars production.

In advancement of bioprocessing, ILs functionalized with acidic groups are new-types of thermally stable catalysts having special properties like providing high-density active sites as liquid acids, non-volatile, easily recyclable and exist as solids even above 100 °C [26]. Several mechanistic studies on cellulose hydrolysis proposed that hydrolysis of cellulose involves breakdown of the hydrogen bond in cellulosic network by the high activity of chloride concentration in ILs [76]. However, water acts as an inhibitor for the dissolution of cellulose and hence can be used to regenerate the cellulose dissolved in ILs. Fascinatingly, during dissolution and regeneration by precipitation of cellulose, its crystallinity reduces significantly and thus, exposing the amorphous part which is much easier to hydrolyze compared with the native cellulose. Furthermore, various ILs specifically hydrophilic imidazolium-based, such as 1-butyl-3-methylimidazolium chloride ([BMIM]Cl), 1-allyl-3-methylimidazolium chloride ([AMIM]Cl), 1-benzyl-3-methylimidazolium chloride ([BZMIM]Cl), and 1-ethyl-3-methylimidazolium acetate ([EMIM] CH_3COO), have been demonstrated for significant dissolution of lignocellulosic materials with remarkable glucose conversion yields (>80%) [14, 45, 64]. Another aspect of ILs in lignocellulosic processing was demonstrated when Lee and

Table 1 Examples of monomeric sugar production from lignocellulosic biomass (adapted from Ref. [88])

Catalyst	Lignocellulose	Operating parameters	Hydrolysis Product	Yield (% wt.)	Ref.
H_2SO_4 (0.175% wt.)	Wood chips	210 °C, 2 min, ~1.9 MPa	Xylose	54	[20]
H_2SO_4 (0.5% wt.)	Corn cobs	125 °C, 165 min	Xylose	25	[66]
H_2SO_4 (6.2 % wt.)	Sugar maple wood extract	95 °C, 50 min, 0.1 MPa	Xylose	161.6 $g.L^{-1}$	[31]
SO_2 Impregnation	Aspen chips	205 °C, 3 min, 1.62 MPa	Glucose Xylose	37 10	[15]
HCl (20% wt.) + [EMIM]Cl	Cellulose	105 °C, 2–4 h	Glucose	~90	[2]

co-workers [44] discovered for dissolution of lignin in ILs, however, exhibited a limited affinity toward cellulose and other constituents of wood flour [44]. These ILs were [MMIM]-[CH_3OSO_3],1,3-dimethylimidazolium trifluoromethanesulfonate ([BMIM][CF_3SO3]), [EMIM][CH_3COO], [AMIM][Cl], [BMIM][Cl], or 1-benzyl-3-methylimidazolium chloride ([BZMIM][Cl]). Despite the advantages offered by ILs, the high cost of ILs limits their large-scale application in biomass pretreatment. However, it can be expected that research will be focused on dropping down the production cost of ILs so as to enable its application in commercial hydrolysis and pretreatment processes for cellulose conversion.

3.2 Heterogeneous Hydrolysis Strategy

Although homogeneous acids have been quite successful in cellulose hydrolysis to yield monomeric glucose, the handling and operational issues associated with these approaches led to the research and development of heterogeneous acid catalysts. However, most heterogeneous catalytic studies are based on commercial cellulose due to difficulties in separation of cellulose and lignin in biomass; nevertheless, few researches have demonstrated for direct lignocellulose conversion. Table 2 summarizes potential applications of heterogeneous solid acid catalysts towards cellulose hydrolysis to glucose.

In modified study, Jiang and co-workers demonstrated self-derived carbonaceous solid acid (CSA) catalysts giving rise to a close loop recycle procedure,

Table 2 Popularly used heterogeneous solid acid catalysts for bio-derived component transformation reactions [29]

Example solids	Class
Zeolite and zeolite-like	X-, Y-zeolites (faujasite), chabasite, ferriertie, beta-zeolite, mordenite, erionite, HZSM-5, MCM-22, metalloaluminophosphate (e.g., silicoaluminophosphate, gallosilicate, beryllosilicate, titanosilicate, stanosilicate
Clay	Montmorillnite, saponite
Metal oxide and mixed metal oxide	Al_2O_3, TiO_2, SiO_2, Nb_2O_5, WO_3, SiO_2–Al_2O_3, SiO_2–ZrO_2, SiO_2–MgO, TiO_2–SiO_2, WO_3–ZrO_2, WO_3–Al_2O_3, WO_3–SnO_2, Nb_2O_5–Al_2O_3, B_2O_3–Al_2O_3
Acid supported	H_3PO_4/SiO_2, $HClO_4/SiO_2$, SO_3H/SiO_2, SO_3H/C, $AlCl_3/SiO_2$, BF_3/SiO_2, SbF_5/SiO_2–Al_2O_3, SbF_5/TiO_2, CF_3SO_3H/SiO_2, heteropoly acids/SiO_2
Sulfated oxide	SO_4^{2-}/ZrO_2, SO_4^{2-}/TiO_2, SO_4^{2-}/SnO_2
Layered transition metal oxide	$HNBMoO_6$, $HTaWO_6$, $HNbWO_6$
Metal salt	$AlPO_4$, $Nb_3(PO_4)_5$, $FePO_4$, $NiSO_4$
Heteropoly compound	$H_3PW_{12}O_{40}$, $H_4SiW_{12}O_{40}$, $H_3PMo_{12}O_{40}$, $H_4SiMo_{12}O_{40}$, and their salts (e.g., $H_{0.5}Cs_{2.5}PW_{12}O_{40}$)
Ion exchange resin	Amberlyst-15, Nafion, Nafion-silica composite/nanocomposite

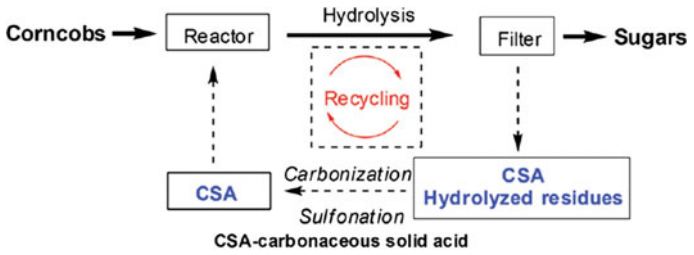

Fig. 7 Process scheme of corncob hydrolysis by CSA derived from the hydrolysis residue [35]

where CSA is prepared under microwave irradiation from hydrolyzed corncob residues and re-used for the hydrolysis of corncob, as illustrated in Fig. 7 [35]. The obvious advantages of this process are two end products as output, first is the sugars derived from cellulose and hemicelluloses and secondly, CSA coming from the unconverted solid residue. Considering the use of inexpensive solid acid catalyst, moderate reaction conditions (130 °C) and appreciable yields of xylose and arabinose (78% wt.) the overall process is postulated to yield good economics. Therefore, it is evident that heterogeneous catalysis offers economic conversion of lignocellulosic biomass into platform sugar compounds. However, efforts are to be made in the direction of overcoming mass-transfer limitations associated with substrate-catalyst interactions without incorporating additional physical pretreatment costs.

4 Thermochemical Catalysis of Carbohydrate Sugars

Depending on the intended end-use of the product, lignocellulosic biomass can be processed in numerous ways like liquefaction, solvo-hydrolysis, pyrolysis, hydrolysis, hydrothermal hydrolysis etc. For instance, synthesis of transportation fuels and chemicals require less oxygen content and consequently, lignocellulosic biomass is depolymerized and deoxygenated prior to catalytic hydrolysis. In favorable, presence of oxygen often provides valuable physical and chemical properties to other value-added chemicals and therefore, require much less deoxygenation. In accordance, with the recent literature cites that 5-hydroxymethylfurfural, lactic acid, acetone-butanol-ethanol (ABE) and lignin has been identified as platform molecules in addition to the previously defined platform chemicals by the US-DOE, which could be obtained from lignocellulose-derived C5 and C6 sugars and also, lignin fraction by any of the chemical or biological processing techniques. Because these molecules can be further processed into value-added chemicals by employing appropriate processing approaches [33].

5-Hydroxymethylfurfural (HMF): A versatile 'value-added' additive molecule, gaining much attention in petroleum and chemical industries due to its reactive features (heterocyclic furan), consisting hydroxide and aldehyde functionalities at

2,5-poistions,and moreover, it is relatively an unsaturated aromatic compound [12]. Thus, HMF is susceptible to many chemical reactions, depending upon the synthesis route (Fig. 8) undergoing favorable changes leading to the production of commercially important chemicals [79].

It is generally produced through acid-catalyzed dehydration of hexose sugars preferably fructose. Synthesis of HMF from biomass-derived glucose is essentially a two-step process i.e., a base and/or Lewis acid catalyzed reaction for isomerization of glucose to fructose followed by Brønsted acid mediated catalysis to the end product. Due to the unstable character of HMF, obtaining high yield and selectivity from glucose is challenging from industrial point of view. In a typical reaction conditions, HMF is more likely to rehydrate to levulinic acid and formic acid at equal proportion under same prevailing reaction conditions. The earliest reports on synthesis of HMF in aqueous phase reaction system employing cheap raw material like wood chips, were restricted by meager selectivity towards HMF owing to instability of HMF in water under acidic conditions. In order to avoid the complications and further product yield improvement, Kuster and Der Van Steen in 1977 [42] attempted to introduce organic solvents, as extracting agents, resulting achieved remarkable conversion yield under modest reaction conditions with appreciable synergistic effects on HMF's rate of formation along with limiting its decomposition to humin species and other side products [42]. Since then numerous solvents including DMSO (dimethyl sulfoxide), DMF (dimethyl formamide), DMA

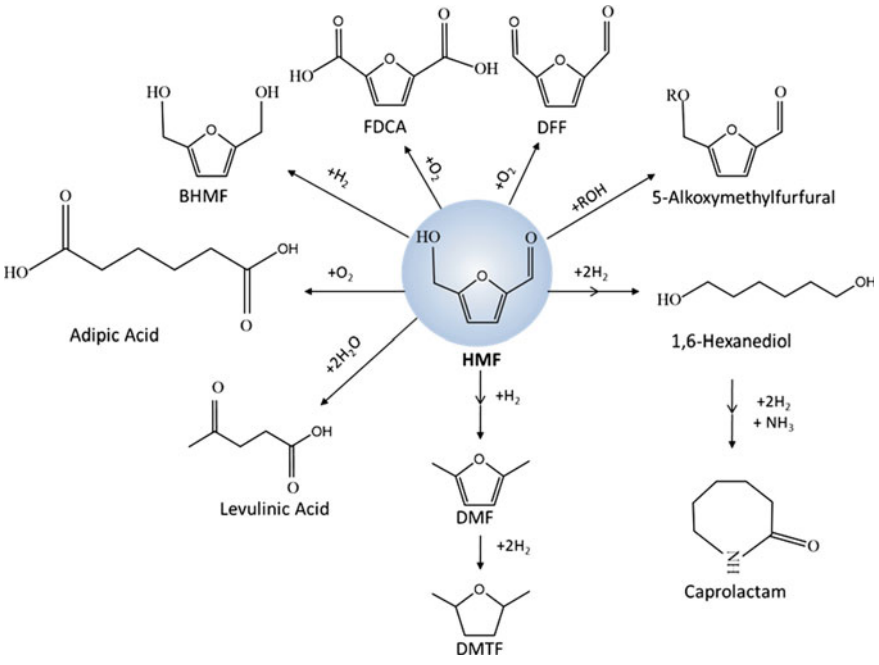

Fig. 8 Potential application of 5-hydroxymethylfurfural as platform molecule

Table 3 Classified catalyst group for HMF synthesis from hexose sugar molecule (reproduced from Ref. [68])

Catalyst group	Example
Organic acids	Carboxylic acids, lactic acid, oxalic acid, levulinic acid, maleic acid, *p*-tolunesulfonic acid, boric acid
Inorganic acids	Sulfuric acid, phosphoric acid, hydrochloric acid, iodine or hydroiodic acid generated in situ
Slats	$MgCl_2$, $(NH_4)_2SO_4/SO_3$, pyridine/PO_4^{-3}, pyridine/HCl, aluminum salts, Th and Zr ions, zirconium phosphate ions: Cr, Al, Ti, Ca, In, $ZrOCl_2$, $VO(SO_4)_2$, TiO_2, V-porphyrine, Zr-, Cr- and Ti-porphyrins, lanthanides ($LaCl_3$, $NdCl_3$, $EuCl_3$, $DyCl_3$ and $YbCl_3$)
Lewis acids	$ZnCl_2$, $AlCl_3$, BF_3
Solid acids	Ion exchange resins, zeolites, supported acids, heteropoly compounds

(dimethyl acetamide), NMP (N-methyl pyrrolidinone), sulfolane etc. have been evaluated and consequently achieved higher HMF yields [70]. For instance, Qi and co-workers [60] successfully tested sulfated zirconia (SZ) for dehydration of fructose reactions achieving 72.8% HMF yield at 180 °C under microwave heating for 20 min in solvent mixture consisting of acetone–dimethylsulfoxide (DMSO) [60]. Recently, Moreno-Recio and co-workers achieved 42% HMF yield with 80% glucose conversion using HZSM-5 (Si/Al ratio of 18.9) in a biphasic system containing 20% NaCl and MIBK, within 30 min reaction at 195 °C [55]. Apprehensively, these processes increase the overall cost economics owing to complex recovery itinerary of such high boiling point solvents. Another advancement in this field is the use of bi-functional heterogeneous catalysts presenting both acidic and basic catalytic sites. In accordance with the literature reports that heterogeneous catalysts have shown superior catalytic activity over homogeneous catalysts in terms of product selectivity [26]. Table 3 lists various catalysts that have been reported for HMF synthesis under various reaction conditions.

With the continuous evaluation of various efficient catalysts for HMF synthesis, complete conversion of biomass derived sugars has been achieved, however, one-pot synthesis still remains a challenge owing to mass-transfer limitations. Due to this, commercialization of HMF from lignocellulosic biomass has not been realized. New heterogeneous catalysts, such as Metal Organic Frameworks (MOFs), Porous Organic Polymer (POP), Covalent Organic Frameworks (COFs) and Covalent Triazine Frameworks (CTFs) have emerged with excellent characteristics, suited the most pivotal being easy functionalization to facilitate direct valorization of lignocellulosic biomass. A recent example of use of such MOFs is hydrolysis of carboxymethylcellulose (CMC) to 5-HMF in aqueous phase at 200 °C for 4 h with aluminum based MIL-53(Al) and achieved a molar yield of 40.3% of 5-HMF [89].

Levulinic acid (LA): Another class platform molecule, which serve as precursor to numerous value-added chemicals production, and is generally prepared from lignocellulose via hydrolysis and dehydration/hydration reactions through intermediate HMF formation.

In popular, the well-established method for LA preparation from biomass is Biofine process, essentially a two-stage processing protocol. Briefly, in the first stage, a plug flow reactor is employed for initial biomass hydrolysis under elevated conditions (210–220 °C, 25 bar for 12 s) and subsequently, the slurry mixture is treated under relatively less severe conditions (190–200 °C, 14 bar and 20 min) at similar acid concentrations to yield ultimately a product mix consisting predominantly LA (50% by wt. of C6 sugar), furfural (50% by wt. of C5 sugar) and formic acid (20% by wt.) along with residual HMF concentrations. So far, variety of carbonaceous feedstocks (biomass) have been evaluated for LA preparation catalysed via both homogeneously and heterogeneously and could achieve up to 40–45% wt. under modest reaction conditions [61]. In a typical reaction setup, LA yields of about two thirds (or even less) than the theoretical value are attainable due to the formation of undesired black insoluble-materials called humins. Recent advancements in LA synthesis include use of $SO3^{-}$ functionalized ionic liquid, 1-(4-sulfonic acid) butyl-3-methylimidazolium hydrogen sulphate ([BSMim]HSO_4), giving the highest yield up to 40% wt. within 120 min in aqueous medium at 120 °C from cellulose [72]. Figure 9 illustrates various value-added commodities which are synthesized from biomass derived levulinic acid.

Sorbitol: A sugar alcohol, which is generally produced by the hydrogenation of glucose in the presence of suitable catalyst either homogenous or heterogeneous.

The earliest reports of sorbitol production from cellulose dates back to 1950 employing mineral acid and supported Ru catalysts under H_2 pressure (7 MPa) giving 99% recovery of sorbitol. Figure 10 summarizes use of sorbitol as potential platform molecule. Although literature cites on direct conversion of biomass

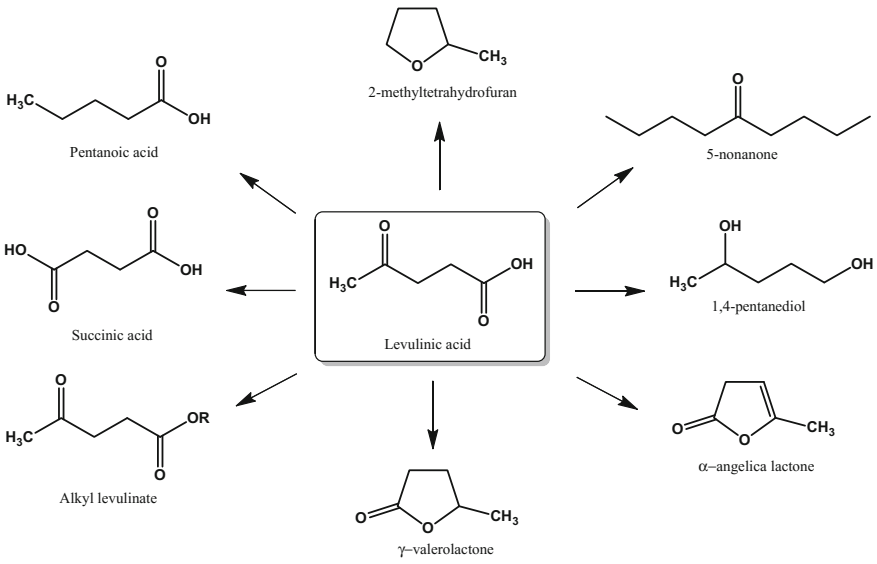

Fig. 9 Summary of end products derived from levulinic acid as building block [50]

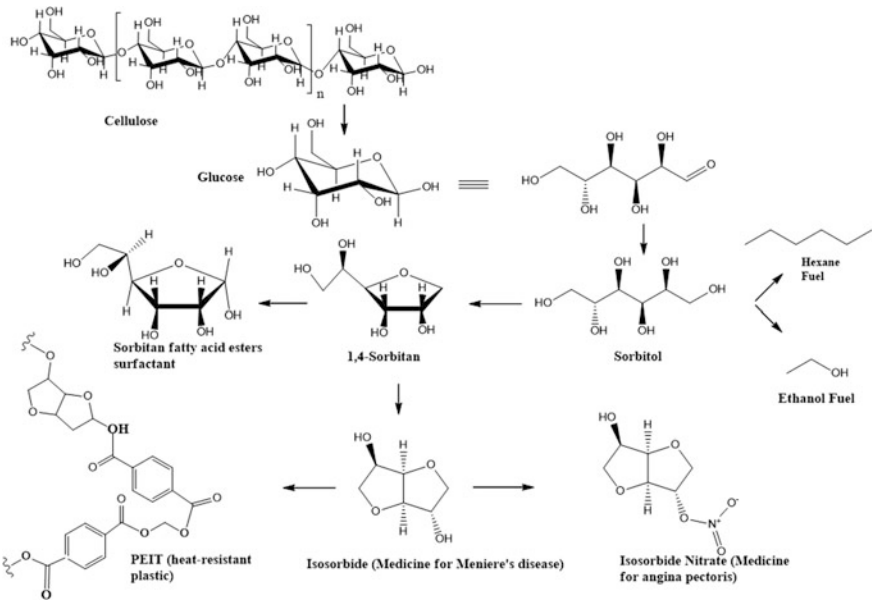

Fig. 10 Reaction scheme for sorbitol production from cellulose and its end-use [39]

substrates for sorbitol production is scarce, commercial D-glucose has been transformed into sorbitol by various researchers [13]. For instance, Käldström and co-workers [37] employed hydrolytic hydrogenation of bleached birch kraft pulp in aqueous medium at 185 °C under 20 bar H_2 over H-MCM-48 and Pt/MCM-48 synthesis zeolite catalysts and identified that former was able to convert cellulosic and hemicellulosic fractions into variety of products include glucose, xylose, 5-HMF, furfural and furfuryl alcohol. The later catalyst was able to further transform the synthesized glucose and fructose molecules into sorbitol and xylitol products, respectively [37]. Subsequently, Kobyashi and co-workers [39] evaluated transformation of Avicel microcrystalline cellulose to sugar alcohols using γ-Al_2O_3-supported Pt catalyst and Pt(Cl)/γ-Al_2O_3 in the presence of H_2 pressure (5 MPa) at 190 °C for 24 h, resultantly achieved 25% wt. sorbitol along with considerable mannitol (6% wt.) as co-product [39]. Overall, reviews convey that cellulosic fraction of lignocellulosic biomass is an extensive source of platform compounds for production of value added chemicals. However, successful conversion of commercial cellulose appears to be promising technique.

Furfural: Furfural (2,5-furandicarboxyaldehyde) is the principal product of C5 sugar derived via dehydration reaction in the presence of mild acid under typical reaction conditions. It can be used as precursor for the production of wide range of high value chemicals and energy fuels, as depicted in Fig. 11. This value added product is exclusively produced from lignocellulose biomass even at commercial scale. The first known commercial production of furfural is accredited to the Quaker

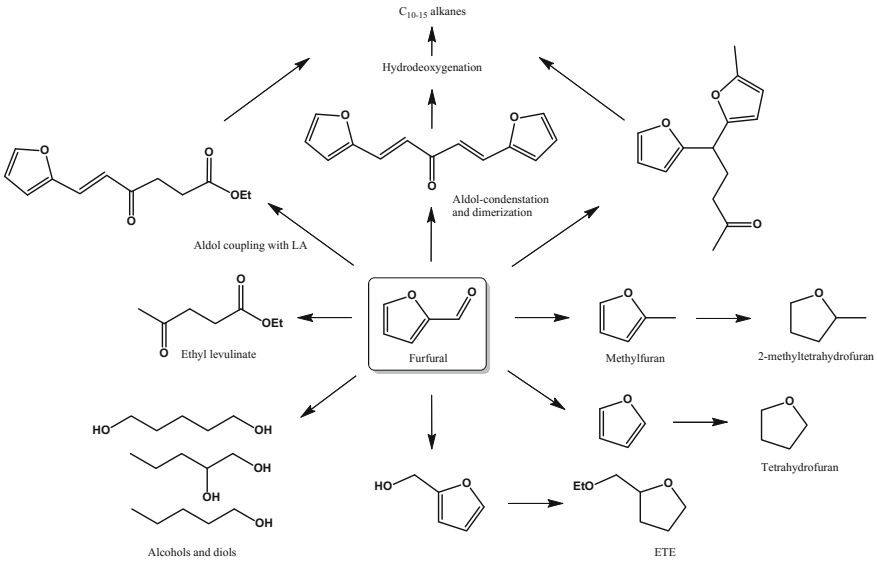

Fig. 11 Potential application of furfural as an industrial precursor

Oats technology established in 1921 and later, various modifications have been made to create new processes with improved furfural yields, recovery, and purity by groups like Westpro modified Huaxia Technology and Supra yield [38]. Despite commercialization of furfural, low yields are obtained which probably is due to the evolution of side reactions as well as cross-polymerization that involve sugars, furfural, and reaction intermediates in an acidic aqueous environment. Till date, varied furfural yields have been reported at bench scale level through employing variety of approaches, which are mainly governed by operating conditions. For instance, maximum up to 87% wt. furfural concentrations have been achieved in an integrated two stage processing i.e., hot water hydrolysis followed by homogenous catalysis (H_2SO_4), of various lignocellulosic biomass (hybrid poplar, miscanthus, switchgrass and corn stover) [51]. In another study, Lewis acid metal chloride catalysts ($CrCl_3$ and $CrCl_2$) have been employed as alternative to mineral acids for furfural production in a monophasic solvent system (N,N-dimethylacetamide/LiCl) and reported maximum furfural yield (56% wt.) [2]. In another approach, use of microwave irradiation has been demonstrated to be effective in reducing the residence time without compromising overall yields [84]. Alternatively, solid catalysts have been employed for furfural synthesis and achieved remarkable yields and conversion performance. For instance, Lima and co-workers [48] employed microporous silicoaluminophosphates (SAPO-5, SAPO-11 and SAPO-40), as solid acid catalysts during dehydration of xylose into furfural under biphasic conditions, and obtained maximum furfural yield (65% wt.) at 170 °C in 24 h [48]. In a recent study, increased furfural yield (relatively 21% wt.) was obtained by Chen and

co-workers [9] in a process employing HZSM-5 with the addition of 4-Methoxyphenol, a polymerization inhibitor, due to less formation of humins [9]. Recent advancements in the area of utilization of biomass derived hemicellulosic fraction, including integrated two-stage strategies, application of microwave irradiation resulting in decreased residence time, addition of polymerization inhibitors for decreased humin formation have exerted the cumulative effect of increased furfural yield, resulting in improved economical aspect of industrial scale furfural production. Overall, it is therefore recommended to be carry forwarded towards application in biomass to value addition to realize the concept of biorefineries, in the context of substitute to petroleum derivatives.

5 Catalytic Valorization of Bio-derived Lignin

Lignin is the third most abundant natural polymer after cellulose and hemicellulose. It is composed of phenylpropane units which are bonded together by various C–C bonds such as aryl–aryl; aryl–aliphatic and aliphatic–aliphatic as well as ether and aryl ether C–O bonds. Various value added products that are synthesized from processing of lignin through hydrodeoxygenation, hydrolysis, oxidation, biotechnological conversions are represented in Fig. 12 [25].

Although lignin forms a large proportion of the non-food biomass eligible for production of renewable and carbon-neutral liquid fuels and chemical compounds, its separation from its covalently linked materials like cellulose and hemicelluose is one of many technical hurdles needed to be overcome for economical production of

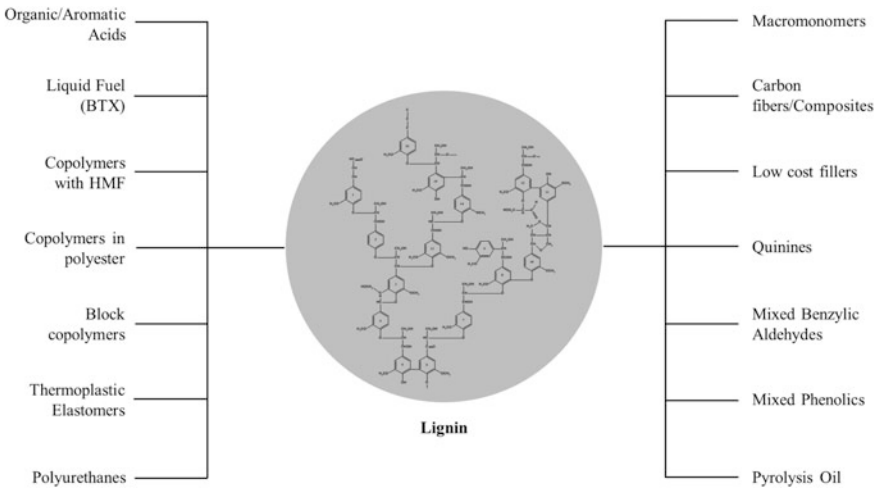

Fig. 12 Value added products from processing of bio-derived lignin through various conversion methodologies [25]

biofuels from cellulosic wastes. To realize this objective, various traditional lignin-isolation methods have been employed such as sulfite (SO_2 and alkali/acid), kraft or sulfate (Na_2S and NaOH) and soda (NaOH) processes. With time several non-conventional chemical methods, such as ammonia fiber expansion (AFEX), aqueous NH_3, dilute and concentrated acids(e.g., H_2SO_4, HCl, HNO_3, H_3PO_4), alkaline (e.g., NaOH, KOH, $Ca(OH)_2$),organic solvents (e.g., ethanol, formic acid, acetic acid, methanol), and ionic liquids have evolved, which offer the advantage of lignin production with little or no sulfur compounds and thus, increasing the applicability for manufacture of value-added products [17]. Although lignin obtained by organic solvents, called organosolv lignin, is beneficial over sulfonated and kraft lignins due to greater ability to be derivatised, lower ash content, higher purity (due to lower carbohydrate content), generally lower molecular weight and more hydrophobicity, it is not used widely developed because of the lower quality of the pulp produced and extensive corrosion of the process equipment. Recent advancements in the area of lignin extraction and precipitation is employing of ionic liquids, where lignins can be recovered from IL by precipitation, allowing the IL to be recycled. Mostly alkylmidazolium based IL have been employed as biomass solvents for dissolution of cellulose. There are reports on use of N-methylimidozole indimethyl sulfoxide for lignin isolation from wood and later precipitation using dioxane/water mixture [22]. Recently, Tan and co-workers [78] utilized ionic liquid mixture consisting 1-ethyl-3-methylimidazolium cation and a mixture of alkylbenzene sulfonates with xylene sulfonate to extract lignin from sugarcane bagasse at elevated temperatures of 170–190 °C under atmospheric condition [78].

High energy content and presence of highly reactive functional groups represent lignin as a potential substrate for synthesis of wide range of renewable chemicals. Further lignin polymer is susceptible to a wide range of chemical transformations, principally cracking or hydrolysis reactions, catalytic reduction, and catalytic oxidation reactions to form valuable chemicals. Normally, lignin catalytic reduction reactions aim at removal of the extensive functionality of the lignin subunits to generate simpler monomeric compounds like phenols, benzene, toluene, or xylene, which can be then hydrogenated to alkanes (carbon atoms C7–C18) via coupling reactions or used as platform chemicals under appropriate reaction environment. Lignin valorisation is often realized through thermal hydrogenolysis (depolymerisation) which could be base-catalyzed, acid-catalyzed, metallic catalyzed and ionic liquids-assisted depolymerization for synthesis of various phenolics (Table 4). However, very meagre yields have been reported indicating pyrolysis to be better methodology for phenolics generation [1, 83].

Heterogeneous hydrogenation of lignin was reported in as early as 1938 when Harris and co-workers obtained monomeric propylcyclohexanols (substituted alkyl phenols) and methanol when lignin was reacted with hydrogen over copper-chromium oxide [28]. Later, many patented processes were reported, for example Noguchi process, which employed an Fe(II)-sulfide along with copper oxide as co-catalyst in phenol at 250–450 °C with an initial hydrogen pressure of 15.2–45.6 MPa and obtained 40% yield of C6–C9 mono phenols [57]. In another patented

Table 4 Production of aromatic phenolics from lignin through various catalytic reactions (reproduced from Ref. [80])

Lignin	Catalyst	Reaction conditions	Major products	Yields (% wt.)	Ref.
Base-catalyzed					
Steam explosion hemp lignin	5% wt. NaOH	300–330 °C, 3.5 MPa	Guaiacol, Catechol Vanilin	0.9–2.8 0.8–3.0 0.5–0.8	[43]
Steam explosion softwood lignin			Guaiacol Catechol Vanilin	1.2–2.1 0.1–3.2 0.3–0.5	
Organosolv lignin	2% wt. NaOH	300 °C, 25 MPa	Syringol Hydroxyacetophenone Guaiacol	4.1 1.6 1.1	[67]
Acid-catalyzed					
Wheat straw lignin	10% wt. formic acid 77% ethanol	360 °C, 25 MPa	Methoxyphenols Catechols Phenols	1.3 0.5 0.3	[24]
Wheat straw lignin	10% wt. formic acid 81% wt. ethanol	380 °C, 25 MPa	Methoxyphenols Catechols Phenols	2.9 1.5 2.0	[23]
Metallic-catalyzed					
Kraft lignin	Si–Al catalyst/ H_2O/butanol	200–350 °C, 1.1–23 MPa	Phenols	6.5	[82]
Acidic hydrolysis spruce lignin	4.4% wt. formic acid 0.15% wt. Pd catalyst 0.94% wt. Nafion SAC-13	300 °C, 9.6 MPa	Guaiacol Pyrocatechol Resorcinol	2.0 1.8 0.5	[47]

(continued)

Table 4 (continued)

Lignin	Catalyst	Reaction conditions	Major products	Yields (% wt.)	Ref.
Birch sawdust lignin	Ni/C	200 °C	Propenylguaiacol Propenylsyringol	12 36	[73]
Ionic-liquid-catalysed					
Organosolv beech lignin	[EMIM][CF_3SO_3]/Mn(NO_3)$_2$	100 °C, 8.4 MPa	2,6-Dimethoxy-1,4-benzoquinone	11.5	[74]
Guaiacylglycerol-β-guaiacyl ether	[BdMIM]Cl/1,5,7-triazabicyclo [4.4.0]dec-5-ene	150 °C	Guaiacol	71.5	[34]

work, Inventa AG employed ferrous sulfate for the fragmentation of lignin into distillable products containing a substantial amount of monophenols [36]. Subsequently, Misson and co-workers [54] investigated catalytic pyrolysis of the pretreated empty palm fruit bunches using NaOH, H_2O_2, and $Ca(OH)_2$ and yielded up to 90 and 80% wt. phenolic monomers in the presence of AlMCM-41 and H-ZSM-5, respectively, when processed at 300 °C [54]. In recent work, Chan and co-workers [8] employed vanadium based catalysts for conversion of dioxasolv-lignin derived from Miscanthus giganteus (under 80 °C for 24 h in 10:1 acetonitrile/THF and 8:1 ethyl acetate/THF mixtures) and obtained a mixture of monophenolics, such as vanillin, syringic acid, syringaldehyde, 4-hydroxybenzaldehyde, vanillic acid, in major proportions [8]. However, utilization of lignin fraction of lignocellulosic biomass for value-added commodities synthesis has not been well established due to its heterogeneity nature.

Further improvements in the existing techniques along with development of novel protocols specifically heterogeneous based are emerging, which will enable the researchers to exploit the potential of lignin at industrial scale.

6 Summary and Perspectives

Lignocellulosic biomass is an abundant source of renewable energy with the potential to be successful alternative to petroleum-based economy. A large pool of value-added chemicals and fuel additives have been devised from cellulosic, hemicellulosic and lignin biogenic polymers and their scope as industrial commodities is revealed in this chapter. Considering the predicted opportunities of lignocellulosic biomass valorization, various catalytic processes that have been evolved for biomass processing, namely hydrolysis, liquefaction, gasification, pyrolysis and deoxygenation/hydrogenation have received increasing attention. However, irrespective of catalytic processes employed, present techniques have not yet offered complete commercialization barring only few bio-products. Although catalytic hydrolysis has evolved as simple process over present liquefaction, gasification and pyrolysis methods of lignocellulosic biomass processing, operational issues such as reactor corrosion, energy-intensive product separation and catalyst recycle remains a challenge in industrial scale production. Advent of heterogeneous as well as ionic liquid-mediated catalysis has emerged as acceptable alternatives, developments in the valorization of lignocellulose still remains a great challenge together with many opportunities. Nevertheless, efforts are being made to develop specific catalysts to overcome various limitations including mass-transfer and catalytic activity loss on reuse and certain novel candidates viz. MOF, POP, COF and CTFs, which finds considerable application in certain fields of biomass valorization. It is postulated that use of such tailored catalysts would bring remarkable improvements in process economics of biomass into biovalue. Commercial

considerations can be further improved through continued research and development and in support, recent trends suggest that chemical catalysis of lignocellulosic biomass will be a key player in establishing a worldwide bio-based economy to substitute conventional petroleum dependent industries.

Acknowledgements The authors gratefully thank Department of Biotechnology, New Delhi, India for their consistent financial support. Authors BA and SE thank Department of Science and Technology (DST-SERB), New Delhi for providing financial assistance through Grant No. PDF/2015/000285 and Grant No. YSS/2014/000031, respectively.

References

1. Amen-Chen C, Pakdel H, Roy C (2001) Production of monomeric phenols by thermochemical conversion of biomass: a review. Bioresour Technol 79(3):277–299
2. Binder JB, Raines RT (2010) Fermentable sugars by chemical hydrolysis of biomass. Proc Natl Acad Sci 107(10):4516–4521
3. Brody T (1999) Nutrients that resist or escape digestion. Nutritional Biochemistry 2nd edition, Academic Press, San Diego, pp 53–61
4. Brunow G, Lundquist K (2010) Functional groups and bonding patterns in lignin (including the lignin-carbohydrate complexes). CRC Press, Taylor Francis Group, New York, NY, USA
5. Cao N-J, Xu Q, Chen C-S, Gong CS, Chen LF (1994) Cellulose hydrolysis using zinc chloride as a solvent and catalyst. Appl Biochem Biotechnol 45(1):521–530
6. Carvalheiro F, Duarte LC, GÃrio FM (2008) Hemicellulose biorefineries: a review on biomass pretreatments. J Sci Ind Res 849–864
7. Cengiz M, Dincturk OD, Sahin HT (2010) Fractional extraction and structural characterization of opium poppy and cotton stalks hemicelluloses. Pharm Mag 6(24):315
8. Chan JMW, Bauer S, Sorek H, Sreekumar S, Wang K, Toste FD (2013) Studies on the vanadium-catalyzed nonoxidative depolymerization of miscanthus giganteus-derived lignin. ACS Catal 3(6):1369–1377
9. Chen H, Qin L, Yu B (2015) Furfural production from steam explosion liquor of rice straw by solid acid catalysts (HZSM-5). Biomass Bioenerg 73:77–83
10. Chiaramonti D, Prussi M, Ferrero S, Oriani L, Ottonello P, Torre P, Cherchi F (2012) Review of pretreatment processes for lignocellulosic ethanol production, and development of an innovative method. Biomass Bioenerg 46:25–35
11. Ciolacu D, Ciolacu F, Popa VI (2011) Amorphous cellulose—structure and characterization. Cellul Chem Technol 45(1):13
12. Corma A, Iborra S, Velty A (2007) Chemical routes for the transformation of biomass into chemicals. Chem Rev 107(6):2411–2502
13. Crezee E, Hoffer BW, Berger RJ, Makkee M, Kapteijn F, Moulijn JA (2003) Three-phase hydrogenation of D-glucose over a carbon supported ruthenium catalyst: mass transfer and kinetics. Appl Catal A 251(1):1–17
14. da Costa Lopes AM, Joo KG, Morais ARC, Bogel-Łukasik E, Bogel-Łukasik R (2013) Ionic liquids as a tool for lignocellulosic biomass fractionation. Sustain Chem Processes 1(1):1
15. De Bari I, Nanna F, Braccio G (2007) SO2-catalyzed steam fractionation of aspen chips for bioethanol production: optimization of the catalyst impregnation. Ind Eng Chem Res 46(23):7711–7720
16. Dhar S, Shukla PR (2015) Low carbon scenarios for transport in India: co-benefits analysis. Energy Policy 81:186–198
17. Doherty WOS, Mousavioun P, Fellows CM (2011) Value-adding to cellulosic ethanol: lignin polymers. Ind Crops Prod 33(2):259–276

19. Elumalai S, Pan XJ (2011) Chemistry and reactions of forest biomass in biorefining. In: Sustainable production of fuels, chemicals, and fibers from forest biomass. ACS symposium series, vol 1067. American Chemical Society, pp 109–144
18. Elumalai S, Agarwal B, Sangwan RS (2016) Thermo-chemical pretreatment of rice straw for further processing for levulinic acid production. Bioresour Technol 218:232–246
20. Emmel A, Mathias AL, Wypych F, Ramos LP (2003) Fractionation of Eucalyptus grandis chips by dilute acid-catalysed steam explosion. Bioresour Technol 86(2):105–115
21. Farmer TJ, Mascal M (2015) Platform molecules. In: Introduction to chemicals from biomass. John Wiley & Sons, Ltd, pp 89–155
22. Fasching M, Schroder P, Wollboldt RP, Weber HK, Sixta H (2008) A new and facile method for isolation of lignin from wood based on complete wood dissolution. Holzforschung 62(1):15–23
23. Forchheim D, Gasson JR, Hornung U, Kruse A, Barth T (2012) Modeling the lignin degradation kinetics in a ethanol/formic acid solvolysis approach. Part 2. validation and transfer to variable conditions. Ind Eng Chem Res 51(46):15053–15063
24. Gasson JR, Forchheim D, Sutter T, Hornung U, Kruse A, Barth T (2012) Modeling the lignin degradation kinetics in an ethanol/formic acid solvolysis approach. Part 1. Kinetic model development. Ind Eng Chem Res 51(32):10595–10606
25. Grestini C (2011) Conversion of lignin: chemical technologies and biotechnologies. EuroBioRef Summer School, Universita Degli Studi di Roma, Castro Marina, Lecce, Italy
26. Guo F, Fang Z, Xu CC, Smith RL (2012) Solid acid mediated hydrolysis of biomass for producing biofuels. Prog Energy Combust Sci 38(5):672–690
27. Haberl H, Erb K-H, Krausmann F, Bondeau A, Lauk C, Müller C, Plutzar C, Steinberger JK (2011) Global bioenergy potentials from agricultural land in 2050: sensitivity to climate change, diets and yields. Biomass Bioenerg 35(12):4753–4769
28. Harris EE, D'Ianni J, Adkins H (1938) Reaction of hardwood lignin with hydrogen. J Am Chem Soc 60(6):1467–1470
29. Hattori H, Ono Y (2015) Solid acid catalysis: from fundamentals to applications. CRC Press
30. Herrera A, Tallez-Luis SJ, Ramarez JA, Vazquez M (2003) Production of xylose from sorghum straw using hydrochloric acid. J Cereal Sci 37(3):267–274
31. Hu R, Lin L, Liu T, Liu S (2010) Dilute sulfuric acid hydrolysis of sugar maple wood extract at atmospheric pressure. Bioresour Technol 101(10):3586–3594
32. IEA (2014) World energy outlook 2014. International Energy Agency (IEA), Paris
33. Isikgor FH, Becer CR (2015) Lignocellulosic biomass: a sustainable platform for the production of bio-based chemicals and polymers. Polym Chem 6(25):4497–4559
34. Jia S, Cox BJ, Guo X, Zhang ZC, Ekerdt JG (2010) Decomposition of a phenolic lignin model compound over organic N-bases in an ionic liquid. Holzforschung 64(5):577–580
35. Jiang Y, Li X, Wang X, Meng L, Wang H, Peng G, Wang X, Mu X (2012) Effective saccharification of lignocellulosic biomass over hydrolysis residue derived solid acid under microwave irradiation. Green Chem 14(8):2162–2167
36. Johann G (1959) Production of phenols by catalytic hydrogenation of lignin. US2870133 A
37. Kaldstrom M, Kumar N, Murzin DY (2011) Valorization of cellulose over metal supported mesoporous materials. Catal Today 167(1):91–95
38. Karinen R, Vilonen K, Niemel M (2011) Biorefining: heterogeneously catalyzed reactions of carbohydrates for the production of furfural and hydroxymethylfurfural. ChemSusChem 4 (8):1002–1016
39. Kobayashi H, Ohta H, Fukuoka A (2012) Conversion of lignocellulose into renewable chemicals by heterogeneous catalysis. Catal Sci Technol 2(5):869–883
40. Kootstra AMJ, Beeftink HH, Scott EL, Sanders JPM (2009) Comparison of dilute mineral and organic acid pretreatment for enzymatic hydrolysis of wheat straw. Biochem Eng J 46(2):126–131
41. Kumar P, Barrett DM, Delwiche MJ, Stroeve P (2009) Methods for pretreatment of lignocellulosic biomass for efficient hydrolysis and biofuel production. Ind Eng Chem Res 48(8):3713–3729

42. Kuster BFM, Der Van Steen HJC (1977) Preparation of 5-hydroxymethylfurfural Part I. Dehydration of fructose in a continuous stirred tank reactor. Starch 29(3):99–103
43. Lavoie J-M, Bara W, Bilodeau M (2011) Depolymerization of steam-treated lignin for the production of green chemicals. Bioresour Technol 102(7):4917–4920
44. Lee SH, Doherty TV, Linhardt RJ, Dordick JS (2009) Ionic liquid-mediated selective extraction of lignin from wood leading to enhanced enzymatic cellulose hydrolysis. Biotechnol Bioeng 102(5):1368–1376
45. Li C, Zhao ZK (2007) Efficient acid catalyzed hydrolysis of cellulose in ionic liquid. Adv Synth Catal 349(11–12):1847–1850
46. Li H, Qu Y, Xu J (2015) Microwave-Assisted conversion of lignin. In: Fang Z, Smith JLR, Qi X (eds) Production of biofuels and chemicals with microwave. Springer, Netherlands, Dordrecht, pp 61–82
47. Liguori L, Barth T (2011) Palladium-Nafion SAC-13 catalysed depolymerisation of lignin to phenols in formic acid and water. J Anal Appl Pyrol 92(2):477–484
48. Lima S, Fernandes A, Antunes MM, Pillinger M, Ribeiro F, Valente AA (2010) Dehydration of xylose into furfural in the presence of crystalline microporous silicoaluminophosphates. Catal Lett 135(1–2):41–47
49. Lloyd TA, Wyman CE (2005) Combined sugar yields for dilute sulfuric acid pretreatment of corn stover followed by enzymatic hydrolysis of the remaining solids. Bioresour Technol 96(18):1967–1977
50. Luterbacher JS, Rand JM, Alonso DM, Han J, Youngquist JT, Maravelias CT, Pfleger BF, Dumesic JA (2014) Nonenzymatic sugar production from biomass using biomass-derived gamma-valerolactone. Science 343(6168):277–280
51. Mandalika A, Runge T (2012) Enabling integrated biorefineries through high-yield conversion of fractionated pentosans into furfural. Green Chem 14(11):3175–3184
52. Marzialetti T, Valenzuela Olarte MB, Sievers C, Hoskins TJC, Agrawal PK, Jones CW (2008) Dilute acid hydrolysis of Loblolly pine: a comprehensive approach. Ind Eng Chem Res 47(19):7131–7140
53. McIntosh S, Vancov T (2010) Enhanced enzyme saccharification of Sorghum bicolor straw using dilute alkali pretreatment. Bioresour Technol 101(17):6718–6727
54. Misson M, Haron R, Kamaroddin MFA, Amin NAS (2009) Pretreatment of empty palm fruit bunch for production of chemicals via catalytic pyrolysis. Bioresour Technol 100(11):2867–2873
55. Moreno-Recio M, Santamaría-González J, Maireles-Torres P (2016) Brönsted and Lewis acid ZSM-5 zeolites for the catalytic dehydration of glucose into 5-hydroxymethylfurfural. Chem Eng J 303:22–30
56. Mosier N, Wyman C, Dale B, Elander R, Lee YY, Holtzapple M, Ladisch M (2005) Features of promising technologies for pretreatment of lignocellulosic biomass. Bioresour Technol 96(6):673–686
57. Motoyoshi O, Yoshio M, Kan K (1963) Process of liquefaction of lignin
58. Panagiotou G, Olsson L (2007) Effect of compounds released during pretreatment of wheat straw on microbial growth and enzymatic hydrolysis rates. Biotechnol Bioeng 96(2):250–258
59. J-Y Park, Shiroma R, Al-Haq MI, Zhang Y, Ike M, Arai-Sanoh Y, Ida A, Kondo M, Tokuyasu K (2010) A novel lime pretreatment for subsequent bioethanol production from rice straw calcium capturing by carbonation (CaCCO) process. Bioresour Technol 101(17):6805–6811
60. Qi X, Guo H, Li L (2011) Efficient conversion of fructose to 5-hydroxymethylfurfural catalyzed by sulfated zirconia in ionic liquids. Ind Eng Chem Res 50(13):7985–7989
61. Rackemann DW, Doherty WO (2011) The conversion of lignocellulosics to levulinic acid. Biofuels, Bioprod Biorefin 5(2):198–214
62. Ragg PL, Fields PR, Tinker PB (1987) The development of a process for the hydrolysis of lignocellulosic waste [and discussion]. Philos Trans R Soc Lond A: Math, Phys Eng Sci 321(1561):537–547

63. Raven PH, Evert, R.F. (1992) Biology of plants. 6th Edition edn. W.H. Freeman and Company/Worth Publishers
64. Rinaldi R, Palkovits R, Schath F (2008) Depolymerization of cellulose using solid catalysts in ionic liquids. Angew Chem Int Ed 47(42):8047–8050
65. Rita de Cassia LB, Rocha GJM, Rodrigues D, Helcio Filho JI, Maria das Gracas AF, Pessoa A (2010) Scale-up of diluted sulfuric acid hydrolysis for producing sugarcane bagasse hemicellulosic hydrolysate (SBHH). Bioresour Technol 101(4):1247–1253
66. Rivas B, Domanguez JM, Domanguez H, Paraji JC (2002) Bioconversion of posthydrolysed autohydrolysis liquors: an alternative for xylitol production from corn cobs. Enzyme Microb Technol 31(4):431–438
67. Roberts V, Stein V, Reiner T, Lemonidou A, Li X, Lercher JA (2011) Towards quantitative catalytic lignin depolymerization. Chem A: Eur J 17(21):5939–5948
68. Rosatella AA, Simeonov SP, Frade RF, Afonso CA (2011) 5-hydroxymethylfurfural (HMF) as a building block platform: Biological properties, synthesis and synthetic applications. Green Chem 13(4):754–793
69. Rubin EM (2008) Genomics of cellulosic biofuels. Nature 454(7206):841–845
70. Saha B, Abu-Omar MM (2014) Advances in 5-hydroxymethylfurfural production from biomass in biphasic solvents. Green Chem 16(1):24–38
71. Saha BC, Iten LB, Cotta MA, Wu YV (2005) Dilute acid pretreatment, enzymatic saccharification and fermentation of wheat straw to ethanol. Process Biochem 40(12):3693–3700
72. Shen Y, Sun J-K, Yi Y-X, Wang B, Xu F, Sun R-C (2015) One-pot synthesis of levulinic acid from cellulose in ionic liquids. Bioresour Technol 192:812–816
73. Song Q, Wang F, Cai J, Wang Y, Zhang J, Yu W, Xu J (2013) Lignin depolymerization (LDP) in alcohol over nickel-based catalysts via a fragmentation/hydrogenolysis process. Energy Environ Sci 6(3):994–1007
74. Stark K, Taccardi N, Basmann A, Wasserscheid P (2010) Oxidative depolymerization of lignin in ionic liquids. ChemSusChem 3(6):719–723
75. Sun Y, Cheng J (2002) Hydrolysis of lignocellulosic materials for ethanol production: a review. Bioresour Technol 83(1):1–11
76. Swatloski RP, Spear SK, Holbrey JD, Rogers RD (2002) Dissolution of cellose with ionic liquids. J Am Chem Soc 124(18):4974–4975
77. Taherzadeh MJ, Karimi K (2008) Pretreatment of lignocellulosic wastes to improve ethanol and biogas production: a review. Int J Mol Sci 9(9):1621–1651
78. Tan SSY, MacFarlane DR, Upfal J, Edye LA, Doherty WOS, Patti AF, Pringle JM, Scott JL (2009) Extraction of lignin from lignocellulose at atmospheric pressure using alkylbenzene-sulfonate ionic liquid. Green Chem 11(3):339–345
79. Teong SP, Yi G, Zhang Y (2015) Hydroxymethylfurfural production from bioresources: past, present and future. Green Chem 16(4):2015–2026
80. Wang H, Tucker M, Ji Y (2013) Recent development in chemical depolymerization of lignin: a review. J Appl Chem
81. Werpy T, Petersen G, Aden A, Bozell J, Holladay J, White J, Manheim A, Eliot D, Lasure L, Jones S (2004) Top value added chemicals from biomass. Volume 1-results of screening for potential candidates from sugars and synthesis gas. DTIC Document
82. Yoshikawa T, Yagi T, Shinohara S, Fukunaga T, Nakasaka Y, Tago T, Masuda T (2012) Production of phenols from lignin via depolymerization and catalytic cracking. Fuel Process Technol 108:69–75
83. Zakzeski J, Bruijnincx PCA, Jongerius AL, Weckhuysen BM (2010) The catalytic valorization of lignin for the production of renewable chemicals. Chem Rev 110(6):3552–3599
85. Zhang Z, Zhao ZK (2010) Microwave-assisted conversion of lignocellulosic biomass into furans in ionic liquid. Bioresour Technol 101(3):1111–1114

84. Zhang D, Ong YL, Li Z, Wu JC (2012) Optimization of dilute acid-catalyzed hydrolysis of oil palm empty fruit bunch for high yield production of xylose. Chem Eng J 181:636–642
86. Zhao X, Cheng K, Liu D (2009) Organosolv pretreatment of lignocellulosic biomass for enzymatic hydrolysis. Appl Microbiol Biotechnol 82(5):815–827
87. Zheng Y, Zhao J, Xu F, Li Y (2014) Pretreatment of lignocellulosic biomass for enhanced biogas production. Prog Energy Combust Sci 42:35–53
88. Zhou C-H, Xia X, Lin C-X, Tong D-S, Beltramini J (2011) Catalytic conversion of lignocellulosic biomass to fine chemicals and fuels. Chem Soc Rev 40(11):5588–5617
89. Zi G, Yan Z, Wang Y, Chen Y, Guo Y, Yuan F, Gao W, Wang Y, Wang J (2015) Catalytic hydrothermal conversion of carboxymethyl cellulose to value-added chemicals over metal–organic framework MIL-53 (Al). Carbohydr Polym 115:146–151

Microbial Electrochemical Platform: Biofactory with Diverse Applications

S. Venkata Mohan, G. Velvizhi and P. Chiranjeevi

Abstract Microbial electrochemical technologies (MET) have significant potential to negate the impending energy, and renewable feedstock crisis. METs have evolved into a sustainable and eco-friendly solutions owing to their diverse applications like microbial fuel cell (MFC), for power generation, bioelectrochemical treatment (BET) for wastewater remeduiation, microbial desalination cell (MDC) for salt removal and resource recovery, microbial electrolysis cell (MEC) for the production of Hydrogen by applying external potential and bioelectrochemical syntheis (BES) for value-added products production and other applications such as plant microbial fuel cells (P-MFC) and artificially constructed wetlands fuel cells (CW-MFC) utilize the root exudates for power generation, biosensor applications, etc. This chapter draws light upon the multifaceted application of MET and their specific operational mechanism along with their futuristic integrations and developmental models.

Keywords Electro-fermentation · Bioelectrochemical treatment (BET) · Microbial fuel cell (MFC) · Microbial desalination cell (MDC)

1 Introduction

Microbial catalyzed electrochemical systems (MES) are multi-disciplinary hybrid systems emerging as a potential platform with multi-facet applications. Exo-electrogens has become an increasingly important platform for the production of biofuels and chemicals from renewable resources [22, 77, 78]. Microbes are effective cleavers of organic substrate to generate electrons and protons. Few microbes are

S. Venkata Mohan (✉) · G. Velvizhi · P. Chiranjeevi
Bioengineering and Environmental Science (BEES), CSIR-Indian Institute of Chemical Technology (CSIR-IICT), Hyderabad 500 007, India
e-mail: vmohan_s@yahoo.com

A.K. Agarwal et al. (eds.), *Biofuels*, Green Energy and Technology,
DOI 10.1007/978-981-10-3791-7_3

able to transport electrons beyond their cell boundaries and thereby, electrically interacting with the external environment creating a specific niche to be developed into an advanced bio-processes by harnessing these electrons with the insertion of the electrodes [37]. Bacteria–electrode interactions exchange the electrons and uses for wider applications such as bioelectricity, wastewater treatment, production of value-added products etc. Research has been originally initiated for harvesting power from microbial fuel cell (MFC) taking advantage of biocatalyst metabolic function. Then, MES nurtured and fragmented into various processes which increased the scope in utilizing the reducing equivalents (electrons and protons) for the remediation of wastewater as bio-electrochemical treatment (BET) [75, 76] and desalinating salt water as microbial desalination cell (MDC) [51], supplying external energy in addition to in situ potential for the production of hydrogen as microbial electro-synthesis cell (MEC) [77] and synthesis of value-added products as bioelectrochemical systems (BES) [44]. Other applications like utilizing root of plant and utilizing artificially constructed wetlands (CW) for power generation and biosensor application, etc. were also reported [2, 3, 11, 79]. Overcoming metabolic redox limitations by electron exchange between microbes and electrodes enhances the yield [37, 59, 77, 78]. This chapter outlines the principles associated with MES operation with particular emphasis on its multifaceted applications (Fig. 1).

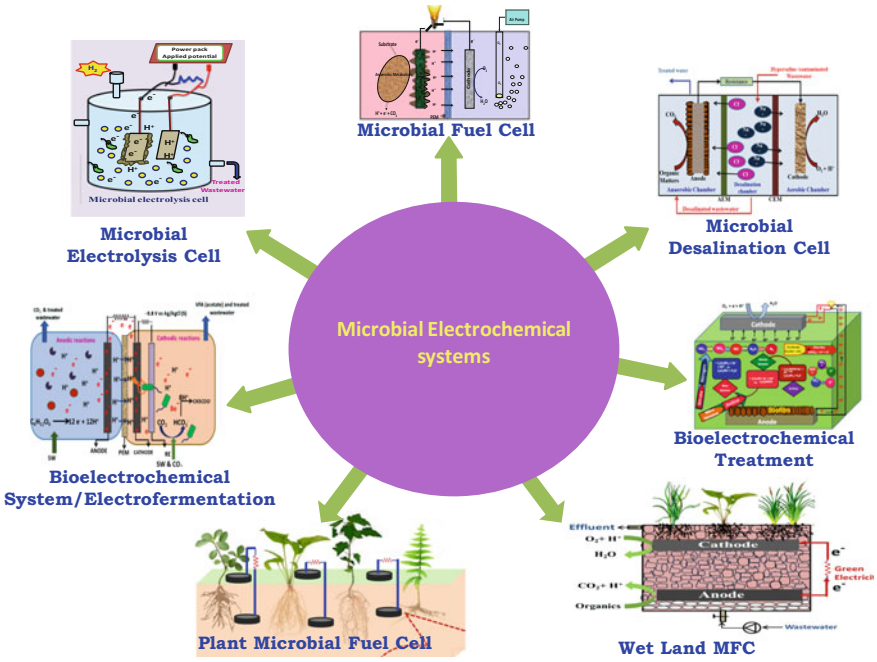

Fig. 1 Multi-faceted applications of microbial catalyzed electrochemical systems

2 Electron Transfer

Few microorganisms have a unique mechanism to transfer electrons extracellularly to electrodes that are distant from the cell surface through microbial electron transport chains. The microbes utilize the substrates and generate the electrons and protons, and these reducing equivalents move via series of redox mediators towards an available terminal electron acceptor (TEA). This facilitates generation of energy-rich phosphate bonds that are useful for the microbial growth and subsequent metabolic activities which occur inside the cell. Bacteria can communicate with external electron acceptors from the cell to the artificially placed electrode through direct contact and electron shuttling mediators and through electrically conductive appendages (nanowires/pilin) [56, 59]. Microorganisms transfer electrons between their cytoplasmic membrane and extracellular electrodes through a network of redox and structural proteins. These proteins often form specific pathway that are electrically and physically connected to intracellular metabolic processes with redox transformation to extracellular electron acceptors that are beyond the outer membrane. Various 'C' type cytochromes present on the bacterial plasma membrane transfer electrons to the electrode through Mtr pathway which is the main route for the reduction of external inorganic electron acceptors or electrodes by both direct and mediated exo-electron transport (EET) [16, 77]. Geobacter, Rhodoferax and Shewanella are reported bacterial species for their exo-cellular electron transfer through membrane-bound organelles [41, 56].

3 Applications of MES

The application of MES depends upon the efficiency of electron transfer machinery based on the electrode-bacterial interactions in the system. The electron flux manifested by bacteria can be harnessed for power generation, pollutant remediation and production of commercial viable value-added product (Fig. 1).

3.1 Microbial Fuel Cell (MFC)

Microbial fuel cells (MFCs) configures with an arrangement of anode and cathode sandwiched with a membrane, in the anode chamber anaerobic bacteria oxidizes the substrates to release electrons and protons, the protons pass through the membrane to the cathode and the electrons pass through the external circuit originating as a measurable direct current flow (Table 1). The potential difference developed by the solid electrode based on the bacterial activity will be used as overall cell electromotive force to harvest electricity. The biochemical reactions occurring during the operation of MFC with glucose is represented below.

Table 1 Bioelectrogenesis with respect to fuel cell configuration

Configuration	Power	Reference
Single chamber	150 mW/m^2	Min and Logan [43]
Flat plate MFC	72 mW/m^2	Min and Logan [43]
Double chamber	1.3 mA/cm^2	Niessen et al. [49]
Single chamber	305 mW/m^2	Liu et al. [40]
Single chamber	354 mW/m^2	Heilmann and Logan [28]
Single chamber	269 mW/m^2	Heilmann and Logan [28]
Stacked MFC	258 W/m^3	Aelterman et al. [4]
Double chamber	170 mW/m^2	He et al. (2008)
Single chamber	211 mA/m^2	Venkata Mohan et al. [69]
Single chamber	182.85 mA/m^2	Venkata Mohan et al. [71]
Benthic MFC	35.08 mW/m^2	Venkata Mohan et al. [76]
Single chamber	401 mW/m^2	Sharma and Li [58]
Single chamber	107.89 mW/m^2	Goud et al. [27]
Basic stack MFC	1184 mW/m^2	Kim et al. [34]
Double chamber	66.21 mW/m^2	Venkata Mohan et al. [81]

$$C_6H_{12}O_6 + 6H_2O \rightarrow 6CO_2 + 24H^+ + 24e^- \quad \text{(Anode)} \tag{1}$$

$$4e^- + 4H^+ + O_2 \rightarrow 2H_2O \quad \text{(Cathode)} \tag{2}$$

$$C_6H_{12}O_6 + 6H_2O + 6\ O_2 \rightarrow 6CO_2 + 12H_2O \quad \text{(Overall)} \tag{3}$$

MFC was originated with the dual chamber by separating both the anode and cathode chamber through the membrane where the oxidation and reduction reactions could occur respectively [66, 69–72, 77]. In single chambered systems the cathodic chamber is eliminated by providing an open-air cathode, which accounts for economics in construction and operation. Research was carried out by eliminating the membrane, though the performance of single chamber is relatively low compared to the double chamber in terms of electrogenic activity due to the inherent limitations in the cathodic reduction reactions but single chamber membrane-less are cost effective and could be easily commercialized. Irrespective of the configuration, MFC performance is independent of reactor volume because the possible theoretical potential in MFC is around 1.2 V [higher electron donors and acceptors NAD+ (−0.32 V) and O_2 (+0.816 V) are available in the biological system]. Henceforth, to enhance the power generation stacked MFCs were designed by connecting multiple MFCs in series connection [34, 60, 87, 94]. Four MFC's were stacked by sandwiching multifunctional paper layers for two-chambered fuel cell configuration for potentially powering on-chip paper based MFCs [24]. A stacked MFC with a total volume of 72 L was constructed with granular activated carbon (GAC) packed bed electrodes [13]. Various applications of MFC are discussed as follows.

3.1.1 Plant-MFC

Plant rhizo-deposition (root exudates) constitutes major photosynthetic product and provides the supplementation of the carbon required for the propagation of microbial consortia which in turn, simplify the nutrients in the soil and make them amenable for the plant root system to absorb. The plant-microbial interactions at rhizosphere represent a favorable microenvironment for both bacterial and plant growth (utilizing plant rhizo-deposits) as well as mediate reducing equivalents for harnessing bioelectricity by incorporation of solid non-catalyzed electrode assembly (MFC system) which facilitates the transformation of solar energy into green electricity (Fig. 2 and Table 2). P-MFC (Plant MFC) with Reed mannagrass (*Glyceria maxima*) using cation exchange membrane for harnessing of power was well studied [62]. Rice field embedded MFC was also reported to produce good power [10, 18, 33]. Bio-cathode was successfully integrated into P-MFC and operated for long term, wherein power density increased with the continuous growth of the plant and due to the high redox potential of oxygen which was effectively catalyzed by microorganisms in the cathode [85]. The new composition of the plant-growth medium (modified Hoagland medium) with fewer nitrates, high-ammonium based macro and micro-nutrients, balanced amount of bicarbonate buffer and addition of sulfates helped to maximize current production of P-MFC [30, 31]. The theoretical calculations between *Spartina anglica* salt marsh and *Phragmites australis* peat

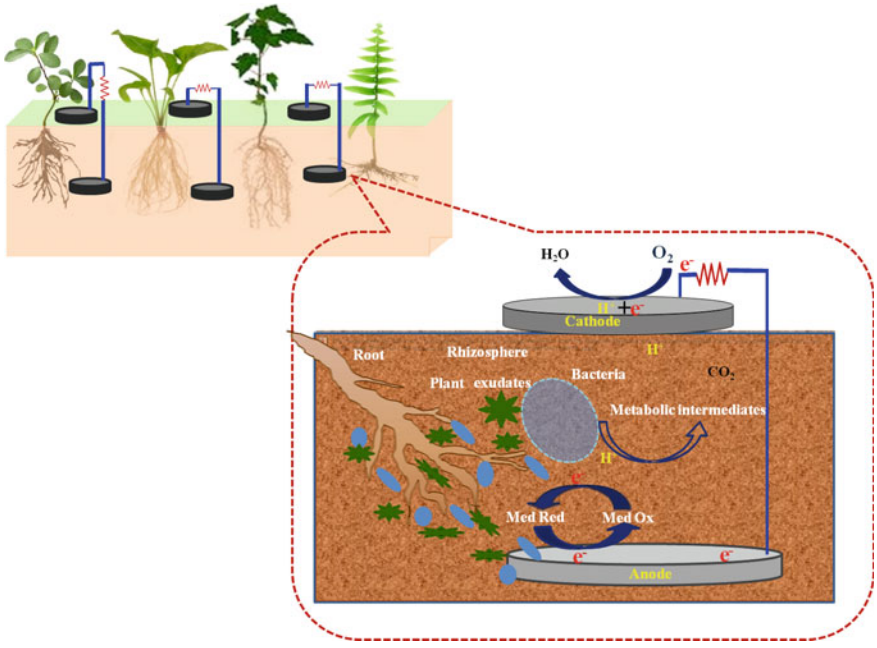

Fig. 2 Plant-microbial fuel cell (P-MFC)

Table 2 Plant-microbial fuel with respect to plant species for harnessing power

Plant species	Power	Reference
Glyceria Maxima	67 mW/m^2	Strik et al. [62]
Oryza sativa L. cv. Sasanishiki	6 mW/m^2	Kaku et al. [33]
Oryza sativa sp. indica	33 mW/m^2	De Schamphelaire et al. [18, 19]
Spartina anglica	222 mW/m^2	Helder et al. [29]
Oryza sativa L. cv. Satojiman	14 mW/m^2	Takanezawa et al. [63]
Floating macrophyte based ecosystem	224 mA/m^2	Venkata Mohan et al. [79]
Flat plate plant MFC	5.8 W/m^3	Helder et al. [30, 31]
Pennisetum setaceum	163 mW/m^2	Chiranjeevi et al. [11]
Submerged and emergent macrophytes	179.78 mW/m^2	Chiranjeevi et al. [12]

soil in P-MFC setup showed that salt marsh generated 10 times more power than the P-MFC in peat soil due to the tidal advection [86]. The tubular P-MFC was designed to increase the feasibility of the P-MFC with the graphite felt and graphite granules respectively. Graphite felt exhibited 15 times higher power output than the P-MFC with the graphite granules based on the mass of the electrode material due to the reduction of anode electrode material while achieving higher power outputs per square meter of the membrane [65]. The feasibility of power generation by non-destructive usage of rhizo-deposits of *Pennisetum setaceum* plant was studied in rhizosphere based MFC (R-MFC) [11]. Miniatured ecologically engineered system with submerged emergent and floating macrophytes embedded with fuel cells were studied for harnessing bioelectricity along with simultaneous wastewater treatment [12, 79].

3.1.2 Wetland Constructed MFC

Apart from power generation, sediment microbial fuel cell (S-MFCs) enhances the oxidation of reduced compounds at the anode, thus bringing about the removal of excessive or unwanted reducing equivalents from submerged soils (Fig. 3). The two biologically mediated cathodic reactions, oxygen reduction, and manganese cycle imply a low cost and high electrode potential. They are of particular interest for reactor-type S-MFCs and go beyond energy generation for low-power applications [18]. The light/dark effect on power output were studied and found fluctuations due to the photosynthetic activity of the macrophytes (*Phragmites australis*) at dark condition (night time). A pilot-scale subsurface constructed wetland system for treating domestic wastewater was studied with horizontal flow (HF) and under vertical flow (VF) modes [6]. A low-cost PVC-made structure is constructed to harvest electricity from mangrove environment located in French Guiana [54]. A bench-scale constructed wetland was operated for 400 days with groundwater

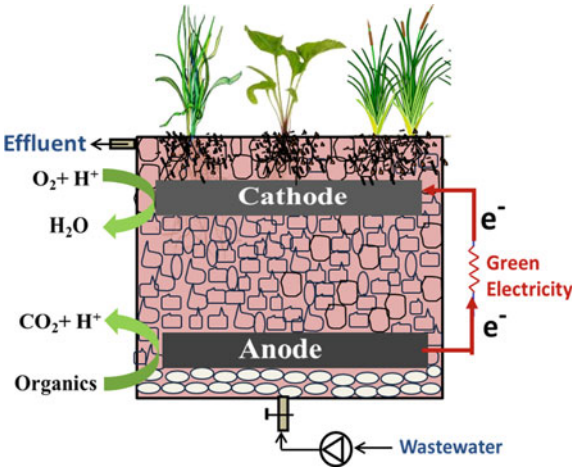

Fig. 3 Constructed wetland systems integrated with MFC

contaminated with benzene, methyl-test-butyl ether (MTBE), and ammonium (NH_4^+) [84]. Upflow constructed wetland–microbial fuel cell (UFCW–MFC) planted with cattail was used for simultaneous wastewater treatment and electricity generation by using carbon felt as an electrode material. Dewatered alum sludge (DAS) based vertical upflow constructed wetland (CW) was integrated with MFC. Powdered activated carbon (PAC) was used in the anode area in varied percentage with DAS to explore its influences on the performance of CW-MFC system [88].

3.2 Bioelectrochemical Treatment (BET)

Bioelectrochemical treatment (BET) systems functions with electrodes as electron acceptor and exploit microbial catabolic activities to degrad organic molecules [36, 66, 75, 76]. BET has the advantage of coupling both electrochemical and anaerobic biological processes, which triggers the redox reactions for the degradation of complex pollutants with simultaneous power generation [45, 76, 91]. When waste/wastewater functions as an electron donor or acceptor, its remediation is accomplished by anodic oxidation or cathodic reduction under defined conditions. In addition to in situ bio-potential, anodic oxidation and cathodic reduction reactions have a positive influence on pollutant removal [67]. BET was reported to treat wastewater viz., distillery [45], dairy waste [77], Complex chemical wastewater [21, 73–75], Pharmaceutical wastewater [66]; petrochemical wastewater [8] Paper and pulp [38], Azo dye based wastewater [61], breweries wastewater [17], pre-irrigation treatment wastewater etc. [1]. Various application of BET are discussed as follows.

3.2.1 Metal Recovery

Bioelectrochemical treatments (BET) have emerged as a potential technological platform for recovery of metal ions from metallurgical waste. The general approach of bio-electrochemical metal recovery is using metals as the electron acceptor in the cathode chamber and organic waste as the electron donor in the anode chamber [47, 83]. The bio-potential/in situ potential developed in bio-electrochemical systems acts as the driving force towards metal removal and recovery. Some of the metal ions can be recovered by using the in situ generated potential, whereas other metal ions can be recovered by the ex situ or externally applied potential [32, 39, 64, 82]. Bacteria play a crucial role in the biotic systems by utilizing the organic substrate and thereby liberate reducing equivalents which act as the power source in reducing the metal species. Various metals, viz. Ag, Au, V, Pb, Cd, Cr and Cu, Se(IV), V(V), Ag(I), Cu(II), Mn(IV) and Cr(VI) have been recovered in the bio-electrochemical systems by the action of a biotic anode and abiotic cathode [47, 48, 82, 92]. The metal compounds act as good electron sinks due to their high electronegativity and can be reduced to a different oxidation states [35]. Since, many metals have effective electron accepting conditions the bio-cathodes have shown good performances in removing and recovering metals, but high concentration metal solutions generally inhibit microbial activities and reduce system efficacy. The electrostatic interactions between the cathode and metal ions affect metal recovery efficiency, the electrostatic attraction facilitates metal cations to move toward the cathode, while electrostatic repulsion inhibits the approaching of metal anions to the cathode [83]. The scope for future research in metal reduction through bioelectrochemical systems include the strategies on developing efficient cathode materials, optimum fuel cell configurations, circuit design and biocatalyst enrichment to improve the reduction reactions towards metal removal/recovery.

3.3 Bioelectrochemical System (BES)

Bioelectrochemical systems (BES) synthesize electricity driven chemical compounds through a series of microbial catalyzed reactions based on the electrode-bacteria interactions [20, 26, 52, 55, 93]. The reduction mechanism in MES processes could be used for the production of reduced end product rather than pollutant degradation. Some of the product formations require less redox potential which can be accomplished by the in situ bio-potential generated in the system, while some reactions require more redox potential at cathode which could be applied externally to meet the energy necessary to cross the thermodynamic barrier for product formation [80]. BES have been gaining prominence for sequestering CO_2, where the electro-lithoautotrophs act as biocatalysts for the reduction of CO_2 to platform chemicals (C1-C6) by utilizing electrons directly derived from

solid-inorganic electron donors (electrode) [44, 81]. Carbon chain elongation from C1 to higher-chain compounds originates from acetate (C2) towards propionate (C3), butyrate (C4), or caproate (C6) and derived from the chain elongation processes.

3.4 Microbial Electrolysis

Hydrogen is one of the alternative renewable fuels having high impact in the present bioenergy research. H_2 production through acidogenic fermentation was well established and understood with respect to the operational and regulating factors [14, 68, 71]. However, there are some drawbacks for the fermentative H_2 production, due to its low substrate conversion efficiency, accumulation of carbon-rich acid intermediates, an imbalance in buffering the system by a sudden drop in system pH, etc. [68, 72]. Microbial electrolysis cell (MEC) combines the conventional acidogenic process with electrochemical hydrolysis [5, 78, 89]. The reducing equivalents generated during fermentation move through a series of redox components towards an available terminal electron acceptor. However, the electron flow slows down due to the thermodynamic feasibility which requires additional drive for the electrons to flow. Hence external potential is applied to the system to drive the electrons for the hydrogen production. External potential results in the growth of electrochemically active microbes on anode which can discharge electrons more effectively [32]. MEC has potential for application within the wastewater industry, reducing energy and operation costs [15].

3.5 Microbial Desalination

Conventionally, desalination process involves high energy inputs and are operated using very expensive setups. Therefore, developing sustainable desalination technologies is being seriously considered. In this context, microbial desalination cell (MDC) is an emerging area which requires less energy inputs and also harnesses energy from the process [23, 53]. MDC is configured with three chambers introducing an additional salt water chamber separated from an anode chamber with an anion exchange membrane (AEM), and from a cathode chamber with a cation exchange membrane (CEM) [90]. The anode chamber is responsible for organic degradation and electricity production, the middle chamber is responsible for salt removal while the cathode chamber completes the electrical loop [46]. Continuously operated upflow, stacked MDC, simultaneous desalination and hydrogen production are also being evaluated in MDC. The performance of MDC depends on the internal resistance, including ohmic, charge transfer, and mass transfer resistances. Apart from low energy inputs, it can also simultaneously tackle

multi-pollutant removal, saline water desalination, resource recovery and value addition advocating sustainable water infrastructure [51].

3.6 Electro-Fermentation

Electro-fermentation (EF) melds conventional microbial fermentative on with electrochemistry. By application of very low potentials of electrical field across the electrodes incorporated in the fermentation medium which influences the fermentative environment and microbial metabolism. This electromotive induced regulation of anaerobic fermentation is termed electro-fermentation and can be employed to produce desirable biochemicals. EF is improved with selectively enriched microbial cultures, increases carbon efficiency, reducing the use of chemicals for pH control; in some cases enhance product recovery. Regulating the potentials of the electrical inputs to drive fermentation can also be used to maneuver both pure culture and mixed microbial fermentations. This innovative EF paves a new avenue to the existing industrial fermentation processes, to utilize organic waste towards the value-added product in a biorefinery approach [50].

3.7 Other Applications

Apart from the above applications MES are also used as Photosynthetic fuel cells (PhFC) which is similar to the MFC in operation but instead of chemotrophic mechanism, phototrophic bacteria will act as biocatalyst [7]. MEC are also being used as biosensors [2, 3, 9, 25, 42, 57]. Micro-MFC was developed for high-throughput screening and sensitivity analyses of biological and electrochemical performance parameters.

4 Conclusion

Great efforts are being made to improve the performance of MES and advance their translational potential toward real-world applications. Significant improvement in MES performance can be achieved with the development of new techniques in synthetic biology that can regulate microbial metabolic pathways or control their gene expression and generate high-throughput rapid screening tools for microbial bio-power production. To enhance the efficacy of its application, a special focus on the essential connection of redox reactions and energy metabolism, should be analyzed in depth. Synergistic interaction between the MES components and biocatalyst needs to be optimized to maximize the product recovery and energy generation. MES has wide scope in upgrading the existing effluent treatment plants

(ETP) by integrating with BET which might be an added advantage with dual benefit of treatment and bioelectricity generation. The value-added products synthesized by elector-fermentation is also an emerging field which requires more focus on electrical potential and impact on the metabolism of the organism for exploiting external electron transfer for the enhanced yield.

Acknowledgements The authors wish to thank the Director, CSIR-IICT for support and encouragement. Authors sincerely acknowledges support from Council of Scientific and Industrial Research (CSIR; SETCA (CSC-0113)), Department of Biotechnology (DBT) and Department of Science and Technology (DST) in the form of research grants.

References

1. Abourached C, English MJ, Liu H (2016) Wastewater treatment by Microbial Fuel Cell (MFC) prior irrigation water reuse. J Cleaner Prod 137:144–149
2. Abrevaya XC, Sacco Natalia J, Bonetto Maria C, Hilding-Ohlsson Astrid, Cortón E (2015) Analytical applications of microbial fuel cells. part I: biochemical oxygen demand. Biosens Bioelectron 63:580–590
3. Abrevaya XC, Sacco NJ, Bonetto MC, Hilding-Ohlsson A, Corton E (2015) Analytical applications of microbial fuel cells. part ii: toxicity, microbial activity and quantification, single analyte detection and other uses. Biosens Bioelectron 15(63):591–601
4. Aelterman P, Rabaey K, Pham HT, Boon N, Verstraete W (2006) Continuous electricity generation at high voltages and currents using stacked microbial fuel cells. Environ Sci Technol 40:3388–3394
5. Call D, Logan BE (2008) Hydrogen production in a single chamber microbial electrolysis cell lacking a membrane. Environ Sci Technol 42:3401–3406
6. Camacho JV, Montano C, Andrés M, Rodrigo R, Jesús F, Morales F et al (2014) Energy production from wastewater using horizontal and vertical subsurface flow constructed wetlands 13:2517–2523
7. Chandra R, Subhash GV, Venkata Mohan S (2012) Mixotrophic operation of photo-bioelectrocatalytic fuel cell under anoxygenic microenvironment enhances the light dependent bioelectrogenic activity. Bioresource Technol 109:46–56
8. Chandrasekhar K, Venkata Mohan S (2012) Bio-electrochemical remediation of real field petroleum sludge as an electron donor with simultaneous power generation facilitates biotransformation of PAH: effect of substrate concentration. Bioresour Technol 110:517–525
9. Chang IS, Jang JK, Gil GC, Kim M, Kim HJ, Cho BW, Kim BH (2004) Continuous determination of biochemical oxygen demand using microbial fuel cell type biosensor. Biosens Bioelectron 19:607–613
10. Chen Z, Huang YC, Liang JH, Zhao F, Zhu YG (2012) A novel sediment microbial fuel cell with a biocathode in the rice rhizosphere. Bioresour Technol 108:55–59
11. Chiranjeevi P, Mohanakrishna G, Venkata Mohan S (2012) Rhizosphere mediated electrogenesis with the function of anode placement for harnessing bioenergy through CO_2 sequestration. Bioresour Technol 124(2012):364–370
12. Chiranjeevi P, Chandra Rashmi, Venkata Mohan S (2013) Ecologically engineered submerged and emergent macrophyte based system: an integrated eco-electrogenic design for harnessing power with simultaneous wastewater treatment. Ecol Eng 51(2013):181–190
13. Chouler J, Padgett GA, Cameron PJ, Preuss K, Titirici M-M, Ieropoulos I, Lorenzo MD (2016) Towards effective small scale microbial fuel cells for energy generation from urine. Electrochimica Acta 192:89–98

14. Clauwaert P, Verstraete W (2009) Methanogenesis in membrane less microbial electrolysis cells. Appl Microbiol Biotechnol 82:829–836
15. Cotterill SE, Curtis HT (2016) Microbial electrolysis cells for hydrogen production [chapter]. [book] Microbial electrochemical and fuel cells, pp 287–319. doi:10.1016/B978-1-78242-375-1.00009-5In
16. Coursolle D, Baron DB, Bond DR, Gralnick JA (2010) The Mtr respiratory pathway is essential for reducing flavins and electrodes in Shewanella oneidensis. J Bacteriol 192:467–474
17. Dannys E, Green T, Wettlaufer A, Madhurnathakam CMR, Elkamel A (2016) Wastewater treatment with microbial fuel cells: a design and feasibility study for scale-up in microbreweries. J Bioprocess Biotech 6:1–6
18. De Schamphelaire L et al (2008) Microbial fuel cells generating electricity from rhizodeposits of rice plants. Environ Sci Technol 42:3053–3058
19. De Schamphelaire L et al (2010) Microbial community analysis of anodes from sediment microbial fuel cells powered by rhizodeposits of living rice plants. Appl Environ Microbiol 76:2002–2008
20. Dennis PG, Harnisch F, Yeoh YK, Tyson GW, Rabaey K (2013) Dynamics of cathode-associated microbial communities and metabolite profiles in a glycerol-fed bioelectrochemical system. Appl Environ Microbiol 79:4008–4014
21. Dileep Y, Velvizhi G Venkata, Mohan S (2016) Coupling sequential batch reactor and bioelectrochemical treatment systems for treatment of complex wastewater associated with bioelectricity generation. Renew Energy 98:171–177
22. Du J, Shao Z (2011) Engineering microbial factories for synthesis of value-added products. J Ind Microbiol Biotechnol 38:873–890
23. ElMekawy A, Hanaa Ab, Hegabcde M, Pant D (2014) The near-future integration of microbial desalination cells with reverse osmosis technology. Energy Environ Sci 7:3921
24. Fraiwan A, Choi S (2016) A stackable, two-chambered, paper-based microbial fuel cell. Biosens Bioelectron 15(83):27–32
25. Gil GC, Chang IS, Kim BH, Kim M, Jang JK, Park HS, Kim J (2003) Operational parameters affecting the performance of a mediator-less microbial fuel cell. Biosens Bioelectron 18:327–334
26. Gildemyn S, Verbeeck K, Slabbinck R, Andersen SJ, Prévoteau A, Rabaey K (2015). Integrated production, extraction, and concentration of acetic acid from CO_2 through microbial electrosynthesis. Environ Sci Technol Lett 2:325–328
27. Goud RK, Babu PS, Venkata Mohan S (2011) Canteen based composite food waste as potential anodic fuel for bioelectricity generation in single chambered microbial fuel cell (MFC): bio-electrochemical evaluation under increasing substrate loading condition. Int J Hydrogen Energy 36:6210–6218
28. Heilmann J, Logan BE (2006) Production of electricity from proteins using a microbial fuel cell. Water Environ Res 78:531–537
29. Helder M et al (2010) Concurrent bio-electricity and biomass production in three plant–microbial fuel cells using Spartina anglica, Arundinella anomala and Arundo donax. Bioresour Technol 101:3541–3547
30. Helder M, Strik DPBTB, Hamelers HVM, Buisman CJN (2012a) The flat-plate plant-microbial fuel cell: the effect of a new design on internal resistances. Biotechnol Biofuels 5:70
31. Helder M, Strik DPBTB, Hamelers HVM, Kuijken RCP, Buisman CJN (2012b) New plant-growth medium for increased power output of the plant-microbial fuel cell. Bioresour Technol 104:417–423
32. Huang L, Chai X, Chen G, Logan BE (2011) Effect of set potential on hexavalent chromium reduction and electricity generation from biocathode microbial fuel cells. Environ Sci Technol 45:5025–5031
33. Kaku N et al (2008) Plant/microbe cooperation for electricity generation in a rice paddy field. Appl Microbiol Biotechnol 79:43–49

34. Kim D, An J, Kim B, Jang JK, Kim BH, Chang IS (2012) Scaling-up microbial fuel cells: configuration and potential drop phenomenon at series connection of unit cells in shared anolyte. Chem Sus Chem 5:1086–1091
35. Kim HJ, Park HS, Hyun MS, Chang IS, Kim M, Kim BH (2002) A mediator-less microbial fuel cell using a metal reducing bacterium, shewanella putrefaciens. Enzyme Microb Tech 30 (2):145–152
36. Kiran Kumar A, Reddy MV, Chandrasekhar K, Srikanth S, Venkata Mohan S (2012) Endocrine disruptive estrogens role in electron transfer: bio-electrochemical remediation with microbial mediated electrogenesis. Bioresour Technol 104:547–556
37. Kracke F, Vassilev I, Kromer JO (2015) Microbial electron transportand energy conservation–the foundation for optimizing bioelectrochemical systems. Front Microbiol 6:1–18
38. Krishna KV, Sarkar O, Venkata Mohan S (2014) Bioelectrochemical treatment of paper and pulp wastewater in comparison with anaerobic process: integrating chemical coagulation with simultaneous power production. Bioresour Technol 174:142–151
39. Lefebvre O, Neculita CM, Yue X, Ng HY (2012) Bioelectrochemical treatment of acid mine drainage dominated with iron. J Hazard Mater 241–242:411–417
40. Liu H, Cheng SA, Logan BE (2005) Production of electricity from acetate or butyrate using a single-chamber microbial fuel cell. Environ Sci Technol 39:658–662
41. Lovley DR (2006) Microbial fuel cells: novel microbial physiologies and engineering approaches. Cur. Opin Biotechnol 17:327–332
42. Lowy DA, Tender LM, Zeikus J, Park DH, Lovley DR (2006) Harvesting energy from the marine sediment–water interface II: kinetic activity of anode materials. Biosens Bioelectron 21:2058–2063
43. Min B, Logan BE (2004) Continuous electricity generation from domestic wastewater and organic substrates in a flat plate microbial fuel cell. Environ Sci Technol 38:5809–5814
44. Modestra JA, Navaneeth B, Venkata Mohan S (2015) Bioelectrocatalytic reduction of CO_2: enrichment of homoacetogens and pH optimization towards enhancement of carboxylic acids biosynthesis. J CO_2 Utilization 10:78–87
45. Mohana Krishna G, Venkata Mohan S, Sarma PN (2010) Bio-electrochemical treatment of distillery wastewater in microbial fuel cell facilitating decolorization and desalination along with power generation. J Hazard. Mater 177:487–494
46. Morel A, Zuo KC, Xia Xue, Wei JC, Xi L, Liang P, Huang X (2012) Microbial desalination cells packed with ion-exchange resin to enhance water desalination rate. Bioresour Technol 118:43–48
47. Nancharaiah YV, Venkata Mohan S, Lens PNL (2015) Removal and recovery of metal ions in microbial fuel cells: a review. Bioresour Technol 195:102–114
48. Nancharaiah YV, Venkata Mohan S, Lens PNL (2016) Biological and bioelectrochemical recovery of critical and scarce metals. Trends Biotech 137–155
49. Niessen J, Schroder U, Scholz F (2004) Exploiting complex carbohydrates for microbial electricity generation—a bacterial fuel cell operating on starch. Electrochem Commun 6:955–958
50. Nikhil GN, Venkata Subhash G, Yeruva Dileep Kumar, Venkata Mohan S (2015) Synergistic yield of dual energy forms through biocatalyzed electrofermentation of waste: stoichiometric analysis of electron and carbon distribution. Energy 88:281–291
51. Nikhil GN, Yeruva DK, Venkata Mohan S, Swamy YV (2016) Assessing potential cathodes for resource recovery through wastewater treatment and salinity removal using non-buffered microbial electrochemical systems. Bioresour Technol 215:247–253
52. Rabaey K, Rozendal RA (2010) Microbial electrosynthesis—revisiting the electrical route for microbial production. Nat Rev Microbiol 8:706–716
53. Saeed HM, Husseini GA, Yousef S, Saif J, Al-Asheh Sameer, Abu Fara A, Azzam S, Khawaga R, Aidan A (2015) Microbial desalination cell technology: a review and a case study. Desalination 359:1–13
54. Salvin P, Ondel O, Roos C, Robert F (2014) Energy harvest with mangrove benthic microbial fuel cells 39:543–556

55. Schievano A, Sciarria TP, Vanbroekhoven K, Wever HD, Puig S, Andersen SJ, Rabaey K, Deepak P (2016) Electro-fermentation—merging electrochemistry with fermentation in industrial applications. Trends Biotechnol. 34:866–878
56. Schroder U (2007) Anodic electron transfer mechanisms in microbial fuel cells and their energy efficiency. Phys Chem Chem Phys 9:2619–2629
57. Shantaram A, Beyenal H, Veluchamy RRA, Lewandowski Z (2005) Wireless sensors powered by microbial fuel cell. Environ Sci Technol 39:5037–5042
58. Sharma Y, Li BK (2010) The variation of power generation with organic substrates in single-chamber microbial fuel cells (SCMFCs). Bioresour Technol 2010(101):1844
59. Shi L, Dong M, Reguera G, Beyenal H, Lu A, Liu J, Yu H, Fredrickson JF (2016) Extracellular electron transfer mechanisms between microorganisms and minerals. Nat Rev Microbiol 14:651–662
60. Shijia Wu, Hui Li, Chen X, Zhou Peng, Liang, Zhang X, Jiang Y, Huang X (2016) A novel pilot-scale stacked microbial fuel cell for efficient electricity generation and wastewater treatment. Water Res 98:396–403
61. Sreelatha S, Velvizhi G, Naresh Kumar A, Venkata Mohan S (2016) Functional behaviour and treatment efficiency of bio-electrochemical system with increasing azo dye concentration: synergistic interactions of biocatalyst and electrode assembly. Bioresour Technol 213:11–20
62. Strik DPBTB et al (2008) Green electricity production with livingplants and bacteria in a fuel cell. Int J Energy Res 32:870–876
63. Takanezawa K et al (2010) Factors affecting electric output from ricepaddy microbial fuel cells. Biosci Biotechnol Biochem 74:1271–1273
64. Tandukar M, Huber SJ, Onodera T, Pavlostathis SG (2009) Biological chromium(VI) reduction in the cathode of a microbial fuel cell. Environ Sci Technol 43:8159–8165
65. Timmers RA, Strik DPBTB (2010) Long-term performance of a plant microbial fuel cell with Spartina anglica. Appl Microbiol Biotechnol 86:973–981
66. Velvizhi G, Venkata Mohan S (2011) Biocatalyst behaviour under self-induced electrogenic microenvironment in comparison with anaerobic treatment: evaluation with pharmaceutical wastewater for multi-pollutant removal. Bioresour Technol 102:10784–10793
67. Velvizhi G, Venkata Mohan S (2015) Bioelectrogenic role of anoxic microbial anode in the treatment of chemical wastewater: microbial dynamics with bioelectro-characterization. Water Res 70:52–63
68. Venkata Mohan S, Veer Raghuvulu S, Srikanth S, Sarma PN (2007) Bioelectricity production by meditorless microbial fuel cell (MFC) under acidophilic condition using wastewater as substrate: influence of substrate loading rate. Curr Sci 92:1720–1726
69. Venkata Mohan S, Sarvanan R, Raghuvulu SV, Mohana Krishna G, Sarma PN (2008a) Bioelectricity production from wastewater treatment in dual chambered microbial fuel cell (MFC) using selectively enriched mixed microflora: effect of catholyte. Bioresour Technol 99:596–603
70. Venkata Mohan S, Mohana Krishna G, Sarma PN (2008b) Effect of anodic metabolic function on bioelectricity generation and substrate degradation in single chambered microbial fuel cell. Environ Sci Technol 42:8088–8094
71. Venkata Mohan S, Raghuvulu SV, Sarma PN (2008c) Biochemical evaluation of bioelectricity production process from anaerobic wastewater treatment in a single chambered microbial fuel cell (MFC) employing glass wool membrane. Biosen Bioelectron 23:1326–1332
72. Venkata Mohan S, Lalit Babu V, Sarma PN (2008d) Effect of various pretreatment methods on anaerobic mixed microflora to enhance biohydrogen production utilizing dairy wastewater as substrate. Bioresour Technol 99:59–67
73. Venkata Mohan S, Mohana Krishna G, Reddy BP, Sarvanan R, Sarma PN (2008e) Bioelectricity generation from chemical wastewater treatment in mediatorless (anode) microbial fuel cell (MFC) using selectively enriched hydrogen producing mixed culture under acidophilic microenvironment. Biochem Eng J 39:121–130

74. Venkata Mohan S, Mohana Krishna G, Srikanth S, Sarma PN (2008f) Harnessing of bioelectricity in microbial fuel cell (MFC) employing aerated cathode through anaerobic treatment of chemical wastewater using selectively enriched hydrogen producing mixed consortia. Fuel 87, 2667–2676
75. Venkata Mohan S, Veer Raghuvulu S, Dinakar P, Sarma PN (2009a) Integrated function of microbial fuel cell (MFC) as bio-electrochemical treatment system associated with bioelectricity generation under higher substrate load. Biosens Bioelectron 24:2021–2027
76. Venkata Mohan S, Srikanth S, Raghuvulu SV, Mohanakrishna G, Kumar AK, Sarma PN (2009b) Evaluation of the potential of various aquatic eco-systems in harnessing bioelectricity through benthic fuel cell: effect of electrode assembly and water characteristics. Bioresour Technol. 100:2240–2246
77. Venkata Mohan S, Velvizhi G, Vamshi Krishna K, Lenin Babu M (2014a) Microbial catalyzed electrochemical systems: A bio-factory with multi-facet applications. Bioresour Technol 165:355–364
78. Venkata Mohan S, Velvizhi G, Annie J, Srikanth S (2014b) Microbial fuel cells: Critical factors and Recent advancements. Renew Sustainable Energy Rev 40:779–797
79. Venkata Mohan S, Mohanakrishna G, Chiranjeevi P (2011b) Sustainable power generationfrom floating macrophytes based ecological microenvironment through embedded fuel cellsalong with simultaneous wastewater treatment. Bioresour Technol 102:7036–7042
80. Venkata Mohan S, Srikanth S, Velvizhi G, Lenin Babu M (2013) Microbial fuel cells for sustainable bioenergy generation: principles and perspective applications (Chapter 11). In: Gupta VK, Tuohy MG (eds) Biofuel technologies: recent developments, Springer. ISBN 978-3-642-34518-0
81. Venkata Mohan S, Annie J, Amulya K, Butti SK, Velvizhi G (2016) A circular bioeconomy with biobased products from CO_2 sequestration. J Trends Biotechnol 34:506–519
82. Wang G, Huang L, Zhang Y (2008) Cathodic reduction of hexavalent chromium [Cr(VI)] coupled with electricity generation in microbial fuel cells. Biotechnol Lett 30(11):1959–1966
83. Wang H, Ren ZS (2014) Bioelectrochemical metal recovery from wastewater: a review. Water Res 66:219–232
84. Wei M, Rakoczy J, Vogt C, Harnisch F, Schumann R, Richnow HH (2015) Bioresource technology enhancement and monitoring of pollutant removal in a constructed wetland by microbial electrochemical technology. Bioresour Technol 196:490–499
85. Wetser K, Sudirjo E, Buisman CJN, Strik DPBTB (2015) Electricity generation by a plant microbial fuel cell with an integrated oxygen reducing biocathode. Appl Energy 137:151–157. doi:10.1016/j.apenergy.2014.10.006
86. Wetser K, Liu J, Buisman C, Strik D (2015) Biomass and Bioenergy Plant microbial fuel cell applied in wetlands: spatial, temporal and potential electricity generation of Spartina anglica salt marshes and Phragmites australis peat soils. Biomass Bioenergy 83:543–550
87. Wu S, Li H, Zhou X, Liang P, Zhang X, Jiang Y, Huang X (2016) A novel pilot-scale stacked microbial fuel cell for efficient electricity generation and wastewater treatment. Water Res 98:396–403
88. Xu L, Zhao Y, Doherty L, Hu Y, Hao X (2016) Promoting the bio-cathode formation of a constructed wetland-microbial fuel cell by using powder activated carbon modified alum sludge in anode chamber. Nat Publ Gr 1–9
89. Yuan H, Lu Y, Abu-Reesh IM, He Z (2015a) Bioelectrochemical production of hydrogen in an innovative pressure-retarded osmosis/microbial electrolysis cell system: experiments and modeling. Biotechnol Biofuels 8:116. doi:10.1186/s13068-015-0305-0
90. Yuan H, Abu-Reesh IM, He Z (2015b) Enhancing desalination and wastewater treatment by coupling microbial desalination cells with forward osmosis. Chem Eng J 270:437–443
91. Zachary AS, Dolfing J, Ren ZJ, Xu P (2016) Interplay of anode, cathode, and current in microbial fuel cells: implications for wastewater treatment. Energy Technol 4:583–592
92. Zhang LJ, Tao HC, Wei XY, Lei T, Li JB, Wang AJ, Wuc WJ (2012) Bioelectrochemical recovery of ammonia–copper (II) complexes from wastewater using a dual chamber microbial fuel cell. Chemosphere 89:1177–1182

93. Zhao Z et al (2015) Potential for direct interspecies electron transfer in an electric-anaerobic system to increase methane production from sludge digestion. Sci Rep 5:11094
94. Zhuang L, Zheng Y, Zhou S, Yuan Y, Yuan H, Chen Y (2012) Scalable microbial fuel cell (MFC) stacks for continuous real wastewater treatment. Bioresour Technol 106:82–88

Biomass-Derived HMF Oxidation with Various Oxidants

S. Saravanamurugan, Ashok Pandey and Rajender Singh Sangwan

Abstract This chapter describes the conversion of cellulosic biomass-derived 5-hydroxymethylfurfural (HMF) to various oxidation products, such as 2,5-diformylfuran (DFF), 5-hydroxymethyl-2-furancarboxylic acid (HMFCA), and 5-formyl-2-furancarboxylic acid (FFCA), with solid catalysts containing with and without metal(s) in the presence of various solvents including water. This chapter further describes the influence of various oxidant, such as hydrogen peroxide (H_2O_2) and *tert*-butyl hydroperoxide (*t*-BuOOH), air, and molecular oxygen, on the yield of oxidation products under wide range of reaction conditions. This chapter also focuses the influence of metal nanoparticles on the yield of FDCA with and without addition of organic bases.

1 Introduction

Most chemicals and fuels are today being produced from fossil resources, such as coal, oil and natural gas. It has been forecasted that the availability of fossil resources will steadily be dwindling in coming decades as the world population increase, so it is paramount important to find alternative substitutes that can replace fossil resources to keep the value chain. Lignocellulosic biomass has been identified as one of the indispensable, renewable, sustainable, and alternative feedstock sources of carbon for producing wide spectrum of chemicals and fuels such as 5-hydroxymethylfurfural (HMF), levulinate and lactates [11, 17, 18]. In this context, furanic compounds derived from biomass have great potential to replace fossil based chemicals, for example, 2,5-furandicarboxylic acid (FDCA) has been identified as a suitable substituent for terephthalic acid in the synthesis of polyethylene terephthalate (PET)—precursor for making drinks plastic bottles. In connection with this, this book chapter describes solid-catalysed oxidation of biomass-derived furanic compounds, such as HMF, to FDCA via various intermediates, such as 2,5-diformylfuran (DFF),

S. Saravanamurugan (✉) · A. Pandey · R.S. Sangwan
Center of Innovative and Applied Bioprocessing (CIAB), Mohali 160071, Punjab, India
e-mail: saravana@ciab.res.in

A.K. Agarwal et al. (eds.), *Biofuels*, Green Energy and Technology,
DOI 10.1007/978-981-10-3791-7_4

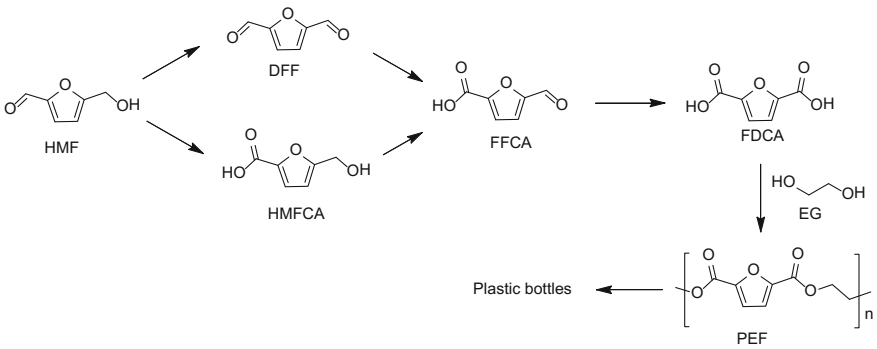

Scheme 1 Oxidation products of HMF to FDCA to polyethylene furanate (PEF)

5-hydroxymethyl-2-furancarboxylic acid (HMFCA), and 5-formyl-2-furancarboxylic acid (FFCA) (Scheme 1) with various solid catalysts due to their relatively high thermal stability, easy recovery and reuse. The influence of H_2O_2/*t*-BuOOH on the yield of DFF, Air on the yield of DFF, FFCA and FDCA, and O_2 on the yield of DFF and FDCA with various heterogeneous solid catalysts, based on articles published over the past few years, are discussed in detail.

2 HMF Oxidation with Peroxides

The peroxides such as hydrogen peroxide (H_2O_2) and *tert*-butyl hydroperoxide (*t*-BuOOH) are known as common oxidant for oxidation of organic compounds. There have been limited number of reports using these peroxides as oxidant for the oxidation of HMF to FDCA via various intermediates as mentioned above and the results are summarised in Table 1. Chen et al. have reported ruthenium complex immobilised on carbon nanotubes (CNT) employed as catalyst for the conversion of HMF to DFF with H_2O_2 and *t*–BuOOH oxidant at 120 °C for 12 h in N, N-dimethylformamide (DMF) as solvent, and the obtained yields of DFF were 32 and 13% with a HMF conversion of 47 and 98%, respectively [9]. It has been claimed that peroxides were too reactive (or quickly decomposed during the reaction) which cleaved the furan ring, resulting in undesired/unwanted products. These observations were in line with other published articles [13, 19, 33, 34]. Similarly, ruthenium nanoparticles supported on N-containing mesoporous polymer (Ru@mPMF) for the oxidation of HMF to DFF in toluene was reported by Kajari et al. in 2016. The yield of DFF was quite low (below 10%) when using 30% H_2O_2 and *t*-BuOOH as oxidant in toluene with Ru@mPMF at 105 °C for 12 h, exhibiting Ru nanoparticles has lower activity than previous mentioned Ru complex on the yield DFF [13].

Table 1 Oxidation of HMF in the presence of peroxides on the yield of DFF with various solid catalysts

Entry	Catalyst	Oxidant	Solvent	HMF conv. (%)	DFF yield (%)	Reaction conditions	Ref.
1	Ru-PVP/CNT	H_2O_2	DMF	47	32	120 °C; 12 h	[9]
		t-BuOOH		98	13		
2.	Ru@mPMF	H_2O_2	Toluene	11	4	105 °C; 12 h	[13]
		t-BuOOH		100	9		
3.	Fe_3O_4/Mn_3O_4	H_2O_2 *t*-BuOOH	DMF	13	5	120 °C; 4 h	[18]
				84	7		
4.	Trimetallic CoCeRu	H_2O_2	MIBK	16.5	5	90 °C; 2 h	[32]
		t-BuOOH		100	7		
5.	Fe_3O_4@SiO_2-NH_2-Ru(III)	H_2O_2	Toluene	8	6	120 °C; 12 h	[33]
		t-BuOOH		100	17	120 °C; 6 h	

Wang et al. studied the oxidation of HMF to DFF with trimetallic catalyst containing Ru, Co, and Ce with peroxides as oxidant at 90 °C for 12 h. In this study, a very low yield of DFF (4%) was obtained along with 18% of FDCA at a quantitative conversion of HMF with $Co_{6.6}Ce_{3.3}Ru_{1.1}$ and *t*-BuOOH as oxygen donor in methyl isobutyl ketone (MIBK) as solvent. When switching the oxidant from *t*-BuOOH to H_2O_2, the yield of DFF (7%) slightly increased, but the yield of FDCA descended from 18 to 8% at a low conversion of HMF (17%) [33]. A similar trend has been observed on the yield of DFF from HMF over Fe_3O_4@SiO_2-NH_2-Ru (III) and with *t*-BuOOH and H_2O_2 at 120 °C in toluene [33]. From these studies one can understand that peroxides are not good oxidant due to their low temperature decomposition and very high reactivity towards HMF oxidation.

Interestingly, Liu et al. reported magnetic Fe_3O_4 supported Mn_3O_4 nanoparticles as catalysts for the transformation of HMF to DFF and FDCA with peroxides as oxygen donor at 120 °C, but gave a very poor yield (<7%) [19]. Montmorillonite K-10 containing molybdenum has also been reported as catalyst for the oxidation of HMF with peroxides at 80 °C for 2 h. It was found that no furanic products such as DFF, HMFCA and FDCA was formed with a quantitative conversion of HMF when using *t*-BuOOH as oxidant. Authors have speculated that the ring opening reaction of HMF could have taken place with highly reactive *t*-BuOOH as mentioned above, leading to formation of no furanics but to unwanted products [35]. Conversely, around 5% of HMFCA with very high selectivity was obtained when the oxidant changed to H_2O_2. The oxidation of HMF with solid acid catalysts in the presence of H_2O_2 to other than furanic compounds has also been reported. The obtained products in this study were 2-oxoglutaric acid (OGA), succinic acid (SA), maleic acid (MA), fumaric acid (FA) and formic acid. Highest yield of OGA and

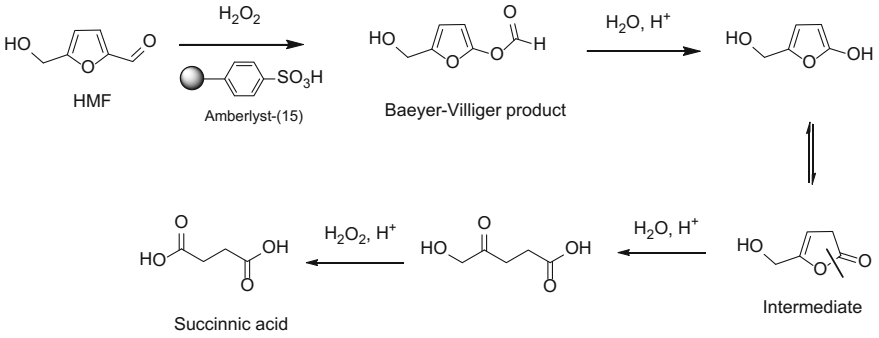

Scheme 2 Proposed reaction pathway for the formation of succinic acid from HMF [10]

SA was found to be 31 and 18%, respectively, apart from formic acid (60%) in water with Amberlyst-15 at 75 °C after 24 h, and the other products found in this study were in trace amounts. It has been proposed that π-π interaction between Amberlyst-15 and HMF took place before forming Baeyer-Villiger product prior to succinic acid formation. The plausible reaction pathway for the formation SA has been proposed by authors as shown in Scheme 2 [10].

3 HMF Oxidation in Air

As the oxidation of HMF with peroxides over various solid catalysts did not give any oxidation products such as DFF, HMFCA, FFCA and FDCA in high yields, there have been many reports for HMF oxidation with air as an alternative green oxidant in various solvents in order to improve the yield of these oxidation products (Table 2).

Saha et al. studied HMF conversion over polymer supported Fe(III) catalyst in water in the presence of air at different pressure ranging from 4 to 10 bar at 100 °C, and it was found to be FDCA was the major product along with minor yields of DFF and FFCA [31]. At 4 bar air, the yield of FDCA was only 14% along with 15 and 12% of DFF and FFCA, respectively, at a conversion of 42% HMF after 5 h. As the pressure increased to 10 bar, the yield of FDCA improved to 53% with a conversion of 80% HMF. FDCA yield further enhanced to 79% from 53% when the reaction time prolonged to 10 h. Pt and Pt–Bi supported on activated carbon were reported to be active catalyst for the transformation of HMF to FDAC. The obtained FDCA yield from HMF was about 70% in water in the presence of $NaHCO_3$ at 100 °C at a high pressure of air (40 bar), with a molar ratio of Pt to HMF 100 [28].

The major intermediate in this study was found to be FFCA, achieving about 80% after 4 h which descended to 30% by converting into FDCA after 24 h. The other intermediates DFF and HMFCA were obtained below 10%. Moreover, the addition of Bi into Pt/C improved the reusability of the catalyst for at least four

Table 2 HMF oxidation in air with various solid catalysts

Entry	Catalyst	Solvent	Conv. HMF (%)	Yield (%)				Reaction conditions	Ref.
				DFF	HMFCA	FFCA	FDCA		
1	Ru/CTF	MTBE	86	64	–	–	Trace	80 °C, 1 h, 20 bar	[5]
2	Bi $(NO_3)_3{\cdot}5H_2O$ and cellulose mediated Cu–NPs.	Acetonitrile	85	82	–	–	–	80 °C, 2 h, atmospheric pressure	[6]
3	Ru@mPMF	Toluene	51	35	–	–	–	105 °C, 12 h, 10 bar	[13]
4	NG-800	Acetonitrile	100	100	–	–	–	100 °C, 3 h, atmospheric pressure	[22, 23]
		Water or methanol	86–88	40–46	–	46–56	–		
5	Pt/C, Pt–Bi/C	Water	0–100	<10	<10	0–80	0–100	100 °C, 0–24 h, 40 bar, inorganic bases	[28]
6	Pt/TiO_2	Water	0–100	0–40	0–12	0–75	0–95	100 °C, 0–12 h, 40 bar, Na_2CO_3, $NaHCO_3$	[29]
7	FeIII–POP-1	Water	42–100	7–15		8–12	4–79	100 °C, 5–10 h; 5–10 bar	[31]
8	Fe_3O_4@SiO_2–NH_2–Ru(III)	Toluene	78–100	68–89	–	–	–	120 °C, 12–16 h, air balloon pressure	[33]
9	$Co_{6.6}Ce_{3.3}Ru_{1.1}$	MIBK	45	38	–	–	5	120 °C, 12 h, atmospheric air	[33]
10	K-10 clay-Mo	Toluene	65–100	–	59–84	–	–	110 °C, 2–8 h, atmospheric air	[35]

runs-maintaining FDCA yields between 90 and 100%, but in the case of Pt/C lost its activity significantly even after third run-FDCA yield dropped from 80% at first run to 30% after third run.

Fe_3O_4@SiO_2-NH_2-Ru(III) was employed as catalysts for HMF conversion in toluene in the presence of air at 120 °C for 12 and 16 h, yielding 68 and 89% of DFF at HMF conversion of 78 and 100%, respectively [34]. The formation of HMFCA and FDCA were not observed in this study under these reaction conditions. Trimetallic catalyst containing Co, Ce and Ru has also been reported for HMF oxidation in MIBK in an atmospheric air pressure at 120 °C for 12, and the obtained yield of DFF and FDCA were 38 and 5%, respectively, with 54% unconverted HMF [33]. Similarly, the HMF oxidation in an atmospheric air with montmorillonite K-10 catalyst containing molybdenum in toluene was also studied by Zhang et al. in [35]. It was reported that 59 and 84% of HMFCA was achieved at 110 °C for 1 and 8 h, with 65% and quantitative conversion of HMF, respectively. No other HMF oxidation furanic intermediates towards FDCA was reported under these reaction conditions [35]. Recently, Lv et al. have also studied the oxidation of HMF to DFF with nitrogen doped graphene (NG) materials in the presence of 2,2,6,6-tetramethylpiperidin-oxyl (TEMPO) as co solvent in an atmospheric air pressure [22, 23]. Gratifyingly, authors found that NG treated at 800 °C (NG-800) gave a quantitative yield of DFF with a quantitative conversion of HMF in acetonitrile at 100 °C after 6 h, due to incorporation of nitrogen into the carbon nanosheets and changing the electronic structure of a sp^2 carbon material and thereby enhancing its activity. They attempted to reuse the catalyst NG-800 and found to be HMF conversion ($\sim$100) and DFF selectivity ($\sim$90) remained unchanged from first through the sixth run. However, authors have reported that when changing solvent from acetonitrile to water and methanol under identical reaction conditions, the selectivity to DFF drastically decrease from 100 to below 50%, concomitantly, the selectivity to FFCA increased to about 50%. In another report, cellulose mediated Cu nanoparticles along with $Bi(NO_3)$. $5H_2O$ were used as catalyst for HMF conversion to DFF in acetonitrile in an atmospheric air at 80 °C for 2 h. The obtained DFF yield was 82% along with 85% HMF conversion [6].

Rass et al. have studied the transformation of HMF over Pt/TiO_2 with and without base $NaHCO_3$ on the yield of FDCA at 100 °C with a pressure of 40 bar air for 12 h [28]. This study clearly indicated that without a base the yield of FDCA was below 10% but DFF and FFCA were the major product, reaching above 30% after 3 h. In order to improve the yield of FDCA at the expense of formed intermediates, authors have introduced 1 to 4 equivalents of $NaHCO_3$ with respect to HMF in the reaction medium and found to be a pronounced effect on the yield of FDCA. The yield of FDCA attained to above 90% after 12 h. The influence of base has also been investigated in this study and reported that addition of Na_2CO_3 favoured the reaction towards the formation of FDCA faster than $NaHCO_3$ under identical reaction conditions. Authors have proposed the reaction pathway for the aqueous oxidation of HMF to FDCA via including various hydrated intermediates as shown in Scheme 3.

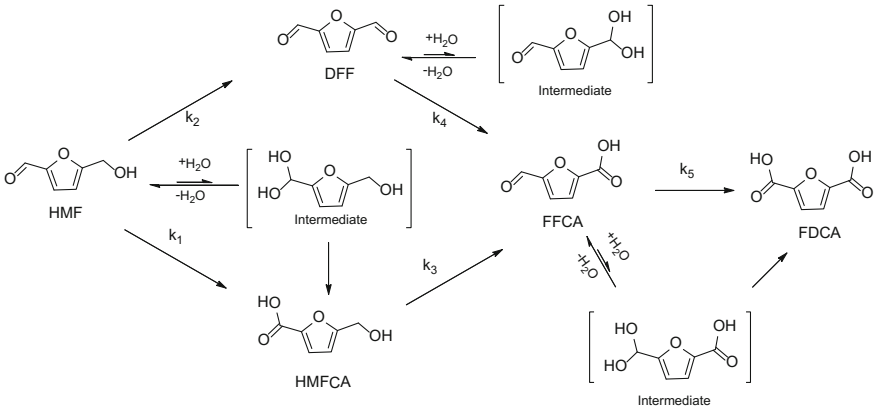

Scheme 3 Reaction pathway for HMF oxidation to FDCA via various intermediates [28]

Artz et al. in [5], comprehensively studied on the yield of DFF from HMF with covalent triazine framework (CTF) supported Ru catalysts (Scheme 4) in various solvents at 80 °C at 20 bar air for 1 h [5]. Among the solvents (toluene, MTBE, 1,4-dioxane, DMSO, H_2O, acetone, and acetonitrile) used, methyl t-butyl ether (MTBE) favoured a highest yield of DFF (44%) at a conversion of 55% HMF. The yield of DFF (10%) was quite low when using DMSO as solvent, claiming that the presence trace amount of water favoured further oxidation to form FDCA. A low selectivity of DFF was also found in this study when using only water as solvent, substantiating the role of water on the formation of FDCA from HMF oxidation. Interestingly, authors have studied the influence of Ru on various supports, such as carbon, alumina, hydrotalcite (HT) and MgO, for HMF oxidation in MTBE at 80 °C at 20 bar air for 1 h and found that CTF showed a superior support than others, yielding 64% DFF over Ru/CTF along with 14% unconverted HMF. Gosh et al. recently reported that ruthenium nanoparticles supported on N-containing mesoporous polymer (Ru@mPMF) could convert HMF to DFF to a moderate selectivity (68%) at a conversion of 51% HMF in toluene at 105 °C at 10 bar air after 12 h [13].

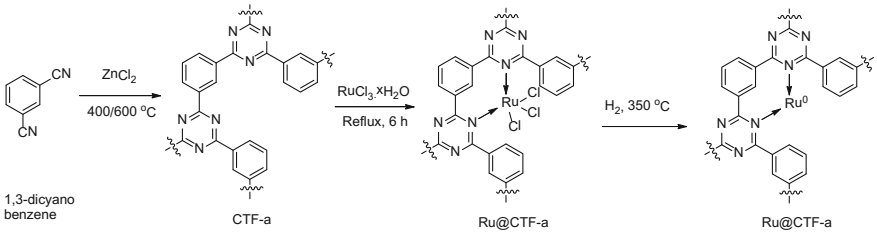

Scheme 4 Proposed synthesis route for stabilisation of Ru nanoparticles in CTF [5]

4 HMF Oxidation in Pure Oxygen

There have been ample numbers of publications dealing with HMF oxidation towards FDCA formation in pure oxygen as it has been considered as green oxidant (Table 3). In this context, Pasini et al. reported Au and Cu supported on TiO_2 as catalysts for HMF oxidation in an oxygen atmosphere in the presence of NaOH as base [27]. Among the catalyst employed, 1.5(AuCu)-TiO_2 (1.14 wt% Au and 0.36 wt% Cu with respect to TiO_2) found to be superior catalytic activity to yield quantitative amount of FDCA in water at 95 °C at 10 bar oxygen pressure after 4 h 30 min, with a ratio of HMF to NaOH $_4$. It has been claimed that aldehyde group of HMF was quite easily oxidised than hydroxyl group to form HMFCA, attaining close to 90% of HMFCA with 1.5(AuCu)-TiO_2after an hour reaction time. In the same year, Gupta et al. reported Au nanoparticle supported on HT as catalyst for the oxidation HMF in water at an atmospheric oxygen pressure without addition of any homogeneous base [15]. In an experiment, a quantitative yield of FDCA from HMF was obtained in water with 1.92 wt% Au/TiO_2 at 95 °C after 7 h, with a ratio of HMF to metal 40 and an oxygen flow rate of 50 ml/min. The size of the Au nanoparticles on HT were found to be an average size of 3.2 nm which were much lower than 2 wt% Au nanoparticles on TiO_2 (6 nm), giving FDCA yield of 31% at 50 °C and 10% at 60 °C, respectively. However, the reaction conditions in both studies were different [15, 27]. A comprehensive study was carried out by Ardemani et al. to get insight to the activity of Au nanoparticles in HT towards HMF oxidation to FDCA [4]. From this study, it has been disclosed that competitive adsorption between HMF and oxidation intermediate, such as HMFCA and FDCA, impeded the active sites on Au/HT, thus disabling further oxidation of HMF. On the other hand, high gold surface concentration on HT without alkali medium can enhance the yield of FDCA from HMF in water. For example, 10 wt% Au/HT yielded 78% FDCA without any soluble base in water at 90 °C under oxygen flow with a rate of 10 ml/min. Below 5 wt% Au/HT gave predominantly HMFCA than FDCA, indicating a high surface concentration of Au required for having higher yield of FDCA. In another study, Gui et al. reported that the role of basicity of the support for Au and Pd nanoparticles for HMF oxidation [14]. The employed supports were zinc hydroxy carbonate (ZOC), hydrotalcite (MG20), TiO_2, CeO_2 and activated carbon and revealed that ZOC possessed a higher basicity than other supports. In an experiment, a quantitative yield of FDCA over Au–Pd/ZOC (Au to Pd ratio was 1:1) was obtained in water in the presence of $NaHCO_3$ at 80 °C at 3 bar O_2 after 4 h, the basicity of ZOC support alone in water was pH = 8.05.

Albonetti et al. reported the influence on the ratio of Au and Cu on TiO_2 for the oxidation of HMF to FDCA, as an extension of their previous studies [1]. Interestingly, they found that introducing Cu into the nanoparticle of Au on TiO_2 seemed to be decreasing the overall particle size (from 4 to 3 nm), estimated by using XRD through Scherrer equation and TEM analysis. It has been found from this study that the ratio of Au to Cu 3 on TiO_2 was optimal to give a higher selectivity

Table 3 HMF oxidation with molecular oxygen over various solid catalysts

Entry	Catalyst	Solvent	HMF conv. (%)	Yield (%)				Reactions conditions	Ref.
				DFF	HMFCA	FFCA	FDCA		
1	10wt% Au/HT	Water	–		20		78	90 °C, O_2 flow	[4]
2	Ru/γ-alumina	Toluene	100	97	–	3	–	120 °C, 4 h, 2.7 bar	[2]
3	V_2O_5/AC	MIBK or Toluene	>95	>96	–	<2	–	100 °C, 4 h, 2.8 bar	[3]
4	1.5wt% Au/HY	Water	>99	–	–	–	>99	60 °C, 6 h, 3 bar O_2, NaOH	[7]
5	Ru–PVP/CNT	DMF	100	94	–	–	–	120 °C, 12 h, 20 bar	[9]
6	Au–Pd/ZOC	Water	>99	–	–	–	>99	80 °C, 4 h, 3 bar, NaHCO3	[14]
7	1.9 wt% Au/HT	Water	100	–	–	–	100	95 °C, 7 h, O_2 flow	[15]
8	Pt/C–O–Mg	Water	>99	–	–	–	97	110 °C, 12 h, 10 bar	[16]
9	Fe_3O_4/Mn_3O_4	DMF	95	80	–	–	10	120 °C, 2 h, O_2 flow	[19]
10	Pd/C@Fe_3O_4	Water	80	98			87	80 °C, 6 h, O_2 flow, K_2CO_3	[20]
11	$Ni_3(BTP)_2$	Water	27	27	–	–	–	120 °C, 24 h, 30 bar	[18]
12	GO	DMSO	100	90	–	8	–	140 °C, 24 h, O_2 flow	[22, 23]
13	$Mn_{0.70}Cu_{0.05}Al_{0.25}$-c	Water	96	89	–	–	6	90°C, 24 h, 12 bar	[25]
14	NNC-900	Water	100	–	–	–	80	80 °C, 48 h, O_2 flow, K_2CO_3	[26]
15	1.5(AuCu)–TiO_2	Water	0–100	–	0–90	–	0–100	60–115 °C, 0–5 h, 5–20 bar, NaOH	[27]
16	Pt/C Pt–Bi/C	Water	100	–	0–10	17–47	44–83	100 °C, 1 h, 40 bar, Na_2CO_3	[27]
17	FeIII–POP-1	Water	100	9	–	5	75	100°C, 5 h 5 bar	[30]

(continued)

Table 3 (continued)

Entry	Catalyst	Solvent	HMF conv. (%)	Yield (%)				Reactions conditions	Ref.
				DFF	HMFCA	FFCA	FDCA		
18	1 wt% V_2O_5/H-beta [24]	DMSO	84	82	–	–	–	125 °C, 3 h, 10 bar	[29]
19	Au-Pd/AC or Au–Pt/AC	Water	100	–	0–38		62–100	60 °C, 2–6 h, 3 bar	[31]
20	K-10 clay-Mo	MIBK	97	–	81	–	–	110 °C, 8 h, O_2 flow	[35]
21	γ-Fe_2O_3@HAP–Pd(0)	Water	97	–	–	–	93	100 °C, 6 h, K_2CO_3	[36]
22	Fe_3O_4@C@Pt	Water	100	–	–	–	100	90 °C, 4 h, O_2 flow, Na_2CO_3	[37]
23	$Co_{6.6}Ce_{3.3}Ru_{1.1}$	MIBK	84–97	72–83	–	–	7–8	120 °C, 12 h, O_2 flow and balloon	[33]
24	Fe_3O_4@SiO_2–NH_2-Ru(III)	Toluene	>99	86	–	–	–	110 °C, 4 h, O_2 flow	[34]

towards FDCA compared to ratio of Au to Cu 1 in water at 95 °C at 10 bar O_2 after 4 h, in the presence of NaOH as base. In a similar approach, Villa et al. reported the modification of Au on activated carbon by introducing Pd and Pt to enhance its catalytic activity towards formation of FDCA from HMF [32]. A quantitative and near quantitative yield of FDCA was achieved in this study with Au_6–Pd_4/AC and Au_8–Pd_2/AC catalysts, respectively, than individual monometallic catalysts (Au/AC and Pd/AC yielded 36 and 8% of FDCA, respectively) in water in the presence of NaOH at 60 °C after 2 h, with a pressure of 3 bar O_2. In another study, it has been reported that changing the metal combination on activated carbon could enhance the activity of the material towards HMF oxidation. In this context, Rass et al. have reported that introducing bismuth into Pt/C to get Pt–Bi/C could reduce the particle size of Pt to 2 nm from 6 nm (Pt/C), particle size estimated by TEM technique. The catalytic activity Pt/C was compared with various ratio of Bi to Pt on C (Pt–Bi/C), ranging from 0 to 0.96. It has been clearly demonstrated that Pt/C yielded 51% of FDCA along with 10 and 35% of HMFCA and FFCA, respectively, with a full conversion of HMF in the presence of Na_2CO_3after 1 h. The FDCA yield significantly improved to 83% at the expense of other formed intermediates over Pi–Bi/C (Pt to Bi ratio 0.2) under identical reaction conditions [28]. Another Pt based catalyst (Pt/C–O–Mg) was also reported and found to be efficient catalyst for the transformation of HMF to FDCA (97%) in water at 110 °C at an oxygen pressure of 10 bar after 12 h. It was further revealed that the other solvents, such as acetonitrile, DMSO, DMF, γ-valerolactone (GVL), 1,4-dioxane, and MIBK, used in this study had no significant effect on the yield of FDCA under identical reaction conditions, highest yield of FDCA was found to be 19% in MIBK, but GVL yielded 35% DFF [16].

Ru/γ-alumina exhibited as promising catalyst for the oxidation of HMF to DFF in high selectivities. Among the solvents employed, a near quantitative yield of DFF was obtained with Ru/γ-alumina in toluene at 120 °C at 2.7 bar O_2 after 4 h. The other organic solvents (DMF, 1,4-dioxane, acetonitrile, ethanol, 1-butanol, isopropanol (IPA), MIBK) used in this study showed either a lower selectivity (DFF) with higher conversion or higher selectivity (DFF) with lower conversion of HMF [2]. Similarly, a high yield of DFF (94%) was achieved with a quantitative conversion of HMF using ruthenium complex immobilised on poly (4-vinylpyridine)-functionalized carbon-nanotube (PVP/CNT), (Ru-PVP/CNT), in DMF at 120 °C at 20 bar O_2 after 12 h [9]. In related to HMF oxidation, various zeolites, such as Beta, ZSM-5, mordenite and Y, have also been used as supports for vanadia for the oxidation of HMF to DFF in different organic solvents, such as N,N-dimethylformamide (DMF), MIBK, toluene, trifluorotoluene and DMSO. The best results obtained in this study was in DMSO as solvent where 98% selectivity towards DFF along with 84% conversion of HMF was observed with 1 wt% V_2O_5/H-beta [25] at 125 °C after 3 h, with an oxygen pressure of 10 bar [30]. However, the major drawback in this study was leaching of vanadia into the solution which partly contributed to the oxidation of HMF to DFF. Cai et al. have reported the synthesis of Au nanoparticle in various supports including zeolites and their catalytic activity towards HMF oxidation. A full conversion to FDCA (>99%) was

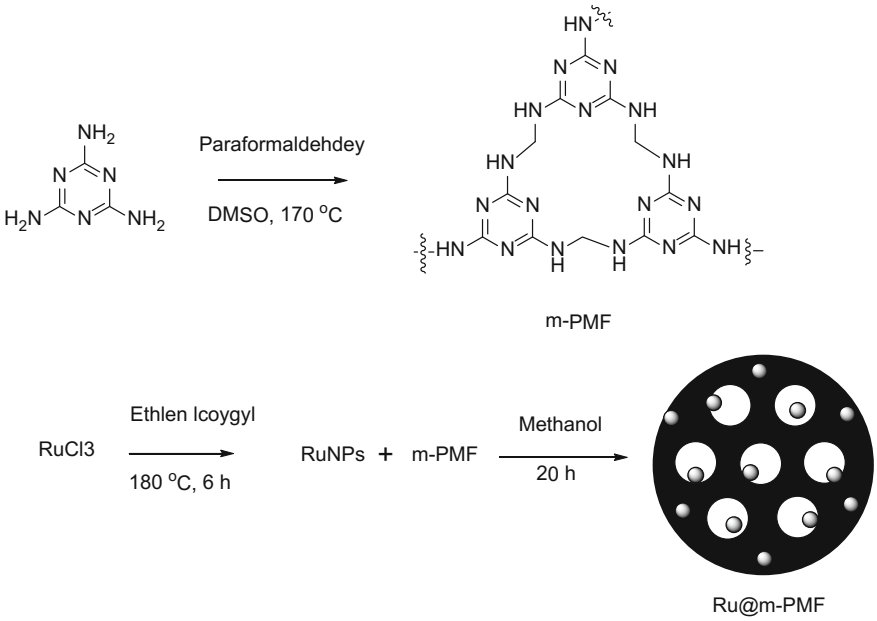

Scheme 5 Schematic representation for synthesis of mesoporous Ru@m-PMF [13]

obtained with 1.5 wt% Au/HY zeolite (average Au nanoparticle size of 1 nm) in water in the presence of NaOH at 60 °C at 3 bar O_2 after 6 h. It has been proposed that small Au nanoparticles were encapsulated in the cages of HY zeolites and claimed that confined Au nanoparticles exhibited a higher catalytic activity than using others supports, such as $Mg(OH)_2$, TiO_2, CeO_2, mordenite, ZSM-5 [7].

Fe(III)–porous organic polymer(FeIII–POP-1) was also examined as catalyst for the transformation of HMF to FDCA in water at 100 °C at 5 bar O_2 for 5 h and found that the obtained FDCA yield was 75% along with 9 and 5% or DFF and FFCA, respectively, with a quantitative conversion of HMF. However, the concentration of HMF was quite low. As the concentration of HMF increased with decreasing FDCA yield but enhancing DFF yield (up to 31%) [31]. In a similar kind of approach, a fair yield of FDCA (85%) at full conversion of HMF was obtained but in toluene with mesoporous poly-melamine-formaldehyde containing Ru nanoparticles (Ru@mPMF) (Scheme 5) at 105 °C with 20 bar of O_2 pressure after 12 h [13].

Wang et al. reported trimetallic mixed metal oxides (Co, Ce and Ru) for the oxidation of HMF to DFF in MIBK solvent under the oxygen flow or oxygen pressure in the balloon. The obtained results were quite interesting that 83% of DFF along with 8% of FDCA was observed at a conversion of 97% HMF at 120 °C under the flow of oxygen (20 ml/min) after 12 h. However, the yield of DFF dropped down to 72% when using oxygen balloon under identical reaction conditions. It has also been shown that this trimetallic mixed oxides can be reused for

four times without significant loss of its activity [33]. The combination of another trimetal mixed oxides (nanocrystalline spinel $Li_2CoMn_3O_8$) as catalyst for HMF oxidation was reported and found to be the obtained isolated yield of FDCA was 80% [8]. Yet another manganese based trimetal mixed oxides was also reported for the conversion of HMF with molecular oxygen, but in this case the major product was DFF rather than FDCA. HMF conversion of 96% with DFF and FDCA selectivity of 93 and 6%, respectively, was obtained over $Mn_{0.70}Cu_{0.05}Al_{0.25}$-c in water at 90 °C at 12 bar O_2 after 24 h [24]. However, a significant yield of HMFCA (22%) was observed at low oxygen pressure (4 bar) under identical reaction conditions. In this context, a bimetallic mixed oxides (Mn and Fe) exhibited as a promising catalysts on the yield of FDCA from HMF. The selectivity towards FDCA and FFCA were 32 and 68%, respectively, with 93% conversion of HMF with Mn0.75/Fe0.25 in water at 90 °C at 8 bar O_2 after 24 h, with a HMF to NaOH ratio of 1:4. However, a quantitative yield of FDCA was attained when using FFCA as substrate under similar reaction conditions [24].

Zhang et al. extended their previous work on HMF oxidation using immobilised molybdenum acetylacetonate in montmorillonite K-10 as catalysts under the flow of oxygen. The activity of this catalyst substantially changed the selectivity towards HMFCA rather than DFF. For example, 81% HMFCA was obtained along with near quantitative conversion of HMF in MIBK with molecular oxygen at 110 °C after 8 h. A similar HMFCA yield was observed with other solvents such as p-chlorotoluene, toluene and trifluortoluene in this study [35].

In 2014, Antonyraj et al. have also reported the transformation of HMF to DFF in MIBK as solvent using vanadia supported on activated carbon as catalyst and found greater than 90% yield of DFF with HMF conversion of about 95% at 100 °C at 2.8 bar O_2. A high selectivity towards DFF (98%) with 95% conversion of HMF in toluene was also obtained at 100 °C at 2.8 bar O_2 after 4 h [3]. On the other hand, a poor yield of DFF (11%) was obtained when using MIBK as solvent and Fe_3O_4/Mn_3O_4 (magnetic separation approach) as catalyst with an oxygen flow rate of 20 ml/min. However, the DFF yield was drastically improved to 80% with 95% conversion of HMF in DMF with Fe_3O_4/Mn_3O_4 at 120 °C after 2 h, clearly indicating solvent played a crucial role [19]. In a similar strategic approach, the same research group synthesised magnetically separable Ru based catalyst (Fe_3O_4@SiO_2-NH_2-Ru(III)) for the conversion of HMF to DFF. A quantitative conversion of HMF with 86% DFF yield was attained with this catalyst in toluene at 110 °C in molecular oxygen with a flow rate of 20 ml/min [34]. In this context, the same group extended further to synthesise γ-Fe_2O_3 supported Pd-based catalyst (γ-Fe_2O_3@HAP-Pd(0)) (Scheme 6) for HMF oxidation. A high yield of FDCA (93%) was achieved with 97% conversion of HMF in water at 100 °C under flow of oxygen (30 ml/min) after 6 h, with a ratio of K_2CO_3 to HMF 0.5 [36]. The study has been extrapolated further by the same research group synthesising magnetically separable Pd/C@Fe_3O_4 as catalyst for the conversion of HMF. The obtained FDCA yield was 87% at a conversion of 98% HMF in water at 80 °C under flow of oxygen (30 ml/min) after 6 h, but in the presence of K_2CO_3 [20]. Yet another study has also been reported related to magnetic separation approach in which authors

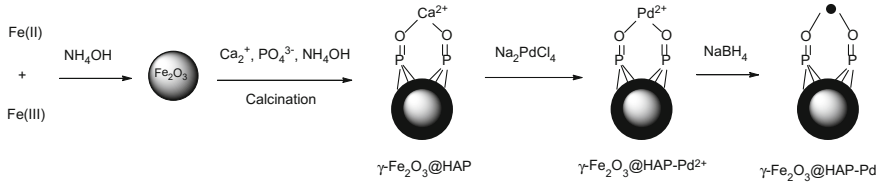

Scheme 6 Pictorial representation of synthesis of magnetically separable γ-Fe_2O_3@HAP–Pd(0) [36]

synthesised Pt nanoparticles on Fe_3O_4@carbon microspheres (Fe_3O_4@C@Pt), employed as catalyst for HMF oxidation and found to be superior activity in terms of FDCA yield (100%) in water in the presence of Na_2CO_3 at 90 °C after 4 h, with an oxygen flow rate of 100 ml/min [37].

Above mentioned articles dealt with metal catalysed oxidation of HMF in various solvents. There have been a very few reports on HMF oxidation with metal free catalytic systems. In connection to this, Lv et al. disclosed a carbon-based (GO) bifunctional material, derived from graphite powder treated with $NaNO_3$, H_2SO_4, H_2O_2, and HCl in a sequence of steps, which did not contain any metal was a promising catalyst for the conversion of HMF to DFF. GO yielded 90% DFF along with 8% FFCA at full conversion of HMF in DMSO at 140 °C at an oxygen flow rate of 20 ml/min after 24 h. Authors also performed an experiment in N_2 atmosphere (20 ml/min) under identical reaction conditions, and no yield of DFF with negligible conversion of HMF was found, substantiating hydroxyl group of HMF was oxidised rather than dehydrogenated [22, 23]. There was another report dealing with metal free zeolitic-imidazole framework (ZIF-8) based, nitrogen-doped nanoporous carbon (NNC) for HMF oxidation. It was found to be NNC-900 gave a highest yield of FDCA (80%) with a full of conversion of HMF in water at 80 °C after 48 h, with three equivalents of K_2CO_3 with respect to HMF and an oxygen flow rate of 100 ml/min [26]. Ni-based metal organic frameworks (MOFs), such as Ni(BDP), Ni(BPEB), and $Ni_3(BTP)_2$, was also reported for the oxidation of HMF and yielded 27% DFF with a selectivity close to 100% in water at 120 °C, at 30 bar O_2 after 24 h [21]. Even though these materials exhibited higher selectivity towards the targeted product, there are some major challenges which limit the implementation of large scale production as follows. Organic moieties adsorbed over these materials during the reaction are difficult to remove by simple wash with aqueous and organic solvents as they strongly bound with the active sites. Moderate thermal stability of these materials further hampers to treat at high temperatures to get rid of the adsorbed organic moieties.

5 Perspective and Outlook

The transformation of HMF to FDCA via oxidation with various oxidants over variety of solid catalysts has been reported. Particularly, a quantitative yield of FDCA was achieved with pure molecular oxygen over Au, Pd and Pt nanoparticle based catalysts. On the other hand, using H_2O_2 of *t*-BuOOH as oxidant for HMF oxidation, Ru nanoparticle based catalysts yielded DFF as a major product. The influence of the size of Au nanoparticles on HT with and without a base on the yield of FDCA well studied and revealed that at high surface Au nanoparticle concentration on HT did not require any base for obtaining a high yield of FDCA. On the contrary, having a low surface concentration of Au nanoparticle did need a base to achieve a high yield of FDCA. In most cases with metal nanoparticles as catalysts, the addition of base entailed as to enhance the yield of FDCA, thus increasing the workup procedure. In general, however, the major problem associated with nobel metal(s) based nanoparticle catalysts are agglomeration and sintering and highly sensitive to fouling, thus preventing the long term activity of the materials, in addition to high cost of precious metals. Therefore, a robust catalyst based on inexpensive metals, including metal nanoparticles, need to be designed for the efficient transformation of HMF to FDCA as well as for economic viability.

The cost of HMF is very expensive today, consequently, the FDCA price is also very high. As to reduce the cost of the process, there has been limited number of studies which focused on the synthesis of FDCA from carbohydrates via cascade reaction. For example, Fang et al. have recently reported sulfonic acid functionalised Fe containing MOF could efficiently dehydrate fructose at quantitative conversion to HMF followed by oxidation to form DFF (>99%) in ethanol at 100 °C [12]. In this context, GO based material possessing bifunctional sites has been reported for the conversion of fructose to DFF where 73% of DFF was obtained in DMSO at 140 °C under flow of oxygen. However, fructose is not an abundant sugar, so the target should be focused on glucose as starting substrate to produce FDCA [21, 22]. On the contrary, this multi-step approach needs a catalyst with various functions; Lewis acid sites for isomerisation of glucose to fructose, Bronsted acid sites for dehydration of fructose to HMF, and metal sites for oxidation of HMF to FDCA. Moreover, from economic point of view, the organic solvents should be replaced with water to enhance the solubility and concentration of starting sugars. Today, the major challenge encountered by researchers is to design such a catalyst and to perform the direct conversion of glucose to FDCA in one-pot multi-step approach. Having such a catalytic system would minimise number of intermediate steps of the process and pave the way towards economically viable to implement the process.

References

1. Albonetti S, Pasinia T, Lolli A et al (2012) Selective oxidation of 5-hydroxymethyl-2-furfural over TiO2-supported gold–copper catalysts prepared from preformed nanoparticles: effect of Au/Cu ratio. Catal Today 195:120–126
2. Antonyraj CA, Jeong J, Kim B et al (2013) Selective oxidation of HMF to DFF using Ru/g-alumina catalyst in moderate boiling solvents toward industrial production. J Ind Eng Chem 19:1056–1059
3. Antonyraj CA, Kim B, Kim Y et al (2014) Heterogeneous selective oxidation of 5-hydroxymethyl-2-furfural (HMF) into 2,5-diformylfuran catalyzed by vanadium supported activated carbon in MIBK, extracting solvent for HMF. Catal Commun 57:64–68
4. Ardimani L, Cibin G, Dent AJ et al (2015) Solid base catalysed 5-HMF oxidation to 2,5-FDCA over Au/hydrotalcites: fact or fiction? Chem Sci 6:4940–4945
5. Artz J, Mallmann S, Palkovits R (2015) Selective aerobic oxidation of HMF to 2,5-diformylfuran on covalent triazine frameworks-supported Ru catalysts. ChemSusChem 8:672–679
6. Baruah D, Hussain FL, Suri M et al (2016) $Bi(NO_3)_3{\cdot}5H_2O$ and cellulose mediated Cu-NPs—a highly efficient and novel catalytic system for aerobic oxidation of alcohols to carbonyls and synthesis of DFF from HMF. Catal Commun 77:9–12
7. Cai J, Ma H, Zhang J et al (2013) Gold nanoclusters confined in a supercage of Y zeolite for aerobic oxidation of HMF under mild conditions. Chem Eur J 19:14215–14223
8. Jain A, Jonnalagadda SC, Ramanujachary KV et al (2015) Selective oxidation of 5-hydroxymethyl-2-furfural to furan-2,5-dicarboxylic acid over spinel mixed metal oxide catalyst. Catal Commun 58:179–182
9. Chen J, Zhong J, Guoa Y et al (2015) Ruthenium complex immobilized on poly (4-vinylpyridine)-functionalized carbon-nanotube for selective aerobic oxidation of 5-hydroxymethylfurfural to 2,5-diformylfuran. RSC Adv 5:5933–5940
10. Choudhary H, Nishimura S, Ebitani K (2013) Metal-free oxidative synthesis of succinic acid from biomass-derived furan compounds using a solid acid catalyst with hydrogen peroxide. Appl Catal A: Gen 458:55–62
11. Corma A, Iborra S, Velty A (2007) Chemical routes for the transformation of biomass into chemicals. Chem Rev 107:2411–2502
12. Fang R, Luque R, Li Y (2016) Efficient one-pot fructose to DFF conversion using sulfonated magnetically separable MOF-derived Fe_3O_4 (111) catalysts. Green Chem. doi:10.1039/c6gc02018f
13. Ghosh K, Mollaa RA, Iqubalb MA et al (2016) Ruthenium nanoparticles supported on N-containing mesoporous polymer catalyzed aerobic oxidation of biomass- derived5-hydroxymethylfurfural (HMF) to 2,5-diformylfuran (DFF). Appl Catal A: Gen 520:44–52
14. Gui Z, Cao W, Saravanamurugan S et al (2016) Efficient Aerobic oxidation of 5-hydroxymethylfurfural in aqueous media with Au–Pd supported on Zinc hydroxycarbonate. ChemCatChem 8:3636–3643
15. Gupta NK, Nishimura S, Takagaki A et al (2011) Hydrotalcite-supported gold-nanoparticle-catalyzed highly efficient base-free aqueous oxidation of 5-hydroxymethylfurfural into 2,5-furandicarboxylic acid under atmospheric oxygen pressure. Green Chem 13:824–827
16. Han X, Geng L, Guo Y et al (2016) Base-free aerobic oxidation of 5-hydroxymethylfurfural to 2,5-furandicarboxylic acid over a Pt/C–O–Mg catalyst. Green Chem 18:1597–1604
17. Holm MS, Saravanamurugan S, Taarning E (2010) Conversion of sugars to lactic acid derivatives using heterogeneous zeotype catalysts. Science 328:602–605
18. Li H, Yang S, Riisager et al (2016) Zeolite and zeotype-catalysed transformations of biofuranic compounds. Green Chem. 18:5701–5735.
19. Liu B, Zhang Z, Lv K (2014) Efficient aerobic oxidation of biomass-derived 5-hydroxymethylfurfural to 2,5-diformylfuran catalyzed by magnetic nanoparticle supported manganese oxide. Appl Catal A: Gen 472:64–71

20. Liu B, Ren Y, Zhang Z (2015) Aerobic oxidation of 5-hydroxymethylfurfural into 2,5-furandicarboxylic acid in water under mild conditions. Green Chem 17:1610–1617
21. Lucarelli C, Galli S, Maspero A et al (2016) Adsorbent—adsorbate interactions in the oxidation of HMF catalyzed by Ni-based MOFs: A DRIFT and FT-IR insight. J Phys Chem C 120:15310–15321
22. Lv G, Wang H, Yang Y et al (2016) Aerobic selective oxidation of 5-hydroxymethylfurfural over nitrogen-doped graphene materials with 2,2,6,6-tetramethylpiperidin-oxyl as cocatalyst. Catal Sci Technol 6:2377–2386
23. Lv G, Wang H, Yang Y et al (2016) Direct synthesis of 2,5-diformylfuran from fructose with graphene oxide as a bifunctional and metal-free catalyst. Green Chem 18:2302–2307
24. Neatu F, Marin RS, Florea M et al (2016) Selective oxidation of 5-hydroxymethyl furfural over non-precious metal heterogeneous catalysts. Appl Catal B: Environ 180:751–757
25. Neatua F, Petreab N, Petreb R et al (2016) Oxidation of 5-hydroxymethyl furfural to 2,5-diformylfuran inaqueous media over heterogeneous manganese based catalysts. Catal Today 278:66–73. doi:10.1016/j.cattod.2016.03.031
26. Nguyen CV, Liao YT, Kang TC et al (2016) A metal-free, high nitrogen-doped nanoporous graphitic carbon catalyst for an effective aerobic HMF-to-FDCA conversion. Green Chem 18:5957–5961. doi:10.1039/c6gc02118b
27. Pasini T, Piccinini M, Blosi M et al (2011) Selective oxidation of 5-hydroxymethyl-2-furfural using supported gold–copper nanoparticles. Green Chem 13:2091–2099
28. Rass HA, Essayem N, Besson M (2013) Selective aqueous phase oxidation of 5-hydroxymethylfurfural to 2,5-furandicarboxylic acid over Pt/C catalysts: influence of the base and effect of bismuth promotion. Green Chem 15:2240–2251
29. Rass HA, Essayem N, Besson M (2015) Selective aerobic oxidation of 5-HMF into 2,5-furandicarboxylic acid with Pt catalysts supported on TiO_2- and ZrO_2- based supports. ChemSusChem 8:1206–1217
30. Sadaba I, Gorbanev YY, Kegnæs S et al (2013) Catalytic performance of zeolite-supported vanadia in the aerobic oxidation of 5-hydroxymethylfurfural to 2,5-diformylfuran. ChemCatChem 5:284–293
31. Saha B, Gupta D, Abu-Omar MM et al (2013) Porphyrin-based porous organic polymer-supported iron(III) catalyst for efficient aerobic oxidation of 5-hydroxymethyl-furfural into 2,5-furandicarboxylic acid. J Catal 299:316–320
32. Villa A, Schiavoni M, Campisi S et al (2013) Pd-modified Au on carbon as an effective and durable catalyst for the direct oxidation of HMF to 2,5-furandicarboxylic acid. ChemSusChem 6:609–612
33. Wang Y, Liu B, Huang K et al (2014) Aerobic oxidation of biomass-derived 5-(hydroxymethyl) furfural into 2,5-Diformylfuran catalyzed by the trimetallic mixed oxide (Co–Ce–Ru). Ind Eng Chem Res 53:1313–1319
34. Wang S, Zhang Z, Liu B et al (2014) Environmentally friendly oxidation of biomass derived5-hydroxymethylfurfural into 2,5-diformylfuran catalyzed by magnetic separation of ruthenium catalyst. Ind Eng Chem Res 53:5820–5827
35. Zhang Z, Liu B, Lv K et al (2014) Aerobic oxidation of biomass derived 5-hydroxymethylfurfural into 5-hydroxymethyl-2-furancarboxylic acid catalysed by a montmorillonite K-10 clay immobilized molybdenum acetylacetonate complex. Green Chem 16:2762–2770
36. Zhang Z, Zhen J, Liu B et al (2015) Selective aerobic oxidation of the biomass-derived precursor 5-hydroxymethylfurfural to 2,5-furandicarboxylic acid under mild conditions over a magnetic palladium nanocatalyst. Green Chem 17:1308–1317
37. Zhang Y, Xue Z, Wang J et al (2016) Controlled deposition of Pt nanoparticles on Fe_3O_4@carbon microspheres for efficient oxidation of 5-hydroxymethylfurfural. RSC Adv 6:51229–51237

Hydrothermal Liquefaction of Lignocellulosic Biomass Components: Effect of Alkaline Catalyst

Rawel Singh, Bhavya B. Krishna and Thallada Bhaskar

Abstract The fundamental studies to understand the role of individual biomass components (cellulose and lignin) on the production of valuable hydrocarbons during hydrothermal liquefaction (HTL) is presented. Thermal and catalytic HTL of cellulose and lignin was performed at 280 °C under biomass:H_2O ratio of 1:6 at 15 min residence time. The use of alkaline catalysts significantly increased both bio-oil yield and conversion for cellulose as well as lignin. Maximum bio-oil yield (28%) and conversion (90%) in case of cellulose was observed with KOH. Similarly in case of lignin maximum bio-oil yield (17 wt%) as well as conversion (72%) was observed with KOH. From the analysis of bio-oil and bio-residue, it was observed both cellulose and lignin have undergone hydrolytic cleavage during HTL to form low molecular weight liquid products. The FTIR and NMR (^{1}H and ^{13}C) of the bio-oil obtained from lignin indicated the presence of phenols and aromatic ethers.

Keywords Cellulose · Lignin · Lignocellulosic biomass · Hydrothermal liquefaction · Subcritical water

1 Introduction

Compared to petroleum feedstocks, biomass contains significant functionality that can be exploited for its conversion to fuels and chemicals by different thermochemical and biochemical routes. Second generation biofuels produced from lignocellulosic biomass is not competing with the food chain. Lignocellulose is a composite material with three biopolymers such as cellulose, hemicelluloses and lignin. Starting feedstock for petroleum refinery is the liquid crude oil whereas in

R. Singh
A. S. College, Samrala Road, Khanna 141402, India

B.B. Krishna · T. Bhaskar (✉)
Thermo-Catalytic Processes Area, Bio-Fuels Division (BFD),
CSIR-Indian Institute of Petroleum (IIP), Dehradun 248005, India
e-mail: tbhaskar@iip.res.in; thalladab@yahoo.com

A.K. Agarwal et al. (eds.), *Biofuels*, Green Energy and Technology,
DOI 10.1007/978-981-10-3791-7_5

case of biorefinery starting material is solid biomass. In order to make biorefinery equivalent to existing and well established petroleum refinery, the first step is to effectively convert the solid biomass to liquid bio-crude thereby converting the whole biomass to liquid products. In order to achieve this, thermochemical methods like pyrolysis and hydrothermal liquefaction (HTL) seems to have a great potential to produce liquid hydrocarbons from biomass. HTL is a process for obtaining fuels/chemicals from biomass in the presence of a sub/supercritical solvent at moderate to high temperature (250–350 °C) and pressure (5–25 MPa). Compared to pyrolysis better quality bio-oil is obtained by HTL. Subcritical water possesses unique properties of high ion product (Kw) and a low dielectric constant and can act as both acid and base catalyst [20].

The major reaction paths of cellulose in subcritical and supercritical water were found to be hydrolysis, retro-aldol condensation, keto-enol tautomerism, and dehydration [3, 5, 7–11]. It was observed using a diamond anvil cell that cellulose swell or dissolved in high-temperature and high-pressure water using in situ observation of its phase behaviour [16]. Microcrystalline cellulose conversion in subcritical and supercritical water was conducted at temperatures between 290 and 400 °C in a continuous-flow-type micro reactor. The main products of the microcrystalline cellulose conversion were hydrolysis products, aqueous degradation products of glucose (fructose, erythrose, glycolaldehyde, glyceraldehyde, 5-HMF, etc.), and undetected aqueous products that were probably organic acids (e.g., acetic acid and formic acid) [17]. Effect of subcritical water on structural changes in microcrystalline cellulose was studied and it was observed that crystallinity remained practically unchanged throughout the treatment, whereas the size of the remaining cellulose crystallites increased. Microcrystalline cellulose underwent significant depolymerisation in subcritical water and cellulose gets dissolved in subcritical water after extensive depolymerisation [25]. The primary liquid products from cellulose hydrolysis contain glucose oligomers and their derivatives with a wide range of degrees of polymerization. The primary hydrolysis reactions on the surface of reacting cellulose particles seem to proceed via the breaking of hydrogen bonds in the structure of microcrystalline cellulose and the random cleavage of the accessible glycosidic bonds in the cellulose and degradation reactions also occur randomly on the surface of cellulose particles, but to a much lesser extent, in comparison to the primary hydrolysis reactions [32]. The behaviour of cellulose in high temperature and high pressure water was studied and it was found that crystalline cellulose was transformed to an amorphous state in high temperature and high pressure water followed by complete dissolution [2]. Hydrothermal liquefaction of cellulose at different pH of 3, 7 and 14 was conducted at temperatures of 275–320 °C with reaction residence times of 0–30 min [31]. 5-Hydroxymethylfurfural (HMF) was main product obtained under acidic and neutral conditions, whereas the main compounds became $C_{2–5}$ carboxylic acids under alkaline conditions. For bio-oil yields, it was observed that high temperatures and long residence times had negative effects, regardless of the pH levels [31].

Hydrothermal liquefaction of alkaline lignin was studied and bio-oil was mainly composed of phenolics. Hydrothermal decomposition of lignin followed mainly

three steps: hydrolysis and cleavage of the ether bond and the C–C bond, demethoxylation, and alkylation [12]. Hydrothermal oxidative degradation of lignin using 0.1% hydrogen peroxide solution in the flow reactor at 150–200 °C was studied to produce organic acids such as formic, acetic, and succinic acids. In case of alkali lignin total yield of organic acids was obtained after oxidation for 2 min at 200 °C and was 0.45 g/g-lignin. When organosolv lignin was oxidized at 160 °C, lignin was depolymerised into the oligomer of MW = ca. 300 and the total yield of organic acids was 0.20 g/g-lignin [6]. Hydrothermal liquefaction of lignin to substituted phenols and aromatic ethers was performed using methanol and ethanol at various temperatures (200, 250 and 280 °C) and residence times of 15, 30 and 45 min where maximum liquid product yield of 85% was observed [19].

In order to understand and select the conditions for hydrothermal liquefaction of whole biomass, it is essential to understand the hydrothermal liquefaction of cellulose and lignin. The fundamental studies to understand the role of individual biomass components (cellulose and lignin) on the production of valuable hydrocarbons during hydrothermal liquefaction (HTL) is presented in this manuscript. Hydrothermal liquefaction of cellulose and lignin was carried out under thermal as well as catalytic conditions to understand the product distribution and nature of products formed.

2 Materials and Experimental Procedures

2.1 Materials

Micro crystalline cellulose has been purchased from Sigma-Aldrich (CAS No: 9004-34-6) and dealkaline lignin and has been procured from TCI (Lot No. REA6C). Carbon, hydrogen, nitrogen and sulfur content in lignin were found to be 45.69, 5.21, 0, 4.48% respectively. Total organic carbon in lignin was 44.79%. Calorific value of lignin was 17.92 MJ Kg^{-1}. ICP analysis of de-alkaline lignin is shown in Table 1. Na amount was very high in lignin compared to other elements.

2.2 Apparatus and Experimental Procedure

Hydrothermal liquefaction experiments of cellulose and lignin were conducted in a 500 ml high pressure autoclave (Autoclave Engineers) at 280 °C, 15 min residence time, 1:6 H_2O:biomass ratio and alkaline catalysts (KOH) under N_2. Hydrothermal liquefaction of cellulose was also carried out in presence of CO_2. The detailed

Table 1 ICP analysis of de-alkaline lignin

Element	Ca	Si	Cu	Cr	Ni	Pb	Al	Mn	Na	K	Mg	Fe	Co
Lignin, ppm	380	120	15	3	3	<1	30	15	40,305	278	994	85	<1

experimental procedure can be found in our earlier papers [18, 21]. Ether soluble fraction after extraction from aqueous phase was weighed and designated as bio-oil1. After extraction, the remaining water phase contained the water-soluble oxygenated hydrocarbons. Solid products were extracted with acetone in a Soxhlet extraction apparatus until the solvent in the thimble became colorless. After removal of the acetone under reduced pressure in a rotary evaporator, this fraction was weighed and designated as bio-oil2. Acetone insoluble fraction was dried at 80 °C then weighed, called as bio-residue.

2.3 Analysis of Feed and Reaction Products

Cellulose, lignin and reaction products obtained after the hydrothermal liquefaction were analyzed by thermo gravimetric analysis, powder XRD, SEM and FTIR. The bio-oil samples were analyzed using FTIR and NMR (^{1}H NMR, ^{13}C NMR). Powder XRD patterns were collected on a Bruker D8 advance X-ray diffractometer fitted with a Lynx eye high-speed strip detector and a Cu Kα radiation source. Diffraction patterns in the 2°–80° region are recorded with a 0.04 step size (step time = 4 s). SEM images have been collected on a FEI Quanta 200 F, using tungsten filament doped with lanthanum hexaboride (LaB_6) as an X-ray source, fitted with an ETD (Everhart Thornley Detector), which preferentially work as a secondary electron detector. The sample for SEM has been subjected to disperse on a carbon paper coated adhesive followed by gold coating. TG-DTG of cellulose and lignin was carried out on Shimadzu DTG-60 under N_2 flow of 100 ml min^{-1} at heating rate of 10 °C min^{-1}. The ^{13}C NMR and ^{1}H NMR spectra of the bio-oil samples have been recorded in the Bruker avance 500 plus instrument. $CDCl_3$ has been used as a solvent. The FTIR spectra were recorded on a Nicolet 8700 FTIR spectrometer. The trace metal analysis of feedstock was carried out using DRE, PS-3000 UV, Leeman Labs Inc., Inductively Coupled Plasma-Atomic Emission Spectroscopy. The gross calorific value of the feed has been found out using the Parr 6300 Bomb Calorimeter. The ultimate analysis has been carried out using Elementar vario micro cube unit. TOC analysis of lignin was performed using Shimadzu TOC-L unit with solid sample module SSM-5000A.

3 Results and Discussions

3.1 Properties of Feedstock

3.1.1 Cellulose

TG/DTG of cellulose shows a single decomposition peak in DTG around 341 °C. There was around 90% weight loss in cellulose with temperature up to 400 °C.

FTIR spectrum of cellulose showed broad band of the CH, CH_2 stretching at 2900 cm^{-1} and the CH_2 shearing at 1400 cm^{-1}. The band at 3400 cm^{-1} was identified as corresponding to OH. The peak at 1200 cm^{-1} corresponds to C–O–C stretching. The peak around 1040 cm^{-1} corresponds to C–O stretching. The peak at 899 cm^{-1} corresponds to ring CH_2 rocking.

Lignin

Powder XRD of lignin showed the amorphous nature of de-alkaline lignin. Some sharp peaks were also observed that might be due to the presence of some inorganic compounds in lignin as ICP analysis showed the presence of some inorganic elements in lignin. TG/DTG of de-alkaline lignin showed around 80% weight loss in lignin up to 900 °C. The decomposition pattern of lignin was complex. There were two major decomposition peaks at around 350 and 750 °C. TG/DTG profile of lignin showed that it decomposed in a wider temperature range from 200–800°C. FTIR spectra of de-alkaline (Fig. 3) lignin shows absorbance peak at 1037 cm^{-1} which is due to the C–O stretching vibrations. The peak at 1212 cm^{-1} is due to the C–C and C–O stretching vibrations. The peak at 1426 cm^{-1} is due to the C–H in plane deformation. C–H stretching vibrations in lignin are observed at 2934 cm^{-1}. Peak at 3422 cm^{-1} is due to O–H stretching vibrations and shows the presence of phenolic hydroxyl groups. Peak at 1597 cm^{-1} corresponds to C–C stretch in aromatics. The peak at 1710 cm^{-1} shows presence of C = O groups in lignin. Aromatic ring vibrations are observed at 1513 cm^{-1} [28].

3.2 *Product Distribution from Hydrothermal Liquefaction of Cellulose and Lignin*

Hydrothermal liquefaction (HTL) of cellulose and lignin under non catalytic and catalytic conditions (KOH) was studied to understand the product distribution under different conditions. Non catalytic HTL studies of cellulose were done under nitrogen as well as CO_2 environment to study the effect of gaseous environment on the product distribution and nature of the products. Product distribution from HTL of cellulose and lignin is shown in Table 2.

In case of HTL of cellulose using N_2 at 280 °C, bio-oil1 yield was 6 wt% and bio-oil2 yield was 6 wt%. The total bio-oil yield was 12 wt%. The gas yield was 6 wt%. The yield of bio-residue obtained was 32 wt% and conversion was 68%. The others in the Table 2 corresponds to water soluble oxygenated hydrocarbons and their yield observed was 50 wt%. When reaction was carried out in CO_2 environment bio-oil1 yield observed was 5 wt% and bio-oil2 yield observed was 7 wt%. The total bio-oil yield observed was 12 wt%. Gas yield observed was 8 wt%. The bio-residue yield observed was 31 wt% and conversion was 69%. The yield of

Table 2 Effect of various reaction conditions on hydrothermal liquefaction of cellulose and lignin at 280 °C for 15 min

Feed	Conversion[a] (%)	Bio-oil1[b] (wt%)	Bio-oil2[c] (wt%)	Total oil (wt%)	Gas[d] (wt%)	Residue[e] (wt%)	Others[f] (wt%)
Cellulose, H_2O	68	6	6	12	6	32	50
Cellulose, KOH	90	17	11	28	11	10	51
Cellulose, H_2O, CO_2	69	5	7	12	8	31	49
Lignin, H_2O	66	2	8	10	8	34	48
Lignin, KOH	72	14	3	17	6	28	49

[a]See Appendix Eq. 1
[b]See Appendix Eq. 2
[c]See Appendix Eq. 3
[d]See Appendix Eq. 4
[e]See Appendix Eq. 5
[f]See Appendix Eq. 6

water soluble oxygenated hydrocarbons (others) was 49 wt%. From above data it was observed that the use of CO_2 have a negligible effect on the product distribution of the reaction products. When HTL of cellulose was carried out using KOH bio-oil1 yield observed was 17 wt% and bio-oil2 yield observed was 11 wt%. The total bio-oil yield observed was 28 wt%. Gas yield observed was 11 wt%. The bio-residue yield observed was 10 wt% and conversion was 90%. Use of the catalyst (KOH) significantly increased the conversion and product yields. The conversion was increased to 90% with the use of catalyst from 68% in case of non catalytic studies. The total bio-oil yield was also increased from 12 to 27% using the catalyst. Both the bio-oil1 and bio-oil2 yield gets increased with the use of the catalyst.

In case of HTL of de-alkaline lignin at 280 °C without any catalyst, bio-oil1 yield was 2 wt% and bio-oil2 yield was 8 wt%. The total bio-oil yield was 10 wt%. The gas yield was 8 wt%. The yield of bio-residue obtained was 34 wt% and conversion was 66%. The others' yield observed was 48 wt%. When HTL of de-alkaline lignin was carried out using KOH, bio-oil1 yield observed was 14 wt% and bio-oil2 yield observed was 3 wt%. The total bio-oil yield observed was 17 wt %. Gas yield observed was 6 wt%. The bio-residue yield observed was 28 wt% and conversion was 72%. Here also use of alkaline catalyst increased the conversion as well as liquid products yield similar to cellulose. There was significant increase of the bio-oil1 yield with the use of the catalyst. Gas yield was almost constant under both catalytic as well as non catalytic case.

Use of the alkali based catalyst increased the conversion as well as liquid products yield in case of lignin as well as cellulose. This shows that the catalyst will also be helpful in increasing the conversion and liquid product yield in case of lignocellulosic biomass as whole and same was observed in our earlier reports [18, 21, 22].

The addition of alkali positively influences hydrothermal liquefaction by accelerating the water gas shift and increases liquid yields [14, 27, 29]. Alkaline catalysts also raise the pH and inhibits dehydration of the biomass monomers. Oxygen removal in form of dehydration instead of decarboxylation might result in unsaturated compounds which have tendency to polymerize to char and tar and use of alkali catalysts suppress char and tar formation [26].

3.3 Analysis of Reaction Products

3.3.1 Analysis of Liquid Products

Cellulose

FTIR spectra of bio-oil1 obtained from cellulose under different reaction conditions showed various peaks at 3357, 3964, 1711, 1513, 1451, 1200, 1078 cm^{-1} etc. were observed in all the bio-oil1 obtained under all conditions. FTIR of bio-oil1 obtained under different conditions was similar but intensity of some peaks varies. Peak at around 3300 cm^{-1} were assigned to the O–H of alcohols. The peak was observed at 3344, 3312, and 3357 cm^{-1} in case of liquefaction using H_2O (N_2), H_2O (CO_2), and KOH respectively. Peak at around 2970 cm^{-1} observed in bio-oil1 is assigned to C–H stretch of alkanes. Peak around 1700 cm^{-1} is due to the C = O stretch that may be due to presence of aldehydes or ketone groups in bio-oil1. Peaks from 1350 to 1470 cm^{-1} are assigned to the C–H rocking and C–H bending vibrations in alkanes. Peaks from 1000–1320 cm^{-1} are assigned to the C–O stretch of alcohols, ethers, carboxylic acids, esters etc. Peaks from 910–950 cm^{-1} may be due to O–H bending vibrations of carboxylic acids. FTIR of bio-oil2 also showed similar peaks but the intensity of peaks varies.

^{1}H and ^{13}C NMR of bio-oil1 obtained from hydrothermal liquefaction of cellulose using KOH is shown in Figs. 1 and 2 respectively.

^{1}H NMR spectra have been used to get information regarding the various types of protons present in the bio-oil. The most downfield region 0.5–1.5 ppm corresponds to the protons present in short chain aliphatics attached to carbon atoms which are at least 2 bonds away from C=C or heteroatom. The next region from 1.5 to 3.0 ppm corresponds to protons on aliphatic carbon atoms which are bonded to C=C either aromatic or olefinic or are two bonds away from a heteroatom. The next region 3.0–4.4 ppm corresponds to protons that are attached to carbon atoms next to an aliphatic alcohol. The range 6.0–8.5 ppm represents the aromatic region of the spectrum. It encompasses the protons in benzenoid molecules and heteroaromatics [15].

Bio-oil1 obtained from hydrothermal liquefaction of cellulose using KOH showed high proton percentage in aliphatic region from 0.5–3.0 ppm. Proton percentage in the region from 0.5–1.5 ppm was 28% and in the region from 1.5–3.0 ppm was 39%. Proton percentage in the region from 3.0–4.5 ppm was 12%.

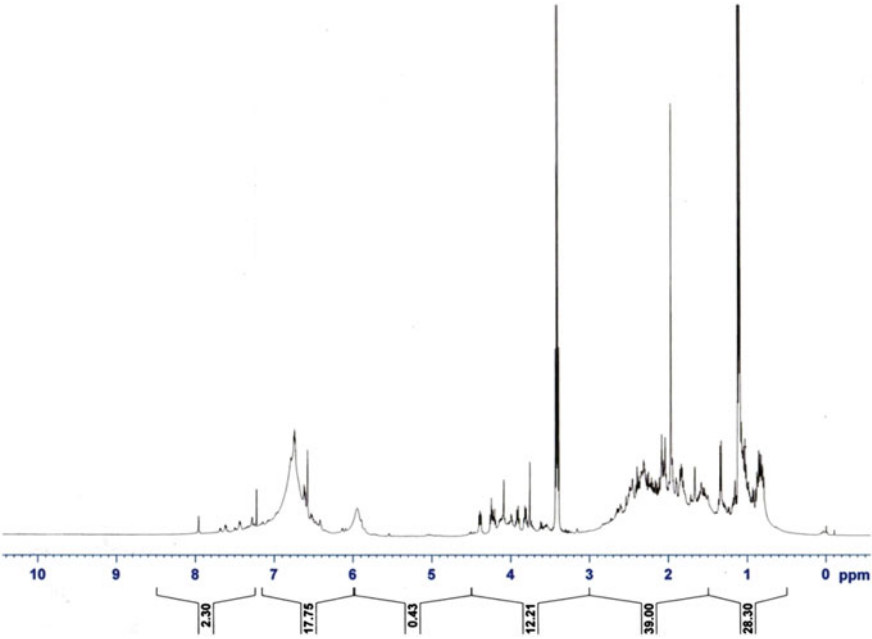

Fig. 1 ^{1}H NMR of bio-oil1 obtained from HTL of cellulose using KOH

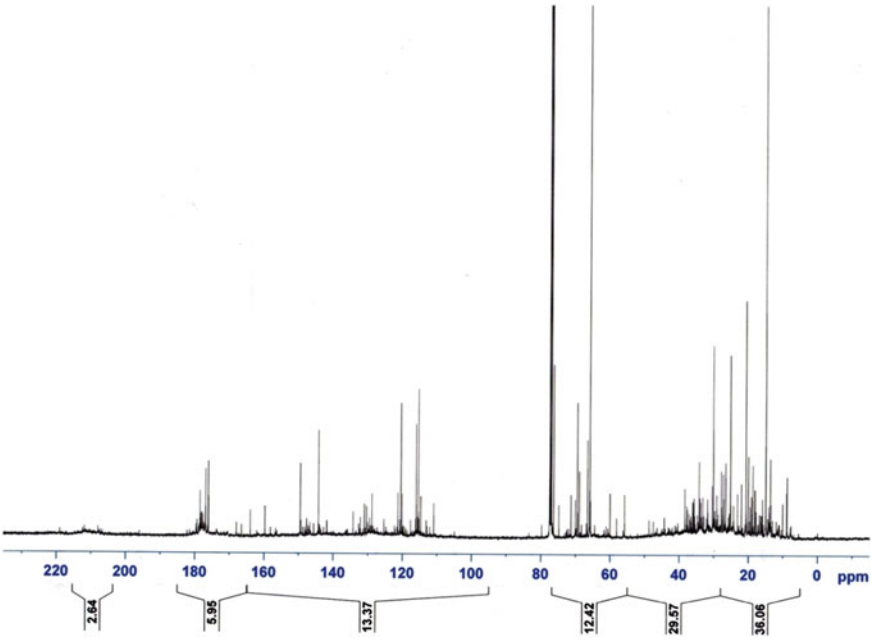

Fig. 2 ^{13}C NMR of bio-oil1 obtained from HTL of cellulose using KOH

Proton percentage in the region from 6.0–8.5 were also observed (20%) that might be due to the heteroaromatics like furan derived compounds, furfural or hydroxymethylfurfural etc. ^{13}C NMR of bio-oil1 pointed to a high aliphatic content (0–55 ppm) similar to ^{1}H NMR that also showed high aliphatic proton percentage. Carbon percentage in region from 0–55 ppm was 66%. The next region of the spectrum is from 55–95 ppm which indicates the presence of alcohol, ethers, and carbohydrate sugars. Carbon percentage in this region was 12%. The aromatics and the olefinic compounds resonate in downfield region and resonate in the region between 95–165 ppm. The carbon percentage in this region was 13%. The region between 165–180 ppm corresponds to the esters and carboxylic acid carbons and carbon percentage in this region was 6%. Further downfield region between 180–215 ppm corresponds to the ketones and aldehydes carbons. Carbon percentage was around 3% in this region. Peaks corresponding to aldehydes, ketones and carboxylic acids were also observed in FTIR of bio-oil. FTIR and NMR of bio-oil indicate that cellulose was decomposed to various aliphatic alcohols, furans, aldehydes, carbohydrate sugars and acids etc.

Lignin

FTIR spectra of bio-oil1 and bio-oil2 obtained after hydrothermal liquefaction of de-alkaline lignin using water at 280 °C is shown in Fig. 3.

It was clear from the figure that bio-oil1 and bio-oil2 has more functionality than de-alkaline lignin indicating that lignin depolymerisation has occurred. The FTIR spectrum of bio-oil1 and bio-oil2 showed absorbance at 1110, 1121, 1215, 1224,

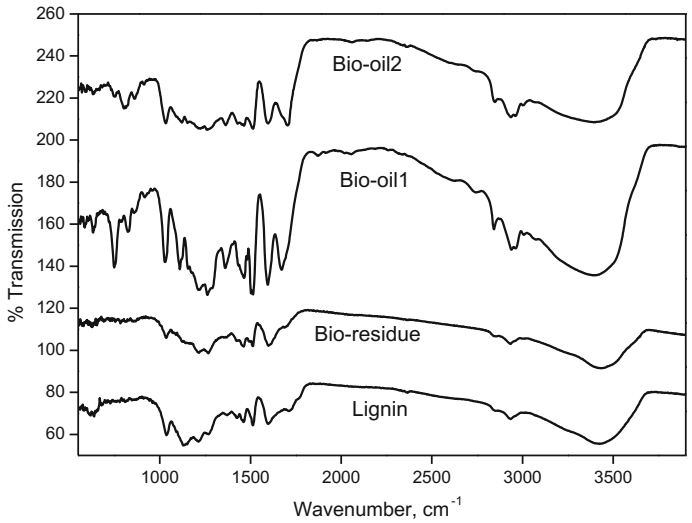

Fig. 3 FTIR analysis of lignin, bio-residue, bio-oil1 and bio-oil2 obtained at 280 °C

1465, 1513, 1595, 1706, and 2934 cm^{-1}. The absorbances at 2847, 2936, 2962 and 1460 cm^{-1} is attributed to C–H stretching vibrations of methyl and methylene and absorbance of these peaks increased in liquid samples and indicates the presence of alkane groups in liquid products. The absorbance at 3007 cm^{-1} in io-oil1 and 3003 cm^{-1} in bio-oil2 corresponds to the C–H stretch of aromatics. The increased absorption peak at 1700 cm^{-1} in bio-oil2 suggests the presence of conjugated aromatic ketones or esters. The absorbances at 1513 and 160 cm^{-1} corresponds to aryl groups and is present in both bio-oil1 and bio-oil2. The peaks around 1220 and 3400 cm^{-1} indicate the presence of phenols which was present in both bio-oil1 as well as bio-oil2. The peak was observed at 1110 Cm^{-1} in bio-oil1 and 1120 cm^{-1} in bio-oil2 belongs to methoxy groups. The peak at 826 cm^{-1} in bio-oil1 indicates the presence of para-substituted aromatic groups [30]. The FTIR spectra of bio-oil1 and bio-oil2 obtained from the hydrothermal liquefaction of lignin using water was almost similar and indicates the presence of phenols and aromatic ethers. Bio-oil1 and bio-oil2 obtained from hydrothermal liquefaction of lignin using water as solvents have same functionality.

NMR spectra provided complementary functional group information to FTIR spectra and enabled to quantify and compare integration areas between spectra. ^{1}H NMR of bio-oil1 obtained after hydrothermal liquefaction of lignin using water is shown in Fig. 4.

The region from 0.5–3.0 is composed of protons on aliphatic carbon. Bio-oil2 obtained from hydrothermal liquefaction of lignin showed high proton percentage

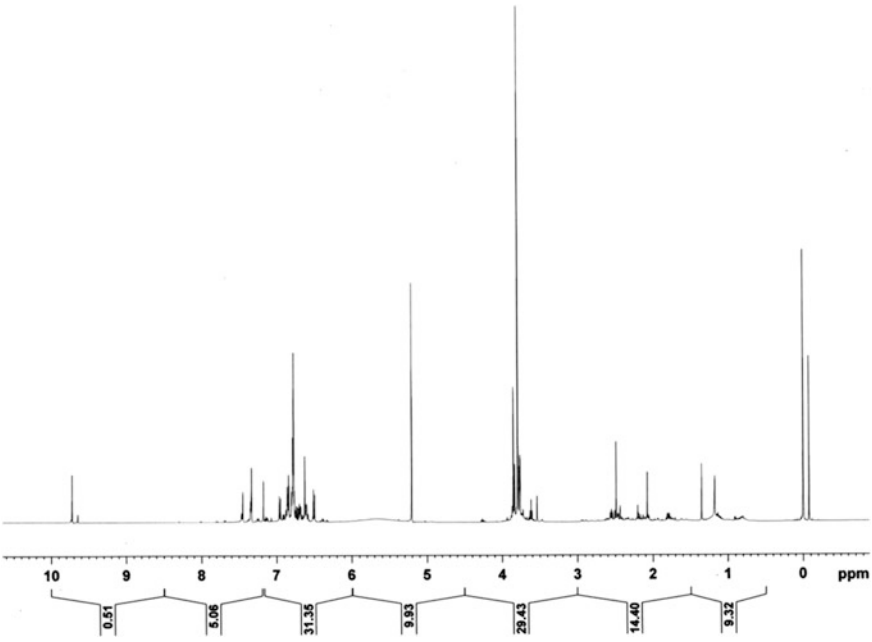

Fig. 4 ^{1}H NMR of bio-oil1 obtained from HTL of de-alkaline lignin using H_2O

in this region. Proton percentage in region from 0.5–3.0 ppm was 14% in case of bio-oil1 whereas it was 65% in case of bio-oil2. The next portion of the ^{1}H NMR spectrum, 3.0–4.5 ppm represents methoxyl protons [13] or methylene group that joins two aromatic rings [15]. Bio-oil1 showed high proton percentage (29%) in this region compared to bio-oil2 (20%). The region between 4.5–6.6 ppm represents aromatic ether protons i.e. lignin derived methoxy phenols. Bio-oil1 (10%) showed high proton percentage in this region than bio-oil2 (1%) The region of the spectrum between 6.0–8.5 ppm corresponds to the aromatic region of spectrum. Both bio-oil1 and bio-oil2 showed significant proton percentage in this region. Proton percentage in this region was 38% in bio-oil1 and 15% in bio-oil2. The downfield spectrum regions (8.5–10 ppm) of the bio-oils arise from the aldehydes and the proton percentage was very low in this region less than 1%.

^{13}C NMR of bio-oil1 is shown in Fig. 5. ^{13}C NMR of bio-oil2 (35%) pointed to a high aliphatic content (0–55 ppm) than bio-oil1 (23%) similar to ^{1}H NMR that also showed high aliphatic proton percentage in bio-oil2 than bio-oil1. The next region of the spectrum is from 55–95 ppm which indicates the presence of alcohol ethers, phenolic methoxys and carbohydrate sugars. Carbon percentage in this region was 7 and 6% in case of bio-oil2 and bio-oil1 respectively. The aromatics and the olefinic compounds resonate in downfield region and resonate in the region between 95–165 ppm. The carbon percentage in this region was very high for both bio-oil1 and bio-oil2. Carbon percentage in this region was 69 and 55% in case of bio-oil1 and bio-oil2 respectively. The region between 165–180 ppm corresponds to the esters and carboxylic acid carbons. Further downfield region between 180–215 ppm corresponds to the ketones and aldehydes carbons. Carbon percentage was around 3% in this region.

The FTIR and NMR (^{1}H and ^{13}C) of the bio-oil1 and bio-oil2 indicated the presence of substituted phenols and aromatic ethers present in bio-oil. This indicated that lignin was depolymerised to low molecular weight phenols and aromatic ethers during hydrothermal liquefaction using water. Similar results were also observed when lignin was depolymerised using methanol and ethanol [19]. The formation of substituted phenols and aromatic ethers may be due to the breakage of various C–C and C–O–C ether bonds (β–O–4 or/and α–O–4) present in lignin. In the hydrothermal liquefaction of lignin, hydrolysis and cleavage of the ether bond and the C–C bond, demethoxylation, alkylation and condensation reactions occur [1, 12]. The aromatic rings are generally not affected by hydrothermal reactions [1] indicating that phenolic monomers could be obtained by preliminary cleavage of ether bond and aliphatic C–C bond in a mild condition of relatively low temperature and short reaction time. Phenolic monomers were also observed during HTL of different lignocellulosic compounds presented in our earlier manuscripts that have been formed by hydrolytic cleavage of lignin in them [23, 24].

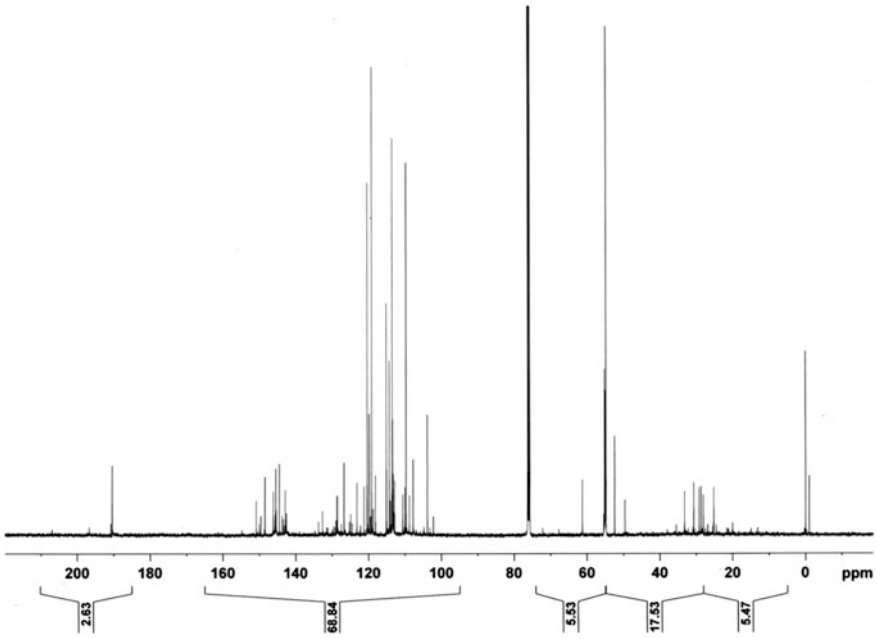

Fig. 5 ^{13}C NMR of bio-oil1 obtained from HTL of de-alkaline lignin using H_2O

3.3.2 Analysis of Bio-Residue

Cellulose

FTIR spectrum of cellulose and bio-residue showed that absorbance peak of the OH stretching vibration (around 3400 cm^{-1}) which corresponds to the hydrogen bonded OH groups in intramolecular and intermolecular cellulose, respectively, decreases in bio-residue sample compared to cellulose. This shows that cellulose has undergone hydrolytic cleavage during HTL.

SEM of cellulose and bio-residue obtained after HTL of cellulose is shown in Fig. 6. SEM showed that under HTL reaction conditions the fibrous structure of cellulose was broken and spherical particles are observed in bio-residue. The fibrous network starts to be disrupted at several points leading to the formation of nano/micro-sized cellulose fragments, which, not being soluble in water, adopt a spherical shape to minimize their contacting interface with the surroundings [4].

Lignin

FTIR spectra of pure lignin and bio-residue obtained after hydrothermal liquefaction of lignin using water at 280 °C is shown in Fig. 3. The absorbances from the

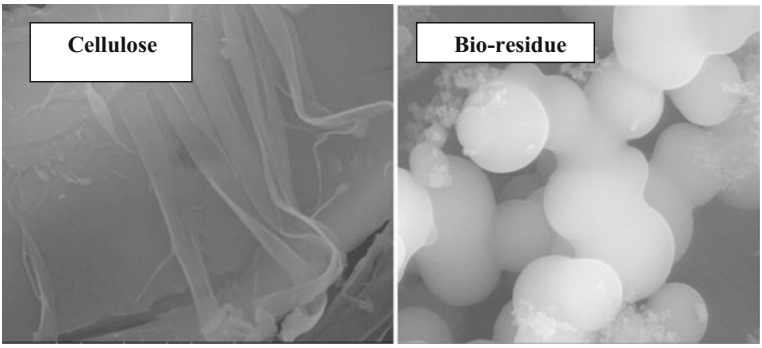

Fig. 6 SEM of cellulose and bio-residue obtained using water at 280 °C

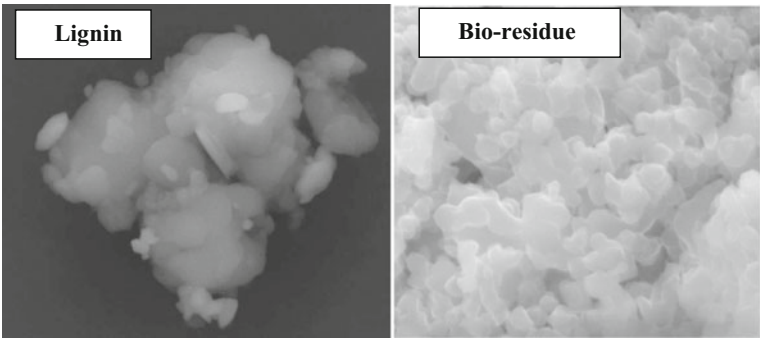

Fig. 7 SEM of lignin and bio-residue

ether bond C–O–C at 1130 and 1037 cm^{-1} weaken in intensity for bio-residue compared to lignin. Peak at 1130 cm^{-1} was not observed in bio-residue. This is possible due to the breakage of β–O–4 and/or α–O–4 ether bonds to form hydroxyl groups and alkyl groups. The weakening of these absorbance peaks in bio-residue samples indicate that the breakage of β–O–4 and/or α–O–4 ether bonds to form hydroxyl groups and alkyl groups have occurred at 280 °C using water [30]. SEM of lignin and bio-residue obtained is shown in Fig. 7. Similar to SEM of cellulose SEM of lignin also showed the formation of spherical particles but the formation was not as good as in cellulose.

4 Conclusions

Thermal and catalytic HTL of cellulose and lignin was performed at 280 °C under biomass:H_2O ratio of 1:6 at 15 min residence time. The use of alkaline catalysts significantly increased both bio-oil yield and conversion for cellulose as well as

lignin. Maximum bio-oil yield (28%) and conversion (90%) in case of cellulose was observed with KOH. Similarly in case of lignin maximum bio-oil yield (17 wt%) as well as conversion (72%) was observed with KOH. Use of the alkali based catalyst increased the conversion as well as liquid products yield in case of lignin as well as cellulose indicating that alkaline catalyst will also be helpful in increasing the conversion and liquid product yield in case of lignocellulosic biomass as whole. From the analysis of bio-oil and bio-residue, it was clear that both cellulose and lignin have undergone hydrolytic cleavage during HTL to form low molecular weight liquid products. The FTIR and NMR (^{1}H and ^{13}C) of the bio-oil1 and bio-oil2 obtained from lignin indicated the presence of phenols and aromatic ethers present in bio-oil.

Acknowledgements The authors thank the Director, CSIR-Indian Institute of Petroleum, Dehradun, for his constant encouragement and support. The authors thank CSIR in the form of XII Five Year Plan project (CSC0116/BioEn) for providing financial support. The authors thank the Analytical Science Division (ASD) of CSIR-IIP for product characterization.

Appendix

$$Converion(\%) = \frac{W_{feed} - W_{residue}}{W_{feed}} \times 100 \tag{1}$$

$$Bio - oil1\ Yeild(wt.\%) = \frac{W_{ether\ soluble}}{W_{feed}} \times 100 \tag{2}$$

$$Bio - oil2\ Yeild(wt.\%) = \frac{W_{acetone\ soluble}}{W_{feed}} \times 100 \tag{3}$$

$$Gas\ Yield(wt.\%) = \frac{w_{(vessel+feed+water)before\ HTU} - w_{(vessel+feed+water)after\ HTU}}{Amount\ of\ feed\ taken\ (g) + Amount\ of\ water\ added\ (g)} \times 100 \tag{4}$$

$$Solid\ residure\ Yield\ (wt.\%) = \frac{w_{solid\ residue}}{w_{feed}} \times 100 \tag{5}$$

$$Other\ Yield(wt.\%) = 100 - (bio - oil1 + bio - oil2 + solid\ residue + gas)Yield \tag{6}$$

W_{feed} is the weight of feed; $W_{residue}$ is the weight of bio-residue; $W_{ether\ soluble}$ is the weight of ether soluble hydrocarbons (bio-oil1); $W_{acetone\ soluble}$ is the weight of acetone soluble hydrocarbons (bio-oil2). Others correspond to the water soluble hydrocarbons and some loses.

References

1. Barbier J, Charon N, Dupassieux N, Loppinet-Serani A, Mahe L, Ponthus J et al (2012) Hydrothermal conversion of lignin compounds. A detailed study of fragmentation and condensation reaction pathways. Biomass Bioenergy 46:479–491
2. Deguchi S, Tsujiib K, Horikoshi K (2008) Crystalline-to-amorphous transformation of cellulose in hot and compressed water and its implications for hydrothermal conversion. Green Chem 10:191–196
3. Ehara K, Saka S (2002) A comparative study on chemical conversion of cellulose between the batch-type and flow-type systems in supercritical water. Cellulose 9:301–311
4. Falco C, Baccile N, Titirici MM (2011) Morphological and structural differences between glucose, cellulose and lignocellulosic biomass derived hydrothermal carbons. Green Chem 13:3273–3281
5. Goto K, Tajima K, Sasaki M, Adschiri T, Arai K (2001) Reaction mechanism of sugar derivatives in subcritical and supercritical water. Kobunshi Ronbunshu 58:685
6. Hasegawa I, Inoue Y, Muranaka Y, Yasukawa T, Mae K (2011) Selective production of organic acids and depolymerization of lignin by hydrothermal oxidation with diluted hydrogen peroxide. Energy Fuels 25:791–796
7. Kabyemela BM, Adschiri T, Malaluan RM, Arai K (1997) Kinetics of glucose epimerization and decomposition in subcritical and supercritical water. Ind Eng Chem Res 36:1552–1558
8. Kabyemela BM, Adschiri T, Malaluan RM, Arai K (1997) Degradation kinetics of dihydroxyacetone and glyceraldehyde in subcritical and supercritical water. Ind Eng Chem Res 36:2025–2030
9. Kabyemela BM, Adschiri T, Malaluan RM, Arai K, Ohzeki H (1997) Rapid and selective conversion of glucose to erythrose in supercritical water. Ind Eng Chem Res 36:5063–5067
10. Kabyemela BM, Takigawa M, Adschiri T, Malauan RM, Arai K (1998) Mechanism and kinetics of cellulose decomposition in sub and supercritical water. Ind Eng Chem Res 37:357–361
11. Kabyemela BM, Adschiri T, Malaluan RM, Arai K (1999) Glucose and fructose decomposition in subcritical and supercritical water: detailed reaction pathway, mechanisms, and kinetics. Ind Eng Chem Res 38:2888–2895
12. Kang S, Li B, Chang J, Fan J (2011) Antioxidant abilities comparison of lignins with their hydrothermal liquefaction products. Bioresources 6:243–252
13. Kosa M, Ben H, Theliander H, Ragauskas AJ (2011) Pyrolysis oils from CO_2 precipitated Kraft lignin. Green Chem 13:3196–3202
14. Mok WSL, Antal MJ, Varhegyi G (1992) Productive and parasitic pathways in dilute acid-catalyzed hydrolysis of cellulose. Ind Eng Chem Res 31:94–100
15. Mullen CA, Strahan GD, Boateng AA (2009) Characterization of various fast-pyrolysis bio-oils by NMR spectroscopy. Energy Fuel 23:2707–2718
16. Sasaki M, Fang Z, Fukushima Y, Adschiri T, Arai K (2000) Dissolution and hydrolysis of cellulose in sub- and supercritical water. Ind Eng Chem Res 39:2883–2890
17. Sasaki M, Adschiri T, Arai K (2004) Kinetics of cellulose conversion at 25 mpa in sub- and supercritical water. AIChE J 50:192–202
18. Singh R, Bhaskar T, Dora S, Balagurumurthy B (2013) Catalytic hydrothermal upgradation of wheat husk. Bioresour Technol 149:446–451
19. Singh R, Prakash A, Dhiman SK, Balagurumurthy B, Arora AK, Puri SK et al (2014) Hydrothermal conversion of lignin to substituted phenols and aromatic ethers. Bioresour Technol 165:319–322
20. Singh R, Prakash A, Balagurumurthy B, Bhaskar T (2015a) Hydrothermal liquefaction of biomass. In: Pandey A, Bhaskar T, Stöcker M, Sukumaran R (eds) Advances in thermochemical conversion of biomass, Elsevier, pp 269–291

21. Singh R, Prakash A, Balagurumurthy B, Singh R, Saran S, Bhaskar T (2015) Hydrothermal liquefaction of agricultural and forest biomass residue: comparative study. J Mater Cycles Waste Manage 17:442–452
22. Singh R, Balagurumurthy B, Prakash A, Bhaskar T (2015) Catalytic hydrothermal liquefaction of water hyacinth. Bioresour Technol 178:157–165
23. Singh R, Chaudhary K, Biswas B, Balagurumurthy B, Bhaskar T (2015) Hydrothermal liquefaction of rice straw: effect of reaction environment. J Supercrit Fluids 104:70–75
24. Singh R, Srivastava V, Chaudhary K, Gupta P, Prakash A, Balagurumurthy B (2015) Conversion of rice straw to monomeric phenols under supercritical methanol and ethanol. Bioresour Technol 188:280–286
25. Tolonen LK, Zuckerstatter G, Penttila PA, Milacher W, Habicht W, Serimaa R, Kruse A, Sixta H (2011) Structural changes in microcrystalline cellulose in subcritical water treatment. Biomacromolecules 12:2544–2551
26. Toor SS, Rosendahl L, Rudolf A (2011) Hydrothermal liquefaction of biomass: a review of subcritical water technologies. Energy 36:2328–2342
27. Watanabe M, Aizawa Y, Iida T, Aida TM, Levy C, Sue K et al (2005) Glucose reactions with acid and base catalysts in hot compressed water at 473 K. Carbohydr Res 340:1925–1930
28. Xu F, Yu J, Tesso T, Dowell F, Wang D (2013) Qualitative and quantitative analysis of lignocellulosic biomass using infrared techniques: a mini-review. Appl Energy 104:801–809
29. Yang BY, Montgomery R (1996) Alkaline degradation of glucose: effect of initial concentration of reactants. Carbohydr Res 280:27–45
30. Ye Y, Zhang Y, Fan J, Chang J (2012) Novel method for production of phenolics by combining lignin extraction with lignin depolymerization in aqueous ethanol. Ind Eng Chem Res 51:103–110
31. Yin S, Tan Z (2012) Hydrothermal liquefaction of cellulose to bio-oil under acidic, neutral and alkaline conditions. Appl Energy 92:234–239
32. Yu Y, Wu H (2010) Understanding the primary liquid products of cellulose hydrolysis in hot-compressed water at various reaction temperatures. Energy Fuels 24:1963–1971

Pretreatment Strategies of Lignocellulosic Biomass Towards Ethanol Yield: Case Study of Pine Needles

Sangeeta Negi

Abstract Today one of the most challenging and noticeable problem is how to supply the vast quantities of energy, fuels and chemicals when oil, gas and coal are depleting exponentially with increase in population. In current scenario lignocellulosic bioethanol seems promising alternative sources of energy and chemicals which is considered a cleaner/or green source also. Lignocellulose, is composed of mainly by three components namely cellulose, hemicelluloses and lignin. However cellulose and hemicellulose are protected by lignin layer, due to which they are not accessible to hydrolytic enzymes and efficiency of the bioethanol production also influenced by crystallinity of cellulose, lignin content, water content and surface area etc. Pretreatment technologies in practice show shortfalls and inefficiency in making cellulose and hemicelluloses free for hydrolysis and also to crack the crystallinity of cellulose. Basically selection of efficient pretreatment process depends on the biomass composition, process economics and environmental impact, therefore in search of an efficient and eco-friendly pretreatment technologies, in current chapter, pretreatment of Pine needles (PN) was carried out by using various methods in combination, such as surfactant assisted acid pretreatment (SAAP), surfactant assisted alkali pretreatment (SABP) and sequential dilute alkali and acid pretreatment (SDAPP) and during pretreatment sugar released (sugar loss) was found to be 0.211, 0.146 and 0.198 g/g, respectively. After pretreatment on enzymatic saccharification of SAAP, SABP and SDAPP liquor, reducing sugar yield was found to be enhanced up to 0.588, 0.477 and 0.582 g/g, respectively under optimized conditions. The PN without pretreatment had released 0.144 g/g of reducing sugar which implied that SDAAP had enhanced the saccharification up to 4 fold. On comparisons of all these pretreatment strategies, sequential acid and alkali pretreatment was found more advantageous in terms of lesser sugar loss and high ethanol yield. However inhibitors generated during pretreatment have to be removed with some potential resins such as Amberlite XAD-4.

S. Negi (✉)
Department of Biotechnology, Motilal Nehru National Institute of Technology, Allahabad 211004, Uttar Pradesh, India

A.K. Agarwal et al. (eds.), *Biofuels*, Green Energy and Technology,
DOI 10.1007/978-981-10-3791-7_6

1 Introduction

As the world population is growing with exponential rate, the existing fossil fuel stock will not be enough to cope up with future energy needs. The continuous consumption of fossil fuels will not only create the energy starvation in the future but it is also harming the environment by enormous emission of green house gases [1, 2]. Therefore, in view of these energy scarcity and environment related issues, the prima facie solution lies in the search of the cost effective alternate green fuel i.e. Bioethanol [3, 4].

Till date, various sugars, starchy substances and lignocelluloses have been explored for the bioethanol production but they have not been found economically viable because of the demand vs. supply economics [4]. The first generation biomasses used for bioethanol production were mostly food grains, which has always generated the food vs. fuel debates. Infact, it doesn't require any debate to conclude that food need always finds predominance over the fuel need. Therefore, there is need of exploration of the readily available non-food based lignocellulosic feedstock, which actually determines the economic feasibility of the lignocellulosic ethanol production [3, 5].

Although, Indian economy is mainly based on agriculture, and India is among the top producers of various crops, still the utilization of food grains for the ethanol production is almost unthinkable when a vast portion of its populations live in poverty. Hence, various nonfood based lignocellulosic biomass, such as Pine needles, Sorghum Stover, Corn Stover, Cotton waste etc., are being explored for the cost effective ethanol production.

1.1 The Roadmap of the Lignocellulosic Biomass to Ethanol Production

The roadmap of the lignocellulosic biomass to ethanol production consists of following steps (Fig. 1):

(i) **Pretreatment of biomass**: In this the biomass is subjected to the deconstruction of the complex network of lignin-cellulose-Hemicellulose. Pretreatment process may involve physical, chemical or biological methods. Physical methods are milling, grinding, extrusion, and irradiation (gamma rays, electron beam, ultrasounds, microwaves); chemical methods include acid, alkali, *ammonia*, organosolve etc.; whereas in biological pretreatment wide range of microorganism have been explored to crack the complex cell wall structure to make cellulose and hemicelluloses accessible for saccharification process.

Although, lots of efforts have been put to make these processes more sustainable, cost effective and echo-friendly, still various drawbacks of the

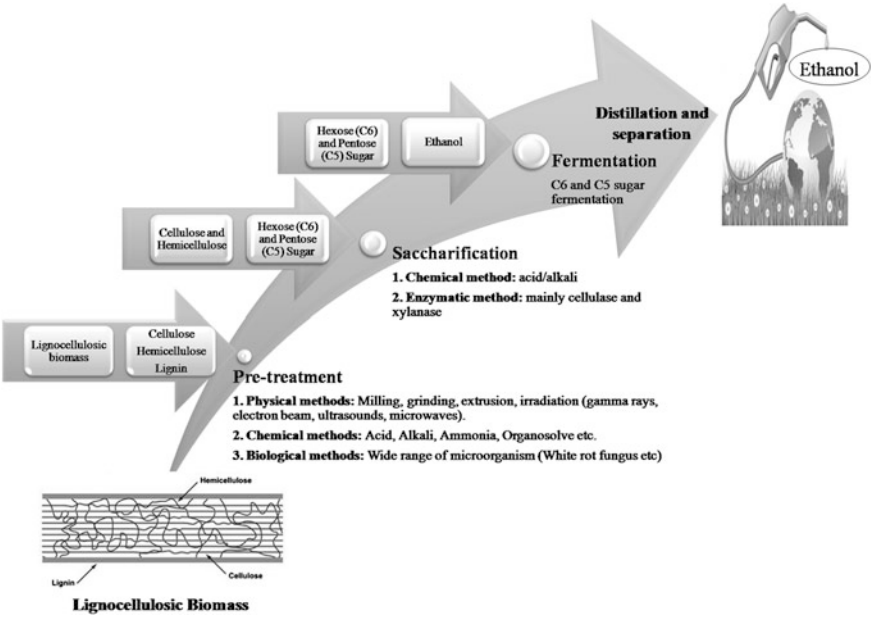

Fig. 1 A schematic roadmap of lignocellulosic biomass to ethanol production

processes are hindering industries to adopt and invest in bioethanol industry [6]. Amongst the drawbacks with existing processes of pretreatment, high power requirement in mechanical pretreatments insufficient separation of cellulose and lignin, generation of sugar and lignin derivatives (e.g. weak acids from hemicellulose, furfurals from hexoses and phenolics from the lignin) which later on adversely affects fermentation process, high use of chemicals and/or energy and production of solid/liquid waste are most challenging [6].

(ii) **Saccharification of pretreated biomass**: In this the pretreated biomass is subjected to hydrolyzing agents such as chemicals (acid) or enzymes (mainly cellulase and xylanase) for the hydrolysis of complex sugars: cellulose and hemicelluloses, into corresponding simple monomeric sugars: hexoses and pentoses, which can easily be fermented by yeast.

(iii) **Fermentation of sugars**: In this the hydrolyzate obtained after the saccharification step (containing fermentable hexoses and pentoses) are exposed to fermentive yeast, generally, under anaerobic condition for ethanol production. The solution containing ethanol further undergoes distillation for separation of pure ethanol.

1.2 Various Aspects of Pretreatment Process Selection

Although each step is important in the lignocellulosic ethanol production but the pretreatment of the lignocellulosic biomass is the key step because it is the major factor affecting the overall efficiency and economy of the entire process, i.e., the yield of fermentable sugar and ethanol, cost of product, plant set up etc.

In bioethanol production through lignocellulosic biomass main culprit is lignin, which reduces the cellulose accessibility for hydrolysis by cellulase enzyme. It is widely postulated that lignin interferes with cellulase and cellulose bindings as it shields more than a quarter of the surface area of cellulose fibers. However, various other mechanisms have also been hypothesized, such as the theory that lignin binds with cellulase via electrostatic or hydrophobic interaction unproductively.

The main aim of pre-treatment processes is basically to reduce the coverage or shielding of cellulose surface by lignin. In crystalline form, cellulose has more affinity towards lignin in comparison to the non-crystalline form. Interaction of cellulase with crystalline form of cellulose is less due to unavailability of hydroxyl group of sugars for action, which remain hidden more in this form than in non-crystalline form. Through selection of right pretreatment strategies crystallinity of cellulose can be reduced along with the removal of lignin.

Another very crucial point with the existing pretreatment strategies is the generation of the various byproduct derivatives, such as furans, phenolics and weak acids, which hinder with the ethanol production activity of the yeast by playing with their enzymatic machinery and reduce their efficiency for ethanol production [7]. Therefore, the hydrolyzate has to be detoxified for the significant removal of inhibitors using the effective detoxification agents, which makes the process more time taking. It should be noticed that during this detoxification the sugar loss should be minimum otherwise it will increase the cost of the overall process. Some processes such as over liming, treatment with hydrophobic and anionic resins, treatment with activated charcoal and enzymatic treatment using laccase are well known detoxification methods but these are not found very efficient in the removal of all types of inhibitors, simultaneously.

Therefore to make pretreatment process more effective, efficient and cost effective, followings aspects needs to be taken care of:

(a) Recalcitrance of biomass should be checked;
(b) Process selected must give high yields of sugars or value added chemicals and/or it must break down the biomass into the components easily accessible to hydrolytic enzymes or agents;
(c) Cellulosic and hemicellulosic layers must be intact (check carbohydrates degradation);
(d) Control formation of inhibitory toxic byproducts;
(e) Value added products should be recovered to make the process cost effective;
(f) Select cost–effective, low energy input and reasonable size reactors or plant set up with least waste generation.

In current scenario demand of ethanol from lignocellulose is growing fast and yield/supply is not able to meet the increased demand. To meet the increase in demand of bioethanol, yield and cost determining aspects of this industry have to be studied well and more attention should be given in process development. Selection of the suitable pretreatment method depends on various factors such as type of lignocellulosic biomass and desired product; therefore, any particular method cannot be categorized as best or right method. A good method of pretreatments should improve the digestibility of lignocellulosic biomaterials with least inhibitor generation at low cost. Each pretreatment has its own impact on the composition and structure of various components of the biomass. In industries, acid-based pretreatment methods are mainly in use for ethanol production. However, with this process lignin is only partially removed and sugar loss is also high. Therefore, more research is needed to be focused on higher removal of lignin with minimum sugar loss, increased solids concentration and higher yield of ethanol.

In this chapter studies on various pretreatment processes, i.e., steam explosion, dilute acid, dilute alkali, sequential dilute alkali and acid, microwave assisted alkali, microwave assisted dilute acid, microwave assisted dilute alkali and surfactant assisted acid pretreatment have been provided. For saccharification chemical processes are not preferred because these lead to degradation of cellulose and hemicelluloses. In a chemical process high chemical charges are required for complete lignin removal. Therefore, for complete removal of lignin, combination of two or three processes may be adopted instead of choosing single process, because at low chemical charges single pretreatment process is not very effective. The pretreatment process should be designed to remove lignin and to disintegrate the cellulose structure without loss (degradation) of cellulose and hemicellulose parts.

In this chapter case studies on various hybrid pretreatment methods, such as surfactant assisted acid pretreatment (SAAP), surfactant assisted alkali pretreatment (SABP) and sequential dilute alkali and acid pretreatment (SDAPP) for the optimized reduction of lignin hindrance and crystallinity in the ethanol production process to make the process commercially viable have been described.

2 Various Pretreatment Methods

2.1 Selection of Pretreatment Method

Biomass varies from each other on the basis of their composition and structure; therefore pretreatment strategies differ for different biomasses. Because selection of feedstock or biomass is one of the major criteria impacting efficiency of the overall process and yield of the product, therefore, criteria of selection of pretreatment method would be dependent on it. The criteria those must be taken into consideration while selecting feedstock are: high biomass production, optimal composition, high harvest index, suitable storage of harvested material, high bulk density,

high biofuel content in harvest biomass, high coproduct potential, high scalability, low harvest cost, high growth rate, high polysaccharide content, no intervention in human food chain etc.

Pretreatment process is directly related to the complexity of biomass. The major factors which makes the difference in the degree of digestibility or hydrolysis of different biomasses are degree of cellulose polymerization and crystallinity; porous surface area (accessibility); thickness of lignin covering cellulose; hemicellulose content intermingled with cellulose (sheathing); and fibre strength [8, 9].

Followings are some of the key criteria for the selection of pretreatment process for lignocellulosic biomass:

- It should be cost effective (low capital and operational cost).
- It should be effective on a broad range of lignocellulosic biomass.
- After the pretreatment various components should be in stable and fermentable form with efficient recovery (separation should be easy).
- It should be simple and without much prerequisite requirement prior to start (or preconditioning steps).
- Minimum inhibitors (sugar and lignin derivative inhibits the fermentation process) should be generated.
- It should have a low energy requirements and waste of the process could be used for heating or value added product formation in order to minimize the impact cost of the downstream processing and trade off [9, 10].

Evaluation and comparison of different pretreatment technologies would not be fully justified unless other aspects involved in the process, such as cost of upstream and downstream processing, investment capita, recycling and waste treatment systems etc. are also considered [11].

In this chapter various treatment methods, such as acid pretreatment, alkali pretreatment, sequential acid and alkali pretreatment, surfactant assisted acid pretreatment and surfactant assisted alkali pretreatment taking pine needles as feedstock for case study have been described with respect to the efficiency of the method for their potential to breakdown the lignocellulosic network, porosity, crystallinity of the cellulose, generation of various fermentation inhibitors etc.

2.2 Weak Acid Pretreatment of the Biomass

Weak acid pretreatment is one of the most common methods for the lignocellulose deconstruction. The major target of this method is hemicelluloses removal and minor target is lignin alteration along with the prime aim of surface area increment for sugar exposures for hydrolysis [12]. Generally, inorganic acids such as H_2SO_4, HCl and HNO_3 are preferred acids for acidic pretreatment but sometimes organic acids such as fumaric acid and maleic acid can also be used [13]. Based on the structural complexity and composition, the efficiency of the particular acid varies.

In pretreatment study on pine needles (PN) various acids, such as H_2SO_4, HCl and HNO_3, have been checked for their pretreatment efficiency and among these sulphuric acid (H_2SO_4) has been found to be the most effective [3]. The pine needles as lignocellulosic biomass were soaked with dilute acids and exposed to steam explosion. Various pretreatment parameters, such as acid concentration (0-5-5% v/v), Biomass loading (5–25% w/v) and autoclaving time (15–60 min), were studied and optimized for the effective release of the sugar during the pretreatment process. Under optimum conditions of 1% (v/v) H_2SO_4, 10% (w/v) and 45 min autoclaving time, a maximum of 0.221 g/g of reducing sugar was obtained from PN and after enzymatic saccharification of the pretreated PN the total reducing sugar yield was found to be enhanced up to 0.511 g/g. These, results indicated that during pretreatment the lignocellulosic network was deconstructed and hemicelluloses were hydrolyzed to generate monomeric reducing sugars [3].

In acidic conditions the most prominent ether bond of the lignin gets converted into hydroxyl group first, followed by conversion into carbonyl/carboxyl group and finally it fragments into C3/C2 molecules [14].

2.2.1 Mechanism of Action of Acid on Sugar Polymer Chain

The acid molecule act as the source of proton for the protonation and charging of the chain through alkyl group (-R). This charged group leaves the polymer chain and gets replaced with the hydroxyl group of the water to form monomers [14].

The sugar polymer chain gets converted into simpler forms by following mechanism (Fig. 2):

2.2.2 Effects of Pretreatment on Biomass Composition

The compositional analysis of the native and dilute acid pretreated PN can be carried out by **National Renewable Energy Laboratory** (NREL) method [3]. The data obtained had indicated that the acid pretreatment has enhanced the cellulose content about 40.1%, whereas hemicelluloses and lignin content were found to be reduced by 41.16 and 9.56%, respectively.

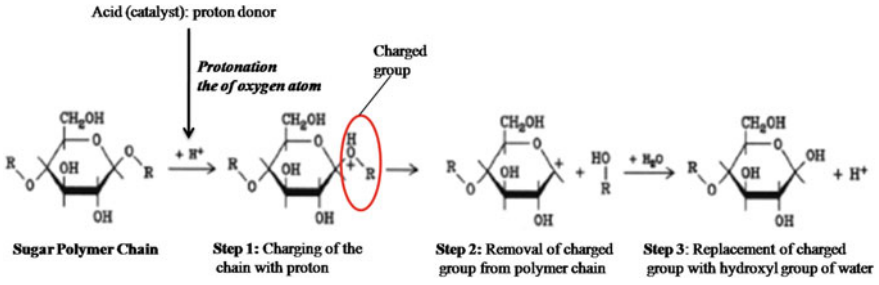

Fig. 2 Mechanism of the action of acid on sugar polymer chain

2.2.3 Drawbacks of Acid Pretreatment

Although, dilute acid pretreatment is the most widely used pretreatment globally due to ease in its mode of action, but this process suffers with the problem of generation of some miscellaneous sugar and lignin derivatives, such as furans (furfural and hydroxyl methyl furfural), weak acids and phenolics. Furan intervenes with the respiration and growth of the yeast, whereas phenolics causes cell membrane's integrity loss which reduces growth and sugar assimilation capability of organisms. Hemicellulose's acetyl group generates acetic acid, which causes cellular pH lowering and slow activity. These inhibitors reduce the ethanol productivity and yield [15, 16].

Therefore, the fermenting yeast should be either adapted to the inhibitors gradually or some efficient detoxification strategy should be employed for effective removal of inhibitors with the least effect on the sugar concentration.

2.3 Alkaline Pretreatment of the Biomass

Removal of lignin, which increases the reactivity of the celluloses and hemicelluloses, from the biomass is the major bottleneck in alkali pretreatment. In this process, saponification of intermolecular ester bonds occur which breaks down the cross linking of lignin with hemicelluloses. Removal of acetyl group along with the substitution of uronic acid on hemicelluloses reduces the surface of cellulose and hemicellulose for enzymes action [17].

Effectiveness of various alkali, such as $Ca(OH)_2$, NaOH and KOH, varies with structural complexity and integrity. Pandey and Negi [3] investigated these alkalis for the pretreatment of the PN and found NaOH as most effective for its pretreatment.

In a case of pretreatment process used for the PN, biomass was soaked with dilute NaOH and exposed to steam explosion. Various pretreatment processes, such as alkali concentration (0-5-5% w/v), Biomass loading (5–25% w/v) and autoclaving time (15–60 min), were studied and optimized for the effective release of the sugar during the pretreatment process. Under optimum conditions, i.e., 1.5% (w/v) NaOH, 15% (w/v) biomass loading and 45 min autoclaving time, a maximum of 0.191 g/g of reducing sugar was obtained from PN and after enzymatic saccharification of the pretreated PN the total reducing sugar yield was found to be enhanced up to 0.454 g/g. These results implied that during pretreatment saponification of the biomass occurred and ester bond cross linking of lignin with sugars was broken down [18].

2.3.1 Mechanism of Action of Alkali Pretreatment of Biomass

During alkaline pretreatment the intra-molecular ether bonds of the lignin molecule breakdown in following manner and the aromatic rings get separated from each other (Fig. 3):

In alkali pretreatment, the breakdown of sugar polymer chain occurs via the formation of an epoxide intermediate of 1,2-anhydro configuration. Since, the ring is formed between one oxygen and two carbon atoms the substitution of hydrogen occurs via nucleophilic substitution mechanism (S_N2) [14] (Fig. 4).

2.3.2 Effects of Pretreatment on Biomass Composition

The compositional analysis of the native and dilute alkali pretreated PN were carried out by using National Renewable Energy Laboratory (NREL) protocol by Pandey and Negi [3]. The data obtained indicated that the alkali pretreatment had enhanced the cellulose content about 48.22%, whereas hemicelluloses and lignin content were found to be reduced by 51.25 and 6.56%, respectively.

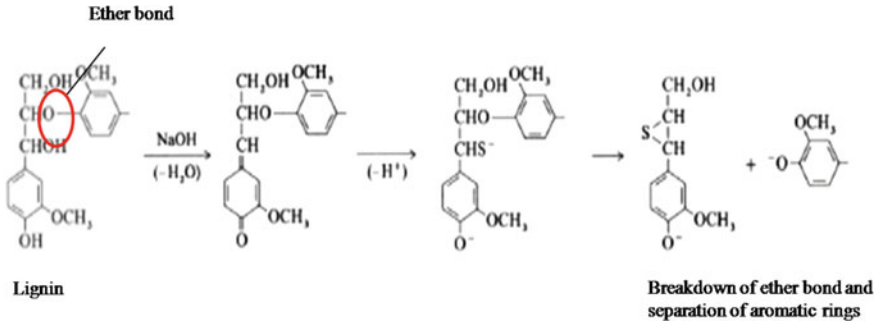

Fig. 3 Mechanism of lignin breakdown during alkali pretreatment

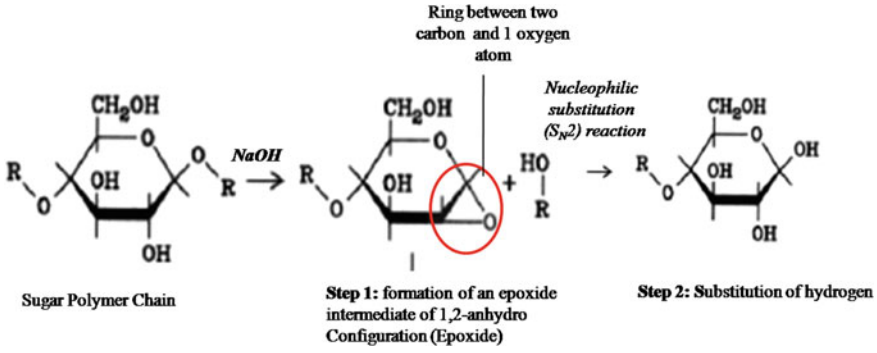

Fig. 4 Mechanism of Sugar polymer chain breakdown during alkali pretreatment

2.3.3 Significance and Drawbacks of Alkaline Pretreatment

In dilute alkali pretreatment significant delignification occurs and overall process input is lesser because it requires low pressure and temperature input in comparison to other pretreatment methods. Since, this process occurs at low temperature the formation of yeast growth inhibiting sugar and lignin derivatives is lesser. This produces less corrosion effect in comparison to acid pretreatment.

The major consequence of alkali pretreatment is formation of irrecoverable salts and production of combined C6 and C5 sugar stream, whereas the dilute acid pretreatment generates C5 rich pretreated liquor and C6 rich solid pretreated residue [8, 9].

2.4 Sequential Dilute Alkali and Dilute Acid Pretreatment (SDAAP)

Primary pretreatment of PN was carried out by using 1% NaOH at 121 °C and 15 lb pressure for 45 min [3]. After pretreatment, the solid residual PN was neutralized by using 1 N HCl, followed by washing under tap water to eliminate salt contamination. The neutralized sample was dried at dried at 45 ± 2 °C to remove moisture. The dilute alkali pretreated biomass was pretreated by using dilute acid for a second time. Under optimum conditions of 1.5% (v/v) H_2SO_4 concentration, 10% (w/v) biomass loading and 45 min incubation time a maximum of 0.296 g/g reducing sugar was released. The possible reason for this could be the affinity of acid towards the solubilization of hemicelluloses fraction of biomass which has made the cellulosic fraction accessible towards the enzyme action. Similar kind of findings was also reported by [16] for the pretreatment of rape seed straw.

In case of SDAAP, the pretreated biomass contained the cellulase, hemicellulose and total lignin content of 42.10 ± 0.21%, 9.87 ± 0.16% and 12.54 ± 0.09%, respectively. The total biomass was found to be degraded by 20% [3].

After hydrolysis of SDAAP-PL carried out for 48 h with 50 FPU/g enzyme loading and 0.15% w/v Tween-80 loading with biomass loading (12.5% w/v), maximum yield of reducing sugar was of 0.582 g/g, whereas reducing sugar release without pretreatment of the PN biomass was only 0.144 g/g, which shows that SDAAP had enhanced the saccharification more than 4 fold [3].

2.5 Surfactant Assisted Acid or Alkali Pretreatment

Cellulases contain hydrophobic residues on its surface, which interact with lignin by hydrophobic interactions and lead to unproductive adsorption on lignin surfaces. This is one of the major drawbacks of pretreatment processes. Surfactants can play

important role in reducing these unproductive enzyme lignin interaction and, thereby, increasing the hydrolytic productivity.

A process involving use of mild acid or alkali along with surfactant can be used to remove lignin and improve the sugar yield from pine needles more effectively. Surfactants interact with hydrolytic enzymes, biomass and enzyme-substrate complex during pretreatment and play following roles:

(a) Thermal deactivation of enzymes during hydrolysis can be reduced;
(b) During saccharification enzymes tend to bind with lignin. Amphiphillic nature of surfactant prevents this unproductive binding and improves enzyme–substrate interactions. Surfactant binds to lignin by hydrophobic interactions and prevents unproductive binding of cellulases to lignin through its hydrophilic head group; thereby, helping in more cellulase being used for hydrolysis of cellulose.
(c) Surface activity of the non-ionic surfactant reduces contact of enzyme with the air–liquid interface.
(d) Surfactant occupies hydrophobic sites on the lignin surface and causes displacement of adsorbed enzyme and reduces further enzyme adsorption. The hydrophilic Ethylene oxide (EO) chains of the adsorbed surfactants at the lignin surface protrude into the water solution and causes repulsion of protein from the lignin surface.

2.5.1 Surfactant Assisted Acid Pretreatment (SAAP) and Surfactant Assisted Base Pretreatment (SABP)

Dilute acid treatment dissolves hemicellulose layer but have very little impact on lignin layer. Dilute acid blending with surfactants can enhance effectiveness of pretreatment. Pandey and Negi [3] investigated effectiveness of the surfactant assisted acid pretreatment (SAAP) for pine needle biomass. In the process 5 g of PN was soaked in 50 ml of 1% H_2SO_4 supplemented with 1% C-TAB (w/w of biomass) for 60 min. The solid liquid separation of the pretreated content was carried out by filtration through double layered muslin cloths. The liquid fraction was neutralized by using 1 M H_2SO_4 and 1 M NaOH. The liquid fraction was analyzed for reducing sugar and the sugar obtained was considered as the sugar loss during the pretreatment (Fig. 5).

For surfactant assisted base pretreatment (SABP) the same set of experiment was carried out using 1% NaOH supplemented with 1% (w/w) PEG-6000. In both SAAP and SABP experiments a flask without any surfactant was used as control [3]. The solid fraction was neutralized by washing with deionized water and considered as pretreated biomass such as SAAP-PN and SABP-PN throughout the study.

The various processes parameters, such as acid/base concentration (0.5–2.5% w/v), biomass loading (5–25% w/v), surfactant concentration (0.5–2.5% w/w) and

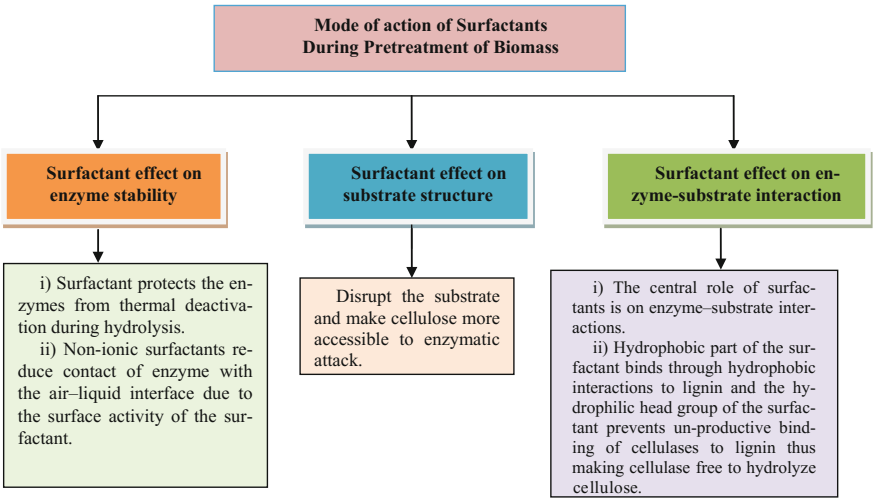

Fig. 5 Mode of action of surfactant assisted acid or alkali pretreatment

incubation time (15–75 min), were optimized by "one parameter at a time approach" [3].

Pretreatment enhanced the content of cellulose and hemicellulose in pretreated biomass up to 43.5 and 37.6% for SAAP-PN and SABP-PN, respectively [3]. The other complex sugar hemicelluloses were found to be 10.2 and 12.9% for SAAP and SABP, respectively. The pretreatment of the biomass was verified by the reduction in the lignin content up to 10.7 and 8.5% in both the pretreated biomasses, respectively.

On the basis of these results, it was concluded that in all the pretreatment processes the complex lignocellulosic network of native pine needle was found to be degraded to exposes the sugars for the further saccharification step.

3 SEM Analysis of Pretreated Biomass

Physical changes in the untreated and pretreated biomass can be done by SEM analysis. Pandey and Negi [3] used SEM for pine foliage. Images of the surfaces of the untreated and pretreated pine foliage were taken at magnification 25x using a Karl Zeiss Make scanning electron microscope (Fig. 6). The specimens were mounted on a conductive tape and observed using a voltage of 2 kV.

The compositional analysis of pretreated PFF revealed the removal of 73.47 ± 1.03% (w/w) lignin & 52.23 ± 1.11% (w/w) hemicelluloses in SABP and 59.53 ± 0.76% (w/w) & 54.46 ± 1.06% (w/w) SAAP which has been supported by the structural analysis. From Fig. 6 it can be revealed that structure of the

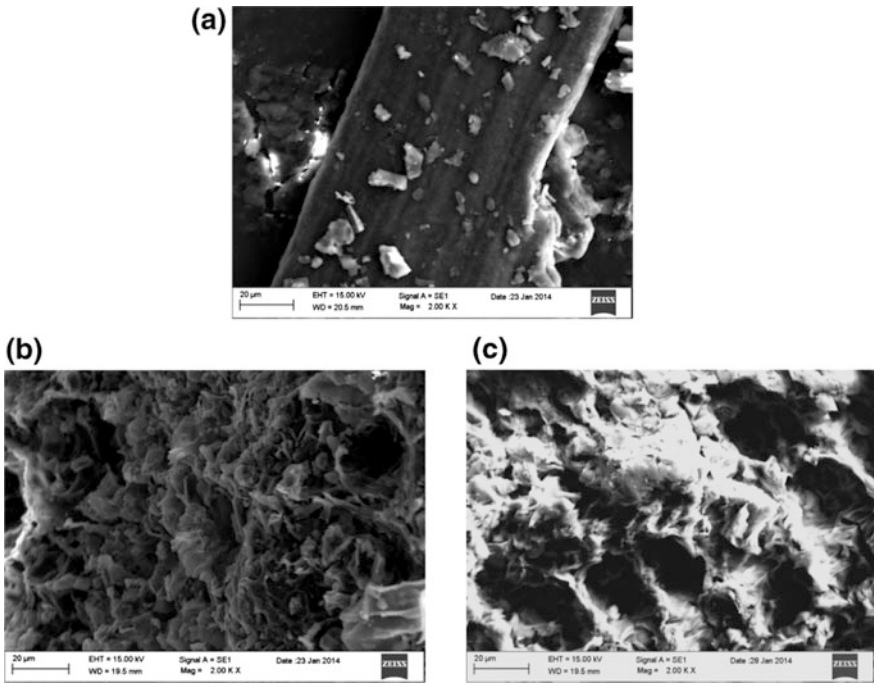

Fig. 6 **a** Pine needle native sample. **b** Pine foliage acid pretreated sample; **c** Pine foliage alkali pretreated sample

cellulose (crystallinity) has been reduced in both the pretreatment methods. These results suggested that during SABP, the saponification of intermolecular ester cross-linkage of lignin and hemicelluloses occurred, which lead to significant increase in biomass porosity, cellulose bulging and overall accessible surface area biomass.

4 Detoxification of Pretreated Liquor

Inhibitors, such as furfural, HMF, phenolic compounds, weak acids etc., are produced during pretreatment processes, such as deliming, adsorption, resins, solvent extraction, biphasic methods etc. These inhibitors can be effectively removed using various detoxification methods. Pandey and Negi [3] used a hydrophobic resin Amberlite XAD-4 for the detoxification of the pretreated liquor. They found the furfural and phenolics concentrations as 0.71 and 1.06 g/l in the dilute acid pretreatment of pine needles with 1% H_2SO_4. After detoxification with the

Table 1 Removal of inhibitors generated during pretreatment through XAD-4

S. No.	Parameters	SAAP-PFN			SABP-PFN			SDAAP-PFN		
		Untreated	Treated	% loss	Untreated	Treated	% loss	Untreated	Treated	% loss
1	Reducing sugar (g/l)	58.8	54.12	7.8	47.7	44.51	6.6	58	54	6.9
2	Furfural (g/l)	0.51	0.133	73.92	–	–	–	0.62	0.133	78.55
3	Phenolics (g/l)	0.98	0.44	55.1	0.718	0.444	38.2	1.02	0.64	37.25

hydrophobic resin Amberlite XAD-4 furfural and phenolics were found to be removed by 86 and 61%, respectively. Further, the ethanol yield of the hydrolyzate was found to be enhanced by 17.3% using the yeast *Saccharomyces cerevisiae* NCIM 3288. Similar results were also reported for the removal of the furfural of about 90% from the corn fiber biomass hydrolyzate using XAD-4 [19, 20]. During SABP only phenolic derivatives were formed and no other inhibitor formation was found. In acid mediated pretreatments furans and phenolics were formed. XAD-4 had removed 73.92% furfural and 55.1% phenolics through adsorption of them with sugar loss of 7.8% in SAAP-PFN hydrolyzate, while 38.2% phenolics removal was found in SABP-PFF hydrolyzate. These results were found in line with the already reported data for inhibitor removal from acid pretreated lignocellulosic hydrolyzate. These results revealed that the XAD-4 is an efficient detoxification agent which adsorbs inhibitors by hydrophobic interaction with lesser effect on sugar content. Summary of detoxication efficiency is given in the Table 1.

5 Enzymatic Saccharification of Pretreated Biomass

The enzymatic saccharification of SAAP-PN and SABP-PN was carried out using crude enzyme (enzyme activity; 7.15 FPU/ml) [3], the pretreated PN samples were mixed with sodium citrate buffer (50 mM, pH 4.8) with biomass loading of 10% w/v and this mixture was inoculated with crude cellulase loading (100 FPU/g). The reaction mixture was supplemented with 0.1% w/w Tween-80 and 0.3% w/v sodium azide (to prevent microbial growth). The reaction mixtures were incubated at 50 °C in an orbital incubator shaker for 48 h at 150 rpm. After incubation, the unhydrolyzed residues were separated by centrifugation at 10,000 rpm for 10 min [2, 21]. The hydrolyzates were analyzed for reducing sugar yield by 2, 5-dinitrosalicylic acid method [22].

Table 2 Fermentation profile of XAD-4 treated and untreated hydrolyzate

S. No.	Samples	Sugar (t = 0 h) (g/l)	Sugar (t = 72 h) (g/l)	Sugar consumed (%)	Ethanol concentration (g/l)	Ethanol yield (g/g)	Ethanol efficiency (%)
1	SAAP	58.8	24.53	58.282	13.98	0.407	79.83
2	SAAP (Treated)	54.12	19.88	63.266	16.31	0.476	93.217
3	SABP	47.7	20.31	57.421	10.95	0.399	78.235
4	SABP (Treated)	44.51	17.71	60.211	11.33	0.422	82.732
5	SDAAP	58	26	55.17	14.14	0.442	86.49
6	SDAAP (Treated)	54	18	66.67	18.2	0.505	98.83

6 Fermentation of Biomass Hydrolyzate for Ethanol Production

Saccharomyces cerevisiae NCIM 3288 was used by Pandey and Negi [3] for preparation of seed inoculums by growing it in Yeast extract peptone dextrose (YEPD) broth (composition in g/L; yeast extract, 10.0; peptone, 20.0; dextrose 20.0; pH 4.5–5.0) for 18 h [3]. The fermentation of the biomass hydrolyzate was carried out using 3% yeast inoculums for ethanol production under anaerobic condition. The ethanol yield was found to be enhanced by 16.1 and 6.01% in XAD-4 detoxified SAAP-PFN and SABP-PFN hydrolyzate, respectively, in comparison to non-detoxified ones after 72 h (Table 2). On the basis of these results Pandey and Negi [3] concluded that XAD-4 is promising inhibitor removal agent and it also enhances the fermentation efficiency of ethanologenic yeast. They carried out ethanol fermentation of SDAAP-PFN hydrolyzate (with sugar concentration 58 g/l) using *S. cerevisiae* (NCIM 3288). After 72 h of incubation, ethanol yield and ethanol efficiency were found to be 0.442 g/g and 86.49%, respectively with 55.17% sugar consumption. Similar kind of the results are also reported for ethanol production from switch grass [23].

7 Summary

See Table 3.

Table 3 Summary of all pretreatment methods employed for ethanol yield

Feedstock used	Pretreatment method	Hydrolysis agent used	Hydrolysis optimization method	Sugar yield (g/g)	Ethanol yield (g/g)	References
Pine needles	Steam explosion	Enzyme consortia (Cellulase: 4.563 IU/ml, laccase: 0.05 IU/ml, Xylanase: 38.32 IU/ml)	RSM (CCD)	0.334	–	[24]
Pine needles	Microwave assisted alkali	(Cellulase: 4.563 IU/ml, Laccase: 0.05 IU/ml, Xylanase: 38.32 IU/ml)	Artificial Neural Network (ANN)	0.669	–	[24]
Pine needles	Surfactant assisted acid	Crude cellulase(7.12 FPU/ml)	RSM (BBD)	0.588	0.476	[3]
Pine needles	Surfactant assisted alkali	Crude cellulase (7.12 FPU/ml)	RSM (BBD)	0.477	0.423	[3]
Pine needles	Surfactant assisted alkali	H_2SO_4 (2%)	One at a time	0.366	–	–
Pine needles	Acid (H_2SO_4 1% v/v)	Crude cellulase (7.12 FPU/ml)	–	0.511	–	–
Pine needles	Alkali (1%)	(Cellulase: 0.673 IU/ml, Laccase: 0.214 IU/ml, Xylanase: 0.032 IU/ml)	–	0.454	–	[24]
Pine needles	Sequential dilute alkali and acid	Commercial cellulase (52.86 FPU/ml)	RSM (BBD)	0.582	0.496	[3]
Kitchen waste	Dilute acid	Crude cellulase (7.12 FPU/ml)	One at a time	0.28	0.455	
Sugarcane tops	Microwave assisted dilute acid	Crude cellulase (20 FPU/ml)	RSM (BBD)	0.595	0.43	[25]
Sugarcane tops	Microwave assiste dilute alkali	Crude cellulase (20 FPU/ml)	RSM (BBD)	0.472	0.427	[25]
Sorghum stover	Acid (H_2SO_4 1% v/v)	Crude cellulase and xylanase	One factor at a time	0.459	0.411 g/g	[2]
Sorghum stover	Alkali (NaOH 1% w/v)	Crude cellulase and xylanase	–	0.366	–	–

8 Conclusions

Out of the various pretreatment strategies discussed in this chapter, SAAP and SDAAP delivered better results with high yield of ethanol after detoxification with hydrophobic resin XAD-4. These strategies significantly improve (about three-four fold) the enzymatic saccharification efficiency. The cellulase from the locally isolated strain *Rhizopus oryzae* SN-5 has potential of a very good hydrolysis agent for the extraction of significant amount of fermentable sugar from lignocellulosic biomass, as it gave very promising results with pine needles biomass. These pretreatment processes along with the XAD-4 detoxification could become a potential tool for the biorefineries for the economical industrial scale production of bioethanol from lignocellulosic biomass.

Acknowledgements The authors are thankful to Department of Science and Technology (DST) and Ministry of New and Renewable Energy (MNRE) Government of India New Delhi, for facilitating current work with financial support and Motilal Nehru National Institute of Technology (MNNIT), Allahabad for providing the space and basic facilities to carry out the research work.

References

1. Kumar P, Barrett DM, Delwiche MJ, Stroeve P (2009) Methods for pre-treatment of lignocellulosic biomass for efficient saccharification and biofuel production. Ind Eng Chem Res 48(8):3713–3729
2. Pandey AK, Negi S (2016) Optimization of concomitant production of cellulase and xylanase from *Rhizopus oryzae* SN5 through EVOP-factorial design technique and application in sorghum stover based bioethanol production. Renew Energy 98:51–56
3. Pandey AK, Negi S (2015) Impact of surfactant assisted acid and alkali pretreatment on lignocellulosic structure of pine foliage and optimization of its saccharification parameters using response surface methodology. Bioresour Technol 192:115–125
4. Sarkar N, Ghosh SK, Bannerjee S, Aikat K (2012) Bioethanol production from agricultural wastes: An overview. Renew Energy 37:19–27
5. Sindhu R, Kuttiraja M, Binod P, Sukumaran RK, Pandey A (2014) Physicochemical characterization of alkali pretreated sugarcane tops and optimization of enzymatic saccharification using response surface methodology. Renew Energy 62:362–368
6. Pandey A, Negi S, Binod P, Larroche C (2015) Pretreatment of biomass processes and technologies. ISBN: 978-0-12-800080-9. Chapter 8—Ionic Liquid Pretreatment, pp 137–155, Sangeeta Negi, Ajay Kumar Pandey. Copyright © 2015 Elsevier B.V. All rights reserved
7. Hawkins GM, Doran-Peterson J (2011) A strain of *Saccharomyces cerevisiae* evolved for fermentation of lignocellulosic biomass displays improved growth and fermentative ability in high solids concentrations and in the presence of inhibitory compounds. Biotechnol Biofuels 4:49
8. Mosier N, Hendrickson R, Brewer M, Ho N, Sedlak M, Dreshel R et al (2005) Industrial scale-up of pH-controlled liquid hot water pretreatment of corn fiber for fuel ethanol production. Appl Biochem Biotechnol 125:77–97
9. Mosier N, Wyman CE, Dale BE, Elander R, Lee YY, Holtzapple MT et al (2005) Features of promising technologies for pretreatment of lignocellulosic biomass. Bioresour Technol 96:673–686

10. Chandra RP, Bura R, Mabee WE, Berlin A, Pan X, Saddler JN (2007) Substrate pretreatment: the key to effective enzymatic hydrolysis of lignocellulosics? Adv Biochem Eng Biotechnol 108:67–93
11. Jeoh T, Ishizawa CI, Davis MF, Himmel ME, Adney WS, Johnson DK (2007) Cellulase digestibility of pretreated biomass is limited by cellulose accessibility. Biotechnol Bioeng 98:112–122
12. Chen H, Qiu W (2010) Key technologies for bioethanol production from lignocellulose. Biotechnol Adv 28:556–562
13. Kootstra AMJ, Beeftink HH, Scott EL, Sanders JPM (2009) Optimization of the dilute maleic acid pretreatment of wheat straw. Biotechnol Biofuels 2(31)
14. Krassig H, Schurz J (2002) Ullmann's encyclopedia of industrial chemistry, 6th edn. Germany, Wiley-VCH, Weinheim
15. McKillip WJ, Collin G (2002) Ullmann's encyclopedia of industrial chemistry, 6th edn. Germany, Wiley-VCH, Weinheim
16. Jeong T, Um B, Kim J, Oh K (2010) Optimizing dilute acid pretreatment of rape seed straw for extraction of hemicelluloses. Appl Biochem Biotechnol 161:22–33
17. Chang VS, Holtzapple MT (2000) Fundamental factors affecting biomass enzymatic reactivity. Appl Biochem Biotechnol Part A Enzym Eng Biotechnol 84–86:5–37
18. Sun Y, Cheng J (2002) Hydrolysis of lignocellulosic materials for ethanol production: A review. Bioresour Technol 83(1):1–11
19. Sandhya SV, Kiran K, Kuttiraja M, Preeti VE, Sindhu R, Vani S, Kumar SR, Pandey A, Bionod P (2013) Evaluation of polymeric adsorbent resins for efficient detoxification of liquor generated during acid pretreatment of lignocellulosic biomass. Indian J Exp Biol 51:1012–1017
20. Weil Joseph R, Dien Bruce, Bothast Rodney, Hendrickson Richard, Mosier Nathan S, Ladisch Michael R (2002) Removal of Fermentation Inhibitors Formed during Pretreatment of Biomass by Polymeric Adsorbents. Ind Eng Chem Res 41(24):6132–6138
21. Harshvardhan K, Mishra A, Jha B (2013) Purification and characterization of cellulase from a marine *Bacillus* sp. H1666: a potential agent for single step saccharification of seaweed biomass. J Mol Catal B Enzy 93:51–56
22. Miller GM (1959) Use of dinitrosalicylic acid reagent for determination of reducing sugar. Anal Chem 31:426–428
23. Dien BS, O'Bryan PJ, Hector RE, Iten LB, Mitchell RB, Qureshi N, Sarath G, Vogel KP, Cotta MA (2013) Conversion of switchgrass to ethanol using dilute ammonium hydroxide pretreatment: influence of ecotype and harvest maturity. Environ Technol 34:1837–1848
24. Vats S, Negi S (2013) Use of artificial neural network (ANN) for the development of bioprocess using *Pinus roxburghii* fallen foliages for the release of polyphenols and reducing sugars. Bioresour Technol 140:392–398
25. Maurya DP, Vats S, Rai S, Negi S (2013) Optimization of enzymatic saccharification of microwave pretreated sugarcane tops through response surface methodology for biofuel. Indian J Exp Biol 51:992–996

Ultrasound-Assisted Biodiesel Synthesis: A Mechanistic Insight

Ritesh S. Malani, Arun Goyal and Vijayanand S. Moholkar

Abstract Use of ultrasound in intensification of biodiesel synthesis process is well-known. However, most of the published literature in this area has focused on results than rationale—in that the exact physical mechanism of the ultrasound-induced enhancement of the biodiesel synthesis has remained unexplored. The research in our group has tried to fulfil this crucial knowledge gap. In this chapter, we have provided an overview and analysis of our studies in establishment of the physical mechanism of ultrasound-assisted biodiesel synthesis. This essentially means identification of the links between physical and chemical effects of ultrasound and cavitation, and the basic chemistry of biodiesel synthesis. The physical effect of cavitation and ultrasound is generation of intense microturbulence in the medium, while the chemical effect is generation of highly reactive radicals through thermal dissociation of the gas and vapor molecules entrapped in the bubble. The basic approach in our research has been concurrent analysis of the experimental results and simulations of cavitation bubble dynamics. We have treated diverse biodiesel synthesis processes that employ edible, non-edible and mixed non-edible feedstocks of oil, both base and acid catalysts in homogeneous form and heterogeneous base catalysts. Our analysis has essentially established that physical effects of ultrasound and cavitation have greater contribution to enhancement and intensification of the transesterification process for biodiesel synthesis. This is essentially manifested through generation of strong emulsion and elimination of mass transfer

R.S. Malani · V.S. Moholkar
Centre for Energy, Indian Institute of Technology, Guwahati, Guwahati, Assam, India

A. Goyal
Department of Biosciences and Bioengineering, Indian Institute of Technology, Guwahati, Guwahati, Assam, India

V.S. Moholkar (✉)
Department of Chemical Engineering, Indian Institute of Technology, Guwahati, Guwahati, Assam, India
e-mail: vmoholkar@iitg.ernet.in

A.K. Agarwal et al. (eds.), *Biofuels*, Green Energy and Technology,
DOI 10.1007/978-981-10-3791-7_7

barriers in the process. However, for heterogeneous catalyzed systems, the mass transfer still remains the rate controlling step, despite intense microconvection generated by sonication.

Keywords Ultrasound · Non-edible oil · Esterification · Transesterification · Catalyst · Modelling

1 Introduction

Principal energy needs of developing economy are in terms of electricity and liquid transportation fuel. Moreover, fast depletion of fossil fuel reserves and growing concerns of global warming and climate change risk has made search for alternate and renewable sources of energy an urgent need of the hour. Among various sources of renewable liquid transportation fuels, bioalcohols (like ethanol and butanol) and biodiesel have shown good promise for blending with conventional gasoline and diesel, respectively [1]. Bioalcohols are manufactured through the fermentation route. Conventionally, fermentation of molasses from sugar industry has been a good source of ethanol. However, due to growing cost of molasses (as a consequence of other potential outlets) and also higher price offered by beverage industry for molasses-based ethanol, the amount of ethanol that ends up in refineries for blending with gasoline is quite low. As far as biobutanol is concerned, the fermentation process has high operating cost due to requirement of strict anaerobic conditions for the microbial culture of *Clostridium acetobutylicum* that carries out the fermentation. The other source of bioalcohol is fermentation of lignocellulosic biomass. However, this route too has low economy due to high cost of pretreatment of biomass (acid pretreatment, delignification and enzymatic hydrolysis). Secondly, cost of concentration of rather dilute solutions of bioalcohols resulting from fermentation through distillation route is also cost intensive. Due to these reasons, commercial implementation of gasoline/bioalcohol blends has been hampered [1–3].

The other popular alternate liquid biofuel is Biodiesel. This essentially is alkyl ester of fatty acids [4]. Biodiesel can be produced through esterification/transesterification of free fatty acid/triglyceride with short chain alcohols like methanol and ethanol. Biodiesel is usually blended with petro-diesel for use in conventional IC engines. Up to 20 wt% biodiesel blends with petro-diesel can be used in existing diesel engines without requiring any modifications, and with no significant deviations in engine performance [5]. Depending on the feedstock used in biodiesel production, biodiesel had been classified as 1st, 2nd and 3rd generation biodiesel [6]. 1st generation biodiesel (manufactured mainly in Latin American countries) utilized relatively low-cost edible oils like palm and soybean as feedstock. However, given tremendous shortage and high cost of edible oils in developing economies like India, this route of biodiesel synthesis is absolutely infeasible. 2nd generation processes for biodiesel production essentially utilized non-edible oils like *Jatropha curcus* (Jatropha), *Pongamia pinnata* (Karanja), *Madhuca indica*

(Mahua), *Ricinus communis* (Castor) or waste cooking oil as feedstock. Nonetheless, this route also lacked attractive economy due to various reasons like low production of oil seeds, low oil content of seeds and high free fatty acid content of feedstock. More recently, microalgal lipids have been investigated as alternate feedstock for biodiesel. Conventionally, microalgae have been cultivated for natural food ingredients like omega-3 fatty acids or natural food colorants and dyes, pharmaceuticals (antioxidants) and nutraceuticals. The algal biomass left after extraction of these ingredients is good fish food. More recently, the microalgal oil or lipid has been considered as low-cost feedstock for biodiesel production. The microalgal lipids, however, contain significant quantities of poly-unsaturated free fatty acids, which are unstable and susceptible to oxidation prior to esterification. Therefore, partial hydrogenation of this feedstock is essential to increase the stability. This route is essentially known as 3rd generation biodiesel. This route also has limitations such as contaminations in the raceway ponds that cultivate the algal species, low lipid content of natural strains, higher susceptibility of genetically modified strains in large-scale open systems and cost of pre-processing of lipids, as noted earlier.

Although the economy of large-scale production of biodiesel is not attractive due to various limitations stated above, there are many feasible solutions. One solution to boosting the economy of commercial biodiesel production is the revenue earned by the side product of transesterification process, viz. glycerol. Glycerol is a versatile chemical and has many potential applications in food, pharmaceutical and cosmetics industry. However, the glycerol from biodiesel industry is contaminated with alkali catalyst and excess alcohol used in the transesterification process, and is thus, not useful for conventional applications [1, 5]. Use of heterogeneous catalysts during transesterification reaction is a possible solution to avoid contamination of the glycerol, which increases its quality and sale value. The literature on biodiesel synthesis is rife with studies reporting use of numerous catalysts for biodiesel synthesis. However, the other side of the coin is slow kinetics of biodiesel synthesis with heterogeneous catalyst (as compared to the homogeneous catalyst) due to triphasic nature of the reaction system. The mass transfer limitations in such system are very marked, which results in slowing down of the kinetics. Mass transfer barrier in heterogeneous reaction systems can be overcome by generation of strong convection in the system. This essentially depends on method of introduction of energy into the system. Conventionally, mechanical agitators have been used for mixing of the reaction mixtures. However, this mixing is essentially macro-scale mixing and does not generate very fine emulsions of organic (oil) and aqueous (alcohol) phases.

A relatively new method of introduction of energy into reaction systems is sonication or ultrasound irradiation of the reaction mixture. Research in past few decades has clearly demonstrated efficacy of sonication in introducing energy in the reaction system on extremely small temporal and spatial scales, which gives higher yield as well as kinetics of desired physical, chemical or biological transformation. Ultrasound is essentially a longitudinal acoustic wave with frequency $\geq$ 20 kHz. Passage of ultrasound wave through the medium in the form of alternate

compression and rarefaction cycles results in sinusoidal static pressure variation in the liquid medium. A secondary effect of this is occurrence of cavitation phenomenon in the medium. In present context, the word "Cavitation" refers to nucleation, volumetric oscillations and implosive collapse of tiny gas or vapor bubbles driven by sinusoidal variation in bulk pressure induced by propagation of ultrasound wave. At sufficiently high amplitude of ultrasound pressure wave, cavitation bubble undergoes transient implosive collapse. This phenomenon causes extreme energy concentration in the medium at an incredibly small temporal ($\sim$50 ns) and spatial scale ($\sim$100 nm) [7]. The temperature and pressure inside the bubble reach extreme ($\sim$5000 K and $\sim$50 MPa) during the transient collapse [8, 9]. Energy concentration generated by transient cavitation has remarkable physical and chemical effects on the reaction system. The physical effect is generation of intense microturbulence (or micro-convection) in the medium. This micro-convection has several fold higher effect in creating interphase mixtures or emulsification as compared to macro-scale mixing generated by mechanical agitation. The micro-convection can enormously boost mass transfer in the system. The chemical effect of transient cavitation includes generation of highly reactive radicals during collapse. These radicals are generated by thermal dissociation of gas and vapor molecules present in the bubble at the moment of transient collapse, when temperature and pressure inside the bubble reach extreme. The bubble may undergo fragmentation during transient collapse, with release of the radicals into the medium. These radicals can then induce/accelerate chemical reactions. This is the well-known sonochemical effect.

Ultrasonic enhancement of various biofuel processes has been an active area of research for past few years. Main applications of ultrasound in biofuel processes include: pretreatment of biomass (delignification/acid hydrolysis), enzymatic hydrolysis of pretreated biomass (or saccharification), fermentation of the hydrolyzates from acid/enzymatic hydrolysis, extraction of lipids from microalgal biomass, biodiesel synthesis with homogeneous/heterogeneous catalysts, and biogas digestion [1]. All previous authors have reported beneficial effects of sonication on the transesterification process for production of biodiesel using both homogeneous and heterogeneous catalysts. These effects mainly include higher yield and faster kinetics. However, the exact physical mechanism underlying ultrasound-induced enhancement of transesterification has not been explored. This essentially means discernment of the links between physical and chemical effects of ultrasound and cavitation (noted above) and the basic physics/chemistry of transesterification. Establishment of the physical mechanism of the ultrasound-assisted transesterification process is not only crucial to understanding fundamental intricacies, but it can also give useful guidelines for optimization and scale-up of the process. In this chapter, an overview of our research in discernment of physical mechanism of ultrasound-assisted biodiesel synthesis is given. Several transesterification systems using homogeneous base or acid catalyst and heterogeneous base catalyst has been treated employing both edible and non-edible feedstocks and also mixed oil feedstock. For feedstocks with relatively high free fatty acid content, two-stage (esterification/transesterification) and single-stage process with in situ water

removal has been discussed. Concurrent analysis of experimental and simulations results reveals interesting mechanistic facets of transesterification process with different combinations of feedstock and catalysts, as outlined in subsequently in this chapter. Brief introduction to basic concepts and principles of ultrasound and cavitation bubble dynamics is given in the next section.

2 Ultrasound and Cavitation Bubble Dynamics: A Brief Overview

2.1 Ultrasound Wave Phenomenon

Sound wave passes through a compressible medium in the form of a longitudinal wave comprising of alternate compression and rarefaction phases. Propagation of the ultrasound wave causes sinusoidal variation in bulk pressure as well as density of the medium. A simple mathematical expression that represents the variation in bulk pressure with passage of ultrasound is:

$$P(t) = P_o - P_A \sin(\omega t) = P_o - P_A \sin(2\pi f t) \quad (1)$$

where, P_o is the hydrostatic pressure in the medium, P_A is the pressure amplitude of the ultrasound wave, ω is the angular frequency of the ultrasound wave, while f is the absolute frequency and t is time in seconds. The pressure amplitude of the ultrasound wave is governed by net power input to the ultrasonic device and the area of the transducer through which ultrasound is generated. The pressure amplitude of the ultrasound wave also determines the oscillatory velocity of the fluid elements. Basic relations between these physical quantities are given in our previous publication [1]. Ultrasound wave undergoes attenuation (or reduction in pressure amplitude due to energy loss) during its passage through the medium. This effect is attributed to three mechanisms, viz. frictional (or viscous) loss, thermal loss and acoustic damping due to bubbles [10, 11]. Viscous dissipation or attenuation is essentially due to absorption of the momentum of the ultrasound wave by the medium due to finite viscosity and this loss is manifested in terms of unidirectional circulatory currents set up in the medium (known as acoustic streaming). The gas bubbles present in the medium also scatter the ultrasound waves that cause severe attenuation. Presence of gas bubbles in the liquid also alters the compressibility of the medium, as a result of which the speed of sound in the medium reduces.

2.2 Cavitation Bubble Dynamics

Ultrasound manifests its physical and chemical effects through phenomenon of cavitation [7, 12]. Cavitation essentially refers to nucleation, growth, oscillations

and implosive transient collapse which results due to the variation in bulk pressure induced by propagation of ultrasound wave through the medium. In ultrasonic cavitation (also known as acoustic cavitation), the liquid medium is usually stagnant during propagation of the ultrasound wave through it. However, in some processes (especially those operating on continuous basis), the liquid medium could be flowing. In this case, variation of bulk pressure can also be created by changing the flow geometry that induces variation in the velocity of the flow. This type of cavitation is termed as hydrodynamic cavitation. Occurrence of acoustic or hydrodynamic cavitation requires presence of nuclei in the bulk liquid medium. The cavitation nuclei could be tiny free-floating gas bubbles already present in the liquid or the gas pockets trapped in the crevices of the solid boundaries in the liquid medium. These gas pockets can grow in response to reduction in ambient pressure with passage of acoustic wave [13]. In case of hydrodynamic cavitation, the cavitation nuclei are also contributed by the gas bubble generated due to release of dissolved gas, as the bulk pressure in the flow falls with rise in velocity. Depending on the level of energy dissipation in the medium, vaporous cavitation can also occur in the medium in case of both acoustic and hydrodynamic cavitation that results in generation of vapor bubbles.

2.3 Radial Motion of Cavitation Bubbles

As noted earlier, transient implosive collapse of the cavitation bubbles creates intense energy concentration on extremely small spatial and temporal scale. This phenomenon has been extensively studied with help of mathematical models for the radial motion (or volumetric oscillations) of the cavitation bubbles. Modeling of cavitation bubble dynamics is a major area of research in physical acoustics with voluminous literature published in past five decades. In this section we very briefly summarize the major contributions in this area for the readers who are not well conversant with this subject matter. The mathematical models for cavitation bubble dynamics described in this section have been developed for the acoustic or ultrasonic cavitation, but these are equally applicable for the hydrodynamic cavitation. For more information on cavitation bubble dynamics, we would like to refer the interested readers to comprehensive treatises by Young [14] or Leighton [10].

The nature of the radial motion (or volumetric oscillations) of the cavitation bubble depends on the pressure amplitude of the acoustic wave. Two forces, viz. inertial force and pressure force, govern the radial motion of the cavitation bubble. For relatively small acoustic pressure amplitudes—typically smaller than the static pressure in the medium, the volume oscillations of the bubble are of small amplitude—driven mainly by the pressure forces, and essentially in phase with the acoustic wave. Volumetric oscillations of the cavitation bubble become

large-amplitude as well as non-linear for larger acoustic pressure amplitudes—typically greater than static pressure in the medium. In this case, the radial motion of the bubble comprises of an initial explosive growth, in which the bubble radius grows at least two times or higher of its initial value. The growth phase is followed by a transient collapse and few after–bounces. In this case, the radial motion of the bubble is dominated by the pressure forces [15].

Lord Rayleigh presented the first–ever mathematical analysis of an empty cavity collapsing under constant static pressure [16]. Subsequent researchers improved the analysis of Lord Rayleigh, which included accounting for the effects of surface tension and viscosity of liquid, and presence of non-condensable gas and solvent vapor inside the bubble. This analysis resulted in the popular Rayleigh–Plesset–Noltingk–Neppiras–Poritsky [17–19] equation for radial motion of bubble which is as follows:

$$R\frac{d^2R}{dt^2}+\frac{3}{2}\left(\frac{dR}{dt}\right)^2=\frac{1}{\rho}\left(P_o+\frac{2\sigma}{R_o}-P_v\right)\left(\frac{R_o}{R}\right)^{3\gamma}+P_v-\frac{2\sigma}{R}-\frac{4\mu}{R}\frac{dR}{dt}-(P_o+P(t)) \tag{2}$$

The above equation did not account for liquid compressibility, which becomes a dominant factor as the bubble wall velocity becomes closer or even exceeds the sonic velocity in the medium during the final moment of transient bubble collapse. The first model for cavitation bubble dynamics accounting for liquid compressibility effect was proposed by Gilmore [20] on the basis of Kirkwood-Bethe hypothesis [21]. Major subsequent contributions in this area are from Keller and Kolodoner [22], Keller and Miksis [23], Prosperetti and Lezzi [24]. These analyses have resulted in more rigorous forms of models for radial motion of cavitation bubbles. Two most popular equations for cavitation bubble dynamics among scientific community are:

(1) Keller and Miksis equation [22, 25]:

$$\left(1-\frac{\dot{R}}{c}\right)R\ddot{R}+\left(1-\frac{3\dot{R}}{c}\right)\frac{3}{2}\dot{R}^2=\frac{1}{\rho}\left(1+\frac{\dot{R}}{c}\right)\left[P_g-P_o-P(t)\right]+\frac{\dot{R}}{\rho c}\frac{dP_g}{dt}-4v\frac{\dot{R}}{R}-\frac{2\sigma}{\rho R} \tag{3}$$

(2) Bubble dynamics equation proposed by Lofstedt et al. [26], Barber et al. [27]:

$$R\ddot{R}+\frac{3}{2}\dot{R}^2=\frac{1}{\rho}\left[P_g-P_o-P(t)\right]+\frac{\dot{R}}{\rho c}\frac{dP_g}{dt}-4v\frac{\dot{R}}{R}-\frac{2\sigma}{\rho R} \tag{4}$$

2.4 Modeling of the Sonochemical and Sonophysical Effects

Ultrasound waves as well as radial motion of cavitation bubbles driven by these waves induce physical and chemical effects in the reaction system or in general liquid medium. The physical effect associated with ultrasound and cavitation is essentially generation of intense micro-mixing in the system as a result of strong micro-convection generated through various mechanisms.

2.4.1 Sonochemical Effect

The chemical effect associated with ultrasound and cavitation (popularly known as sonochemical effect) is generation of highly reactive chemical species, some of which are radical species, which can induce/accelerate numerous chemical reactions in the medium, generated through thermal dissociation of gas and vapor molecules present in the bubble at the moment of transient collapse [12, 28, 29].

Several previous authors have dealt with the physical explanation to the sonochemical effect induced by ultrasound and cavitation. Passage of ultrasound wave through the medium gives rise to sinusoidal variation in the bulk pressure in the liquid medium. In the rarefaction half cycle of ultrasound, when the pressure in the medium falls sufficiently below the ambient or static pressure, the cavitation bubbles grow from the nuclei. These nuclei could be gas pockets trapped in the crevices of solid boundaries in the reactor. If the pressure amplitude of the ultrasound wave is higher than the static pressure in the medium, the radial motion of the bubble is dominated by inertial forces and bubble undergoes an explosive growth to several times its original size. During this expansion, liquid at the bubble interface evaporates with diffusion of the vapor molecules towards the core of the bubble. However, as the bubble gets compressed in the compression half cycle of ultrasound, not all of the vapor present in the bubble can condense and return to the liquid medium. A review of literature on vapor transport across bubble interface and the entrapment of vapor in the bubble during transient collapse is given by Krishnan et al. [28].

Storey and Szeri [29] presented comprehensive analysis of vapor transport and entrapment in the cavitation bubble. This analysis relaxed all of the assumptions and simplifications made in previous analyses. Storey and Szeri [29] showed that in the compression phase of radial bubble motion, counter diffusion of the vapor molecules occurs with condensation at the bubble wall. The principal result of the study of Storey and Szeri [30] was that water vapor transport in the bubble is a two-step process, i.e. diffusion to the bubble wall and condensation at the wall. Thus, it is influenced by two time scales, viz. time scale of diffusion (t_{dif}) and time scale of condensation (t_{cond}) [31], and their magnitudes relative to the time scale of bubble dynamics, t_{osc}.

During the transient motion of cavitation bubble, the velocity of the bubble wall (or the bubble-liquid interface) reaches or even exceeds the sonic velocity in the

medium. At this stage, $t_{osc} << t_{diff}$ condition is reached, and the vapor molecules have insufficient time to diffuse to the bubble wall for undergoing phase change or condensation. The bubble composition gets essentially "*freezed*" with fixed and uneven distribution of vapor molecules in the bubble. In other words, the vapor present inside the bubble is essentially "*trapped*" in the bubble. In addition to diffusion limitation, another mechanism which also contributes to trapping of vapor molecules inside the bubble, is the non-equilibrium phase change at the bubble wall. In the final moments of bubble collapse, the time scale of bubble oscillations becomes lesser than the time scale of phase change or vapor condensation. As a consequence, all of the vapor molecules approaching the bubble wall cannot "stick" to the bubble wall for undergoing a phase change [31]. Storey and Szeri [29] have shown in their analysis that the vapor entrapment in the cavitation bubble occurs predominantly due to diffusion limitation than condensation limitation. As the temperature and pressure inside the bubble reach extreme at transient collapse, the vapor molecules trapped inside the bubble undergo thermal dissociation along with the gas molecules resulting in generation of spectrum of chemical species (with relatively smaller molecular weight) including some radical species. In view of the results of Storey and Szeri [29, 30], Toegel et al. [32] developed a simple diffusion limited model, which has become immensely popular among the sonochemical community. This model, based on ordinary differential equations, has distinct merits of being simple yet physically realistic. Ordinary differential equations and thermodynamic data of the diffusion-limited model of cavitation bubble dynamics are listed in Tables 1 and 2 [33]. The main components of diffusion-limited model are: (1) Keller–Miksis equation for radical motion of cavitation bubbles, (2) Equation for the diffusion of solvent vapor across bubble wall, (3) Equation for heat conduction across bubble wall, and (4) Overall energy balance of cavitation bubble. In overall energy balance, the cavitation bubble is treated as open system. Diffusion coefficient and thermal conductivity of the bubble contents have been determined using Chapmen–Enskog theory with Lennard–Jones 12–6 potential at the bulk temperature of the liquid [34–36]. With assumption of fast condensation of vapor molecules at bubble interface and prevalence of equilibrium, the thermal and diffusive penetration depths are estimated using dimensional analysis as follows [37]:

$$l_{diff} = \min\left(R/\pi, \sqrt{RD_{ij}/|dR/dt|}\right) \tag{5}$$

$$l_{th} = \min\left(R/\pi, \sqrt{R\kappa/|dR/dt|}\right) \tag{6}$$

An important assumption made for estimation of the sonochemical effect is the prevalence of chemical equilibrium in the bubble all through radial motion. This assumption is based on the relative time scales of reactions kinetics inside the bubble and the timescale of bubble dynamics. The temperature and the pressure in the bubble reaches extreme ($\sim$5000 K and $\sim$50 MPa) at the point of maximum compression triggering chemical reactions with large kinetic constants. Moreover,

Table 1 Essential equations (ODE's) of the diffusion-limited ODE model [1, 33]

Model component	Equation	Initial value
1. Radial motion of the cavitation bubble	$\left(1-\frac{dR/dt}{c}\right)R\frac{d^2R}{dt^2}+\frac{3}{2}\left(1-\frac{dR/dt}{3c}\right)\left(\frac{dR}{dt}\right)^2=\frac{1}{\rho_L}\left(1+\frac{dR/dt}{c}\right)(P_i-P_t)+\frac{R}{\rho_L c}\frac{dP_i}{dt}-4v\frac{dR/dt}{R}-\frac{2\sigma}{\rho_L R}$ Internal pressure in the bubble: $P_i=\frac{N_{tot}(t)\,kT}{[4\pi(R^3(t)-h^3)/3]}$ Pressure in bulk liquid medium: $P_t=P_0-P_A\sin(2\pi ft)$	At t = 0, R = R_o, dR/dt = 0
2. Diffusive flux of solvent (methanol) molecules	$\frac{dN_S}{dt}=4\pi R^2 D_S\frac{\partial C_S}{\partial r}\Big\vert_{r=R}\approx 4\pi R^2 D_S\left(\frac{C_{S,R}-C_S}{l_{diff}}\right)$ Instantaneous diffusive penetration depth: $l_{diff}=\min\left(\sqrt{\frac{RD_S}{\vert dR/dt\vert}},\frac{R}{\pi}\right)$	At t = 0, N_S = 0
3. Heat conduction across bubble wall	$\frac{dQ}{dt}=4\pi R^2\lambda\frac{\partial T}{\partial r}\Big\vert_{r=R}\approx 4\pi R^2\lambda\left(\frac{T_0-T}{l_{th}}\right)$ Thermal diffusion length: $l_{th}=\min\left(\sqrt{\frac{R\kappa}{\vert dR/dt\vert}},\frac{R}{\pi}\right)$	At t = 0, Q = 0
4. Overall energy balance	$C_{V,mix}dT/dt=dQ/dt-P_i dV/dt+(h_S-U_S)dN_S/dt$ Mixture heat capacity: $C_{V,mix}=\sum C_{V,i}N_i$ (i = N_2/O_2/Solvent) Molecular properties of solvent: Enthalpy: $h=\left(1+\frac{f_i}{2}\right)kT_o$ Internal energy: $U_S=N_S kT\left(3+\sum_{i=1}^{3}\frac{\theta_i/T}{\exp(\theta_i/T)-1}\right)$ Heat capacity of various species (i = N_2/O_2/Solvent): $C_{V,i}=N_i k\left(f_i/2+\sum\left((\theta_i/T)^2\exp(\theta_i/T)\Big/(\exp(\theta_i/T)-1)^2\right)\right)$	At t = 0, T = T_0

Table 2 Thermodynamic data for the diffusion limited model

Species	Degrees of freedom (translational + rotational) (f_i)	Lennard–Jones force constants		Characteristic vibrational temperatures θ (K)
		σ (10^{-10} m)	ε/k (K)	
N_2	5	3.68	92	3350
O_2	5	3.43	113	2273
CH_3OH	6	3.626	481.8	500.59, 1674.41, 1708.94, 1854.22, 2169.26, 2356.26, 2376.4, 2392.22, 4581.62, 4649.23, 4752.8, 5923.74
Ar	3	3.42	124	–
H_2O	6	2.65	380	2295, 5255, 5400

Reproduced with permission from [1] Copyright © 2015, Springer Science + Business Media Dordrecht

*Data taken from Toegel [33], Hirschfelder et al. [34], Reid et al. [35], Condon and Odishaw [36], Davis [41]

Notations R radius of the bubble; *dR/dt* bubble wall velocity; c velocity of sound in bulk liquid medium; ρ_L density of the liquid; v kinematic viscosity of liquid; σ surface tension of liquid; λ thermal conductivity of bubble contents; κ thermal diffusivity of bubble contents; θ characteristic vibrational temperature(s) of the species; N_S number of solvent molecules in the bubble; N_{N2} number of nitrogen molecules in the bubble; N_{O2} number of oxygen molecules in the bubble; t time, D_S diffusion coefficient of solvent vapor; C_S concentration of solvent molecules in the bubble; $C_{S,R}$ concentration of solvent molecules at the bubble wall or gas–liquid interface; Q heat conducted across bubble wall; T temperature of the bubble contents; T_o ambient (or bulk liquid medium) temperature; k Bolzmann constant; h_S molecular enthalpy of solvent; U_S internal energy of solvent molecules; f_i translational and rotational degrees of freedom; $C_{V,i}$ heat capacity at constant volume for species i; N_{tot} total number of molecules (gas + vapor) in the bubble; h van der Waal's hard core radius; P_o ambient (bulk) pressure in liquid; P_A pressure amplitude of ultrasound wave; f frequency of ultrasound wave

the concentrations of different chemical species in the bubble are very high due to extremely small volume. As a result, the rates of various reactions occurring between chemical species present in the bubble are extremely fast, due to which chemical equilibrium prevails in bubbles all along during the radial motion [28, 38].

2.4.2 Physical Effects of Cavitation Bubble

The principal physical effect of ultrasound and cavitation on a reaction system is generation of intense micro-convection and micro-mixing. This micro-convection essentially helps in elimination of mass transfer barriers in the system. A brief description of different mechanisms of generation of micro-convection is given below [10, 12, 14].

Micro-streaming

This is essentially small amplitude oscillatory motion of fluid elements around a mean position, which is induced by propagation of ultrasound wave. For a typical ultrasound wave with pressure amplitude of 120 kPa in water (ρ = 1000 kg/m^3, C = 1500 m/s), the micro-streaming velocity = 0.08 m/s.

Acoustic Streaming

Due to finite viscosity of the medium through which ultrasound waves propagate, the momentum of the wave is absorbed by the medium. This is manifested in terms of low velocity unidirectional currents of the fluid known as acoustic streaming [39, 40]. Acoustic streaming also generated due to obstruction of the oscillatory motion of the fluid elements in the vicinity of solid boundaries in the medium. This phenomenon results in setting up of unidirectional current parallel to the boundary.

Microturbulence

The oscillatory motion of fluid induced by volume oscillations of the bubble is called microturbulence. During expansion of the cavitation bubble, the liquid surrounding the bubble is displaced away from bubble interface. In the compression phase, fast contraction of the bubble generates "void" around it, and the liquid is pulled towards the bubble as it fills this void. The velocity of microturbulence, is obviously a function of the amplitude of bubble oscillation. The phenomenon of microturbulence is observed only in the close vicinity of the bubble, and diminishes very rapidly away from it.

Acoustic (or Shock) Waves

As noted above, the liquid gushes or spherically converges towards the bubble interface during the contraction phase. The compression of the bubble is mostly adiabatic and the pressure inside the bubble rises rapidly if the bubble contains non-condensable gas such as air. At the point of minimum radius (or maximum compression) during radial motion, the velocity of the bubble wall becomes zero. At this moment, the velocity of the fluid elements converging towards the bubble interface also reduces to zero—almost instantly—which creates rise in pressure (due to conservation of momentum). This generates a high pressure shock wave that propagates through the medium. The bubble may undergo renounces due to the pressure exerted by the non-condensable gas inside the bubble.

Microjets

During radial motion driven by ultrasound wave, the initial spherical geometry of the bubble may be disturbed due to non-uniformity of pressure gradients surrounding it. These non-uniform gradients are induced by phase boundaries, either solid–liquid, gas–liquid or liquid–liquid, due to which the motion of liquid in the vicinity of the cavitation bubble is hindered. Under influence of non-uniform pressure gradient, the bubble undergoes asymmetric radial motion with the portion of bubble exposed to higher pressure collapsing at a faster rate than rest of the bubble. Such asymmetric motion results in formation of a high speed liquid jet. The direction of this jet depends on the type of phase boundary. For a "rigid" boundary such as metal surface, the microjet is directed towards the boundary. For a "free" boundary such as gas–liquid (typically air–water) interface, the microjet is directed away from the boundary. The velocities of these microjets are in the range of 120–150 m/s.

3 Mechanistic Insight into Ultrasound-Assisted Biodiesel Synthesis

The transesterification reaction is essentially a liquid-liquid heterogeneous reaction. With use of solid catalyst, it becomes a tri-phasic reaction, with strong mass transfer limitations. The basic chemical mechanisms of both alkali and acid catalyzed transesterification reactions are well known. Due to heterogeneous nature of the reaction system, the kinetics and yield of transesterification is a major function of the interfacial area. As noted earlier, sonication can have multiple beneficial effects on such reaction system. Our research group has put in significant efforts in deducing the physical mechanism of ultrasound-assisted biodiesel synthesis with variety of feedstocks and catalysts. In this section, we present an overview of these studies.

3.1 Transesterification of Refined Edible Oil

3.1.1: Kalva et al. [42] have deduced the physical mechanism of ultrasound–assisted enhancement of transesterification reaction by discriminating between physical and chemical effects of ultrasound. Kalva et al. [42] investigated the process using refined soybean oil with methanol and sodium hydroxide as the homogeneous alkali catalyst. Experiments were carried out in a beaker made of borosilicate glass with dimensions: height = 95 mm, diameter = 68 mm, and thickness = 2.5 mm. Microprocessor based and programmable ultrasonic processor

was used (Sonics and Materials Inc., Model: VCX 500) with frequency of 20 kHz as a source of ultrasound.

Discrimination between relative contributions of physical and chemical effects of ultrasound and cavitation have been achieved with following experimental categories: (1) no external addition of base catalyst during reaction; (2) sparging of methanol with argon prior to reaction (without addition of external catalyst); (3) addition of Fe^{2+} to methanol prior to reaction; (4) addition of base catalyst (NaOH) in methanol. First three experimental categories were aimed at in situ production of $^{\bullet}OH$ radicals and OH^{-} ions, which would generate methoxide ions by their reaction with methanol. First category experiments aimed at in situ production of $^{\bullet}OH$ radicals through thermal dissociation of methanol vapor in the transient cavitation bubble. The second category experiments were aimed at seeding cavitation nuclei of monatomic gas (argon) in the reaction system so as to boost the cavitation intensity. Third experimental category aimed at generating OH^{-} ions from $^{\bullet}OH$ radicals produced from transient cavitation bubbles through oxidation of Fe^{2+} to Fe^{3+} (Fenton reaction). OH^{-} ions can generate methoxy ions (CH_3O^{-}) required for transesterification by reacting with methanol. These experiments did not yield any biodiesel, which clearly pointed at no role played by the chemical effects of transient cavitation in the transesterification process.

In the fourth category, base catalyst (NaOH) was added to methanol. Two concentrations of NaOH were used, viz., 0.5 and 1% (w/w) of oil. The experiments were carried out using 4 methanol:oil molar ratios, viz. 6:1; 12:1; 16:1 and 24:1. Results of the experimental study were coupled to single bubble dynamics model to establish the physical mechanism of sonication on transesterification reaction. This experimental category produced good yields of biodiesel, and the trends in biodiesel yield with varying alcohol/oil molar ratios was shown in Fig. 1. For both 0.5 and 1% w/w NaOH, the highest yield was obtained for an alcohol to oil molar ratio of 12:1, while the lowest yield was obtained for an alcohol to oil molar ratio of 24:1. Moreover, for any particular alcohol to oil molar ratio, the biodiesel yield for 1% w/w NaOH is higher than 0.5% w/w NaOH.

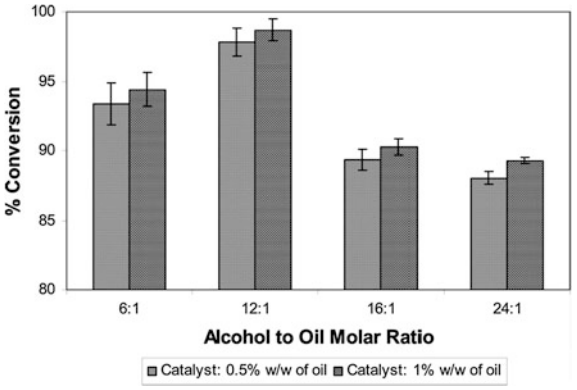

Fig. 1 Biodiesel yield in the fourth category of experiments as a function of alcohol to oil molar ratio (Reproduced with permission from [42], Copyright © 2009, American Chemical Society)

Kalva et al. [42] also performed simulations of radial motion of a single 10 μm argon cavitation bubble using diffusion-limited model in methanol and oil as liquid media. The results of these simulations, viz. radial motion of the cavitation bubble, number of vapor molecules in the bubble and temperature/pressure conditions reached inside the bubble, have been shown in Figs. 2 and 3 for methanol and oil as liquid media, respectively. The results of simulations have been summarized in Table 3, which lists the temperature and pressure peaks reached in the bubble at transient collapse and the magnitude of the microturbulence and acoustic waves generated by the bubble.

Results presented in Figs. 2 and 3 and Table 3 reveal following key facets of radial motion of cavitation bubbles in oil and methanol as liquid media:

(1) Cavitation bubble in methanol undergoes large expansion ($\sim 5 \times$ original size) due to low viscosity of methanol. This expansion is accompanied by significant vaporization of methanol into the bubble. At the final moments of transient collapse, the velocity of the bubble wall becomes extremely fast and not all of the methanol vapor that has entered cavitation bubble during expansion can escape the bubble. Methanol molecules entrapped in the bubble at transient collapse are subjected to extreme conditions of temperature and pressure (viz., 810 K and 1455 atm) generated in the bubble at transient collapse. At these conditions, methanol vapor undergoes thermal dissociation to form smaller chemical species. The chemical composition of the cavitation bubble at transient collapse can be determined by knowing the number of moles of O_2, N_2 and CH_3OH in the bubble and temperature/pressure conditions reached in the bubble, and minimization of the Gibbs energy for this system. Table 3 also gives the equilibrium composition of the bubble contents at conditions of transient collapse. Results presented in Table 3 reveal that the dominant species resulting out of dissociation of O_2, N_2 and methanol molecules in cavitation bubble are CH_4, H_2O, H_2, and CO_2 along with traces of several other species. However, the gamut of these species does not include any radical species (such as $H^{\cdot}$, $OH^{\cdot}$, and $HO_2^{\cdot}$). This result is essentially a consequence of relatively low peak temperature reached inside the bubble during transient collapse, which in turn is a result of large entrapment of methanol vapor molecules in the bubble due to which the net heat capacity of bubble content increases. The mean velocity of microturbulence generated due to bubble motion is ~ 2 cm/s.

(2) The cavitation bubble in oil undergoes marginal initial expansion (just $\sim$ 2 times the initial size) with practically no solvent evaporation in the bubble as a result of very low vapor pressure of oil. Therefore, sonochemical effect of production of radicals in the bubble does not take place. Moreover, peak temperature and pressure conditions reached in the bubble during collapse are also smaller than methanol. Mean microturbulence velocity in oil is ~ 0.3 m/s, which was one order of magnitude smaller than that in methanol. In summary, the cavitation phenomenon in oil was less energetic than methanol, which was

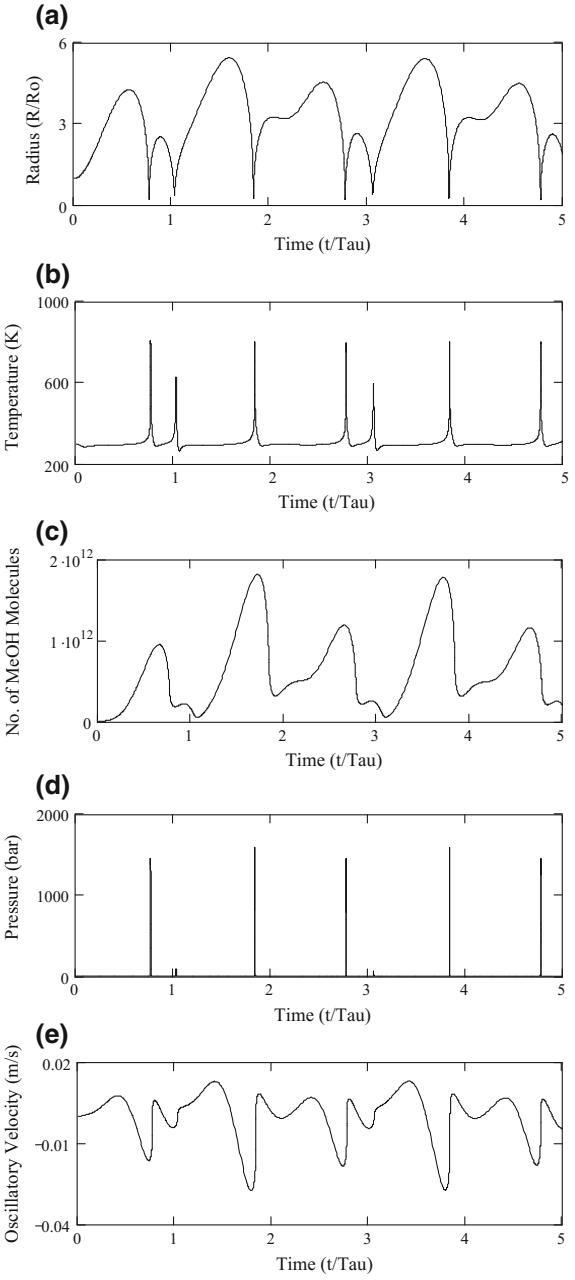

Fig. 2 Simulation results of radial motion of a 10 μm cavitation bubble in methanol medium (Reproduced with permission from [42], Copyright © 2009, American Chemical Society)

attributed due to high viscosity of the oil. The viscosity of the liquid medium essentially offers resistance to radial motion of the bubble, causing reduction in the intensity of the resultant physical and chemical effects.

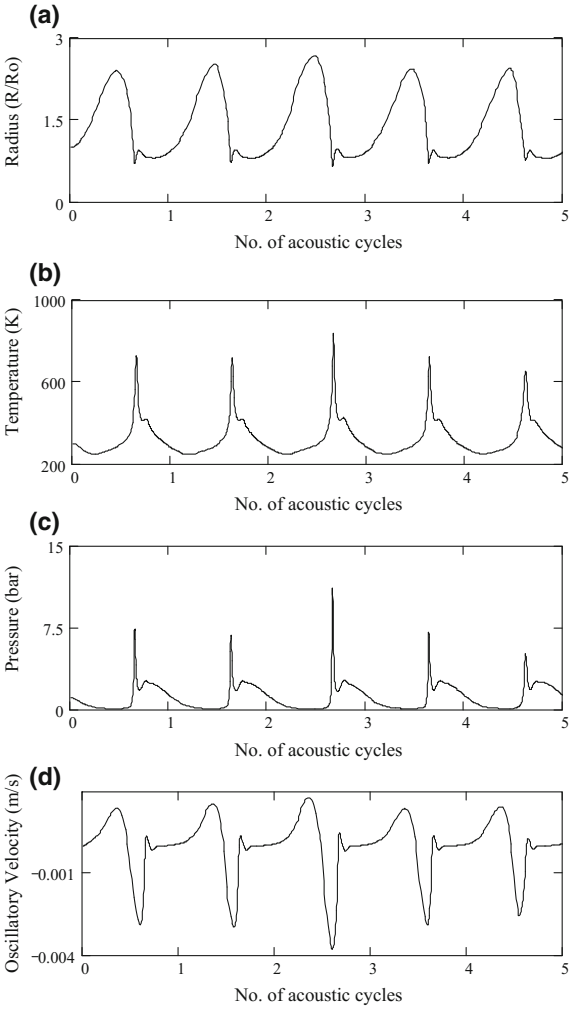

Fig. 3 Simulation results of radial motion of a 10 μm cavitation bubble in oil medium (Reproduced with permission from [42], Copyright © 2009, American Chemical Society)

In the first, second, and third experimental categories, the transesterification reaction was left out of in situ-produced methoxy ions (or methoxy radicals). These methoxy ions were essentially generated from $OH^{\cdot}$ radicals generated by cavitation bubbles. The results of simulations show that no generation of any radical species ($H^{\cdot}$, $OH^{\cdot}$, or $HO_2^{\cdot}$) occurs during transient collapse of argon bubbles in methanol. This essentially rules out in situ generation of methoxide ions. This result points out that the influence of ultrasound and cavitation on the transesterification reaction system has predominantly physical nature, i.e. generation of large interfacial area between oil and methanol due to intense micro-convection.

Table 3 Summary of simulation results

(A) Conditions at the first compression of the cavitation bubble

Parameter	Liquid medium	
	Methanol	Oil
T_{max} (K)	810	727
P_{max} (bar)	1455	7.37
N_{MeOH}	3.88E+011	–
V_{turb} (m/s)	0.0205	0.00277

(B) Equilibrium composition of the cavitation bubble contents in methanol at collapse conditions

Species	Equilibrium composition (mole fraction)
CH_4	7.3213E–01
H_2O	2.2833E–01
H_2	2.0609E–02
CO_2	1.8203E–02
C_2H_6	3.1621E–04
CO	4.1087E–04
CH_3OH	1.5522E–07
C_2H_4	1.2378E–07
CH_3COOH	2.8683E–08
HCOOH	1.3946E–08
H_2CO	2.4576E–08

Reproduced with permission from [42], Copyright © 2009, American Chemical Society

Notations T_{max} Temperature peak reached in the bubble at the time of first collapse; P_{max} pressure peak reached in the bubble at the time of first collapse; N_{MeOH} number of methanol molecules trapped in the bubble at the instance of first collapse; V_{turb} bulk liquid velocity (or the microturbulence velocity) generated by the cavitation bubbles

An interesting trend was seen from the experimental results of the fourth category, the biodiesel yield passing through a maximum for an alcohol to oil molar ratio of 12:1. Moreover, increase in catalyst concentration resulted in higher triglyceride conversion. To explain these trends, we need to analyze the variation in the two principal factors influencing the yield of the reaction, viz., the concentration of methoxide ions and the interfacial area with respect to the alcohol to oil molar ratio and catalyst concentration used in the four sets of experiments in this category. (a) For alcohol/oil molar ratio 6:1, the methanol forms the dispersed phase (20 mL) of the reaction mixture compared to the continuous oil phase (80 mL). Thus, extend of dispersion of methanol in the oil phase decides the availability of interfacial area for the reaction. Due to a high level of microturbulence generated by the cavitation bubbles in methanol in the vicinity of the interface, methanol disperses uniformly in the oil phase. However, due to a small amount of methanol, the RO^- radicals were produced limited. This puts a limit on biodiesel yield. (b) Increasing alcohol/oil

molar ratio to 12:1, the equilibrium of the reaction shifted to produce more RO^- radicals. Greater generation of the RO^- radicals raises the rate of the transesterification reaction. However, dispersion of methanol in oil determined the total interfacial area, as the volume of the methanol was still less (33 mL) compared to the oil (67 mL). Because this dispersion was uniform, the interfacial area for the reaction was large. The highest yield of transesterification reaction was achieved due to combination of favorable factors. (c) For a molar ratio of 16:1, the volume of oil (60 mL) reduces with a corresponding rise in the methanol volume (40 mL). Since the volumes of methanol and oil are now comparable, the interfacial area for the reaction was decided not only by the dispersion of methanol in oil but also the dispersion of oil in methanol. The dispersion of oil in methanol depends on the intensity of microturbulence generated by the cavitation bubbles in oil, located at the interface between two media.

Simulations of the radial motion of the cavitation bubble in methanol and oil were shown in Figs. 2 and 3 respectively. It can be seen that the magnitude of the microturbulence generated by cavitation bubble in oil was very small with velocity ~ 0.3 cm/s, which was an order of magnitude smaller than the velocity in methanol. This was attributed to a high viscosity of oil and low acoustic pressure amplitude sensed by the bubble as a result of high attenuation. Given the large difference in the intensity of microturbulence in methanol and oil, it was obvious that the dispersion of oil in methanol was not as uniform as that of methanol in oil, resulting in lesser interfacial area for the reaction and, hence, reduced yield of biodiesel. (d) For a molar ratio of 24:1, the volumes of oil and methanol become equal (50 mL). With this, the problem of low dispersion of oil becomes more pronounced. In addition, dispersion of methanol in oil may also not be complete due to a rather large volume of methanol. As a result, the interfacial area for the reaction further reduces and so does the overall yield of biodiesel. (e) For all alcohol to oil molar ratios, the yield of the reaction with 1% (w/w) catalyst concentration was higher than 0.5% (w/w) catalyst concentration. This was clearly attributed to the higher production of the RO^- species with a higher concentration of the catalyst. However, the rise in the yield was found to be marginal ($\sim 10\%$) with doubling of the catalyst concentration. This result suggests that the dynamics of the reaction system at catalyst concentration of 1% (w/w) was kinetics (and not mass transfer) limited.

Cavitation phenomenon in oil and methanol phase has different characteristics. As a result of large vapor pressure of methanol, significant evaporation of methanol molecules occurs inside the bubble. Accordingly, the peak temperature and pressure attained during at transient collapse was reduced. The summary of the simulation results has been given in Table 3. Although thermal dissociation of methanol molecules occurs during collapse, the species resulting from this are molecular species such as CH_4, H_2O, H_2 and CO_2. No formation of radical species was seen. This result basically confirmed that intensification of transesterification reaction by ultrasound was due to emulsification effect, which generated enormous interfacial area between oil and methanol phases.

Although cavitation and ultrasound wave phenomenon occurs in both oil and methanol phase, the velocities of micro-streaming and microturbulence are far higher in methanol due to its viscosity being lower than oil. For molar ratio of 6:1, the methanol phase forms the minor fraction of the reaction mixture, as compared with the oil phase. Thus, the dispersion of methanol in oil phase decides the interfacial area for reaction. Due to high level of microturbulence generated by cavitation bubbles in methanol, the dispersion of methanol in oil phase is uniform. However, the production of methoxy (CH_3O^-) ions is limited due to smaller volume of methanol, which places a limit on biodiesel yield.

For alcohol/oil molar ratio of 12:1, formation of methoxide ions was favored due to equilibrium shift towards right hand side. This lead to higher concentration of CH_3O^- resulting in faster kinetics. However, methanol volume was still lesser than oil. This made methanol dispersed phase and oil continuous phase. Intensity of microturbulence and micro-streaming was higher in methanol, which caused uniform dispersion of methanol in oil. This resulted in high interfacial area. Net manifestation of higher CH_3O^- concentration and high interfacial area was larger yield of biodiesel. For alcohol/oil molar ratio of 16:1, oil and methanol volumes in reaction mixture become comparable. In this situation, interfacial area is determined not only by dispersion of methanol in oil, but also vice versa, i.e. dispersion of oil in methanol. However, due to feeble micro-streaming and microturbulence velocities, oil does not get dispersed properly in methanol, resulting in reduced interfacial area. For the highest alcohol/oil molar ratio of 24:1, the effect of weak dispersion of oil was more pronounced resulting in probably the least interfacial area, and thus, slowest kinetics and least biodiesel yield. Thus, Kalva et al. [42] have clearly established the roles of physical and chemical effects of ultrasound and cavitation in alkali-catalyzed transesterification process.

3.1.2: Parker et al. [43] investigated acid catalyzed ultrasonic transesterification of edible grade soybean oil. The major findings of acid catalyzed transesterification study was the reaction mechanism were quite atypical of base catalyzed reaction. Several anomalies were observed when ultrasonic transesterification with acid catalyst was compared to mechanically agitated systems, the anomalies such as the occurrence of reaction at a below atmospheric temperatures (i.e. 15 °C), high reaction rate constants for alcohol ratio of 6:1 despite the high activation energy, and a minimum in reaction rate constant at temperatures in the range of 15–65 °C. These results, when correlated with simulation of cavitation bubble dynamics, revealed interesting physical mechanistic facts of acid–catalyzed transesterification.

The basic chemical mechanisms of base and acid catalyzed transesterification reactions were different [42, 43]. In case of base–catalyzed transesterification, generation of alkoxide anion initiates reaction between alcohol and alkali, whereas in acid-catalyzed transesterification, direct protonation of triglycerides by acid initiates the reaction (Scheme 1). Protonation of triglycerides generates electrophillic center on the carbonyl carbon making it susceptible to nucleophilic attack of methanol. Rate controlling step in acid catalyzed transesterification was probability of interaction between proton in methanol (or aqueous phase) and triglyceride in oil (or organic phase). Acid concentration reduces with increasing alcohol to oil

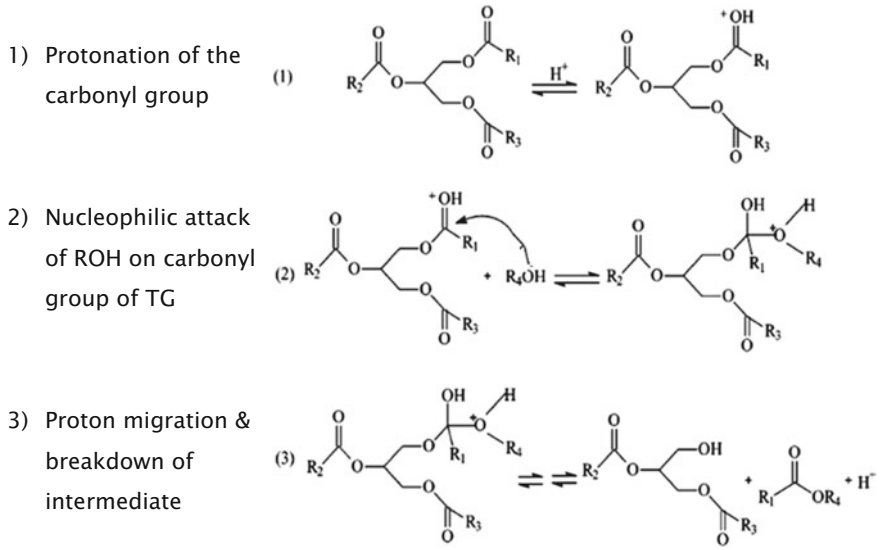

Scheme 1 Chemical mechanism of acid catalyzed transesterification reaction (Reproduced with permission from [1] Copyright © 2015, Springer Science + Business Media Dordrecht)

molar ratio, and so does the probability of interaction between proton and triglyceride. The macroscopic equilibrium constant also shifts towards product. Reduction in the concentration of protons with increasing alcohol ratio results in slowing down of reaction kinetics at any temperature. For the same reason, the highest rate constant and yield was obtained for an alcohol ratio of 6:1, as against 12:1 in case of base–catalyzed process [42]. These results have signified predominant role of intrinsic kinetics of acid catalyzed transesterification, despite elimination of mass transfer barriers due to emulsification and enhancement of interfacial area induced by sonication.

Simulations of cavitation bubble dynamics in methanol reveal that the intensity of the shock waves generated by cavitation bubble at 15 °C was much higher than 25 °C [43]. This essentially means greater emulsification and interfacial area at 15 °C than 25 °C. The emulsification effect overwhelms intrinsic kinetics of transesterification at lower temperature, resulting in higher rate constants at 15 °C than 25 °C. However, at higher temperatures of 45–65 °C, the intrinsic kinetics dominates and higher rate constant than at 15 °C have been obtained. These results have highlighted physical or mechanistic features of ultrasonic biodiesel synthesis. Parkar et al. [43] have also determined the activation energies of transesterification as a function of alcohol to oil molar ratios. Least activation energy of 27.53 kJ/mol was obtained for molar ratio of 12:1. Despite the lowest activation energy (or highest specific rate constant at any temperature), the overall yield and kinetic constant was low for alcohol/oil molar ratio of 12:1 at 15 °C.

3.1.3: Choudhury et al. [44] investigated the mechanistic in ultrasonic biodiesel synthesis were based on statistical design of experiments (DOE) that were coupled with simulation of cavitation bubble dynamics. Box–Behnken statistical design of experiments was employed to optimize the transesterification reaction parameters [44]. The optimization parameters were reaction temperature, alcohol to oil molar ratio and catalyst loading. The transesterification yield was treated as the objective function. Optimization of the process for the highest yield was done through response surface methodology (RSM) using a quadratic model and analysis of variance (ANOVA). The response surface plots resulting from this analysis have been depicted in Fig. 4. Optimum parameters were: Temperature = 62 °C, molar ratio = 10:1 and catalyst loading of 6 wt%. The activation energy at optimum conditions was determined as 82.3 kJ/mol. This was significantly higher than activation energy for homogenous catalyst, which is typically in the range of 20–30 kJ/mol. Transesterification system in the present case was 3-phase heterogeneous (liquid–liquid–solid), with more pronounced mass transfer restrictions than 2-phase (liquid–liquid) system for homogeneous catalyst. The optimum temperature resulted from the RSM analysis was close to boiling point of methanol. At these conditions, very large evaporation of methanol occurred into the bubble, which drastically reduced the intensity of transient collapse of cavitation bubble. The peak temperature reached in the bubble was $\sim$700 K, which is not sufficiently high to generate radical species through thermal dissociation of methanol molecules. The microturbulence generated by cavitation bubble was also less intense. In such situation, the main contribution to the convection in the medium was by micro-streaming process, which is oscillatory motion of fluid elements induced by ultrasound wave propagation. Base catalyst CaO, with hydrophilic surface, preferably stays in the aqueous (or methanol) phase. Generation of methoxy ions in this case is through adsorption of methanol molecules on the catalyst surface, which are transferred to organic phase from interface between phases. Micro-streaming by ultrasound can enhance the rate of adsorption and enhance CH_3O^- production.

Unlike the homogenous base catalyzed process (where high yield of biodiesel have been obtained at ambient temperature); the optimum temperature in the case of heterogeneous base catalyst was 62 °C. This result has essentially indicated that enhancement of mass transfer due to micro-convection generated by ultrasound does not overcome the intrinsic kinetic limitations of the process. This is attributed to high activation energy of the system. However, the optimum alcohol ratio of 10:1 is almost similar to that for the homogenous system (12:1). The explanation for this can be given along similar lines as that for homogenous system. The ANOVA results have indicated strong interactions between effects of all optimization parameters on biodiesel yield. The parameters of catalyst loading and molar ratio and temperature and molar ratio are related through the variation in convection level in the medium, which in turn related to cavitation bubble dynamics and ultrasound wave phenomena. The parameters of catalyst loading and temperature are related through intrinsic kinetics of the process. Impurities in catalyst (such as $CaCO_3$ phase) could have also contributed to a reduction in the yield.

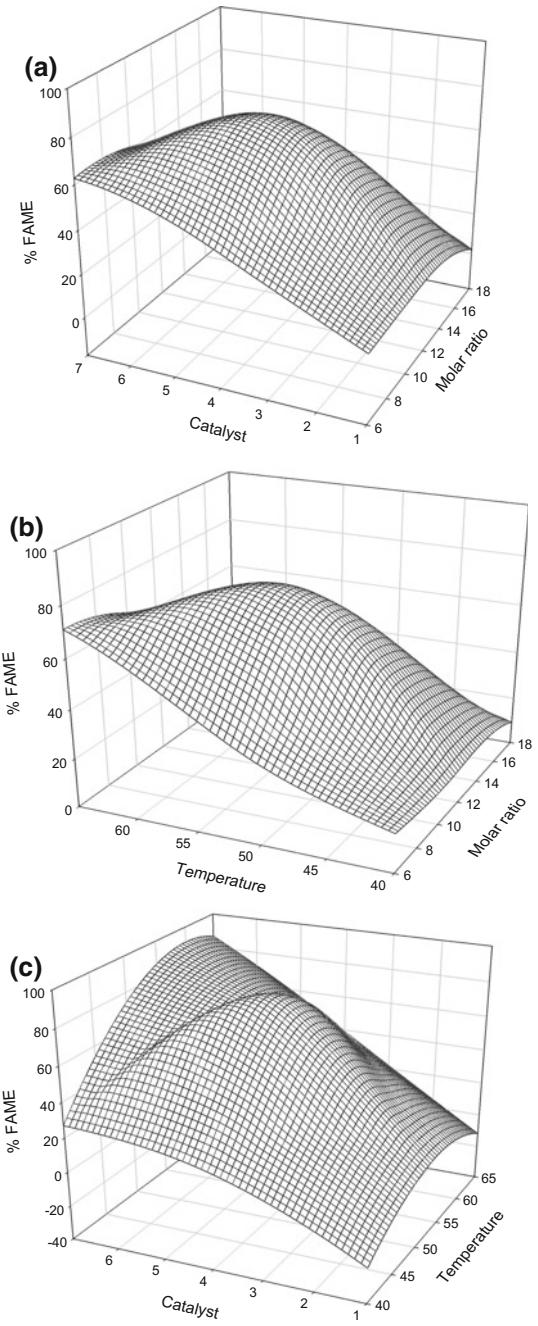

Fig. 4 Response surface plots for percentage of fatty acid methyl ester (FAME) yield as a function of reaction temperature, catalyst loading and methanol-to-oil molar ratio (Reproduced with permission from [44], Copyright © 2014, Elsevier)

3.2 Transesterification of Non-edible Oil

3.2.1: Choudhury et al. [45] have also done mechanistic investigations on acid catalyzed biodiesel synthesis from *Jatropha curcus* oil. The non-edible oil have much higher contents of free fatty acids than conventional refined oils. Therefore, the process was carried out in two stages, viz. esterification of free fatty acids followed by transesterification of triglycerides. The esterification experiments were designed on the results of Deng et al. [46]. The experiments were conducted using mechanical shaking and ultrasound. However, it was found that the time for almost complete esterification (>90%, as indicated by reduction in acid value of oil) was same for both mechanical stirring and sonication. Almost complete reduction of acid value was obtained within 1 h with FAME yield in the range of 17–20%. The important parameters for esterification reaction were alcohol to oil molar ratio and catalyst concentration at a fixed temperature of 65 ± 2 °C with a reaction time of 1 h. Experiments were performed in nine sets, with duplicate runs in each set in order to assess the reproducibility of the results. The acid catalyzed esterification was found to be insensitive to ultrasound irradiation.

Esterified low acid value feedstock was used for transesterification using sonication. Optimization of independent process parameter has been carried out using Box-Behnken statistical design for 3 factors and 3 levels, comprises of 15 combination sets of experiments. The experimental results were complied with diffusion based bubble dynamics model. RSM of the experimental results shows following important results: (a) For experiment with the temperature 85 °C i.e. above optimum, catalyst concentration 6 wt% at optimum, however alcohol/oil molar ratio 4:1 below optimum, and the yield drops to 18%. (b) For experiment with the temperature 70 °C near optimum, catalyst concentration 9 wt% above optimum, and alchol/oil molar ratio 4:1 below optimum, resulted in the yield of 28% only. (c) For experiment with the temperature 70 °C near optimum, catalyst concentration 9 wt% and molar ratio 10:1 above optimum, the yield was relatively higher, i.e., 52.77%. (d) For experiment with the temperature 70 °C near optimum; however, catalyst concentration 3 wt% and molar ratio 4:1 below optimum, again the yield drops to 32%. (e) For experiment with the temperature 55 °C below optimum, catalyst concentration 6 wt% at optimum and molar ratio 10:1 above optimum, and the yield drops to 30.7%. These results revealed that all the three process parameters have strong influence on transesterification reaction.

The kinetic analysis of the transesterification was carried out at the optimum conditions obtained from statistical analysis (RSM). Pseudo 1st order kinetic model was fitted and the activation energy of the reaction system was determined using Arrhenius equation. Activation energy for transesterification reaction was determined as 167.419 kJ/mol. Relatively higher activation energy for homogenous acid catalyzed transesterification (as compared to homogenous base catalyst) results in slower reaction kinetics. Concurrent analysis of experimental and simulation results has revealed important facets of the physical mechanism of the acid catalyzed esterification/transesterification process. The kinetics of esterification reaction was

practically insensitive to sonication. In case of transesterification, intrinsic kinetics plays a predominant role. Simulations of cavitation bubble dynamics have not releaved any sonochemical effect, i.e. formation of any radical species from cavitation bubbles. This essentially means that beneficial effect of ultrasound on the reaction system was through strong micro-mixing and emulsification of oil and alcohol phases [38, 47]. Moreover, the intensity of microturbulence generated by cavitation bubbles was small, and thus, microstreaming by ultrasound mainly contributes to emulsification of oil and alcohol. Due to high viscosity of oil, the intensity of bubble motion was too low to create sufficient convection. In addition, the micro-streaming velocity was also expected to be quite small. Thus, the major contribution to the overall convection in the system was through micro-streaming in methanol.

Assessment of the experimental results corroborates above conjectures. Even for high reaction temperatures (70 or 85 °C), and high catalyst concentration (6 or 9% w/w oil), biodiesel yield was low for smaller molar ratios (4:1). This was attributed to low convection intensity in the medium with low alcohol content, which results in lesser emulsification and lower interfacial area. As a consequence, protonation of carbonyl oxygen of triglyceride was reduced. Quite interestingly, low FAME yield was obtained at 55 °C for alcohol/oil molar ratio of 10:1. This result could possibly be ascribed to dilution of acid concentration in methanol at high molar ratio. Thus, despite higher convection in the reaction system due to larger alcohol content, the net probability of interaction of proton in aqueous phase with carbonyl oxygen could be lower, leading to smaller yield. A rise of catalyst concentration to 9 wt% and temperature to 70 °C almost doubles this yield. These results clearly show the relative influence of mass transfer and intrinsic kinetics on the transesterification reaction system. Mere enhancement of mass transfer with ultrasound was not sufficient to boost the overall kinetics of the process leading to high biodiesel yield. It also depends on factors such as catalyst concentration and temperature that determine the intrinsic kinetics of the reaction. Therefore, for maximum yield of the transesterification process, an overall optimization in terms of all parameters was necessary and mere elimination of mass transfer limitation with sonication will not suffice.

The optimum set of process parameter obtained by the statistical design of experiments was as follows: alcohol/oil molar ratio = 7, catalyst loading = 6 wt%, and reaction temperature = 70 °C. The kinetics of the acid catalyzed transesterification was found to be much slower than base catalyzed process, which is attributed to basic difference in the chemical mechanism of acid and alkali catalyzed transesterification. The transesterification for acid catalyst is initiated by nucleophilic attack of methanol on the protonated carbonyl carbon of triglycerides. Since methanol is a poor nucleophile, its intrinsic reactivity was much less than the methoxide (CH_3O^-) ion, which initiates the transesterification in base catalyzed process. This was essentially manifested in slower kinetics of the reactions. It has been observed from the experimental trends, that enhanced mass transfer with ultrasound was not sufficient to boost the overall kinetics of the process leading to

higher biodiesel yield. Hence, an overall optimization in terms of all parameters was necessary to get high yield of transesterification process.

3.2.2: Choudhury et al. [48] have extended the above theme of two-stage biodiesel synthesis from *Jatropha curcus* oil with acid catalyst in the transesterification step replaced by solid base catalyst. Scheme 2 depicts the chemical mechanism of CaO catalyzed transesterification reaction. The statistical design of experiments resulted optimum set of operating parameters as: alcohol/oil molar ratio = 11, catalyst loading = 5.5 wt% and reaction temperature = 64 °C. The variation on transesterification yield by varying operating parameters were shown in Fig. 5. The X-Ray Diffraction analysis of catalyst powder revealed formation of calcium methoxide $Ca(OMe)_2$ phase, which acts as active sites for transesterification reaction. Activation energy of the ultrasound-assisted transesterification process at optimized conditions found to be 133.5 kJ/mol, and this was attributed to 3 phase heterogeneity of the system. As compared to the previous study of Choudhury et al. [44] using refined soybean oil as a feedstock, which showed an activation energy of 82.3 kJ/mol (the corresponding Arrhenius plot is shown in Fig. 6), ∼50% higher activation energy for *Jatropha curcus oil* could also be attributed to crudeness of oil. The impurities in the oil could poison the catalyst by adsorbing over it and reduces the availability of active sites for the reaction. However, as compared to mechanically stirred system, the ultrasonic system showed ∼30% reduction in activation energy, which could be a consequence of the mass transfer enhancement in the system. The optimum value of alcohol molar ratio of 11 could be justified as follows: For very low catalyst concentration (3 wt%), the amount of methoxy ions generated was less, resulting in lower yields. Although stronger dispersion and emulsification between oil and methanol phases was achieved

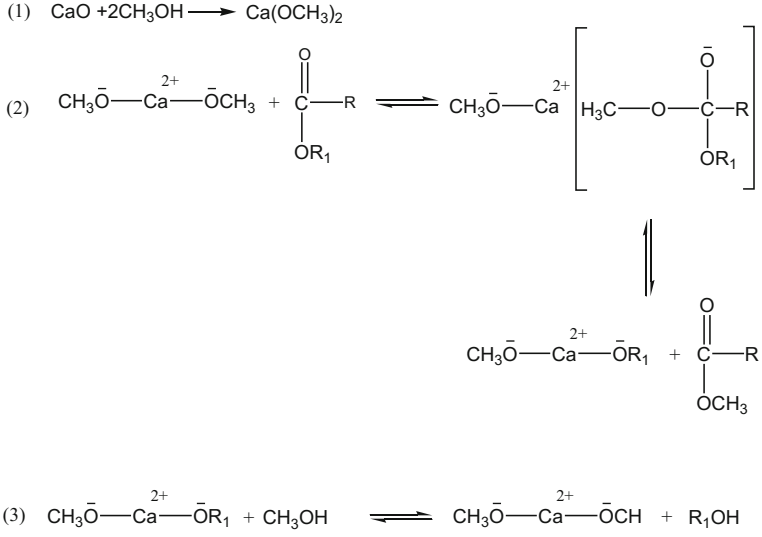

Scheme 2 Proposed chemical mechanism of calcium oxide catalyzed trans-esterification reaction (Reproduced with permission from [48], Copyright © 2014, Elsevier)

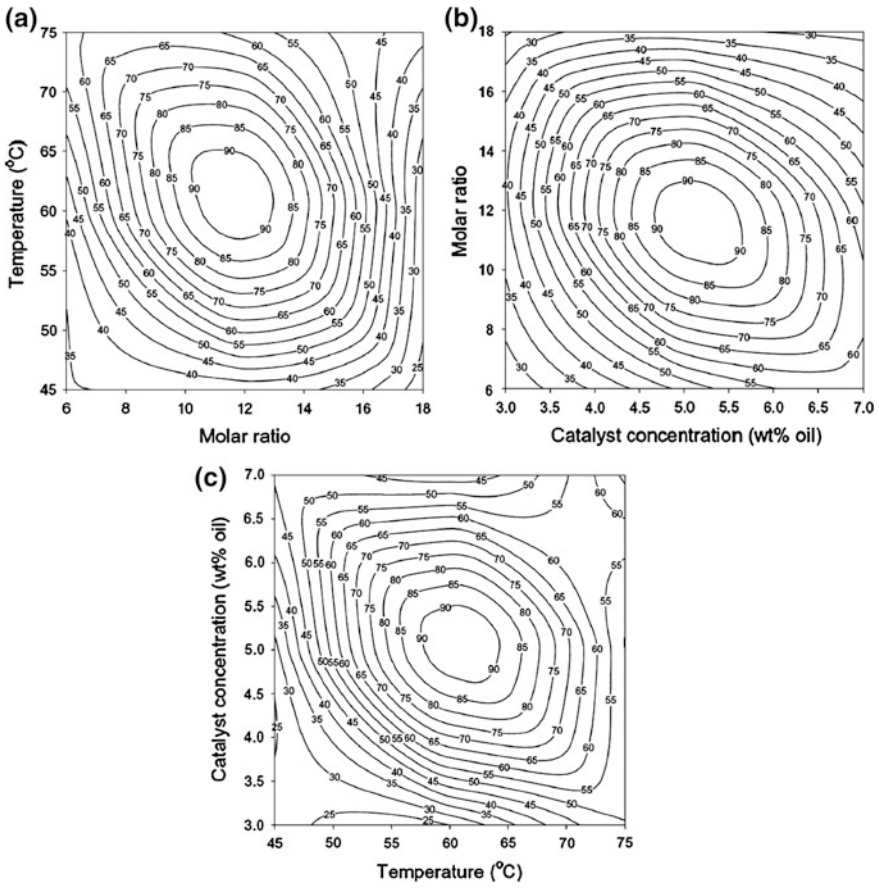

Fig. 5 Contour plots showing variation of transesterification yield (or %FAME yield) as a function of any two experimental parameters. **a** Temperature and molar ratio, **b** molar ratio and catalyst concentration, **c** catalyst concentration and temperature (Reproduced with permission from [48], Copyright © 2014, Elsevier)

at high alcohol molar ratio, the mass transfer resistance for CH_3O^- ions increases. Higher mass transfer resistance can be explained as follows: CH_3O^- ions were generated at the surface of CaO catalyst. The CaO catalyst particles, being hydrophilic in nature, preferentially stay in the methanol phase. As the volume fraction of methanol in the total reaction mixture increases with molar ratio, these ions have to diffuse through larger volume so as to reach the interface and react with triglyceride. For low alcohol molar ratios, the volume fraction of oil in reaction mixture was high and some catalyst particles may also stay in oil phase. The oil can wet the catalyst surface, and hinder adsorption of methanol leading to formation of methoxy ions. Hence, to overcome the mass transfer limitations in 3-phase heterogeneity higher molar ratio of alcohol was required.

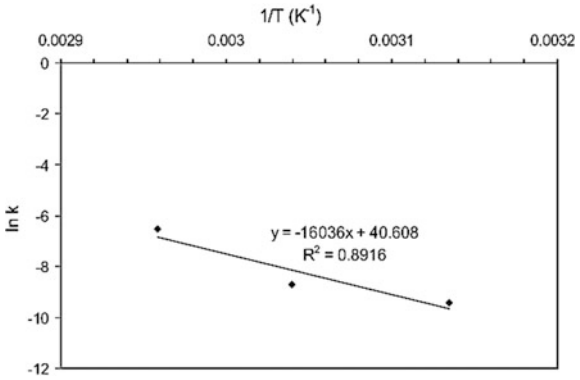

Fig. 6 Arrhenius plot of ln (k) versus 1/T for transesterification reaction considering 3rd order reaction kinetics (with respect to triglyceride) for optimum conditions of methanol to oil molar ratio (11:1) and catalyst concentration (5.5 wt%) as determined by statistical analysis (Reproduced with permission from [48], Copyright © 2014, Elsevier)

3.2.3: Choudhury et al. [49] have also reported a novel single step process for biodiesel synthesis using chlorosulphonic acid as catalyst. The previous process with H_2SO_4 catalyst reported in literature required a two stage approach with separate esterification and transesterification [45]. With the application of chlorosulfonic acid as the catalyst, two steps process was combined in a single step process. The chemical mechanism of this synthesis was shown in Scheme 3. The acid catalyzed esterification of the free fatty acids in *Jatropha curcus* oil releases water, which has serious inhibition effects due to solvation of the protons as well as $CH_3OH_2^+$ (methoxenium) ions. Solvation of the protons reduces their reactivity and accessibility leading to lowering of kinetics. This inhibition was counteracted by chlorosulphonic acid by in-situ removal of water formed during esterification. Water produced in the esterification process reacts with chlorosulfonic acid to produce H_2SO_4. Dissociation of this H_2SO_4 can generate additional protons that catalyze esterification/transesterification reaction. However, generation of H_2SO_4 is accompanied by in-situ removal of water molecules that solvate the H_3O^+ ion and reduce its activity. In this study as well, the statistical design of experiment was used to determine the optimum condition for the highest biodiesel yield. The optimum conditions are: catalyst concentration = 8.358 wt%, alcohol molar ratio = 18:1 and temperature = 60 °C.

The major findings from the optimizations were summarized as follows. The optimum temperature was close to boiling point of methanol, and also that the intensity of transient cavitation was minimal at this temperature, once again demonstrates that the beneficial effect of ultrasound and cavitation on reaction system was merely physical, i.e. emulsification of the phases. The activation energy for the single-step process was determined as 57.3 kJ/mol, which was more than three-fold lower than for H_2SO_4 catalyzed process (i.e. 169 kJ/mol). Choudhury et al. [49] also carried out chlorosulfonic acid catalyzed transesterification in conventional two-step process comprising of esterification and tranesterification. Quite interestingly, the two-step process had 40% less activation energy of 31 kJ/mol. This reduction has been attributed to complete removal of water from reaction system in the two-step process—as compared to single step process, in which some

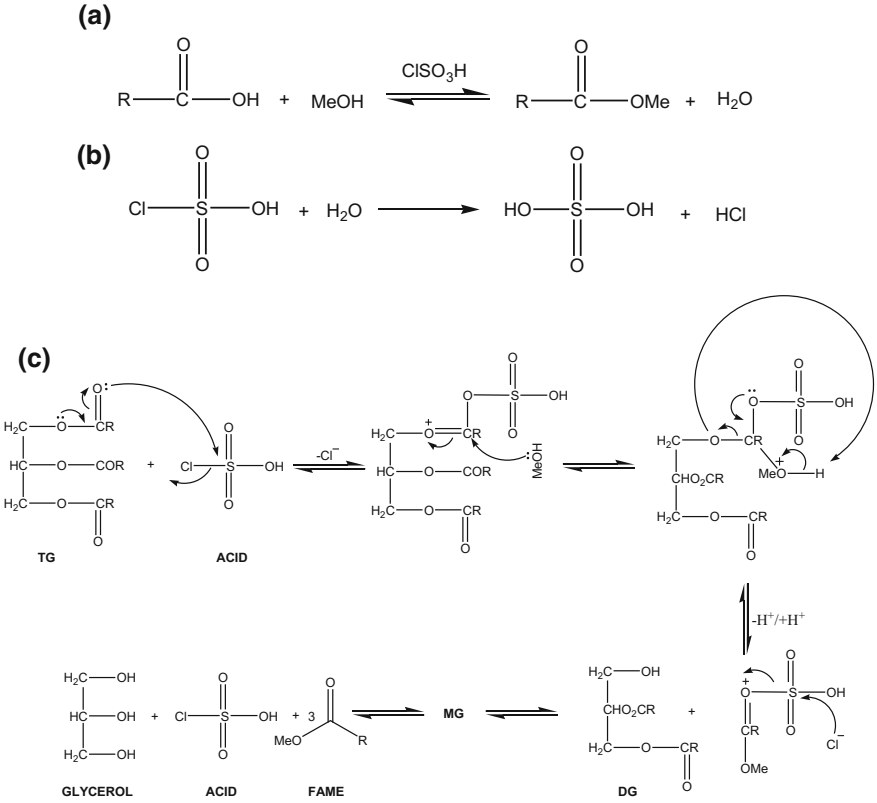

Scheme 3 **a** Reaction of chlorosulfonic acid induced esterification process, **b** removal of water formed during esterification by chlorosulfonic acid, and **c** mechanism of chlorosulfonic acid induced trans-esterification process (Reproduced with permission from [49], Copyright © 2014, Wiley)

trace of water might be left in the system despite the in-situ removal of chlorosulfonic acid, which reduces inhibition effect on the process.

3.3 *Transesterification with Mixed Non-edible Oil Feedstock*

Malani et al. [50] have extended the work to biodiesel production from mixed non-edible oil feedstock in continuous packed bed mode. The approach adopted was two-fold, viz. (1) statistical optimization of the transesterification process in a continuous packed bed reactor with Cu_2O catalyst, coupled with sonication (or

ultrasound irradiation), and (2) kinetic and mechanistic analysis of transesterification process using mathematical model based on Eley–Rideal mechanism. Experiments were conducted in packed bed as well was batch mode using slurry reactor coupled with sonication to get the time dependent profiles of reactants. The experimental data has been fitted to kinetic model to obtain the values of kinetic parameters. Experiments in batch mode with mechanical agitation done to compare the kinetic parameters for sonication and mechanical agitation.

Malani et al. [50] has investigated the mechanistic issues of ultrasound–assisted transesterification process using solid Cu_2O catalyst and mixed feedstock of non-edible oils, which consists of Jatropha oil (15% v/v), castor oil (25% v/v), rubber seed oil (20% v/v), cotton seed oil (25% v/v), waste cooking oil (15% v/v). The optimum conditions for transesterification have been determined using statistical experimental design in packed bed catalytic reactor. The kinetic constants of different steps of transesterification process was determined using kinetic model based on Eley–Rideal mechanism (as depicted in Tables 4 and 5) coupled to time profiles of reactants and products of transesterification in batch slurry reactors.

Table 4 The steps and corresponding kinetic expressions in Eley–Rideal (ER) mechanism of transesterification using a solid heterogeneous catalyst

Step in the mechanism	Chemical equation	Rate expression
1. Methanol adsorption	$* + CH_3OH \leftrightarrows CH_3OH^*$	$r_1 = -k_1[*]_f[CH_3OH]$
2. Transesterification reactions	$CH_3OH^* + T \leftrightarrows D^* + F$	$r_2 = -k_2[T][CH_3OH^*]$
	$CH_3OH^* + D \leftrightarrows M^* + F$	$r_3 = -k_3[D][CH_3OH^*]$
	$CH_3OH^* + M \leftrightarrows G^* + F$	$r_4 = -k_4[M][CH_3OH^*]$
3. Desorption of adsorbed species	$D^* \leftrightarrows D + *$	$r_5 = -k_5[D^*]$
	$M^* \leftrightarrows M + *$	$r_6 = -k_6[M^*]$
	$G^* \leftrightarrows G + *$	$r_7 = -k_7[G^*]$

Symbols * Free catalyst active site, *T* triglyceride, *D* diglyceride, *M* monoglyceride, *G* glycerol, *F* fatty acid methyl ester (biodiesel)

Table 5 The final kinetic rate expressions in Eley–Rideal (ER) mechanism of transesterification using a solid heterogeneous catalyst

Rate of triglyceride consumption	$r_T = \frac{d[T]}{dt} = -\frac{k_2[T]}{1+\frac{k_2[T]}{k_5}+\frac{k_3[D]}{k_6}+\frac{k_4[M]}{k_7}+\frac{k_2[T]+k_3[D]+k_4[M]}{k_1[CH_3OH]}}$
Rate of diglyceride consumption	$r_D = \frac{d[D]}{dt} = -\frac{k_3[D]-k_2[T]}{1+\frac{k_2[T]}{k_5}+\frac{k_3[D]}{k_6}+\frac{k_4[M]}{k_7}+\frac{k_2[T]+k_3[D]+k_4[M]}{k_1[CH_3OH]}}$
Rate of mono-glyceride consumption	$r_M = \frac{d[M]}{dt} = -\frac{k_4[M]-k_3[D]}{1+\frac{k_2[T]}{k_5}+\frac{k_3[D]}{k_6}+\frac{k_4[M]}{k_7}+\frac{k_2[T]+k_3[D]+k_4[M]}{k_1[CH_3OH]}}$
Rate of methanol consumption	$r_{CH_3OH} = \frac{d[CH_3OH]}{dt} = -\frac{k_2[T]+k_3[D]+k_4[M]}{1+\frac{k_2[T]}{k_5}+\frac{k_3[D]}{k_6}+\frac{k_4[M]}{k_7}+\frac{k_2[T]+k_3[D]+k_4[M]}{k_1[CH_3OH]}}$
Rate of glycerol formation	$r_G = \frac{d[G]}{dt} = \frac{k_4[M]}{1+\frac{k_2[T]}{k_5}+\frac{k_3[D]}{k_6}+\frac{k_4[M]}{k_7}+\frac{k_2[T]+k_3[D]+k_4[M]}{k_1[CH_3OH]}}$
Rate of FAME formation	$r_F = \frac{d[F]}{dt} = \frac{(k_2[T]+k_3[D]+k_4[M])}{1+\frac{k_2[T]}{k_5}+\frac{k_3[D]}{k_6}+\frac{k_4[M]}{k_7}+\frac{k_2[T]+k_3[D]+k_4[M]}{k_1[CH_3OH]}}$

The batch experiments were performed at optimum conditions obtained from statistical design of experiments (DoE): alcohol/oil molar ratio = 10.6, temperature = 62.5 °C, catalyst concentration = 7.25 wt% oil. The results revealed that adsorption of methanol was the slowest and rate determining step of transesterification process. Sonication enhanced the kinetics of reaction steps of transesterification process, but its effect on methanol adsorption on Cu_2O catalyst was adverse. The activation energy of overall transesterification process was found to be 90.14 kJ/mol; while, the sum total of activation energies of the three reaction steps of triglyceride conversion (i.e. r_2–r_4) was 40.98 kJ/mol. These results essentially point to strong mass transfer influence on Cu_2O–catalyzed transesterification process, even in presence of sonication. The adsorptive mass transfer of methanol to catalyst sites was not enhanced by microturbulence generated by sonication. Two probable causes leading to this effect were: discrete and intermittent nature of acoustic (or shock) waves generated by the transient cavitation, and secondly, the high temperature of reaction that offsets the methanol adsorption on catalyst free sites.

4 Conclusions and Perspectives

The potential of biodiesel as alternate renewable liquid transportation fuel is well demonstrated. The commercial production of biodiesel would require efficient technologies for the basic esterification/transesterification reactions, which should also be flexible in terms of feedstock and catalyst. The basic reaction system of biodiesel synthesis has heterogeneous character with mass transfer limitations. With use of a solid catalyst for avoiding contamination of the glycerol side product, the mass transfer limitations become even predominant. In order to have sufficiently fast kinetics in such processes that would increase productivity, efficient methods of introduction of energy in the system are required that overcome the mass transfer barriers. Ultrasound is a potential technology for efficient introduction of energy into the reaction system on extremely small temporal and spatial scales. Although ultrasound has been demonstrated to intensify both homogeneous and heterogeneous biodiesel processes, the basic physical mechanism of the process intensification has remained largely unexplored. In order to have efficient design and scale-up of the ultrasound-assisted biodiesel processes, it is utmost essential to establish the basic physical mechanism of the process. In this chapter, we have presented a review of our studies in discerning the physical mechanism of the ultrasound-assisted biodiesel process. Our analysis has clearly established that physical effect of generation of strong micro-convection in the reaction system plays crucial role in enhancement of the biodiesel yield through elimination of the mass transfer barriers. Moreover, for solid catalyzed reaction systems, despite intense micro-convection in the system, the intrinsic kinetics of the reaction still play a dominant role. Quite interestingly, these conclusions are found to hold true for a wide variety of reaction systems employing different edible and non-edible feedstocks and both homogeneous and heterogeneous catalysts. The results

presented in this chapter can form useful guidelines for development and optimization of large scale processes for ultrasound-assisted biodiesel. These results are also expected to give crucial inputs for further research in ultrasound-assisted processes for biodiesel synthesis.

References

1. Moholkar VS, Choudhury HA, Singh S, Khanna S, Ranjan A, Chakma, S Bhasarkar JB (2015) Physical and chemical mechanisms of ultrasound in biofuel synthesis. In: Fang Z, Smith RL, Qi X (eds) Production of biofuels and chemical with ultrasound, biofuels and biorefineries series, vol. 4. Springer Science + Business Media, Dordrecht, pp 35–86
2. Borah AJ, Singh S, Goyal A, Moholkar VS (2016) An assessment of the potential of invasive weeds as multiple feedstocks for biofuel production. RSC Adv 6(52):47151–47163
3. Ranjan A, Singh S, Malani RS, Moholkar VS (2016) Ultrasound-assisted bioalcohol synthesis: review and analysis. RSC Adv 6(70):65541–65562
4. Gerpen JV (2005) Biodiesel processing and production. Fuel Process Technol 86:1097–1107
5. Ma F, Hanna MA (1999) Biodiesel production: a review. Bioresour Technol 70(1):1–5
6. Kumar M, Sharma MP (2015) Assessment of potential of oils for biodiesel production. Renew Sustain Energy Rev 44:814–823
7. Suslick KS (1988) Ultrasound: its physical, chemical and biological effects. VCH, New York
8. Hart EJ, Henglein A (1985) Free radical and free atom reactions in the sonolysis of aqueous iodide and formate solutions. J Phys Chem 89(20):4342–4347
9. Hart EJ, Henglein A (1987) Sonochemistry of aqueous solutions: hydrogen–oxygen combustion in cavitation bubbles. J Phys Chem 91:3654–3656
10. Leighton TG (1994) The acoustic bubble. Academic Press, San Diego
11. Mason TJ, Lorimer JP (2002) Applied sonochemistry: the uses of power ultrasound in chemistry and processing. Wiley–VCH, Coventry
12. Shah YT, Pandit AB, Moholkar VS (1999) Cavitation reaction engineering. Plenum Press, New York
13. Atchley AA, Prosperetti A (1989) The crevice model of bubble nucleation. J Acoust Soc Am 86:1065–1084
14. Young FR (1989) Cavitation. McGraw Hill, London
15. Flynn HG (1964) Physics of acoustic cavitation in liquids. In: Mason WP (ed) Physical Acoustics. Academic Press, New York, pp 57–172
16. Rayleigh L (1917) On the pressure developed in a liquid during the collapse of spherical cavity. Phil Mag 34:94–98
17. Plesset MS (1949) Dynamics of cavitation bubbles. J Appl Mech (Trans. ASME) 16:277–282
18. Noltingk BE, Neppiras EA (1950) Cavitation produced by ultrasonics. Proc Phys Soc B63:674–685
19. Poritsky H (1952) The collapse or growth of a spherical bubble or cavity in a viscous fluid. In: Sternberg E (ed) Proceedings 1st national congress on theoretical and applied mechanics, pp 813–821
20. Gilmore FR (1954) Hydrodynamic Laboratory Report. California Institute of Technology, 26–4
21. Kirkwood JG, Bethe HA (1942) The pressure wave produced by an under water explosion. Office of Science Research and Development, Rep 558
22. Keller JB, Kolodner II (1956) Damping of underwater explosion bubble oscillations. J Appl Phys 27:1152–1161
23. Keller JB, Miksis MJ (1980) Bubble oscillations of large amplitude. J Acoust Soc Am 68:628–633

24. Prosperetti A, Lezzi A (1986) Bubble dynamics in a compressible liquid. Part 1. First order theory. J Fluid Mech 168:457–477
25. Colussi AJ, Weavers LK, Hoffmann MR (1998) Chemical bubble dynamics and quantitative sonochemistry. J Phys Chem A 102(35):6927–6934
26. Lofstedt R, Weninger K, Puttermann SJ, Barber BP (1995) Sonoluminescing bubbles and mass diffusion. Phys Rev E 51:4400–4410
27. Barber BP, Hiller RA, Lofstedt R, Putterman SJ, Weninger KR (1997) Defining the un-knowns of sonoluminescence. Phys Rep 281:65–143
28. Krishnan SJ, Dwivedi P, Moholkar VS (2006) Numerical investigation into the chemistry induced by hydrodynamic cavitation. Ind Eng Chem Res 45:1493–1504
29. Storey BD, Szeri AJ (2000) Water vapor, sonoluminescence and sonochemistry. Proc R Soc Lond Ser A 456:1685–1709
30. Storey BD, Szeri AJ (2001) A reduced model of cavitation physics for use in sonochemistry. Proc R Soc Lond Ser A 457:1685–1700
31. Eames IW, Marr NJ, Sabir H (1997) The evaporation coefficient of water: a review. Int J Heat Mass Transfer 40:2963–2973
32. Toegel R, Gompf B, Pecha R, Lohse D (2000) Does water vapor prevent upscaling sono-luminescence? Phys Rev Lett 85:3165–3168
33. Toegel R (2002) Reaction diffusion kinetics of a single sonoluminescing bubble. Ph.D. Dissertation, University of Twente, Netherlands
34. Hirschfelder JO, Curtiss CF, Bird RB (1954) Molecular theory of gases and liquids. Wiley, New York
35. Reid RC, Prausnitz JM, Poling BE (1987) Properties of gases and liquids. McGraw Hill, New York
36. Condon EU, Odishaw H (1958) Handbook of physics. McGraw Hill, New York
37. Crank J (1975) The mathematics of diffusion. Clarendon Press, Oxford
38. Brennen CE (1995) Cavitation and bubble dynamics. Oxford University Press, Oxford
39. Kolb J, Nyborg WL (1956) Small scale acoustic streaming in liquids. J Acoust Soc Am 28:1237–1242
40. Nyborg WL (1958) Acoustic streaming near a boundary. J Acoust Soc Am 30:329–339
41. Davis SL Vibrational modes of methanol. http://classweb.gmu.edu/sdavis/research/modes.htm. Accessed May 2000
42. Kalva A, Sivasankar T, Moholkar VS (2009) Physical mechanism of ultrasound–assisted synthesis of biodiesel. Ind Eng Chem Res 48:534–544
43. Parkar PA, Choudhary HA, Moholkar VS (2012) Mechanistic and kinetic investigations in ultrasound assisted acid catalyzed biodiesel synthesis. Chem Eng J 187:248–260
44. Choudhury HA, Chakma S, Moholkar VS (2014) Mechanistic insight into sonochemical biodiesel synthesis using heterogeneous base catalyst. Ultrason Sonochem 21:169–181
45. Choudhury HA, Malani RS, Moholkar VS (2013) Acid catalyzed biodiesel synthesis from Jatropha oil: mechanistic aspects of ultrasonic intensification. Chem Eng J 231:262–272
46. Deng X, Fang Z, Liu YH, Yu CL (2011) Production of biodiesel from Jatropha oil catalyzed by nanosized solid basic catalyst. Energy 36(2):777–784
47. Colussi AJ, Hoffmann MR (1999) Vapor supersaturation in collapsing bubbles: relevance to mechanisms of sonochemistry and sonoluminescence. J Phys Chem A 103:11336–11339
48. Choudhury HA, Goswami PP, Malani RS, Moholkar VS (2014) Ultrasonic biodiesel synthesis from crude Jatropha curcas oil with heterogeneous base catalyst: mechanistic insight and statistical optimization. Ultrason Sonochem 21:1050–1064
49. Choudhury HA, Srivastava P, Moholkar VS (2014) Single-step ultrasonic synthesis of biodiesel from crude Jatropha curcas oil. AIChE J 60:1572–1581
50. Malani RS, Patil S, Kuldeep, Chakma S, Goyal A, Moholkar VS (2016) Mechanistic analysis of ultrasound–assisted biodiesel synthesis with Cu_2O catalyst and mixed oil feedstock using continuous (packed bed) and batch (slurry) reactors (communicated)

Thermo-Chemical Ethanol Production from Agricultural Waste Through Polygeneration: Performance Assessment Through a Case Study

Kuntal Jana and Sudipta De

Abstract Substitution of fossil fuels by biofuels over a planned period is an imperative need to meet the energy demand in future with minimum possible environmental impact. Biofuels from food stuff may lead to conflict between energy and food security. However, producing biofuel (say, ethanol) from agricultural waste (say, rice straw) in thermo-chemical process may be a sustainable option through recycling of waste. But energy requirement for this process is significantly higher and independent production of ethanol may not be economically feasible. However, suitable integration of this ethanol production through an efficiently integrated multi-utility system called polygeneration may be economically feasible with low impact on the environment. This has been explored through a case study with thermodynamic, economic and environmental performance assessment. Results show sustainability of such a process with acceptable performance from multidimensional viewpoints.

1 Introduction

Energy is the vital resource for civilization and improvement of living standard of any society. Often per capita energy consumption is considered as the indicator of living standard. Over several decades, fossil fuels have catered to this demand [1]. However, the impact on environment due to energy generated from fossil fuels is also critical. The climate change problem has emerged as the greatest threat to future survival of living species on earth, including human being [2]. Major source of green house gases causing this climate change are fossil fuels that have been used over a long period for rapid industrial and economic growth and improvement of living standard. The concept of 'sustainability' has eventually evolved. This means

K. Jana · S. De (✉)
Department of Mechanical Engineering, Jadavpur University, Kolkata 700032, India
e-mail: de_sudipta@rediffmail.com

K. Jana
e-mail: kuntaljana@gmail.com

A.K. Agarwal et al. (eds.), *Biofuels*, Green Energy and Technology,
DOI 10.1007/978-981-10-3791-7_8

to maintain the living standard with possible future continuation of it even with limited resources and ever increasing population. Present challenge of the energy technologists is to develop sustainable options to meet energy demand over a long period in the future [3]. Use of fossil fuels has to be replaced by alternatives over a reasonable period for future sustainability. Exploring alternative fuels for meeting energy demand is the key issue in this effort.

Biofuels are those which are from any living material and have useful heat energy that can be used substituting fossil fuels [4]. Initially biofuels were produced from agricultural products which were used as food [5]. Though these biofuels have the potential of reduced carbon emission, a serious conflict between food and energy securities emerged for such biofuels. These first generation biofuels thus found to be not sustainable in the long run. 'Waste-to-energy' is considered to be a very good sustainable option if it can be implemented in an economically feasible and environmentally benign way [6]. Ethanol has several usages. It can also be used as fuel. Producing ethanol from agricultural waste can be a sustainable option. However, the thermo-chemical process of waste-to-ethanol involves several steps requiring energy inputs both in the form of heat and work. Thus, the independent process of producing ethanol from agricultural waste may not be cost effective. If this can be integrated in a multiple utility output system formally called 'poly-generation', the process may be economically feasible with less environmental impact [7].

2 Types and Sources of Biomass

Biomass is any matter from plant or animals which is living or was alive a short time ago. It includes plants, organic waste, wood, animals, humans, marine life, etc. Before the invention of fossil fuels, biomass was used for heating, cooking, etc. Still, many developing countries use biomass for cooking in open burner though it causes health hazards and environmental degradation.

Recently, importance of biomass is increasing due to its use as 'carbon neutral' energy source. Biomass is considered as renewable resource because in a typical time-scale for human use, it can be regenerated within the time scale. Regeneration or growing of biomass occurs through photosynthesis process. In the photosynthesis process, solar energy is stored in the form of chemical energy in the plant as shown by the following:

$$6CO_2 + 6H_2O \underset{[sunlight,\, chlorophyll]}{\longrightarrow} C_6H_{12}O_6 + 6O_2, \quad \Delta G^0 = 480\text{kJ/mol} \qquad (1)$$

Plants capture CO_2 from air during their growth phase and emit CO_2 to the atmosphere during the combustion process of biomass. Hence, it is generally called as 'carbon neutral' fuel, after neglecting the soil carbon balance. Apart from its

heating value, biomass is also a good source of carbon and hydrogen. Hence, it can be used for secondary fuel production.

Biomass can be classified in different ways. On the basis of its source, it can be of two types, i.e., (a) farm products and (b) ligno-cellulosic materials. These can be used as a source of synthetic fuels. Biomass available from farms like corn, sugar cane, sugar beet, wheat, etc. may produce ethanol; rape seed, soybean, palm or sunflower seed, jatropha, etc. may produce biodiesel. Ligno-cellulosic material, e.g., straw or cereal plants, husk, wood, etc. have the potential of producing ethanol, bioliquid and synthetic gas. However, depending on the source of its availability, it can be classified as follows:

- Agricultural biomass: rice straw, wheat straw, etc.
- Forest residues: pine, oak, eucalyptus, etc.
- Biomass of food processing industry: sugarcane bagasse, coconut shell, rice husk, etc.
- Urban solid wastes e.g. vegetables, municipal solid wastes, etc.

As mentioned above, most of the farm products used for synthetic fuels are human foods. Hence, bioenergy using farm products has the controversy due to food security issues. Many developing countries like India with large populations and finite fertile land cannot afford these products for secondary energy, though India has a huge amount of ligno-cellulosic biomass from agricultural waste. An estimated 164.5 million metric tonnes of surplus crop residue were available in 2007–08. This was 26.4% of overall biomass generation [8]. Thus, proper technologies for utilization of these wastes as energy resources, increase the energy security of India. It is not only applicable for India but also all over the world without affecting the food security. Biomass can also produce chemicals such as methanol, fertilizer, synthetic fiber, etc.; secondary energy such as heat, electricity; transportation fuels such as gasoline, biodiesel.

3 Logistics and Handling of Agricultural Waste

Unlike fossil fuels, logistics of biomass is very critical for successful long-run operation of biomass based energy system. First of all, supply of biomass should be continuous and sufficient throughout the year for uninterrupted operation. Also cost and emission related to transportation have serious impacts on overall performance of the plant. Hence, the location of the plant should be optimized by considering the availability of biomass and its distribution area. It is even more critical for small-scale distributed plant. However, energy density of biomass is lower than that of fossil fuels. Hence, mass of biomass transportation required for same utility is generally higher. Also it is difficult to handle due to its fibrous and non-spherical nature. In Fig. 1, different steps of logistic and handling of agricultural waste (e.g. rice straw) are shown. Firstly, rice straw is collected from the paddy field. Then it is

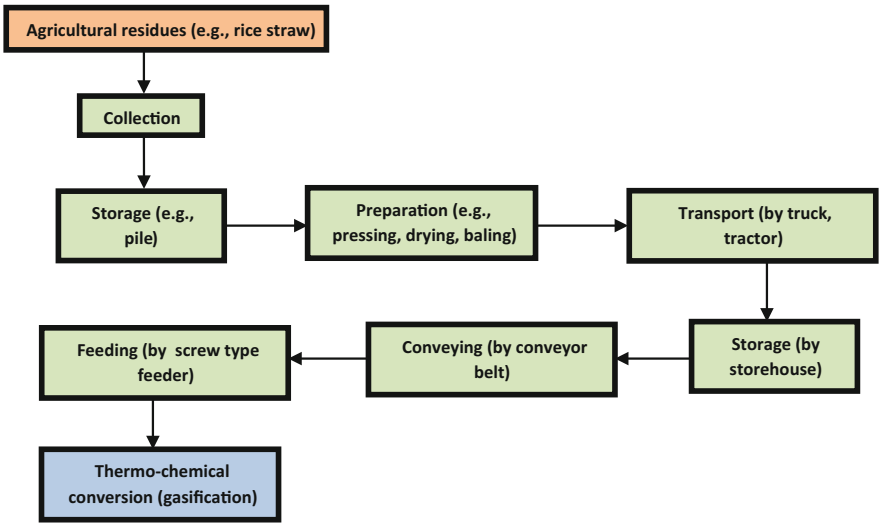

Fig. 1 Schematic of logistic and handling of agricultural waste

stored for a short time in the form of a pile. Drying and pressing of straw are done to reduce the volume of biomass. Straw is baled in cylindrical form for handling and transportation. After that it is transported to the storehouse. Then biomass is fed to the gasifier through different types of feeding systems e.g. conveyor belt.

4 Conversion of Biomass

Biomass is usually available in nature in rather inconvenient form for energy conversion using existing technologies. Hence, biomass needs to be converted to gaseous or liquid fuels for use in conventional energy conversion devices. Conversion of biomass to liquid or gaseous fuels can be achieved by two fundamental ways—(a) bio-chemical and (b) thermo-chemical. These two processes may be executed in different ways as shown in Fig. 2.

In presence of bacteria or enzymes, large biomass molecules are converted into small molecules in bio-chemical route. It is significantly slower than thermo-chemical conversion and no external heat is required. The main products of digestion are methane and CO_2 with solid and liquid wastes. In this process, bacteria take oxygen from biomass. During the fermentation process, alcohols are produced in the presence of bacteria. In thermo-chemical process, biomass is initially converted to synthetic gas. This gas is further treated or synthesized for chemicals or power generation. In this chapter, thermo-chemical conversion of biomass and also gasification is considered as the means of conversion of biomass into synthetic gas.

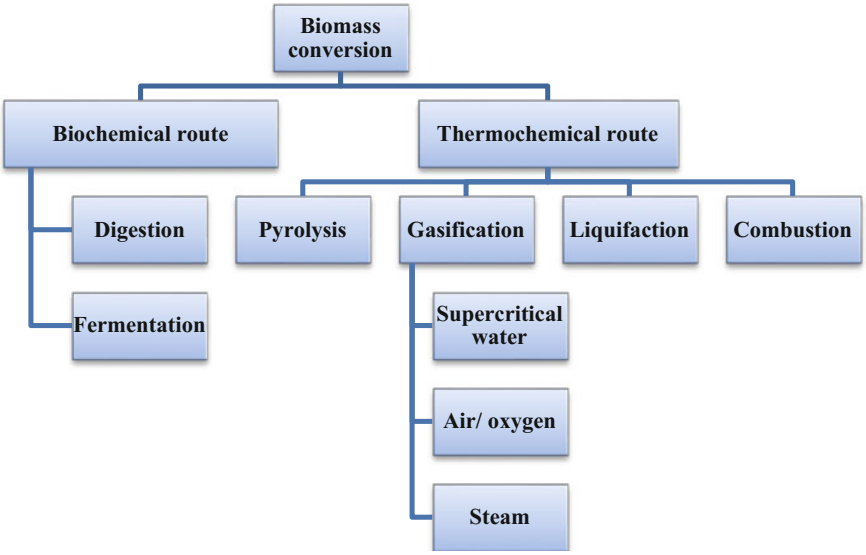

Fig. 2 Conversion routes of biomass into fuels, gases or chemicals

5 Biomass to Thermo-Chemical Ethanol

To produce thermo-chemical ethanol from biomass, gasification route is a possible option. Syngas produced through gasification is processed for alcohol synthesis. Then ethanol is separated. A brief discussion over this topic is given below.

5.1 Gasification

Gasification is the process of thermo-chemical conversion of solid/liquid carbonaceous fuels to synthetic gas with the useful heat value [9]. It is achieved by partial oxidation of fuel at atmospheric pressure or higher than that and at a temperature above ambient as shown in Fig. 3. During the biomass gasification process, biomass is partially oxidized by oxygenating agent (air, steam, oxygen) and produces hot syngas that consists of H_2, CO, CO_2 etc. This hot gas is quenched by water. Then it is cleaned and conditioned according to the requirement of downstream process. In gas cleaning process tar is removed to use the syngas smoothly in downstream processes. Acid gas removal unit may be used additionally for removal of CO_2 and sulfur.

Following physical, chemical and thermal processes occur sequentially or simultaneously within the gasifier depending on the type of gasifier.

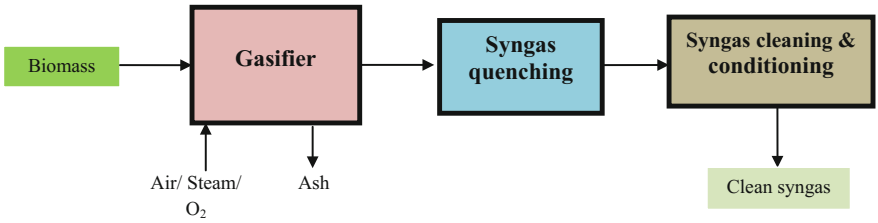

Fig. 3 Basic schematic of gasification process

Drying is the process by which moisture of moist feedstock (biomass) is separated by applying heat at a lower temperature.

$$\text{Moist feedstock} + \text{Heat} = \text{Dry feedstock} + H_2O$$

Then devolatilization of biomass takes place. In this process volatile matter (hydrocarbon with lower molecular weight) is liberated from the dry feedstock by applying heat. Char is produced as a residue of the devolatilization process.

$$\text{Dry feedstock} + \text{Heat} = \text{Char} + \text{volatiles}$$

During the gasification reactions, carbon and hydrogen content of the char is partially oxidized by steam or air. Syngas is produced in the forms of a mixture of gases like CO, CO_2, CH_4, H_2, H_2O. This is a chemical conversion process and reactions are exothermic. Reactions during the gasification process are shown below.

$C + H_2O + \text{Heat} \leftrightarrow CO + H_2$	Water gas reaction
$C + CO_2 + \text{Heat} \leftrightarrow 2CO$	Boudouard reaction
$C + 2H_2 \leftrightarrow CH_4 + \text{Heat}$	Methanation reaction
$CO + 3H_2 + \text{Heat} \leftrightarrow CH_4 + H_2O$	Steam methane reforming
$CO + H_2O + \text{Heat} \leftrightarrow H_2 + CO_2$	CO shift reaction
$C + O_2 \leftrightarrow CO_2 + \text{Heat}$	Combustion of char
$2C + O_2 \leftrightarrow 2CO + \text{Heat}$	Partial combustion of char
$2H_2 + O_2 \leftrightarrow 2H_2O + \text{Heat}$	Hydrogen combustion
$2N_2 + 3H_2 \leftrightarrow 2NH_3$	NH_3formation
$H_2 + S \leftrightarrow H_2S$	H_2S formation

During the gasification process, some portion of char ($\sim 2\%$) is lost through ash. Sometimes it is recycled back to the gasifier. Dust particles from syngas are removed by cyclone separation. However, the type of gasifier should be chosen according to the type of biomass input and required specification of the product gas. In general, there are three types of gasifiers available, i.e., fixed bed, fluidized bed

and entrained flow gasifier. Downdraft and updraft gasifiers are the two types of fixed bed gasifier. Depending on the capacity, operating conditions and characteristics of the biomass, gasifiers are selected.

5.2 Syngas Processing

Gasification at elevated temperature reduces the yield of tar formation. Hence, post-processing of syngas is minimized for treatment of tar. After gasification and before entering to the ethanol synthesis tower, syngas needs to be treated as shown in Fig. 4. Firstly, it is cleaned for ammonia and other impurities. Then water gas shift reaction is required to achieve the desired H_2 and CO ratio (i.e. 2:1) for ethanol synthesis [10]. For sour water gas shift (WGS) reaction, separation of H_2S is not required. Otherwise, H_2S is separated before the water gas shift reactor, depending on the catalyst used for WGS reaction. In this case, WGS reactor operates at a pressure of 4 MPa. Hence, compression of syngas is necessary before WGS. Following is the water gas shift reaction:

$$CO + H_2O \leftrightarrow CO_2 + H_2 \quad \Delta H_{298} = 41.0 \text{ kJ/mol} \tag{2}$$

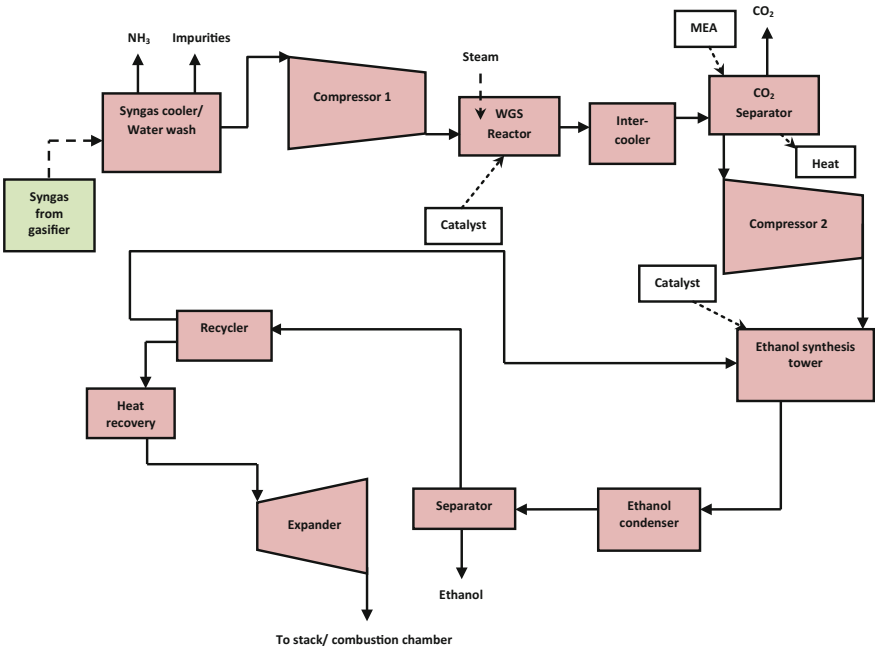

Fig. 4 Schematic of thermo-chemical ethanol production [16]

Conversion percentage of CO is designed according to the desired ratio. For WGS reaction, external input of steam is required depending on the percentage of H_2O in the syngas. After WGS, concentration of CO_2 increases. This CO_2 is separated by an absorption based system using mono-ethanol amine (MEA) or by adsorption based system. However, separation process requires reboiler heating in stripper column. Before entering to the carbon capture process, heat generated in the exothermic WGS reaction is removed/recovered. Then syngas containing N_2 (for gasification with air), CO and H_2 enters to the ethanol synthesis tower. The ethanol synthesis tower is maintained at 9.6 MPa pressure [11]. Hence, syngas is compressed before entering to the ethanol synthesis process and it requires a significant amount of power.

5.3 *Ethanol Synthesis and Separation*

For ethanol synthesis different types of catalyst (e.g. MoS_2 based, Rh based) are used according to the desired product and conversion rate. Direct conversion of syngas to ethanol, i.e., hydrogenation of CO, is highly exothermic as shown below [10]

$$2CO + 4H_2 \leftrightarrow C_2H_5OH + H_2O \quad \Delta H_{298} = -255.7\,\mathrm{kJ/mol} \tag{3}$$

There are many other side reactions during the ethanol synthesis process. To get the desired product, selection of suitable catalyst is important. Other higher alcohols are also produced during ethanol synthesis (like propanol (C_3H_7OH), butanol (C_4H_9OH) and pentanol ($C_5H_{11}OH$)). These alcohols act as excellent additives with gasoline for internal combustion engines.

At the exit of ethanol synthesis reactor, unconverted gases, alcohols (ethanol, methanol, and higher alcohols), and water are obtained. Unconverted gases are separated by pressure reduction in ethanol condenser. The remaining liquid is separated in distillation columns into ethanol, methanol, higher alcohols, and water, which requires additional energy but in the form of heat. A part of the unconverted gases can be used for combustion whereas the remaining part is recycled back to the ethanol synthesis tower.

6 Process Configurations

In this thermo-chemical ethanol production process, heat and materials are lost in many components. Due to different exothermic reactions (as discussed previously), heat is available at different temperatures. In ethanol production process, significant amount of power is consumed during compression of the syngas. The waste heat can be utilized and power can be generated within an efficiently integrated system. Also production of other utilities from this integrated system may influence the

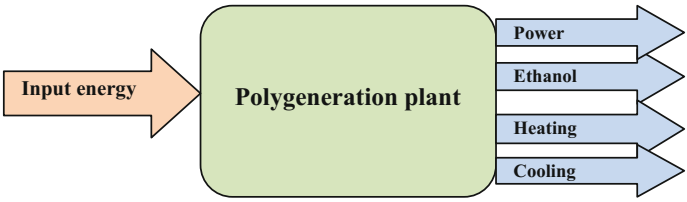

Fig. 5 Basic concept of a polygeneration

economic and environmental performance of the plant. Hence, there is a significant scope to increase the energy efficiency through proper system integration. This system integration can be obtained through polygeneration (Fig. 5).

6.1 Polygeneration

When multiple utilities are produced in a single plant that is called polygeneration. Input energy sources may be single or multiple. In polygeneration, multiple outputs are obtained through process integration. Depending on the utility demands at the place of operation, outputs of polygeneration may be energy services, synthetic fuels or other types of utilities like potable water etc. [12]. However, proper integration of processes is critical to increase energy efficiency and flexibility of the system. Output amounts can be adjusted according to the demand. Also the economic performance of the polygeneration plant improves due to the production of multiple utilities. Polygeneration also reduces waste and emission to the environment. Decentralized polygeneration in remote areas also increases energy access to rural people [13]. For coal and biomass based polygeneration, capture of CO_2 may be integrated to reduce the greenhouse gas emission. The available waste heat of the system can be utilized for this carbon capture. This kind of polygeneration reduces the energy penalty of GHG mitigation.

6.2 Ethanol Production Through Polygeneration—A Case Study

For this study, rice straw is utilized as the source of energy input to the polygeneration plant. Rice straw has useful calorific value to be used as an energy resource though there are some serious challenges during gasification. Thermo-chemical properties of rice straw are shown in Table 1. Different units of polygeneration are shown in Fig. 6. The proposed polygeneration consists of syngas production by gasification unit, combined cycle gas turbine (CCGT) for power generation, CO_2 separation unit using MEA, ethanol production unit, heat recovery and ammonia

Table 1 Feedstock properties and ultimate and proximate analyses (mass percent) (dry basis)

	Rice straw
Higher calorific value (MJ/kg)	14.56
Lower calorific value (MJ/kg)	13.76
FC	13.33
VCM	62.31
Ash	24.36
C	34.6
H	3.93
O	35.38
N	0.93
S	0.16
Ash	25

based vapor absorption refrigeration system. The power required for ethanol production is supplied by the CCGT unit. Heat recovered from gasification and flue gas is used for vapor absorption cooling. Also from ethanol production, a significant amount of heat is obtained. Detailed schematics of the CCGT power generation is shown in Fig. 7. Produced syngas is utilized by two processes—either in power

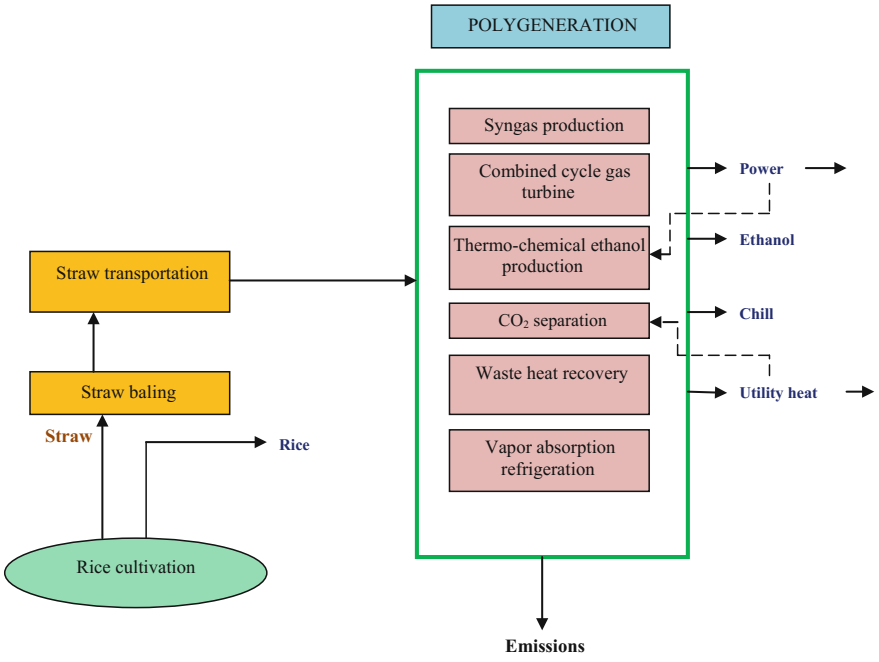

Fig. 6 Integration of multiple units in a polygeneration [17]

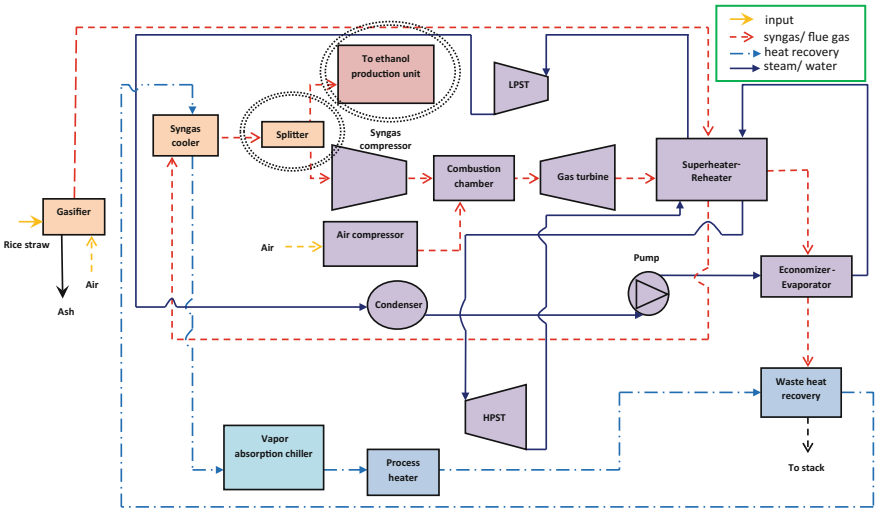

Fig. 7 Detailed schematic of biomass based power generation integrated with ethanol production [14]

generation or in ethanol production. The percentage of syngas between these two processes can be varied according to demand. In Fig. 8, heat recovery from the WGS reaction and ethanol synthesis reaction shown.

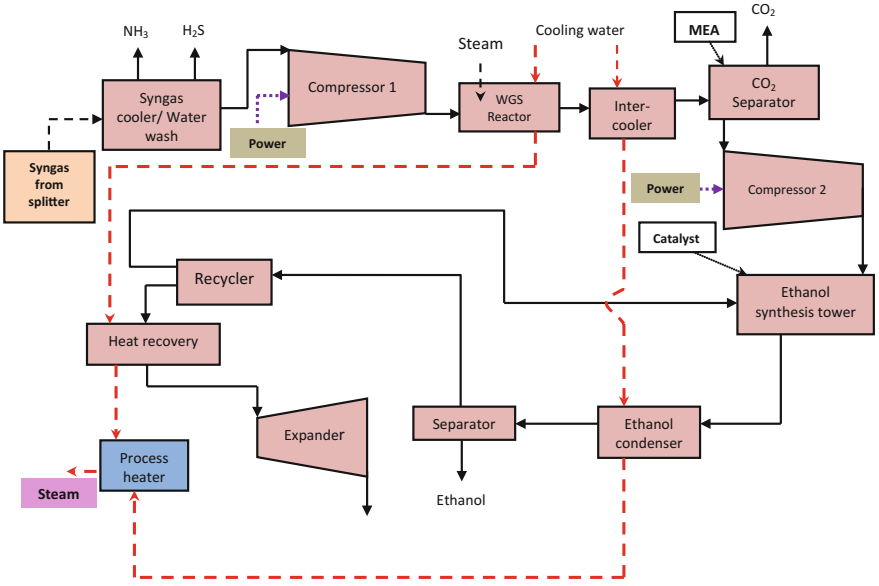

Fig. 8 Detailed schematic of ethanol production integrated with polygeneration [14]

6.3 *Net-CO_2 Negative Ethanol*

In the ethanol production unit, after WGS reaction, CO_2 is separated from the syngas to maintain the desired composition of the syngas for ethanol synthesis. Hence, there is a possibility of sequestration of CO_2 as shown in Fig. 9. By sequestering this CO_2, concentration of GHG gases in the atmosphere can be reduced. In order to store CO_2, it must be transported to a proper site of sequestration. Hence, liquefaction of CO_2 is necessary for transportation by pipeline or by vessels. Liquefaction can be done by pressurization and it requires a significant amount of power which is supplied by the polygeneration itself.

Input energy of this polygeneration is obtained from rice straw which is an agricultural waste. As it is a by-product of paddy cultivation, it may be treated as a CO_2-neutral fuel. After CO_2 sequestration, this energy system may become a net CO_2-negative one and this production of ethanol by this process may even be a

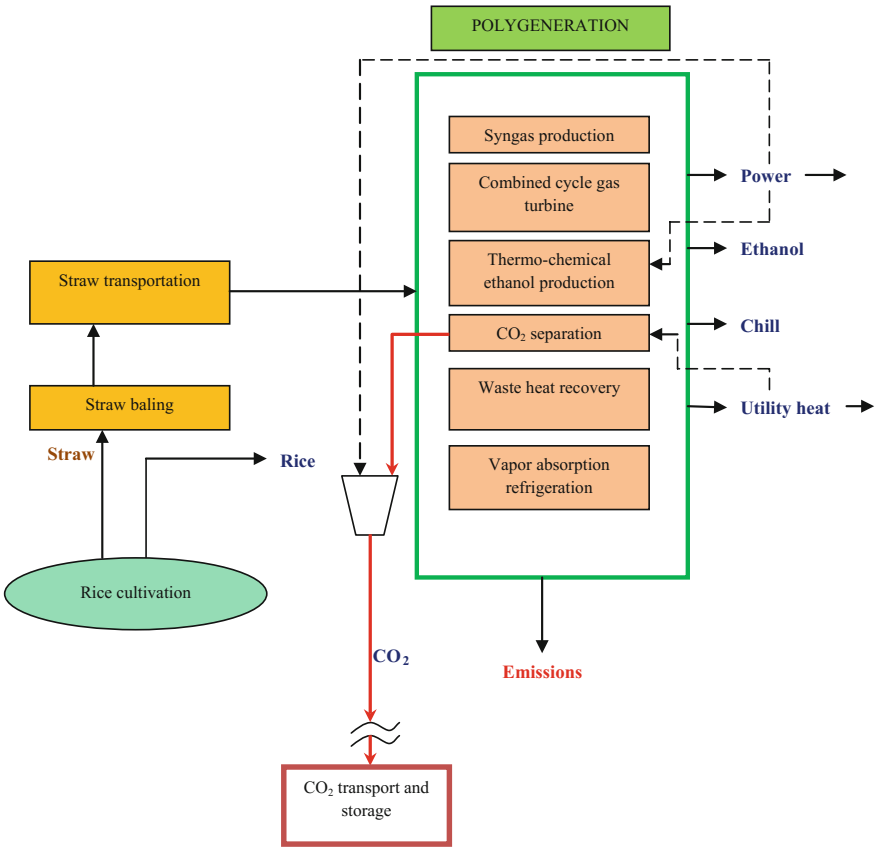

Fig. 9 Polygeneration with CO_2 capture and storage [17]

net-CO_2 negative one. To assess the net-CO_2 emission, life cycle analysis (LCA) is the most scientific tool for this purpose.

7 Assessment of the Ethanol Production Process

To assess a sustainable energy solution, assessment should be multi-dimensional [13]. Technological feasibility may be assessed through thermodynamic analysis. Simultaneously, this system should be economically viable for its sustainability. Economic viability of this system is tested through techno-economic analysis. One of the major objectives of bio-ethanol production and use is to reduce the GHG emission from transportation sector. This reduction of GHG emission is assessed most scientifically through life cycle analysis (LCA). LCA study also identifies environmental benefits/burdens from this polygeneration. However, it also explores the net-CO_2 negativity of this energy solution.

7.1 Thermodynamic Assessment

Thermodynamic simulation of the polygeneration plant is done by using Aspen Plus®. As performance of a biomass based plant is highly dependent on confirmed availability of biomass, this polygeneration is designed according to the availability of rice straw of an Indian district [15, 16]. The operating parameters of the plant are given in Table 2.

Table 2 Plant operating parameters [14]

Parameters	Value
Biomass feed rate	62 t/h
Gasification equivalence ratio	25%
Produced syngas in ethanol production unit	30%
GT-cycle pressure ratio	14
Water circulation rate in steam cycle	70 t/h
Make-up water for steam cycle	10%
HP-Steam turbine inlet temperature	538 °C
HP-Steam turbine inlet pressure	12.4 MPa
LP-Steam turbine inlet pressure	3.2 MPa
NH_3 circulation rate in cold storage	124 t/h
Cold storage evaporator temperature	−5 °C
H_2:CO in WGS	2:1
Ethanol synthesis pressure	9.6 MPa
Recycling of unconverted syngas in ethanol synthesis tower	70%
Flue gas exhaust temperature	200 °C
Lean amine loading	30% (wt./wt.)

Table 3 Thermodynamic performance of the polygeneration plant for an Indian district (30% syngas used for ethanol production) [14]

Item	Value
Net gas turbine power output	33.5 MW
Steam turbine power output	28 MW
Power requirement for ethanol production	5.3 MW
Ethanol production rate	3.6 t/h
Cooling rate	3.7 MW
Utility heat rate	3 MW
CO_2 capture rate	8.9 t/h

In this simulation, 30% of produced syngas is utilized for ethanol production and the rest is used for power generation. However, heat recovered from both of these units is used for either heating or cooling. Cooling is used for cold storage for preservation of foods and agricultural products. The results of the simulation are given in Table 3 which shows that a significant amount of power, ethanol, heating and cooling can be produced through this polygeneration. Rate of ethanol production may be decided according to utility demands and economic value of each of the products.

7.2 Economic Assessment

For sustainable operation of the polygeneration plant, it must be economically feasible. The cost of produced ethanol should be competitive with other available liquid fuels to be acceptable to the consumers. By taking the market value of ethanol as the input, economic performance of the polygeneration plant is assessed. Inputs and assumptions of the techno-economic performance are given in Table 4.

The results of the economic performance of the polygeneration plant are given in Table 5. Though this plant needs a large capital investment, its payback period is quite reasonable, i.e., within 5 years. Net present value of the polygeneration plant is also high. Hence, ethanol production through polygeneration is an economically feasible solution.

7.3 Environmental Impact Assessment

The main incentive for using ethanol as the secondary fuel is the possible decarbonization of the transport sector. Use of ethanol reduces the dependency on oil import and hence, increases energy security also. To assess the environmental impact, assessment of GHG emission throughout the life cycle of the ethanol production process is necessary. LCA is the most scientific tool to measure the GHG emission. Cradle-to-gate LCA is used to show the environmental impact of ethanol production from straw. For the LCA, basic assumptions for life cycle

Table 4 Basic assumptions and prices for economic calculation [14]

Parameters	Value
Year of study	September 2013
Plant life	10 years
Start-up period	3 years (20, 45, 35%)
Plant location factor	1.02
Plant overheads	10% of FCI
Working capital	15% of FCI
Depreciation method	Linear
Salvage value after 10 years	15% of FCI
Plant discount rate	10%
Plant O&M	2.8% of FCI
Insurance and taxes	1% of FCI
Sales tax	4%
Operating hours per annum	8000
Biomass purchasing cost	13.33 USD/t
MoS_2 Catalyst cost	11.57 USD/kg
Catalyst replacement per year	20%
Catalyst's alcohol productivity	300 g/kg-catalyst/hr
Water cost	0.28 USD/m^3
Thermal energy requirement for CO_2 capture	3 GJ/t CO_2
Specific MEA price	1416.7 USD/t
MEA degradation rate	1.5 kg/t CO_2
CO_2 transport and storage cost	14.2 USD/t CO_2
Carbon credit	21.25 USD/t CO_2
Electricity price	72.67 USD/MWh
Ethanol price	1.6 USD/gallon
Cooling price	20 USD/MMBtu
Utility heating price	13.33 USD/MWh

Table 5 Economic performance of the polygeneration plant [14]

Parameters	Value
Total capital investment	257 million USD
Annual operating cost	16 million USD
Annual net profit (after tax)	40 million USD
Payback period	4.76 years
Return on investment (ROI)	15.5%
Net present value (NPV)	97 million USD

inventory are given in Table 6. The system boundary of polygeneration is shown in Figs. 6 and 9. In Fig. 9, the polygeneration is explored with carbon sequestration option.

Table 6 Basic assumptions for inventory of LCA

Parameters	Value
Rice straw generation (kt/y)	4966.8
Rice straw surplus (kt/y)	496.7
Vehicle capacity (t)	10
Plant operating hours	8000 h/y
Plant life time	20 y
MoS_2 catalyst degradation rate per year	20%
Catalyst's alcohol productivity	350 g/kg-catalyst/h
Ammonia leakage rate per year	20%
MEA degradation rate	1.5 kg/t CO_2
Heat duty for CO_2 separation	3 GJ/t CO_2
CO_2 transport distance	1000 km

This polygeneration produces multiple utilities. Hence, finding the environmental impact of individual product is not a straight forward process like single utility systems. In Fig. 10, effect of different allocation methods is shown. Though the outputs are some forms of energy, qualities of these energy outputs are different. Hence, the gross energy allocation method is not suitable for this case. The economic allocation method is not suitable due to its varying market value. Exergy based allocation is the best option for this case.

To assess the net-GHG emission during cradle-to-gate life cycle of the polygeneration, IPCC 100a method [15] is selected. The net GHG emission of the polygeneration without CO_2 sequestration is shown in Fig. 11a. From this figure, it is noted that a significant amount of GHG is emitted for this polygeneration though biomass is considered as carbon-neutral fuel. When this polygeneration is integrated with the carbon sequestration process, net GHG emission becomes negative as shown in Fig. 11b.

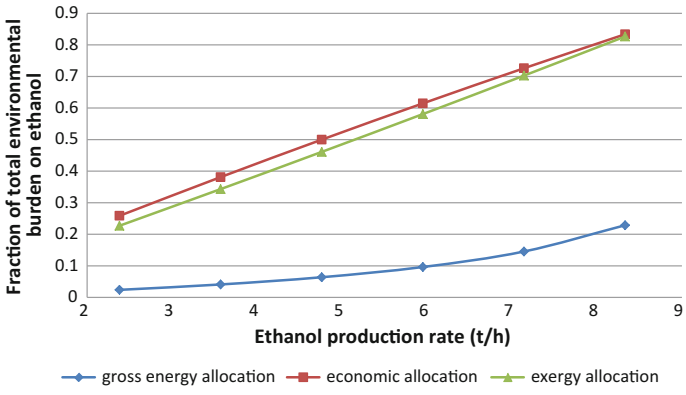

Fig. 10 Effect on allocation of environmental burden [17]

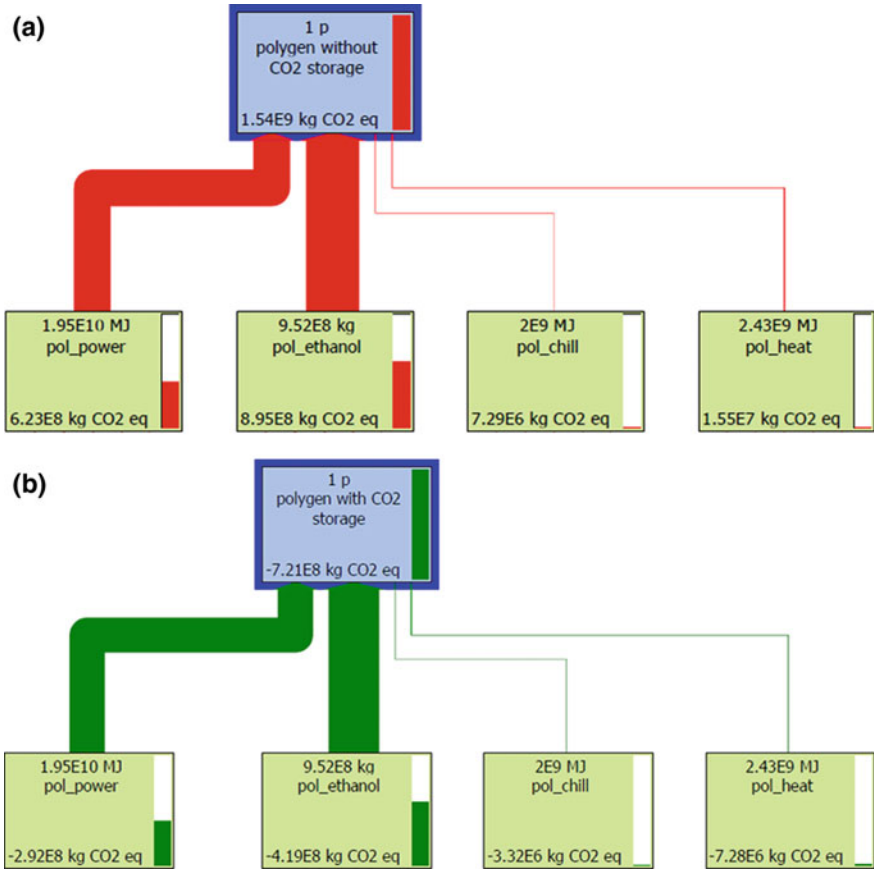

Fig. 11 Comparison of net GHG (IPCC 100a) emission from polygeneration **a** without CO_2 storage and **b** with CO_2 storage [17]

8 Conclusion

Replacing fossil fuels by some low carbon alternatives is a critical challenge at present. However, producing fuels from food stuff may lead to the conflict between food and energy securities. Recycling waste, specifically agricultural waste, may be a possible sustainable option for this transition from fossil to renewable regime. However, the performance of such option must be economically feasible with acceptable environmental impact in spite of being technologically feasible. A case study is presented with production of ethanol from rice straw. As a significant amount of energy is required for this process, independent production of ethanol in this process may not be cost effective. However, integrating this process into a polygeneration can lead to economic feasibility with acceptable environmental performance. Results of a case study for production of ethanol from rice straw in

thermo-chemical process in a polygeneration system and estimated performance from multi-dimensional viewpoint are reported. The results show that with the availability of rice straw, the system will be economically attractive with existing options. A payback period of less than 5 years will be required for recovery of investment of capital. The system may be integrated with CO_2 sequestration for a net CO_2-negative option as observed from a cradle-to-gate life cycle analysis.

Acknowledgements Mr. Kuntal Jana gratefully acknowledges to the Council of Scientific and Industrial Research (CSIR), India for awarding Senior Research Fellowship during this work toward Ph.D.

References

1. IEA (2015) World energy outlook. International Energy Agency, Paris
2. IPCC (2015) Climate change 2014, Synthesis Report (AR5). Cambridge University Press, Intergovernmental Panel on Climate Change
3. Tester JW, Drake EM, Driscoll MJ, Golay MW, Peters WA (2012) Sustainable energy: choosing among options. MIT press, MA
4. de Freitas LC, Kaneko S (2011) Ethanol demand in Brazil: regional approach. Energy Policy 39:2289–2298
5. Hira A (2011) Sugar rush: prospects for a global ethanol market. Energy Policy 39:6925–6935
6. Kalyani KA, Pandey KK (2014) Waste to energy status in India: a short review. Renew Sustain Energy Rev 31:113–120
7. Meerman JC, Ramirez A, Turkenburg WC, Faaij APC (2011) Performance of simulated flexible integrated gasification polygeneration facilities. part A: technical energetic assessment. Renew Sustain Energy Rev 15:2563–2587
8. TIFAC (2009) Availability of Indian biomass resources for exploitation. http://www.tifac.org.in/index.php?option=com_content&view=article&id=747&Itemid=208. Accessed 17 Oct 2016
9. Higman C, Burgt MVD (2008) Gasification. Elsevier, UK
10. Van der Heijden H, Ptasinski KJ (2012) Exergy analysis of thermochemical ethanol production via biomass gasification and catalytic synthesis. Energy 46:200–221
11. Perales ALV, Valle CR, Ollero P, Gomez-Bare A (2011) Technoeconomic assessment of ethanol production via thermochemical conversion of biomass by entrained flow gasification. Energy 36:4097–4108
12. Jana K, De S (2015) Sustainable polygeneration design and assessment through combined thermodynamic, economic and environmental analysis. Energy 91:540–555
13. Chicco G, Mancarella P (2009) Distributed multi-generation: a comprehensive view. Renew Sust Energy Rev 13(3):535–551
14. Jana K, De S (2015) Polygeneration performance assessments: multi-dimensional viewpoint. Clean Technol Environ Policy 17:1547–1561
15. CGPL (2010) Biomass resource atlas of India. Combustion, gasification and propulsion laboratory, IISc Bangalore, India. http://lab.cgpl.iisc.ernet.in/Atlas/Tables.aspx Accessed 05 May 2014
16. Jana K, De S (2015) Techno-economic evaluation of a polygeneration—a case study for an Indian district. Bioresour Technol 181:163–173
17. IPCC (2007) Climate change 2007: working group I: the physical science basis. Intergovernmental Panel on Climate Change

18. Jana K, De S (2015) Polygeneration using agricultural waste: thermodynamic and economic feasibility study. Renew Energy 74:648–660
19. Jana K, De S (2016) Environmental impact of an agro-waste based polygeneration without and with CO_2 storage: life cycle assessment approach. Bioresour Technol 216:931–940

Microalgae Based Biofuel: Challenges and Opportunities

Richa Katiyar, Amit Kumar and B.R. Gurjar

Abstract The growing demand of conventional fuels and its limited reservoir has ignited attention of scientific communities to produce alternative fuels including biofuels from renewable sources. The renewable sources include wood, plants, agro-waste, fruit pulps and other waste materials with nutrients. The use of biomass based bioenergy or biofuel is gaining public attention due to their environment friendly aspects. Earlier the biofuel was produced from food and non food crops which puts pressure on land resource. To circumvent such negative impacts, scientific communities have explored the use of microalgae for production of biofuels. Microalgae can produce high oil (more than 300 times) than other existing resources such as terrestrial plants. The added advantage of microalgae also includes the use of non cultivable soil and waste water for its cultivation which renders the process more efficient from cost perspective. Thus, the usage of microalgae for biofuel production doesn't affect the agriculture land resource and drinking water balance in the environment. Using microalgae based biofuel has been shown to be a carbon neutral process because the carbon generated in the fuel combustion is almost neutralized by the carbon consumption during micro-algal growth. Moreover, the different species of microalgae produce bio-sustainable novel products which can be used as raw materials in a number of industries like energy, power generation, feed and food industry and cosmetics. In this way, the multi usage of microalgae can contribute toward cost effectiveness with development of nation in terms of health, industry establishment and job creation.

R. Katiyar · A. Kumar · B.R. Gurjar (✉)
Centre for Transportation Systems, Indian Institute of Technology Roorkee, Roorkee 247667, Uttarakhand, India
e-mail: brgurjar@gmail.com

B.R. Gurjar
Department of Civil Engineering, Indian Institute of Technology Roorkee, Roorkee 247667, Uttarakhand, India

A.K. Agarwal et al. (eds.), *Biofuels*, Green Energy and Technology,
DOI 10.1007/978-981-10-3791-7_9

Graphical Abstract

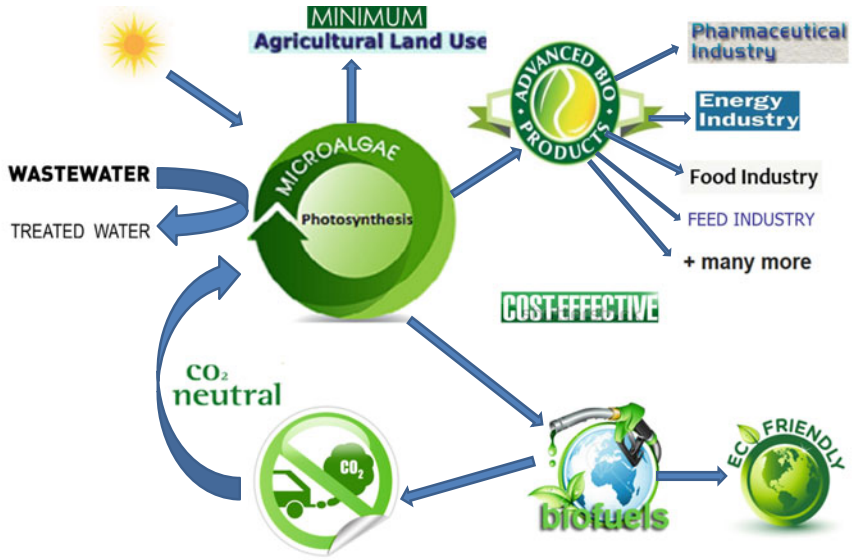

Keywords Carbon · Bioenergy · Biofuel · Renewable energy · Environment

1 Introduction

Negative environmental repercussions of anthropogenic activities such as burning of fossil fuels include release of various greenhouse gas emissions to the environment. The non renewable nature of fossil fuels causes degradation of environmental components and consequently hazards to human health. To avoid these negative effects of non-renewable sources, researchers have created interest in production of renewable energy sources including biofuels [86]. Biofuels can be produced from several resources such as food crops (first generation biofuels), non-food crops (second generation biofuels) and biomass based energy resources (advanced or third generation biofuels). Commercially the cultivation of energy crops (food and non food crops) for fuel generation has created a lot of issues related to food prices and land requirement. This has shifted idea toward biomass based energy resources which are gaining more scientific attention due to its high yield and advantages over other resources. Biomass based resources such as microalgae can utilize animal fat, agro waste materials, fruit pulps, municipal waste materials for production of biofuels. Biofuels produced from microalgae are considered as carbon neutral in nature because the CO_2 liberated in combustion process of biofuel is equilibrated by the CO_2 taken by the new ones sowed to replace

harvested ones [8, 43, 73]. On account of these positive aspects, biofuels have emerged as a viable alternative to diesel/petroleum fuels used in the transport sector [24]. This article critically reviews and presents the biofuel production from microalgae, and associated advantages and challenges.

2 Demand and Production of Biofuel

Human dependency on transportation vehicles for their livelihood across the world is increasing the demand of biofuels generation globally. As the reservoirs of petroleum based fuels are limited and non-renewable, it further stresses the need for development of production of alternate energy fuels for future including biofuels. To produce biofuels and its byproducts in 2004, about 14 million hectare crops were used globally that has accounted about 1% of global cropland area [85]. Many countries like Germany, India, USA, China and Japan are using blending of biodiesel with conventional fuel in transportation sector [72]. Volkswagen Group has used B20 (20% biodiesel and 80% conventional diesel) in their vehicles.

While India produces 30% of its crude oil needs, yet India has demanded 3.6 Million Metric Tons of biodiesel in 2011–12 [29, 41]. In 2004, many busses in Gujrat and some trains like Jan Shatabdi have run successfully using B5 and B20 in India [68]. In India, total production of biodiesel was 6 million gallons in 2009 [81] and the demand for biofuel is estimated to grow at the rate of 5.8% annually till 2030 [41]. For production of biofuels in India, many private companies have already planted safflower, castor and Argemone over 400 ha in Gujarat, Karnataka and Maharashtra for production of biofuel in India [29].

To fulfill the growing demand of biofuel globally, biofuel production is continuously increasing in number of countries including Germany, India, Brazil, U.S. and China. The biodiesel production in US has started in 2000 and hiked from 25 million gallons in 2004 to 678 million gallons in 2008 [81]. In 2009, the biodiesel production was 6 million gallons in India, whereas the biodiesel production in Brazil was recorded as 500 million gallons in year 2010 [13].

3 Microalgae

Microalgae are unicellular microscopic miniatures which perform photosynthesis with high efficiency than crops [60]. Microalgae generally have a higher production rate, growth rate, product accumulation rate, less doubling time and high photosynthetic rate than other biomass feedstocks and plants [44]. Hence, they can propagate within a day and can be harvested in about 1–10 days [83]. For instance, doubling time for microalgae can be as short as 3–8 h, while jatropha takes 2–3 years [44]. Moreover, microalgae are oxygen (O_2) producing miniatures,

generally autotrophs, consume inorganic carbon in the form of carbon dioxide (CO_2) to produce organic compounds such as carbohydrates, proteins and lipids. Some species of microalgae can grow efficiently in heterotrophic as well as mixotrophic conditions in the presence of organic carbon compounds. Hence, a single cell can follow three different modes of growth patterns. Moreover, microalgae have ability to resist in different environments ranging from fresh water to high alkalinity water and, in wet to dryrocks [34]. Thus microalgae, having the ability to adapt to different environments, is suitable to grow in extreme of stress conditions such as nutrient limitation and extremes of pH. Moreover under some stress conditions i.e. under extremes of pH and nutrient limitation, microalgae produces maximum lipids this ultimately leads to highest yield of biofuels. Different species of microalgae can increase oil yield up to 70% under stress condition [37]. Microalgae based biofuels are also capable to be used with the existing infrastructure for storage and distribution. Microalgae based biodiesel has been proposed as one of the most popular choices these days [71].

3.1 *Use of Microalgae as a Single Cell for Production of Biofuel and Its Byproducts*

The production of biofuel and other byproducts from microalgae is carried out in three steps (Fig. 1). (i) Cultivation of microalgae (ii) Cell harvesting, drying and extraction of oil bodies and (iii) Transesterification.

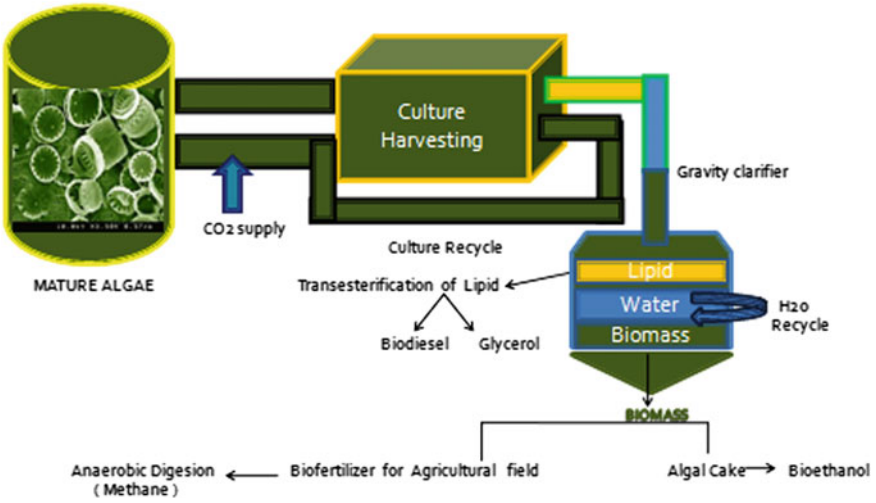

Fig. 1 Single step biofuel production from microalgae with production of its byproducts

3.1.1 Cultivation of Microalgae

Photobioreactor

Photo-bioreactors (PBRs) are closed transparent structures equipped with all facilities required for growth of microalgae. PBRs are available in different sizes, shapes, designs and varieties such as flat panel reactors (FPR), tubular PBRs (horizontal and vertical column reactors), bubble column reactors (BCR), air lift reactors (ALR), and stirred tank PBR. Amongst these, tubular PBRs and FPR are most popular and used in mass cultivation of microalgae due to its easy handling, high surface to volume ratio and large illuminating surface area [80]. Samson and Leduy [70] designed a FPR equipped with fluorescence lamps and Ramos de Ortega and Roux [63] have designed an outdoor FPR with thick translucent PVC materials to reduce cost. With time and extensive research work in this area, various designs of tubular PBRs and FPR have been reported for mass cultivation of different algae [40, 78]. The advantages of using PBR for cultivation of microalgae are to reduce risk of contamination and high productivity. PBRs are designed in such a way that they can utilize sunlight as well as artificial light like light emitting diodes (LED), tungsten or fluorescent tube lights and bulbs. LEDs are preferred due to minimum heat generation and low power consumption. Yet another advantage is that LEDs can be used to study the effect of different wavelength on growth of microalgae. For example—microalgae, *Nannochloropsis* sp. has shown a higher growth rate and lipid productivity under blue light (470 nm) than white, red or green [19, 20] (Table 1).

Table 1 Advantages and limitations of different types of PBRs

PBR types	Advantages	Limitations
Tubular PBRs	Cost effective; good biomass productivity; large illuminating surface area and fairly good for outdoor cultures	Difficulty in handling in pH and CO_2/O_2 ratio; require large space [77]
Vertical PBRs	Reduced photo inhibition and photooxidation; efficient mixing; good for immobilization of microalgae; low shear force and energy consumption	Decrease illumination on scaling up
FPR	Low oxygen buildup; easy to clean; large illuminating surface; cost effective and good biomass productivity	Difficulty in scaling up the process and temperature control [77]
ALR and BCR	Used for increasing photosynthetic efficiency and light flashing effect	Suitable for indoor operation [57]
Stirred tank reactor	–	High shear force, mechanical agitation required and low surface to volume ratio [57]

Open Ponds System

Open pond systems are performed in the natural open environment. These systems are constructed in simple and inexpensive way with attachment of paddle wheels for mixing of nutrients and uniformity of media. Open pond systems require high volume of water because water evaporation is a major issue due to minimum depth and large surface area. To overcome this problem, sea water, brackish water and waste water can be used instead of fresh water. Another issue associated with this system is the risk of contamination as unwanted microorganisms may start growing and competing with microalgae for various resources. The problem can be overcome with the use of high inoculum size because majority of cells will compete for nutrients availability with other microorganisms.

In terms of cost effectiveness, open system has the advantage over PBR as the installation and maintenance cost of PBRs are very high. However, these high costs of PBRs can be justified in case of high value products such as PUFAs and carotenoides. Moreover, PBRs show better results in terms of productivity of lipid as the cells get the controlled environment inside the reactor providing high yield e.g. Rodolphi et al. [68] showed high lipid productivity (204 mg L^{-1} d^{-1}) of microalgae grown in PBR, while [53] described the lipid productivity of microalgae ranging from 20 to 50 mg L^{-1} day^{-1} grown in open systems. An advance approach involves the hybrid system in which biomass obtained from PBRs is transferred to open ponds or raceways to get maximum biomass yield [31, 30].

3.1.2 Harvesting, Drying and Oil Extraction from Microalgae

A number of methods are employed for harvesting of microalgae such as sedimentation, centrifugation, filtration and flocculation. The studies in literature have employed and analyzed different methods for harvesting of microalgae e.g. Pragyaa et al. [61] observed that sedimentation combined with flocculation is efficient among simple sedimentation, filtration and flocculation. Young et al. [90] have experimentally proved that new modified nanoparticle engineering based method for microalgae cell harvesting is more efficient than sedimentation, filtration and flocculation. After harvesting, disruption of micro algal cell is necessary to release oil bodies and cellular components.

The cell disruption can be accomplished by several methods [44], including ultrasonic assisted method, press machine, chemical method, supercritical fluid, enzymatic method, microwave, autoclaving, bead beating, osmotic pressure method, soxhlet method and homogenizer e.g. Mata et al. [48] and Jae Yon et al. [42] reported that microwave oven method is one of the simpler and powerful methods among autoclaving, osmotic shock and bead beating for microalgal cell explosion. The general criteria for selection of harvesting and disruption methods

include the species of microalgae used for cultivation and cost criteria of energy extraction process.

After harvesting and cell disruption the oil bodies and other cellular components are needs to be separated and extracted. Hence, the most common and applicable extraction method is solvent extraction method, which includes organic solvents such as hexane, dichloromethane, methanol, chloroform and toluene [55]. For extraction of lipid, two most commonly used solvents include methanol and chloroform [6, 28]. Solvent extraction method is then followed by trans-esterification, an energy intensive process for biofuels production from oil bodies. A diverse range of studies are under way with the goal of obtaining high biofuels yield in a cost effective manner with minimum use of toxic solvents [44].

3.1.3 Transesterification

Triacylglycerols (TAGs) or oil bodies have to undergo for transesterification to form biodiesel. Transesterification process includes methanolysis or ethanolysis which produces the fatty acid methyl esters (FAMEs) called biodiesel. For increasing the rate of the transesterification process, catalysts are required. The catalysts can be acidic or alkaline in nature e.g. Carrapiso and Garcia [12] used a combination of a basic catalyst in methanol, followed by an acid catalyst for better transesterification. Transesterification process also yields glycerin as byproduct of biodiesel production, which can be used as substrate for many industries such as cosmetics and food.

Furthermore, the remaining biomass of biodiesel production can be utilized for production of methane by anaerobic digestion [33] and bioethanol production by fermentation [69] (Fig. 1). Thus, a single cell (microalgae) can be used to produce three different energy sources together in a same cycle (Fig. 1).

3.2 Photosynthesis and Metabolic Route for Production of Lipid in Microalgae

The photosynthesis process in algae involves capturing carbon dioxide (CO_2) from the environment and converting it into sugar using light energy. The mechanism for CO_2 acquisition in algae includes active bicarbonate accumulation. Carbonic anhydrase (enzyme) that inter converts CO_2 and bicarbonate, which supply the enzyme (Rubisco) with CO_2 from the pool of bicarbonate. The major antenna pigments (important in absorbing light energy) in algae including chlorophylls, phycobiliproteins and carotenoids give distinctive colour to algae. Algae and higher plants have about equal capacity to utilize light energy and fix it into chemical

energy by photosysnthesis. Algae and plants can convert as much as 20% of photosynthetically active radiation [PAR ~ visible light] at very low light intensity, while at full light intensity the conversion in plants and algae is reduced to 2–3% of PAR [7]. Algal photosynthesis can be stimulated with increase in nutrients (N, P and Fe) availability and through metabolic engineering. Increase in photosysnthesis of algae causes sequestration of more CO_2 from the environment. Algae can grow faster and are capable of converting solar energy into chemical energy, which is mainly in the form of lipids (triacylglycerols), know as oil bodies.

In lipid synthesis pathway, microalgae use CO_2 to produce acetyl-CoA (coenzyme A) by more than one pathway. Acetyl-CoA acts as the initiator in the fatty acid (FA) synthetic pathway, which takes place in chloroplast genome. FAs are basic units of many cellular lipids including triacylglycerols (TAGs) commonly called as oil bodies. In FA synthetic pathway, a multifunctional enzyme complex (acetyl-CoA carboxylase) plays an important role by producing malonyl-CoA from acetyl-CoA and bicarbonate. Finally, these FA moieties enter into the endoplasmic reticulum (ER) for glycerolipid synthesis. TAGs synthesis in microalgae varies due to alteration in acetyl-CoA carboxylase (ACCase) activity participated in TAGs synthesis pathway [39]. In further steps, TAGs are formed by the sequential acylation of glycerol-3-phosphate (G3P) backbone with three acyl-Co-A, in ER. The TAGs accumulated in a specific domain of ER, which buds out from the ER forming distinct cellular organelles.

Depending upon the species of microalgae the TAGs content yield may vary. Microalgae may yield high TAGs amount due to its high surface/volume ratio in contrast to other energy crops. This ratio leads to more nutrients uptake rate and enhances acquisition of desired product such as lipid/TAGs for biodiesel production. Additionally, this ratio also provides microalgae to tolerate the environmental stresses, which make them an attractive alternative for energy extraction than other terrestrial plants.

3.3 Benefits of Using Microalgae as Biofuel Source

3.3.1 Oil Content of Microalgae

Microalgae have carbon fixation ability to converts solar energy into chemical energy [72] in the form energy rich compounds such as carbohydrates, protein and lipids. Further, these compounds are converted into value-added products e.g. lipid gets converted into oil or biodiesel; carbohydrate into bioethanol or acetone butanol and protein into fertilizers and manure. Microalgae can yield up to 300 times more oil (lipid content) per acre than other cropping species [59] such as soybeans, coconut, rapeseed or jatrophaetc [16, 66] (Table 2).

Table 2 Oil content of microalgae and other crops (Adapted from [24])

Serial no.	Species of microalgae	Oil content (% dry weight)	Reference
1.	*Botryococcus* braunii	29–75	[5, 51]
2.	*Chlorella* sp.	29	[75]
3.	*Thalassiosira* pseudonana	21–31	[9]
4.	*Schizochytrium* sp.	50–77	[81]
5.	*Heterotrophic C.* protothecoides	57.9	[52]
6.	*Chlorella* sorokiniana	22	[46]
7.	*Nitzchia* sp.	45–47	[15]
8.	*Cylindrotheca* sp.	16–37	[67]
9.	*C. marina*	70.00	[67]
Other crops			
10.	*Jatropha*	62.20	[67]
11.	*Coconut*	57.40	[67]
12.	*Soyabean*	9.40–37.80	[67]

3.3.2 Other Products of Microalgae

Microalgae have capability to produce more than 15,000 novel products which can supplement raw materials for other industries [62, 79]. One of the known and essential metabolic product of microalgae is PUFA (poly unsaturated fatty acids), an essential fatty acid of human diet [11], e.g. PUFA content of *Cadophora* fracta has been reported about 51% which is mainly used in aquacultures [23]. Other novel products of microalgae are listed in Table 3.

Table 3 Products of microalgae with their applications

Serial no.	Other products of microalgae	Applications
1.	Caretenoide	Rich source of pro-vitamin A [84]
2.	Phycocolloids	Having antitumor, anticoagulant, antioxidant capability [50]
3.	Lectins	Carbohydrates binding proteins [3]
4.	Terpens and latexes	Pharmacological activities [21, 22, 65]
5	PUFA (poly unsaturated fatty acids)	Food industry as food supplement [11]
6	Polyketides	Used as chemotherapeutic agents in pharmaceuticals for synthesis of many antibiotics such as tetracycline [26]

3.3.3 Use of Low Cost Feed Stocks for Cultivation of Microalgae for Biodiesel Production

In order to produce biodiesel/oil from microalgae, it is essential to enhance lipid production. The oil content of microalgae can be enhanced with application of organic carbon sources in growth media as a result of which cells exhibit mixotrophic or heterotrophic growth patterns. Micro-algal cultivation in mixotrophic and heterotrophic modes gives better result in terms of lipid and biomass [4] (Table 4). The wide availability of lipid extracted algal biomass, orange peel extract, waste from municipal and dairy industry makes them low cost organic carbon rich feed stocks for cultivation of microalgae (Table 5), e.g. lipid extracted algal biomass accounts for approximately 70% of cell dry weight rich in protein and carbohydrates [64].

Table 4 Productivity and lipid content of different micro algal species under different cultivation conditions

Microalgae species	Mode of growth	Biomass productivity (mg/L/day)	Lipid productivity (mg/L/day)	Lipid content (%)	References
Botryococcus braunii UTEX 572	Phototrophic	30	5.5	20.8	[89]
Chlorella protothecoides	Heterotrophic	4000	1881.3–1840.0	43.0–46.0	[14]
Chlorella vulgaris #259	Heterotrophic	80–150	27.0–35.0	23.0–36.0	[45]
Chlorella vulgaris #259	Mixotrophic	90–250	22.0–54.0	21.0–34.0	[45]
Scenedesmus obliquus	Mixotrophic	100–510	11.6–58.6	6.6–11.8	[49]
Spirulina maxima LB 2342	Phototrophic	210	8.6	4.1	[30]
Scenedesmus obliquus	Phototrophic	60	7.14	12.7	[49]

Table 5 Low cost feed stocks for microalgae cultivation in terms of high biomass and lipid productivity for more biodiesel production

Microalgae species	Feedstocks	Biomass productivity (mg/L/day)	Lipid productivity (mg/L/day)	References
C. vulgaris	Enzymatic hydrolysed lipid extracted algal biomass	164	116	[91]
C. vulgaris	Dairy industrial waste	750	253	[1]
C. minutissima	Wastewater	800	57	[47]
C. vulgaris	Orange peel extract	183.33	22.7	[58]

3.3.4 Use of Waste Water for Cultivation of Microalgae

The use of water in industries and agriculture releases number of organic and inorganic substances which leads water pollution that has been aggravating continuously. Wastewater produced from dairy plants, domestic households, paper mills and sewage has high source of nutrients. The carbon in these wastewater is in the form of reducing and non reducing sugars, organic and inorganic forms of nitrogen and phosphorous [2, 76]. Microalgae have the capability to utilize both organic and inorganic forms of nitrogen, carbon and phosphorus for their growth [38, 88]. The removal of various pollutants from wastewater depend on the species of microalgae being employed e.g. C. debaryana removes 53% of total phosphate and 88% of total nitrogen from swine waste water [36]; *Scenedesmus* sp. removes 98% of total nitrogen and phosphate from secondary effluent [88]. Consequently, microalgae treat this wastewater while producing their biomass (by mixotrophic growth) used for biofuel production (Table 6). Because of these benefits, microalgae make it fantastic alternative among other existing species for biofuel production using waste water. Waste utilizing capability of microalgae reduces the cost of dispose of waste water and energy inputs for its treatment. Furthermore, utilization of waste water for cultivation of microalgae preserves water resource in the environment.

3.3.5 Land Requirement by Microalgae for Their Cultivation

Another problem associated with the production of biofuel from existing energy crops (food and non food crops) is continuous shrinkage of cultivable land [26] and its quality, which can pose an immediate problem for food security on earth. The data from India shows that as many as 20 states have reported a decrease in cultivable land to the extent of 790,000 ha in 4 years from 2007–08 to 2010–11, mainly attributable to diversion of land to non agricultural purposes [54]. The use of arable land to grow the crop is the major drawback associated with the use of first and second generation biofuels generating resources e.g. U.S.A. has consumed about 220 trillion liters of diesel in 2010. To replace this volume of alternative fuel

Table 6 Biomass productivity of different micro algal species in different waste source

Species	Type of WW	Biomass productivity (mg/L/day)	References
C. vulgaris	Municipal WW	138	[27]
C. minutissima	Wastewater	800	[47]
C. vulgaris	Orange peel extract	183.33	[58]

Table 7 Oil yield and required land area for microalgae and other crops (Adapted from [71])

Source	Yield of oil (L/ha)
Corn	172
Jatropha	1892
Microalgae (40% oil (% dry wt) in biomass)	70,405
Microalgae (20% oil (% dry wt) in biomass)	35,202
Rapeseed	1190

from soybean may require 367 Mha (million hectares) arable land while 178 Mha (million hectares) land is only available for cropping out of 930 Mha total land area of U.S.A. [85]. Microalgae based biofuels have thus emerged as a partial solution to these problems [17, 78] (Table 7) because, as stated earlier, it does not compete with food crops and can be grown on land which is not suitable for crops, for instance, arid land, land with excessively saline soil, and drought stricken land. Moreover, the soil fertility also increases after cultivation of microalgae.

3.3.6 Carbon Neutral Process of Microalgae

Carbon neutral means zero increase in amount of carbon in the atmosphere from carbon based fuel combustion. When carbon based fuels burn, the carbon molecule of the fuel combines with oxygen molecule present in the environment which forms CO_2. As CO_2 generated in the fuel combustion is not a part of the natural carbon cycle, it enters in the atmosphere and increase net amount of CO_2. Microalgae show carbons neutral processes because the amount of carbon generated in the fuel combustion is utilized by new algae grow, resulting net zero emission (Fig. 2). Inorganic carbon in the form of CO_2 serves as food for microalgae to perform photosynthesis to build their biomass. Algae can also be considered as a marine and freshwater plant bodies that have higher photosynthetic efficiencies and carbon capturing than terrestrial plants [56]. Microalgae require more fossil-based carbon to produce the same amount of bioenergy as other crops [18] (Fig. 2).

3.3.7 Cost Effectiveness of Using Microalgae

Using microalgae has its own cost and benefits. Before the production of biofuel is scaled up, the important aspects to be considered are type of cultivation system and mode, net energy input and output, environmental impacts, and economical analysis. The selection of type of cultivation method and mode for algal cultivation depends on species of microalgae used for biofuel production. Also, after extraction of biodiesel form microalgae, the oil biomass extract can be utilized for production of methane by anaerobic digestion [33] and bioethanol production by fermentation [69] (Fig. 1), a secondary source of energy leading to cost cutting and efficient use of resources. Moreover the recycling of nutrient utilized in cultivation of microalgae can improve

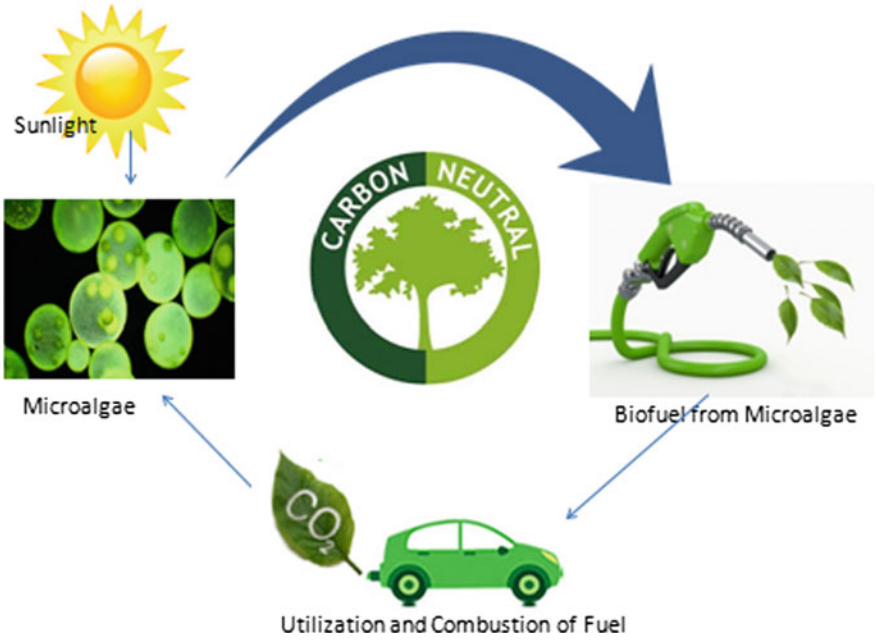

Fig. 2 Carbon neutral process of microalgae

economic feasibility for oil extraction process. Crude glycerol, a by-product of algal biodiesel production can be utilized as substrate or organic carbon source for algae to produce more biodiesel. Glycerol, another by-product of the process, can also be used as substrate for production of acetone butanol or bioethnol (Fig. 1), another secondary source of energy. Hence, the use of microalgae based biofuels is cost effective by designing low cost reactors, recycling of nutrients and use of bio-products for different purposes. Moreover, the solvents such as chloroform, methanol and hexane utilized in extraction of biofuel can be extracted in rotary evaporator at 80 °C for its utilization in next cycle provides cost cutting results [44].

4 Drawbacks and Challenges of Utilizing Microalgae for Biofuel Production

Despite all the advantages discussed above, the process of biofuel production from microalgae has its drawbacks and challenges associated, as discussed below:

- For commercialization, it is necessary to scale up the process of biofuel production from microalgae. The scaling up would require large space and fertilizers, e.g. Buchele and Zimba [10] have stated in their report that 3000 L of water is required for production of at least 1 L of biofuel using microalgae when

grown in arid soil. To overcome this issue many scientific communities are using waste water, salt water and brackish water for cultivation of microalgae without disturbing the fresh water balance in the environment.

- Commercially, biofuel production from microalgae is not viable presently as the cost of different algal species are normally in the range of $5–10 per kilogram [35].
- Glycerin is the co-product of biodiesel production which requires separation and purification for its utilization in feed industry. The glycerine and biodiesel is produced in the ratio of about 1:10 by the transesterification process [82]. The separation of glycerin can be done by using different techniques such as distillation units and membrane separation techniques [74]. Production of biodiesel could be economical but combination of downstream processes for purification of end products may increase the overall production cost. Hence, the economically feasibility of the purification processes is challenging.
- Microalgae require controlled temperature conditions for high yield in terms of biofuel.
- The genetic engineering approach used to improve photosynthetic efficiency [87], enhance biomass production rate, alteration in transcriptional factors linked up with the enzymes involved in TAG synthesis pathway, further escalates the cost of biofuel production using microalgae.
- Microalgae require phosphorous as a fertilizer which has detrimental effects on human health.
- Another problem associated with algal cultivation for biofuel generation in open system is contamination from unwanted microorganisms. To resolve these issues many researchers are continuously trying to design inexpensive photo-bioreactors for cultivation of algae. Bioreactors have proved to be the most effective systems that produce high quality algae.

5 Conclusions and Future Outlook

Microalgae based biofuel can contribute towards the useful solutions for existing global problems like fossil fuel shortage and hazardous emission resulting from fossil fuel combustion. Microalgae utilize solar energy and capture CO_2 which is converted into different variety of biofuels such as bioethanol and biodiesel through photosynthesis. Microalgae are robust microorganisms capable of fast growth under wide range of conditions including high alkalinity and extreme of temperature and pH range. Furthermore, microalgae have ability to produce high biofuel under modified growth conditions or metabolic engineering. Hence, microalgae offer promising results in the production of biofuel due to its potential to utilize waste land, waste water and low feed stock. However, a large extent of research is still required before the realistic production of biofuels using microalgae due to uncertainties in behavior of various species of microalgae species and lack of cost

effective harvesting, disruption, oil extraction and biodiesel conversion strategies. Thus, these recent challenges are encouraging scientific communities to take up research in various domains of biofuel production on large scale using microalgae. The overview of microalgae as a source for energy and useful byproducts presented in this study shows that microalgae are able to not only produce biofuel in very efficient manner but also to generate numerous biorefinery products, which increases the overall cost effectiveness of its production process. The biorefinery products of microalgae can be used in number of industries including automotive, pharmaceutical, feed industry, energy and chemical. The rapid urbanization and industrialization is exerting pressure on land resources in developing countries including India, in contrast the production of biofuels from microalgae do not compete for land and water resources. Moreover, microalgae offer sustainable results in terms of almost zero carbon to the environment than through conventional energy crops. Thus, besides meeting the energy demand through efficient biofuel production, microalgae can also enhance the human developmental index through providing nutrition, health, jobs and overall socio-economic welfare.

Acknowledgements The authors thank the Ministry of Human Resources and Development, New Delhi for providing funds for the research and Indian Institute of Technology, Roorkee for providing resources and platform for this study.

References

1. Abreu AP, Fernandes B, Vicente AA, Teixeira J, Dragone G (2012) Mixotrophic cultivation of Chlorella vulgaris using industrial dairy waste as organic carbon source. Bioresour Technol 118:61–66
2. Amini M, Younesi H, Zinatizadeh Lorestani AA, Najafpour G (2013) Determination of optimum conditions for dairy wastewater treatment in UAASB reactor for removal of nutrients. Bioresour Technol 145:71–79
3. Andrade LR, Salgado LT, Farina M, Pereira MS, Mourao PAS, Amado-Filho GM (2004) Ultrastructure of acidic polysaccharides from the cell walls of brown algae. J Struct Biol 145:216–225
4. Arora N, Patel A, Pruthi PA, Pruthi V (2016) Boosting TAG accumulation with improved biodiesel production from novel oleaginous microalgae Scenedesmus sp. IITRIND2 utilizing waste sugarcane bagasse aqueous extract (SBAE). Appl Biochem Biotechnol (Accepted)
5. Banerjee A, Sharma R, Chisti Y, Banerjee UC (2002) Botryococcusbraunii: a renewable source of hydrocarbons and other chemicals. J Crit Rev Biotechnol 22:245–279
6. Bligh EG, Dyer WJ (1959) A rapid method of total lipid extraction and purification. Biochem Physiol 8:911–917
7. Benemann J (2012) Photosynthetic efficiency and biomass productivity of microalgae mass cultures John Benemann. Algae biomass summit, San Diego, CA, pp 1–29. http://algaebiomass.org/wp-content/gallery/2012-algae-biomass-summit/2010/06/T1_Wed_1030_JBenemann.pdf. Accessed 08 Nov 2016
8. Brennan L, Owende P (2010) Biofuels from microalgae: a review of technologies for production, processing, and extractions of biofuels and co-products. Renew Sustain Energy Rev 14:557–577

9. Brown MR, Dunstan GA, Norwood SJ, Miller KA (1996) Effects of harvested stage and light on the biochemical composition of the diatom Thalassiosira pseudonana. J Phycol 32:64–73
10. Buchele M, Zimba P (2012) A report on—the downside of using algae as a biofuel. University of Texas
11. Cardozo KH, Guaratini T, Barros MP, Falcao VR, Tonon AP, Lopesm NP (2007) Metabolites from algae with economical impact. J Compar Biochem Physiol C Toxicol Pharmacol 146:60–78
12. Carrapiso AI, Garcıa C (2000) Development in lipid analysis: some new extraction techniques and in situ transesterification. Lipids 11:1167–1177
13. Cesar ADS, Batalha MO (2010) Biodiesel production from castor oil in Brazil: a difficult reality. Energy Policy 38:4031–4039
14. Cheng Y, Zhou WG, Gao CF, Lan K, Gao Y, Wu QY (2009) Biodiesel production from Jerusalem artichoke (Helianthus Tuberosus L.) tuber by heterotrophic microalgae Chlorella protothecoides. J Chem Technol Biotechnol 84:777–781
15. Christi Y (2007) Biodiesel from microalgae. J Biotechnol Adv 25:294–306
16. Chisti Y (2008) Response to reijnders: do biofuels from microalgae beat biofuels from terrestrial plants. Trends Biotechnol 26(7):351–352
17. Chisti Y (2008) Do biofuels from microalgae beat biofuels from terrestrial plants. Trends Biotechnol 26(7):351–352
18. Clarens AF, Resurreccion EP, White MA, Colosi LM (2010) Environmental life cycle comparison of algae to other bioenergy feedstocks. Environ Sci Technol 44:1813–1819
19. Das P, Aziz SS, Obbard JP (2011) Two phase microalgae growth in the open system for enhanced lipid productivity. Renew Energy 36:2524–2528
20. Das P, Lei W, Aziz SS, Obbard JP (2011) Enhanced algae growth in both phototrophic and mixotrophic culture under blue light. Bioresour Technol 102:3883–3887
21. Dembitsky VM, Srebnik M (2002) Natural halogenated fatty acids: their analogues and derivatives. J Progress Lipid Res 41:315–367
22. Demirbas A (2009) Progress and recent trends in biodiesel fuels. J Energy Convers Manag 50:14–34
23. Demirbas A, Demirbas MF (2010) Biodiesel from algae. In: Algae energy book, chapter 6, pp 139–157
24. Demirbas A, Demirbas MF (2011) Importance of algae oil as a source of biodiesel. Energy Convers Manag 52:163–170
25. Dos Santos MD, Guaratini T, Lopes JLC, Colepicolo P, Lopes NP (2005) Plant cell and microalgae culture. In: Modern biotechnology in medicinal chemistry and industry. Research signpost, Kerala, India
26. Duncan GR (2011) Beyond food versus fuel. Nature 474:6–8
27. Ebrahimian A, Kariminia HR, Vosoughi M (2014) Lipid production in mixotrophic cultivation of Chlorella vulgaris in a mixture of primary and secondary municipal wastewater. Renewable Energy 71:502–508
28. Folch J, Lees M Sloane, Stanley GH (1957) A simple method for the isolation and purification of total lipids from animal tissues. Biol Chem 226:497–509
29. Gahukar RT (2012) New sources of feed stocks for biofuels production: Indian perspectives. Petroleum Technol Altern Fuels 3(3):24–28
30. Gouveia L, Oliveira AC (2009) Microalgae as a raw material for biofuels production. J Ind Microbiol Biotechnol 36:269–274
31. Greenwell HC, Laurens LML, Shields RJ, Lovitt RW, Flynn KJ (2010) Placing microalgae on the biofuels priority list: a review of the technological challenges. J R Soc Interface 7(46):703–726
32. Grobbelaar JU (2000) Physiological and technological considerations for optimising mass algal cultures. J Appl Phycol 12(3–5):201–206
33. Gunaseelan NV (1997) Anaerobic digestion of biomass for methane production: a review. Biomass Bioenergy 13(1–2):83–114

34. Gustavo BL, Abdelaziz EMA, Hallenbeck CP (2013) Algal biofuels: challenges and opportunities. Bioresour Technol 145:134–141
35. Haluzan N (2010) Biofuels from algae advantages and disadvantages. http://www.renewablesinfo.com/drawbacks_and_benefits/biofuels_from_algae_advantages_and_disadvantages.html. Accessed 05 Nov 2016
36. Hasan R (2014) Bioremediation of swine wastewater and biofuel potential by using Chlorella vulgaris, Chlamydomonas reinhardtii, and Chlamydomonas debaryana. J Petroleum Environ Biotechnol 5(3):175–180
37. Hashemi NM, Tabatabaei M, Mansourpanah Y, Khatami FM, Javani A (2011) Upstream and downstream strategies to economize biodiesel production. Bioresour Technol 102:461–468
38. Hena S, Fatimah S, Tabassum S (2015) Cultivation of algae consortium in a dairy farm wastewater for biodiesel production. Water Resour Indus 10:1–14
39. Hildebrand M, Davis AK, Smith RS, Traller CJ, Abbriano R (2012) A review: the place of diatoms in the biofuels industry. Biofuels 3:221–240
40. Hoekema S, Douma RD, Janssen M, Tramper J, Wijffles RH (2002) A pneumatically agitated flat panel photo bioreactor with gas recirculation: anaerobic photohetrotrophic cultivation of a purple non sulfur bacterium. Int J Hydrogen Energy 27:1228–1331
41. Jadhav CS (2009) Demand for biodiesel will see a steady rise. Biospectrum 54–55
42. Jae-Yon L, Chan Y, So-Young J, Chi-Yong A, Hee-Mock O (2010) Comparison of several methods for effective lipid extraction from microalgae. Bioresour Technol 101:S75–S77
43. Karen M, Dougall M, McNichol J, McGinn JP, O'Leary SJB, Melanson JE (2011) Triacylglycerol profiling of microalgae strains for Biofuel feedstock by liquid chromatography–high-resolution mass spectrometry. J Bioanal Chem 401:2609–2616
44. Katiyar R, Gurjar BR, Biswas S, Pruthi V, Kumar N, Kumar P (2016) Microalgae: an emerging source of energy based bio-products and a solution for environmental issues. Renew Sustain Energy Rev (accepted)
45. Liang YN, Sarkany N, Cui Y (2009) Biomass and lipid productivities of Chlorella vulgaris under autotrophic, heterotrophic and mixotrophic growth conditions. Biotechnol Lett 31:1043–1049
46. Li Q, Du W, Liu D (2008) Perspectives of microbial oils for biodiesel production. J Appl Microbiol Biotechnol 80:749–756
47. Malla FA, Khan SA, Sharma R, Gupta GK, Abraham G (2015) Phycoremediation potential of Chlorella minutissima on primary and tertiary treated wastewater for nutrient removal and biodiesel production. Ecol Eng 75:343–349
48. Mata Teresa M, Antonio Martins A, Nidia Caetano S (2010) A review: microalgae for biodiesel production and other applications. Renew Sustain Energy Rev 14:217–232
49. Mandal S, Mallick N (2009) Microalga Scenedesmusobliquus as a potential source for biodiesel production. J Appl Microbiol Biotechnol 84:281–291
50. Mayer AMS, Lehmann VKB (2001) Marine pharmacology in 1999: antitumor and cytotoxic compounds. J Anticancer Res 21:2489–2500
51. Metzger P, Largeau C (2005) Botryococcus braunii: a rich source for hydrocarbons and related ether lipids. J Appl Microbiol Biotechnol 66:486–496
52. Miao XL, Wu QY (2004) High yield bio-oil production from fast pyrolysis by metabolic controlling of Chlorella protothecoides. J Biotechnol 110:85–93
53. Moazami N, Ashori A, Ranjbar R, Tangestani M, Eghtesadi R, Nejad AS (2012) Large-scale biodiesel production using microalgae biomass of nannochloropsis. Biomass Bioenergy 39:449–453
54. Mohan V (2013) Cultivable land continues to shrink, The Times of India. Aug 16, 2013, p 7
55. Mubaraka M, Shaijaa A, Suchithrab TV (2015) A review—the extraction of lipid from microalgae for biodiesel production. Algal Res 7:117–123
56. Packer M (2009) Algal capture of carbon dioxide; biomass generation as a tool for greenhouse gas mitigation with reference to New Zealand energy strategy and policy. Energy Policy 37 (9):3428–3437
57. Pandey A, Lee JD, Chisti Y (2014) Biofuel from algae, chapter-8, algae oils as fuel, pp 1–4

58. Park WK, Moon M, Kwak MS, Jeon S, Choi GG, Yang JW, Lee B (2014) Use of orange peel extract for mixotrophic cultivation of Chlorella vulgaris increased production of biomass and FAMEs. Bioresour Technol 171:343–349
59. Peng W, Wu Q, Tu P (2001) Pyrolytic characteristics of heterotrophic Chlorella protothecoides for renewable bio-fuel production. J Appl Phycol 13:5–12
60. Pirt SJ, Tansley (1986) A review (4) the thermodynamic efficiency (quantum demand) and dynamics of photosynthetic growth. J New Phytol 102:3–37
61. Pragyaa N, Pandeya KK, Sahoo PK (2013) A review on harvesting, oil extraction and biofuels production technologies from microalgae. Renew Sustain Energy Rev 24:159–171
62. Qiang H, Sommerfeld M, Jarvis E, Ghirardi M, Posewitz M, Seibert M, Darzins A (2008) Microalgal triacylglycerols as feedstocks for biofuel production: perspectives and advances. Plant J 54:621–639
63. Ramos de Ortega A, Roux JC (1986) Production of Chlorella biomass in different types of Flat bioreactor in temperate zones. Biomass 10:141–156
64. Rashid N, Rehman MSU, Han JI (2013) Recycling and reuse of spent microalgal biomass for sustainable biofuels. Biochem Eng J 75:101–107
65. Rawat I, Ranjith R, Mutanda T, Bux F (2011) Dual role of microalgae: phycoremediation of domestic wastewater and biomass production for sustainable biofuels production. J Appl Energy 88:3411–3424
66. Reijnders L (2008) Do biofuels from microalgae beat biofuels from terrestrial plants? Trends Biotechnol 26(7):349–350
67. Rekha V, Gurusami R, Santhanam P, ShenbagaDevi A, Ananth S (2012) Culture and biofuel production efficiency of Marine Microalgae Chlorella Marina and Skeletonema costatum. Ind J Geo-Marine Sci 41(2):152–158
68. Rodolphi L, Zittelli GC, Bassi N, Padovani G, Biondi N, Bonini G, Tredici MR (2009) Microalgae for oil: strain selection, induction of lipid synthesis and outdoor mass cultivation in a low-cost photobioreactor. J Biotechnol Bioeng 102:100–112
69. Rojan P, Johna GS, Anishab K, Nampoothiric M, Pandey A (2011) Micro and macroalgal biomass: a renewable source for bioethanol. Bioresour Technol 102(1):186–193
70. Samson R, Leduy A (1985) A multistage continuos cultivation of blue green alga Spirulina maxima in the flat photobioreactor. J Chem Eng 63:105–112
71. Satyanarayana KG, Mariano AB, Vargas JVC (2011) A review: microalgae, a versatile source for sustainable energy and materials. J Integrated Energy Res 35:291–311
72. Schenk MP, Skye R, Hall T, Stephens E, Marx UC, Mussgnug JH, Posten C, Kruse O, Hankamer B (2008) Second generation biofuels—high-efficiency microalgae for biodiesel production. J Bioenergy Res 1:20–43
73. Scott SA, Davey MP, Dennis JS, Horst I, Howe CJ, LeaSmith DJ, Smith AG (2010) Biodiesel from algae: challenges and prospects. J Curr Opinion Biotechnol 21:277–286
74. Sdrula N (2010) A study using classical or membrane separation in the biodiesel process. Desalination 250:1070–1072
75. Sheehan J, Dunahay T, Benemann J, Roessler P (1998) A look back at the US Department of Energy's Aquatic Species Program—biodiesel from algae. National Renewable Energy Laboratory (NREL) report: NREL/TP-580-24190, Golden, CO
76. Shen QH, Jiang JW, Chen LP, Cheng LH, Xu XH, Chen HL (2015) Effect of carbon source on biomass growth and nutrients removal of Scenedesmusobliquus for wastewater advanced treatment and lipid production. Bioresour Technol 190:257–263
77. Sherif SA, Goswami YD, Stefanakos KE, Steinfeld A (2014) A Hand book of hydrogen energy, p 337
78. Singh A, Nigam PS, Murphy JD (2011) Renewable fuels from algae: an answer to debatable land based fuels. Bioresour Technol 102:10–16
79. Spolaore P, Joannis-Cassan C, Duran E, Isambert A (2006) Commercial applications of microalgae. J Biosci Bioeng 101(2):87–96
80. Suali E, Sarbatly R (2012) Conversion of microalgae to biofuel. Renew Sustain Energy Rev 16:4316–4342

81. Subramaniam R, Dufreche S, Zappi M, Bajpai R (2010) Microbial lipids from renewable resources: production and characterization. J Indus Microbiol Biotechnol 37:1271–1287
82. Sun F, Chen H (2008) Organosolv pretreatment by crude glycerol from oleochemicals industry for enzymatic hydrolysis of wheat straw. Bioresour Technol 99:5474–5479
83. Tabatabaei M, Masoud T, Salehi JG, Mohammadreza S, Mohammad P (2011) Biodiesel production from genetically engineered microalgae: future of bioenergy in Iran. Renew Sustain Energy Rev 15:1918–1927
84. Tapiero H, Townsend DM, Tew KD (2004) The role of carotenoids in the prevention of human pathologies. J Biomed Pharmacol 58:100–110
85. USEIA (2012) Annual energy outlook. US Energy Information Administration. http://www.eia.gov/forecasts/aeo/pdf/0383(2012).pdf
86. Verbruggen A, Mohamed Marchohi, Marchohi Mohamed Al (2010) Views on peak oil and its relation to climate change policy. J Energy Policy 38:5572–5581
87. Victoria HW, Sarah DA, Radakovits R, Jinkerson RE, Posewitz MC (2012) Improving photosynthesis and metabolic networks for the competitive production of phototroph-derived biofuels. Curr Opin Biotechnol 23:290–297
88. Xin L, Hong-ying H, Ke G, Ying-xue S (2010) Effects of different nitrogen and phosphorus concentrations on the growth, nutrient uptake, and lipid accumulation of a freshwater microalga Scenedesmus sp. Bioresour Technol 101:5494–5500
89. Yoo C, Jun SY, Lee JY, Ahn CY, Oh HM (2010) Selection of microalgae for lipid production under high levels carbon dioxide. Bioresour Technol 101:S71–S74
90. Young LC, Kyubock L, You-Kwan O (2015) A review-Recent nanoparticle engineering advances in microalgal cultivation and harvesting processes of biodiesel production. Bioresour Technol 184:63–72
91. Zheng H, Gao Z, Yin F, Ji X, Huang H (2012) Lipid production of Chlorella vulgaris from lipid extracted microalgal biomass residues through two-step enzymatic hydrolysis. Bioresour Technol 117:1–6

Surrogates for Biodiesel: Review and Challenges

Aditya Dilip Lele, Krishnasamy Anand and Krithika Narayanaswamy

Abstract Biodiesel is being considered as a renewable fuel candidate to completely or partially replace fossil diesel. Understanding its combustion is key to assess its applicability in practical compression ignition engines. Significant progress has been made in understanding biodiesel combustion through experimental studies, development of reaction kinetics to describe its oxidation, and simulations in typical engine environments. The use of surrogates in place of the real biodiesels plays a crucial role in this endeavour. This chapter reviews the existing studies revolving around surrogate fuels for biodiesels. Thereafter, the challenges ahead in this context to further enhance our knowledge of biodiesel combustion are presented, and possible options to address these are discussed where appropriate.

Keywords Biodiesel · Surrogate · Chemical kinetics · Challenges

List of Abbreviations

MB	Methyl butanoate
MB2D	Methyl crotonate
MD	Methyl decanoate
MD5D	Methyl-5-decanoate
MD9D	Methyl-9-decanoate
nC7	*n*-heptane
CN	Cetane number
NTC	Negative temperature coefficient
LHV	Lower heating value
CFPP	Cold filter plugging point
JSR	Jet stirred reactor
RME	Rapeseed methyl ester
PME	Palm methyl ester
HCCI	Homogeneous charge compression ignition
NO_x	Nitrogen oxides

A.D. Lele · K. Anand · K. Narayanaswamy (✉)
Department of Mechanical Engineering, Indian Institute of Technology Madras, Chennai, India
e-mail: krithika@iitm.ac.in

A.K. Agarwal et al. (eds.), *Biofuels*, Green Energy and Technology,
DOI 10.1007/978-981-10-3791-7_10

1 Introduction

In the wake of depleting fossil fuel resources, the use of renewable and alternate fuels has gathered momentum. Biodiesel is one such fuel, which has shown the potential to partially or completely substitute diesel fuel [1]. Biodiesel is typically derived from plant oil or animal fat using trans-esterification [2]. Existing engine design and operating strategies have evolved with fossil fuels as the principal focus. The use of biodiesel in compression ignition (CI) engines requires no major engine modifications, and therefore makes it an attractive replacement for diesel fuel [3]. To assess and quantify the use of these alternative fuels in practical engines, understand their combustion behavior, reactivity, and emission characteristics using computations, it is important to incorporate finite rate chemistry in these studies.

In the case of fossil derived fuels, which are a mixture of several hundreds of species belonging to different hydrocarbon classes, a reaction mechanism that describes the oxidation of the complex mixture is impractical. Therefore, in computational studies, the notion of using a representative simpler surrogate fuel in place of the real fuel, which reproduces certain target properties of the real fuel is the practical way forward when dealing with fuels such as kerosene [4, 5], diesel [6, 7], and gasoline [8]. On the contrary, most biodiesels, consist of only a few major components (4–6) as shown in Table 1, which permits detailed kinetic description of the actual fuel. However, these components being long chain ester molecules, detailed kinetic mechanisms for the real biodiesel typically runs into several thousands of species and reactions [9]. Since reactive flow computations of combustion dynamics in the engine scale are expensive, there is a severe restriction on the size of chemical kinetic mechanism that can be coupled with the simulations. To simplify the kinetic description of biodiesel in computations, surrogates made of simpler well-studied molecules are used in place of the actual fuel, for which accurate and compact reaction mechanisms are proposed. In this short write-up, the focus is to present a review of the existing work on surrogate fuels for biodiesels that represent their gas phase combustion characteristics, kinetic model

Table 1 Chemical composition of biodiesels obtained from different sources [11]

Source	Methyl palmitate (C16:0)	Methyl stearate (C18:0)	Methyl oleate (C18:1)	Methyl linoleate (C18:2)	Methyl linolenate (C18:3)
Soybean	11.3	3.6	24.9	53.0	6.1
Rapeseed	4.9	1.6	33	20.4	7.9
Animal fat	25.2	19.2	48.9	2.7	0.5
Canola	3.9	3.1	60.2	21.1	11.1
Lard	25.5	15.5	47.1	8.9	1.1
Karanja	11.1	2.9	60.6	16.9	0

Note that the amount of different components in a particular biodiesel will also vary depending on the source of the fuel

development for these surrogate fuels, and a brief note on formulating surrogates for liquid phase fuel spray representation.

In the remainder of this section, the chemical composition and properties of biodiesel are reviewed. This provides the necessary background for the discussion on surrogates and their kinetic modeling, which follows in Sect. 2. Thereafter, challenges and scope for future work are summarized in Sect. 3. All numerical calculations presented here have been performed using the FlameMaster code (version 3.3.9, [10]).

1.1 Chemical Composition

As stated earlier, biodiesel can be derived from number of vegetable oil or animal fat sources using trans-esterification. The readers are referred to Demirbas [2] for a detailed discussion on biodiesel production process. The chemical composition of biodiesel varies depending on its source and alcohol used in trans-esterification, a process which converts a fatty acid into an alkyl ester using an alcohol. With methanol being the preferred choice for alcohol, a majority of biodiesels are a mixture of methyl esters. A large database on the properties and composition of biodiesel is available [11–14], which is summarized in the table below.

Most commonly found methyl esters in biodiesel include methyl palmitate (C17:0), stearate (C19:0), oleate (C19:1), linoleate (C19:2) and linolenate (C19:3) as listed in Table 1 (see Fig. 1). In the short names, for instance, C19:1, the first number indicates the total number of carbon atoms in the hydrocarbon chain attached to ester group. Methyl esters with longer chain display higher reactivity. The second number corresponds to the number of double bonds present in the chain. The degree of unsaturation has been found to have significant impact on the reactivity of the biodiesel as well [15] and this will be discussed in detail in Sect. 2.2. The presence of oxygen in the fuel molecule gives it distinct combustion features such as early CO_2 formation [16] and also results in lesser lower heating value (LHV) compared to diesel.

1.2 Properties

Properties of the biodiesel are almost similar to that of diesel, which makes it an viable replacement for diesel. Table 2 compares important properties of a typical biodiesel with those of diesel.

Properties such as density, viscosity, surface tension, vapor pressure and boiling point are important in determining spray characteristics of biodiesel, whereas C, H, O atom content, lower heating value, and cetane number are key in determining the heat release and ease of ignition during its gas-phase combustion. A mixture designed to mimic the important physical properties of the real fuel is called a

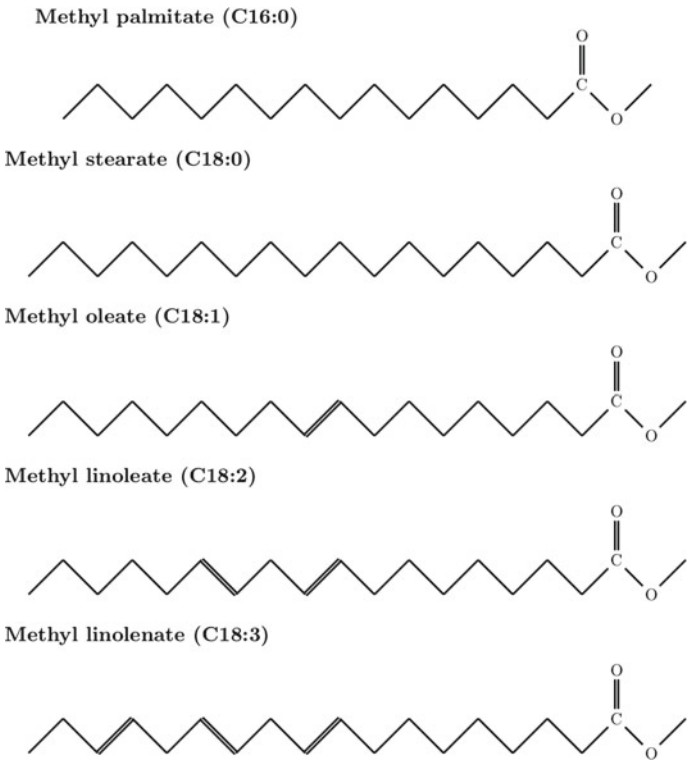

Fig. 1 Chemical structures of commonly found methyl esters in biodiesels

Table 2 Comparison of biodiesel and diesel properties [17]

Properties	Biodiesel	Diesel
C, H O, wt%	77, 12, 11	84–87, 13–16, 0
Molecular weight	292	195
Density @ 20 °C (kg/L)	0.870–0.892	0.831
Viscosity @ 40 °C (mm^2/s)	3.1–5.4	3
Boiling point °C	330–340	160–380
Lower heating value (MJ/kg)	37.4–40.1	42.6
Flash point °C	135–180	74
Stoichiometric A/F, (by wt)	13	14.7
Cetane number	42–61	>45
CFPP	−11–12	17

physical surrogate, which can be different from a chemical surrogate, which is formulated to capture the gas-phase combustion targets [18]. The focus of the present discussion will primarily center around chemical surrogates.

2 Surrogates for Biodiesels and Their Kinetic Modeling

The target application of the surrogate drives its selection for any fuel. In case of biodiesel, its application is mainly in compression ignition engines where it is used as a neat fuel or in the form of blends with diesel. Furthermore, depending on the specific target that the surrogate is intended for, it can be defined to emulate those key properties of the real fuel that are necessary to predict the desired combustion characteristics. For instance, surrogates may be defined specific to capturing heat release rate alone versus onset of ignition or emission predictions. Such surrogates could also be defined to account for the biodiesel composition itself, which varies depending on its source.

Thus, there are three main aspects to formulating a surrogate: (a) choice of surrogate components, (b) identification of target properties to match between the surrogate and the real fuel, and (c) determination of the amounts of each component in the surrogate to define the surrogate. Note that the set of properties to be reproduced between the surrogate and the real fuel itself plays a key role in determining the suitable components of the surrogate. This aspect is highlighted with specific examples in the discussion in Sect. 2.2. Additionally, the accuracy of the individual component's kinetic mechanism should also be paid attention to while choosing the components in a surrogate, since this has a direct bearing on the accuracy of the kinetic description of the multi-component surrogate itself. Once the components of the surrogate mixture are chosen and the target properties are identified, one strategy to define a surrogate is using a constrained optimization approach, such as those employed in Refs. [5, 19–21] to define gasoline, diesel, and jet fuel surrogates. Another attractive approach for surrogate definition is briefly presented in Sect. 3.

Several surrogates have been proposed for biodiesels [16, 22–34]. Based on the compositional analysis of biodiesels presented in Table 1, methyl ester molecules of differing chain lengths and degrees of unsaturation have been used as components in these surrogate mixtures. It is interesting to note that a surrogate comprising just a normal alkane can still reproduce the reactivity of biodiesels [35], although not the ester specific characteristics of biodiesel oxidation, mandating an ester representative in the surrogate mixture. The choice of the ester molecule in the surrogate used in these studies has been influenced both by the availability of accurate kinetics for the ester molecules and the size of their chemical mechanisms. A brief summary of kinetic models for ester molecules relevant to biodiesels is presented first, followed by a discussion of surrogate mixtures proposed in the literature.

2.1 Kinetics of Methyl Ester Molecules

2.1.1 Kinetic Models for Saturated Methyl Esters

The earliest studies on ester kinetics focusing on methyl formate, the smallest member of the methyl ester group, and methyl butanoate (MB), a candidate for biodiesel surrogate, were conducted by Fisher et al. [36]. In their reaction mechanism, rules for estimating kinetic parameters were adopted from hydrocarbon combustion. The kinetic model showed qualitative agreement with the low temperature sub-atmospheric experiments available then. Gail et al. [22] updated this mechanism and compared against experimental data obtained in jet stirred reactor (JSR) at 0.101 MPa, $\phi = 1.13$ and 800 K < T < 1350 K. This mechanism was further validated against more experiments using opposed flow diffusion flame and Princeton variable pressure flow reactor data with good agreement. Metcalfe et al. [37] also developed a detailed mechanism for $C_5H_{10}O_2$ ethyl and methyl esters. Their comparison in shock tubes indicated that ethyl propanoate is more reactive than methyl butanoate. The reader is referred to Refs. [9, 38–41] for further details on kinetic modeling of saturated methyl esters.

While the kinetics of methyl butanoate serves as a prototype for methyl ester kinetics, it does not exhibit the NTC behavior that is characteristic to long chain methyl esters found in biodiesel [22, 36] (see Fig. 2). As a remedy, methyl decanoate was proposed as a representative of the ester content in biodiesel surrogates in later studies, which possessing a longer carbon chain than methyl butanoate, shows Negative Temperature Coefficient (NTC) behavior. A detailed kinetic mechanism for methyl decanoate (MD) was developed by Herbinet et al. [16] based on the reaction class description by Curran et al. [42, 43] and using ester specific kinetics from methyl butanoate mechanism [36]. Including methyl decanoate component in the surrogate also permitted to predict the early CO_2 formation characteristic to biodiesel combustion. A surrogate comprised of methyl decanoate

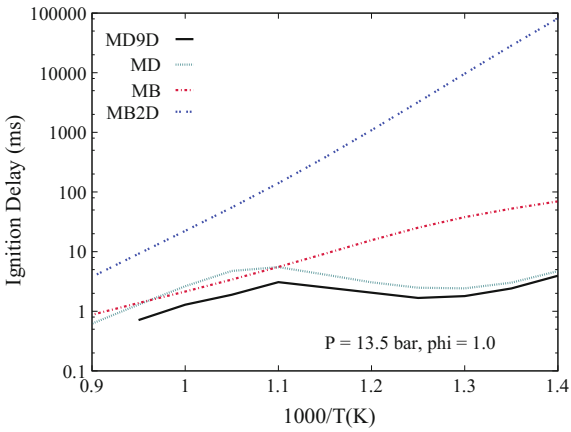

Fig. 2 Comparison of simulated ignition delay times for different methyl esters surrogates (MB, MB2D [45], MD, MD9D [34]) at P = 13.5 bar and ϕ = 1; lines-simulations

and *n*-heptane was found to give qualitatively good results against JSR experiments performed with Rapeseed methyl ester (RME) as the fuel [35]. Based on the chemical reaction scheme constructed by Herbinet et al. [16], a new chemical kinetic model was developed for methyl decanoate by Diévart et al. [44]. This model adapts the kinetic and thermochemical parameters of methyl decanoate from those of methyl butanoate oxidation, and thereby achieves improved predictions for ignition delays, species profiles in jet stirred reactors, and flame speeds.

2.1.2 Kinetic Models for Unsaturated Methyl Esters

Most of the biodiesels contain significant amount of unsaturated methyl esters, whose importance as a surrogate component needs to be understood. Gail et al. [45] further developed their methyl butanoate mechanism to include methyl crotonate (MB2D) to account for the unsaturated ester content of biodiesels. This mechanism has been validated at moderate to high temperatures, 900–1400 K and equivalence ratios of 0.5–1.13. While methyl crotonate has its advantages similar to that of methyl butanoate, in that it can be represented by a compact scheme, it does not exhibit the NTC behavior characteristic of biodiesels (see Fig. 2), and this motivated the need to study longer unsaturated methyl esters in surrogates.

Based on their methyl decanoate mechanism, Herbinet et al. [34] further developed reaction schemes for methyl-5-decanoate (MD5D) and methyl-9-decanoate (MD9D). These are unsaturated methyl esters with a C10 carbon chain having one double bond at the 5th and 9th C atom away from ester group, respectively. Methyl-5-decanoate has a C=C bond in the middle of the chain, which is similar in position to that found in many biodiesel components such as methyl stearate, whereas methyl-9-decanoate mimics the distance of the C=C bond in biodiesel components from the ester group. These mechanisms were also compared against JSR experiments with RME. Their comparison indicated that MD9D is better at representing major species profiles than MD5D and hence a better candidate to represent the unsaturated ester content of biodiesels in a surrogate.

2.1.3 Kinetic Models for Biodiesels

This picture is completed by noting that detailed chemical kinetic schemes for the ester molecules present in actual biodiesel components, such as methyl palmitate, methyl stearate, methyl oleate, methyl linoleate and methyl linolenate, have been developed recently [9]. This mechanism based on the work for methyl decanoate and its unsaturated counterparts, consists of $\sim$4800 species and $\sim$30,000 reactions. Herbinet et al. [46] also generated mechanisms for C11–C19 saturated methyl esters using a reaction mechanism generation software, EXGAS. A mechanism generated in this manner for methyl stearate is huge, with $\sim$6203 species and $\sim$43,444 reactions. Recent studies have focused on obtaining reduced mechanisms starting with the detailed kinetic scheme proposed by Westbrook et al. [9], for instance, Ref. [47].

With this discussion providing a brief account of the development of ester kinetics specific to biodiesels, surrogates proposed for biodiesels are detailed next. Readers may refer to more comprehensive reviews [48, 49] for elaborate accounts of ester kinetics.

2.2 Components of Surrogate Mixtures

Due to the lack of long chain methyl ester kinetic models, initial studies used a small methyl ester component usually combined with *n*-alkane to define surrogates for biodiesels. Several works have used a combination of methyl butanoate and *n*-heptane in different proportions as a surrogate for the desired biodiesel [23, 25]. Long chain *n*-alkanes, such as *n*-hexadecane, have been found to replicate the reactivity of rapeseed methyl esters in jet stirred reactor experiments [35]. However, it can be surmised that a normal alkane alone may not be well suited to predict the ignition delays and major intermediates in the case of biodiesels, which have larger amounts of unsaturated components. In fact, significant differences in ignition delays of saturated and unsaturated methyl esters at low temperatures are suggested by the kinetic scheme proposed by Westbrook et al. [9] for the actual biodiesel components, and this is also corroborated by shock tube experiments [15]. As a representative of the unsaturated ester content in biodiesels, a small molecule, methyl crotonate has been used in addition to methyl butanoate and *n*-heptane in some other studies [24, 26].

Later studies substituted methyl decanoate in place of methyl butanoate in the surrogate, owing to its ability to reproduce the reactivity, NTC behavior, and early CO_2 rise, which are characteristic of the long chain methyl esters in biodiesels [16, 27–30, 50].

Reactivity of biodiesel, represented by its cetane number, is also found to be a function of its degree of unsaturation. Four components have been used to represent unsaturated ester content of biodiesel, namely MB2D, MD9D, MD5D and methyl linoleate. Herbinet et al. [34] concluded that MD9D is a better candidate to represent unsaturated ester based on JSR experiments. But shock tube experiments [15] with MD5D and MD9D have suggested otherwise. It has been found that MD5D has ignition delays that are longer by almost a factor of two at $T < 900$ K compared to MD, while those of MD9D are comparable to MD. This observation has prompted many researchers [29, 32, 33] to choose MD5D as the unsaturated methyl ester candidate in their surrogates, while others have opted for MD9D [27–30].

Recently, Liu et al. [32], included methyl linoleate itself as a surrogate component to represent the multiple C=C bonds present in biodiesels (see Table 1), since no existing surrogate candidate belonged to the diene hydrocarbon class. Reduced kinetic schemes for several of these surrogate combinations have also been developed invoking state-of-art model reduction strategies, and are discussed briefly in Sect. 2.3.

From the above discussion, we see that the presence of at least one methyl ester component is typical of all surrogates proposed to represent biodiesel. Addition of *n*-alkane in the surrogate helps to match reactivity as well as the heat content of the biodiesel. The importance of a representative for the unsaturated ester content of the biodiesel to mimic ignition as well as major species profiles is also acknowledged in the literature. Most of the above combinations perform well in predicting engine parameters like pressure rise rate and ignition delays, but improved accuracy is desirable. A list of various surrogate mixtures proposed for biodiesel is summarized in Appendix.

Analysis on the Choice of Surrogate Components

A comparison between two surrogates with the same carbon content: one comprising of 2.75 mol of 20% methyl butanoate and 80% *n*-heptane (by mole %), while the other having 2 mol of 25% methyl decanoate, 25% methyl-9-decanoate, and 50% *n*-heptane, is provided here to examine their usability as surrogates for different target applications. The kinetic schemes for these surrogates come from the compact schemes derived by Liu et al. [23] for the surrogate containing methyl butanoate and Luo et al. [31] for the surrogate containing methyl decanoate, using Fisher et al. [36] and Herbinet et al. [34] as the reference mechanisms, respectively.

Figure 3 shows that the differences in predictions between the two surrogates for soot precursors such as ethylene and acetylene concentrations in a plug flow reactor are small, within 20%, whereas this increases up to 100% for ethane. In this case, considering the soot precursors alone, although both surrogates show similar predictions (equally good or bad depending on actual values for the real fuel), the compact size of the methyl butanoate and *n*-heptane kinetic scheme can make it an attractive choice compared to surrogates made of long chain methyl esters such as methyl decanoate. Further, being a small molecule, methyl butanoate has attracted many experimental studies [22, 40, 41, 45, 51–53], compared to the longer methyl esters such as methyl decanoate [53–55], and has thereby facilitated the development of accurate kinetic schemes for methyl butanoate [45, 51].

The ignition delays of the two surrogates at low through high temperatures are shown in Fig. 4. Note that although methyl butanoate does not exhibit the NTC behavior [51] characteristic of biodiesel by itself, when combined with a *n*-alkane, for instance, a mixture of methyl butanoate and *n*-heptane does exhibit NTC behavior due to the alkane component [23]. More importantly, Fig. 4 shows that significant differences are seen in ignition delays between the two surrogates, which could place one more suitable for determining the onset of ignition, depending on the reactivity of the real fuel. Similar extents of differences are also observed at equivalence ratios other than the stoichiometric conditions examined in Fig. 4 (not shown here).

Laminar flame speeds of the surrogates are compared in Fig. 5. Similar to ignition delays, the surrogates show significant differences in laminar flame speed predictions, up to 45%. It can be seen that the surrogate containing methyl

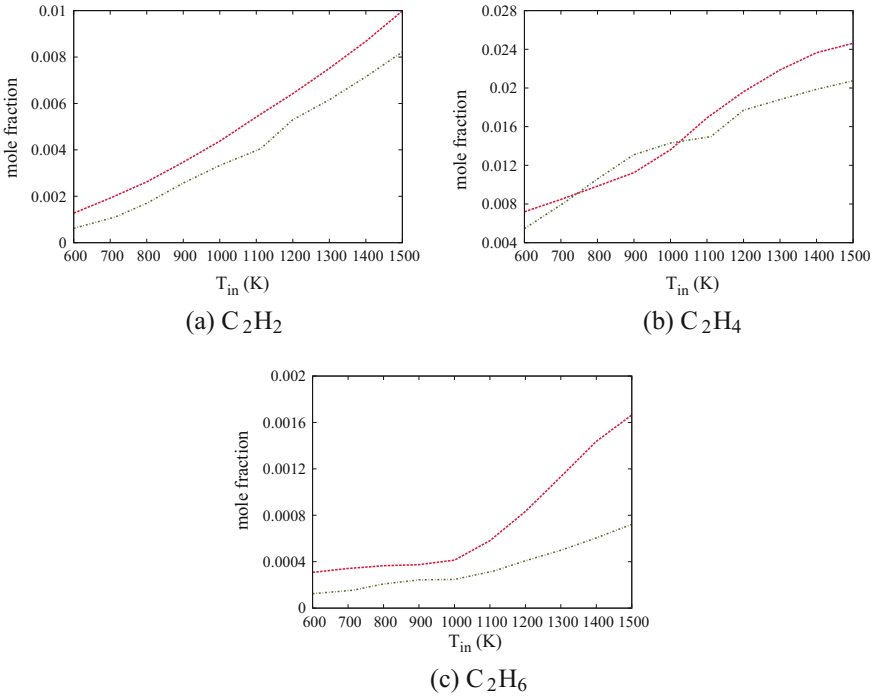

Fig. 3 Comparison of computed species profiles for C_2H_2, C_2H_4, C_2H_6 in plug flow reactor for initial $T = 1000$ K, $\phi = 1$ and $P = 20$ atm; *lines* simulations results for two surrogates: (i) MB + n-heptane (-·-·-) [23] and (ii) MD + MD9D + n-heptane (···) [31]

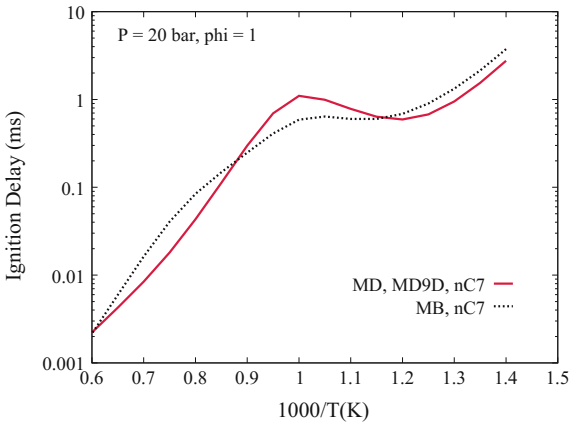

Fig. 4 Comparison of ignition delay times; *lines* simulations for two surrogates: (i) MB + n-heptane (···) [23], (ii) MD + MD9D + n-heptane (—) [31]

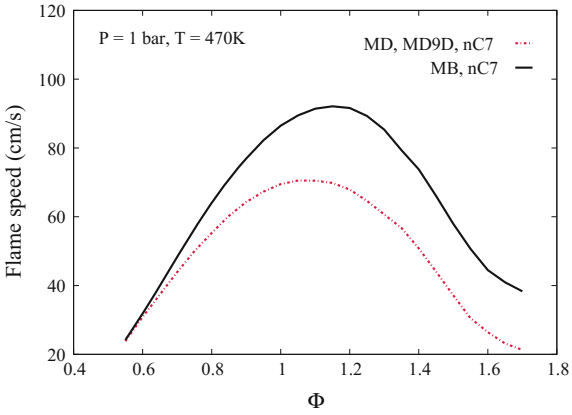

Fig. 5 Comparison of laminar flame speeds; *lines* simulations results for two surrogates: (i) MB + n-heptane (—) [23], (ii) MD + MD9D + n-heptane (-···-) [31]

butanoate [23] exhibits larger burning speeds compared to the other containing methyl decanoate [31]. These relative differences would have a direct bearing on the predictions of fuel burning rate in internal combustion engines and thereby the engine's thermal efficiency [56, 57] and emissions, when using one surrogate in place of the other.

Therefore, while both surrogates having the same carbon content can predict the amount of ethylene and acetylene in engine simulations, the choice of surrogate components can certainly impact the predictions of onset of ignition and flame speeds. This discussion asserts the importance of the choice of surrogate components, and how this decision has to be arrived at tailoring to the specific application that the surrogate is intended for.

2.3 Surrogate Definition and Kinetic Modeling

Given a set of target properties to emulate between the surrogate and the real fuel, a surrogate can be constituted and defined to best reproduce them. As noted earlier, these target properties will depend on the application for which the surrogate is intended. Matching or closely matching the carbon content of the real fuel is a criterion used by most of the studies [25, 31, 34]. Other criteria have also been used to define surrogate composition in addition to carbon content, such as matching the heating value [25], cetane number [23] and ester content [34]. The different surrogate criteria used in the literature are summarized in Appendix.

2.3.1 Comparing Different Surrogate Definition Criteria

Figure 6 compares simulated ignition delays of surrogates made of methyl butanoate and *n*-heptane mixture defined based on two different criteria. In the first case, fuel is taken as a mixture of 20% MB and 80% *n*-heptane (by mole), whose cetane number is closer to that of the real fuel [23]. Whereas, in the second case, one mole of fuel is assumed to be composed of 1 mol of methyl butanoate and 2 mol of *n*-heptane [25], so that its heating value is closer to the real fuel. This case translates into a surrogate with 33% of methyl butanoate and 67% of *n*-heptane (by mole). The two surrogates, comprising the same components, depict similar predictive capabilities for major species in flow reactors (not shown here). However, they show different ignition delays at moderate and low temperatures, which can have an impact on the onset of ignition in a compression ignition engine. Thus, the criteria employed in the surrogate definition can play an key role in predicting the combustion dynamics in engine simulations.

2.3.2 Kinetic Models for Surrogates

Although the size of mechanisms for biodiesel surrogates are smaller compared to the detailed mechanism for actual biodiesel components, they still remain computationally expensive to be incorporated in turbulent combustion simulations. Several studies [23, 26, 28, 32] use a combination of existing graph based reduction methods such as DRG [58], DRGEP [59], DRGEPSA [60] and species and reaction lumping to derive compact kinetic schemes to be coupled with reactive flow simulations [30–32].

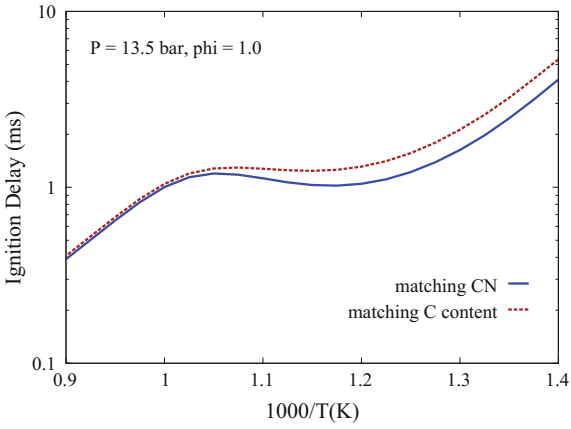

Fig. 6 Comparison of ignition delay times at $P = 13.5$ bar and $\phi = 1$ computed with two different surrogates comprised of methyl butanoate and n-heptane, defined by (i) matching cetane number and (ii) matching carbon content

In a nutshell, these reduction techniques rely on eliminating species and reactions not important at the desired target conditions. To compensate for the errors due to reduction, in a few studies [26, 28, 30, 32], pre-exponential factors in the rate constants of reactions with high sensitivity towards parameters such as ignition delays have been adjusted. Other studies [29, 32] have opted for the development of skeletal mechanism using a decoupling methodology. In this approach, a reduced C_2–C_3 mechanism and a detailed H_2/CO/C_1 forms the basis. Thereafter, this mechanism is extended to include the overall reaction pathways for the fuel under consideration. Following this, the kinetic parameters are optimized using available experimental results. Both these approaches result in compact surrogate mechanisms suitable for the computationally demanding combustion models (for instance, see Refs. [61–63]). Some remarks on deriving such reduced mechanisms are presented in the following section.

It is interesting to note that the definition of the surrogate composition also plays an important role in deriving combustion kinetic models for the multi-component fuel oxidation. In the context of gasoline surrogates, it has been demonstrated that depending on the composition of the multicomponent surrogate for which the reduced mechanism is derived, different reduced schemes can be obtained, specific to the precise surrogate composition [64]. In fact, most of the reduced reaction schemes for biodiesel surrogates follow this trend and tend to be specific to the proposed surrogate composition.

While kinetic models developed in this manner have been assessed for the specific surrogate, they do not guarantee similar accuracy for changes in surrogate composition. When it is of interest to understand the specificities arising out of the variabilities in biodiesels (depending on its source), reaction mechanisms that also allow examining surrogates for different biodiesel compositions are preferred. Recently, Cheng et al. [30] developed such a *generic* reduced surrogate mechanism using methyl decanoate, methyl-5-decanoate, and *n*-heptane as components that is applicable for biodiesels arising out of different sources. Furthermore, these generic kinetic schemes are also particularly useful to evaluate different surrogate definition criteria by proposing several surrogate mixtures with varying component compositions (still comprised of the same chosen components) and thereby crystallize the best approach to define a surrogate for a particular type of biodiesel fuel and a desired target application.

3 Challenges

Having summarized the recent work on biodiesel surrogates, this section focus on the challenges ahead in this field.

3.1 Widening the Experimental Database for the Real Fuel and its Components

Experimental data for biodiesels lag behind other hydrocarbons, especially when it comes to ignition delay measurements at moderate and low temperatures ($T < 900$ K). With advanced combustion technologies such as HCCI or ultra lean combustion, which are more chemical kinetically driven compared to conventional combustion strategies, it is imperative to experimentally study the behavior of the fuels in wider operating ranges, especially in the low temperature regime, yet in simple reactor configurations, to facilitate the development of accurate kinetics for the real fuel. Low vapor pressure of biodiesel fuels and their components pose considerable challenges to conducting heated shock tube experiments at these temperatures. Aerosol shock tubes have been proposed as a viable alternative for measuring ignition delays of these fuels [65].

Experimental data for ignition delays of the actual biodiesel fuel can pave way to propose better surrogates for the specific biodiesel. Recently, a surrogate definition strategy has been proposed for jet fuels [66], which suggests that in place of the cetane number used as a criteria for matching reactivity between real fuel and the surrogates, the experimental ignition delay data of the real fuel over a wide range of pressures and temperatures themselves be used. This strategy has been found promising and demonstrates that a better jet fuel surrogate, than one defined based on cetane number, can be proposed using the same components. The idea can be similarly extended to defining biodiesel surrogates, if experimental data for ignition delays of the real fuel at wide temperature and pressure ranges become available.

Further, the existing literature lacks ignition delay measurements for the components of the real biodiesel at moderate and low temperatures. These experimental datasets are valuable to validate the component kinetics, which show widely different reactivities depending on their degree of unsaturation (see Fig. 7). Such well-validated kinetic schemes for the actual components of biodiesels will form a

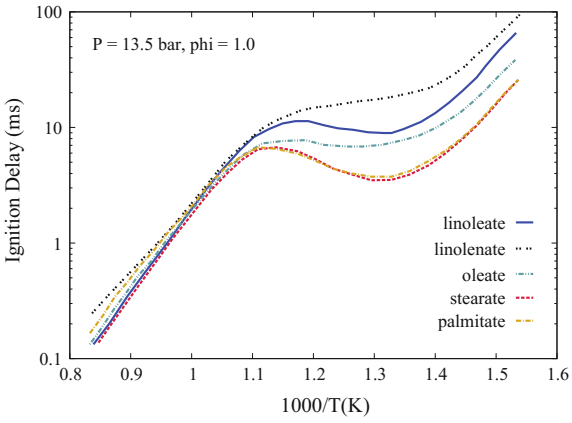

Fig. 7 Comparison of ignition delays of different methyl esters present in biodiesels at $P = 13.5$ bar and $\phi = 1$; *lines* simulations [9]

solid base for selecting suitable representatives for the different types of methyl esters to form a surrogate mixture, which can emulate the same ignition behavior as the real fuel.

3.2 Accuracy of Surrogate Component Kinetics

A non-exhaustive summary of methyl ester kinetic modeling and the significant progress made until recently has been provided earlier. Noneless, there is still a need to further refine the present detailed mechanisms for the ester components of the surrogates. In fact, it has been noted by Wang et al. [15] when comparing the reactivities of different C10 methyl esters: methyl decanoate (MD), methyl-9-decanoate (MD9D), and methyl-5-decanoate (MD5D) in a shock tube that MD9D is close in reactivity to MD, while this aspect is not predicted by the existing detailed mechanisms for these methyl esters. While the ignition delay data from Wang et al. provide a useful target for validation of kinetic models proposed for these components, the development of accurate kinetics for these methyl esters and a comprehensive assessment will greatly benefit from additional experimental data for the oxidation of these methyl esters in flow reactors and flame configurations as well.

3.3 Surrogate Definition Criteria for Gas Phase Applications

It has been noted in the earlier discussion that several criteria have been used for surrogate definition, such as carbon content, heating value, cetane number, ester content, and unsaturated molecule content. A general agreement on the most important set of definition criteria has been suggested and agreed upon for formulating jet fuel surrogates [4], diesel fuel surrogates [6], and gasoline surrogates, whereas such a consensus is yet to be reached for biodiesel surrogates. This needs a systematic and careful assessment of the different surrogate definition criteria (and additionally others if relevant) and their significance to the target applications, which they are intended for.

3.4 Deriving Reduced Mechanisms for Surrogates

Several studies have derived reduced mechanisms for surrogate mixtures and optimized the reduced kinetics against experimental data or with the corresponding reference detailed mechanism [26, 29, 30, 32, 33]. The changes in rate parameters

are justified in order to compensate for the errors due to reduction, nevertheless, the optimized mechanism compromises on the kinetic accuracy.

As a consequence, this procedure may not guarantee similar accuracy in configurations for which the mechanism has not been optimized for. The authors believe that this approach, which is the viable one in the absence of accurate kinetics for the surrogates components, must be revisited when the surrogate component kinetics are better described. Reduced and compact mechanisms must ideally be derived starting from a reference mechanism that is well-validated, using reduction strategies to prune out insignificant species and pathways pertaining to the target conditions.

3.5 *Surrogates for Liquid Phase Applications*

The discussion in this chapter has entirely been on chemical surrogates, which are intended for gas-phase applications. To represent fuel spray characteristics, such as atomization, vaporization and mixing, the physical properties, such as density, viscosity, and surface tension, are particularly important to be matched between the real fuel and the surrogate. Table 3 shows some of these properties for the typical components used in gas-phase surrogates and for an actual biodiesel. It is not surprising to note that no combination of these components can emulate some of the key liquid phase properties, such as kinematic viscosity and boiling point. Hence, it becomes important to describe liquid phase properties using a separate surrogate.

As highlighted in the previous section, biodiesels are less complex in terms of number of components in its chemical composition (only 4–6) compared to diesel, gasoline or jet fuels. Considering this, liquid phase properties of biodiesel could be represented precisely by its actual methyl ester constituents. Thus, a model fuel for biodiesel can use two groups of surrogates: one to represent the liquid phase properties and the other to represent the gas phase kinetics of biodiesel. As indicated earlier, in the case of biodiesel, its actual methyl ester constituents can be used to represent the liquid phase fuel spray properties, while a simpler well characterized chemical surrogate (comprising of two or three components) can represent the gas phase chemical kinetics.

Table 3 Biodiesel and surrogate property comparison at standard conditions

Properties	Methyl butanoate	Methyl decanoate	n-heptane	n-decane	Biodiesel [17]
Density (kg/L) @ 298 K [67, 68]	0.892	0.873	0.679	0.726	0.870–0.892
Kinematic viscosity (mm^2/s)	0.510	1.72	0.499	0.969	3.1–4.5
@ 313 K [69, 70]					
Boiling point °C [71, 72]	102	224	98	174	330–340

This strategy referred to as the *hybrid surrogate modeling* approach, would be a way forward to model biodiesel fuel characteristics as it (i) provides a more accurate representation of liquid phase properties and (ii) is also computationally less expensive due to use of a simpler surrogate to represent gas phase kinetics, for which a compact kinetic scheme can be derived. The components in the liquid phase surrogates can be interfaced to gas phase surrogates by using a *Group Chemistry Representation* (GCR) approach proposed by Anand et al. [73] for diesel fuel. The hybrid surrogate modeling approach has been found to accurately represent diesel fuel characteristics under conventional and low temperature combustion engine conditions [74, 75]. Extending this approach to the case of biodiesel fuels will enable the use of a surrogate whose physical and chemical properties match the real fuel in computational studies.

4 Concluding Remarks

This exposition summarizes the recent progress in surrogate formulation for biodiesels and their kinetic models. Since biodiesels are made up of methyl esters of varying degrees of unsaturation, representative methyl esters have been considered as a part of most biodiesel surrogates. Therefore, in this chapter, kinetic model development for methyl esters has been discussed in detail. Surrogate definition methods used in the literature have been reviewed as well and the need for careful assessment of different criteria and their importance to target applications has been emphasized. The authors have also availed this opportunity to highlight several impending challenges in the field of biodiesel surrogates and their kinetic modeling.

As commonly agreed upon in the combustion community, while being renewable, the one main downside to the use of biodiesels in conventional engines is the increase in NO_x potential as compared to diesel [76]. When coupled with NO_x chemistry, a well-validated kinetic mechanism for an appropriately defined biodiesel surrogate can shed light into the NO_x formation pathways and possible strategies to mitigate NO_x. Such molecular level kinetics based understanding of global emissions can also be immensely useful in designing the next generation fuels with desirable emission and performance characteristics.

Acknowledgements The last author gratefully acknowledges support from the New Faculty Initiation Grant, Project no. MEE/15–16/845/NFIG offered by the Indian Institute of Technology Madras.

Appendix: List of Biodiesel Surrogates and Their Kinetic Models

See Table 4.

Table 4 Summary of available studies on surrogates for biodiesels and their kinetic models in chronological order: Detailed[a] and reduced[b] schemes

Surrogates	Type and size		Surrogate definition criteria	Year
	# species	# reactions		
n-hexadecane[a]	225	1841	Carbon content	2007 [35]
Methyl butanoate + n-heptane[b]	53	156	LHV, O_2 content of real biodiesel (by mass)	2008 [25]
Methyl decanoate	3012	8820	Carbon content	2008 [16]
Methyl decanoate + n-heptane			Carbon content	2008 [16]
Methyl-9-decanoate			Carbon content	2010 [34]
Methyl-5-decanoate			Carbon content	2010 [34]
Methyl decanoate + n-heptane + methyl-9-decanoate			C content, ester group content	2010 [34]
Methyl decanoate + methyl-9-decanoate + n-heptane	118	837	Equal mole fraction of surrogates	2010 [27]
Methyl decanoate + n-heptane + methyl-9-decanoate	115	460	25% MD, 25% MD9D and 50% n-heptane by mole	2012 [31]
Methyl butanoate + n-heptane	145		Cetane number	2012 [23]
Methyl crotonate + methyl butanoate + n-heptane	80	299	Saturated and unsaturated methyl ester ratios, molecular mass, LHV and fuel-bound oxygen content	2012 [24]
Methyl butanoate + methyl crotonate + n-heptane	113	399	Saturated and unsaturated methyl ester ratios	2012 [26]

(continued)

Table 4 (continued)

Surrogates	Type and size		Surrogate definition criteria	Year
	# species	# reactions		
Methyl decanoate + n-heptane + methyl-9-decanoate	112	498	25% MD, 25% MD9D and 50% n-heptane	2014 [28]
Methyl decanoate + n-decane + methyl-5-decanoate	60	172	Saturated and unsaturated methyl ester ratios, energy content and C/H/O ratio	2014 [29]
Methyl mecanoate + n-heptane + methyl-9-decanoate	92	360	Saturated and unsaturated methyl ester ratios	2015 [30]
Methyl decanoate + methyl-5-decanoate + n-decane + methyl linoleate	106	263	Energy content, C/H/O ratio and methyl ester content with two double bonds	2015 [32]
Methyl decanoate + methyl-5-decanoate + n-decane + methyl linoleate	134	475	Energy content, C/H/O ratio and methyl ester content with two double bonds	2016 [33]

References

1. Anand K, Sharma RP, Mehta PS (2008) Experimental investigations on combustion of jatropha methyl ester in a turbocharged direct-injection diesel engine. Proc Inst Mech Eng Part D: J Autom Eng 222(10):1865–1877
2. Demirbas A (2009) Progress and recent trends in biodiesel fuels. Energy Convers Manag 50 (1):14–34
3. Wang W-G, Lyons W, Clark N, Gautam M, Norton P (2000) Emissions from nine heavy trucks fueled by diesel and biodiesel blend without engine modification. Environ Sci Technol 34(6):933–939
4. Colket M, Edwards T, Williams S, Cernansky NP, Miller DL, Egolfopoulos F, Lindstedt P, Seshadri K, Dryer FL, Law CK, Friend D, Lenhert DB, Pitsch v, Sarofim A, Smooke M, Tsang W (2007) Development of an experimental database and kinetic models for surrogate jet fuels. In: 45th AIAA aerospace sciences meeting and exhibit, pp 2007–770
5. Narayanaswamy K, Pitsch H, Pepiot P (2016) A component library framework for deriving kinetic mechanisms for multi-component fuel surrogates: application for jet fuel surrogates. Combust Flame 165:288–309
6. Farrell JT, Cernansky NP, Dryer FL, Friend DG, Hergart CA, Law CK, McDavid RM, Mueller CJ, Patel AK, Pitsch H (2007) Development of an experimental database and kinetic models for surrogate diesel fuels. SAE Paper No. 2007-01-0201
7. Pitz WJ, Mueller CJ (2011) Recent progress in the development of diesel surrogate fuels. Prog Energy Combust Sci 37(3):330–350
8. Mehl M, Chen J-Y, Pitz WJ, Mani Sarathy S, Westbrook CK (2011) An approach for formulating surrogates for gasoline with application toward a reduced surrogate mechanism for CFD engine modeling. Energy Fuels 25(11):5215–5223
9. Westbrook CK, Naik CV, Herbinet O, Pitz W, Mehl M, Sarathy SM, Curran HJ (2011) Detailed chemical kinetic reaction mechanisms for soy and rapeseed biodiesel fuels. Combust Flame 158(4):742–755
10. Pitsch H, Bollig M (1993) Flamemaster, a computer code for homogeneous and one-dimensional laminar flame calculations. Institut fur Technische Mechanik, RWTH Aachen
11. Thangaraja J, Anand K, Pramod S (2016) Mehta. Biodiesel no x penalty and control measures-a review. Renew Sustain Energy Rev 61:1–24
12. Goodrum JW (2002) Volatility and boiling points of biodiesel from vegetable oils and tallow. Biomass Bioenergy 22(3):205–211
13. Yanowitz J, Ratcliff MA, McCormick RL, Taylor JD, Murphy MJ (2014) Compendium of experimental cetane numbers. Technical Repot, National Renewable Energy Laboratory
14. Takase M, Zhao T, Zhang M, Chen Y, Liu H, Yang L, Xiangyang W (2015) An expatiate review of neem, jatropha, rubber and karanja as multipurpose non-edible biodiesel resources and comparison of their fuel, engine and emission properties. Renew Sustain Energy Rev 43:495–520
15. Wang W, Gowdagiri S, Oehlschlaeger MA (2013) Comparative study of the autoignition of methyl decanoates, unsaturated biodiesel fuel surrogates. Energy Fuels 27(9):5527–5532
16. Herbinet O, Pitz WJ, Westbrook CK (2008) Detailed chemical kinetic oxidation mechanism for a biodiesel surrogate. Combust Flame 154(3):507–528
17. Anand K, Sharma RP, Pramod S (2011) Mehta. Experimental investigations on combustion, performance and emissions characteristics of neat karanji biodiesel and its methanol blend in a diesel engine. Biomass Bioenergy 35(1):533–541
18. Edwards T, Maurice LQ (2000) Surrogate mixtures to represent complex aviation and rocket fuels. J Prop Power 17:461–466

19. Mueller CJ, Cannella WJ, Bruno TJ, Bunting B, Dettman HD, Franz JA, Huber ML, Natarajan M, Pitz WJ, Ratcliff MA, Wright K (2012) Methodology for formulating diesel surrogate fuels with accurate compositional, ignition-quality, and volatility characteristics. Energy & Fuels 26(6):3284–3303
20. Ahmed A, Goteng G, Shankar VSB, Al-Qurashi K, Roberts WL, Mani Sarathy S (2015) A computational methodology for formulating gasoline surrogate fuels with accurate physical and chemical kinetic properties. Fuel 143:290–300
21. Pepiot-Desjardins P (2008) Automatic strategies for chemical mechanism reduction. PhD thesis, Stanford University, Department of Mechanical Engineering, June 2008
22. Gal S, Thomson MJ, Mani Sarathy S, Syed SA, Dagaut P, Diévart P, Marchese AJ, Dryer FL (2007) A wide-ranging kinetic modeling study of methyl butanoate combustion. Proc Combustion Inst 31(1):305–311
23. Liu W, Sivaramakrishnan R, Davis MJ, Som S, Longman DE, Lu TF (2013) Development of a reduced biodiesel surrogate model for compression ignition engine modeling. Proc Combustion Inst 34(1):401–409
24. Kiat Ng H, Gan S, Ng J-H, Mun Pang K (2013) Development and validation of a reduced combined biodiesel–diesel reaction mechanism. Fuel 104:620–634
25. Brakora JL, Ra Y, Reitz RD, McFarlane J, Stuart Daw C (2008) Development and validation of a reduced reaction mechanism for biodiesel-fueled engine simulations. SAE Int J Fuels Lubricants 1(2008-01-1378):675–702
26. Mohamed Ismail H, Kiat Ng H, Gan S, Lucchini T, Onorati A (2013) Development of a reduced biodiesel combustion kinetics mechanism for CFD modelling of a light-duty diesel engine. Fuel 106:388–400
27. Luo Z, Tianfeng L, Maciaszek MJ, Som S, Longman DE (2010) A reduced mechanism for high-temperature oxidation of biodiesel surrogates. Energy Fuels 24(12):6283–6293
28. An H, Yang WM, Maghbouli A, Li J, Chua KJ (2014) A skeletal mechanism for biodiesel blend surrogates combustion. Energy Convers Manag 81:51–59
29. Chang Y, Jia M, Li Y, Zhang Y, Xie M, Wang H, Reitz RD (2015) Development of a skeletal oxidation mechanism for biodiesel surrogate. Proc Combustion Inst 35(3):3037–3044
30. Cheng X, Kiat Ng H, Gan S, Hou Ho J, Mun Pang K (2015) Development and validation of a generic reduced chemical kinetic mechanism for CFD spray combustion modelling of biodiesel fuels. Combustion Flame 162(6):2354–2370
31. Luo Z, Plomer M, Lu T, Som S, Longman DE, Mani Sarathy S, and William J. Pitz. A reduced mechanism for biodiesel surrogates for compression ignition engine applications. Fuel, 99:143–153, 2012
32. Liu T, Jiaqiang E, Yang W, Hui A, Hao Cai (2016) Development of a skeletal mechanism for biodiesel blend surrogates with varying fatty acid methyl esters proportion. Appl Energy 162 (x):278–288
33. Jiaqiang E, Liu T, Yang W, Deng Y, Gong J (2016) A skeletal mechanism modeling on soot emission characteristics for biodiesel surrogates with varying fatty acid methyl esters proportion. Appl Energy 181:322–331
34. Herbinet O, Pitz WJ, Westbrook CK (2010) Detailed chemical kinetic mechanism for the oxidation of biodiesel fuels blend surrogate. Combust Flame 157(5):893–908
35. Dagaut P, Gail S, Sahasrabudhe M (2007) Rapeseed oil methyl ester oxidation over extended ranges of pressure, temperature, and equivalence ratio: Experimental and modeling kinetic study. Proc Combustion Inst 31 II:2955–2961
36. Fisher EM, Pitz WJ, Curran HJ, Westbrook CK (2000) Detailed chemical kinetic mechanisms for combustion of oxygenated fuels. Proc Combust Inst 28:1579–1586
37. Metcalfe WK, Dooley S, Curran HJ, Simmie JM, El-Nahas AM, Navarro MV (2007) Experimental and modeling study of $C_5H_{10}O_2$ ethyl and methyl esters. J Phys Chem A 111 (19):4001–4014
38. Hakka MH, Glaude PA, Herbinet O, Battin-Leclerc F (2009) Experimental study of the oxidation of large surrogates for diesel and biodiesel fuels. Combustion Flame 156(11):2129–2144

39. Grana R, Frassoldati A, Cuoci A, Faravelli T, Ranzi E (2012) A wide range kinetic modeling study of pyrolysis and oxidation of methyl butanoate and methyl decanoate. note i: Lumped kinetic model of methyl butanoate and small methyl esters. Energy 43(1):124–139
40. Parandaman A, Balaganesh M, Rajakumar B (2015) Experimental and theoretical study on thermal decomposition of methyl butanoate behind reflected shock waves. RSC Advances 5 (105):86536–86550
41. Diévart P, Hee Won S, Gong J, Dooley S, Ju Y (2013) A comparative study of the chemical kinetic characteristics of small methyl esters in diffusion flame extinction. Proc Combustion Inst 34(1):821–829
42. Curran HJ, Gaffuri P, Pitz WJ, Westbrook CK (1998) A comprehensive modeling study of n-heptane oxidation. Combustion Flame, 114(1):149–177
43. Curran HJ, Gaffuri P, Pitz WJ, Westbrook CK (2002) A comprehensive modeling study of iso-octane oxidation. Combustion Flame 129(3):253–280
44. Diévart P, Hee Won S, Dooley S, Dryer FL, Ju Y (2012) A kinetic model for methyl decanoate combustion. Combustion Flame 159(5):1793–1805
45. Gal S, Sarathy SM, Thomson MJ, Diévart P, Dagaut P (2008) Experimental and chemical kinetic modeling study of small methyl esters oxidation: Methyl (e)-2-butenoate and methyl butanoate. Combust Flame 155(4):635–650
46. Herbinet O, Biet J, Hichem Hakka M, Warth V, Alexandre Glaude P, Nicolle A, Battin-Leclerc F (2011) Modeling study of the low-temperature oxidation of large methyl esters from C11 to C19. Proc Combustion Inst 33(1):391–398
47. Saggese C, Frassoldati A, Cuoci A, Faravelli T, Ranzi E (2013) A lumped approach to the kinetic modeling of pyrolysis and combustion of biodiesel fuels. Proc Combust Inst 34 (1):427–434
48. Coniglio L, Bennadji H, Alexandre Glaude P, Herbinet O, Billaud F (2013) Combustion chemical kinetics of biodiesel and related compounds (methyl and ethyl esters): experiments and modeling–advances and future refinements. Progr Energy Combustion Sci 39(4):340–382
49. Lai JYW, Lin KC, Violi A (2011) Biodiesel combustion: advances in chemical kinetic modeling. Progr Energy Combustion Sci 37(1):1–14
50. Sarathy SM, Thomson MJ, Pitz WJ, Lu T (2011) An experimental and kinetic modeling study of methyl decanoate combustion. Proc Combust Inst 33(1):399–405
51. Dooley S, Curran HJ, Simmie JM (2008) Autoignition measurements and a validated kinetic model for the biodiesel surrogate, methyl butanoate. Combust Flame 153(1):2–32
52. Wang YL, Lee DJ, Westbrook CK, Egolfopoulos FN, Tsotsis TT (2014) Oxidation of small alkyl esters in flames. Combust Flame 161(3):810–817
53. Wang YL, Feng Q, Egolfopoulos FN, Tsotsis TT (2011) Studies of C_4 and C_{10} methyl ester flames. Combust Flame 158(8):1507–1519
54. Alexandre Glaude P, Herbinet O, Bax S, Biet J, Warth V, Battin-Leclerc F (2010) Modeling of the oxidation of methyl esters—validation for methyl hexanoate, methyl heptanoate, and methyl decanoate in a jet-stirred reactor. Combust Flame 157(11):2035–2050
55. Seshadri K, Tianfeng L, Herbinet O, Humer S, Niemann U, Pitz WJ, Seiser R, Law CK (2009) Experimental and kinetic modeling study of extinction and ignition of methyl decanoate in laminar non-premixed flows. Proc Combust Inst 32(1):1067–1074
56. Farrel JT, Weissman W, Johnston RJ, Nishimura J, Ueda T, Iwashita Y (2003) Fuel effects on sidi efficiency and emissions. SAE Publication 2003-01-3186 (2003)
57. Kuo TW (1990) J Eng Gas Turbines Power 112:348–356
58. Tianfeng L, Law CK (2005) A directed relation graph method for mechanism reduction. Proc Combust Inst 30(1):1333–1341
59. Pepiot-Desjardins P, Pitsch H (2008) An efficient error-propagation-based reduction method for large chemical kinetic mechanisms. Combust Flame 154(1–2):67–81
60. Niemeyer KE, Sung C-J, Raju MP (2010) Skeletal mechanism generation for surrogate fuels using directed relation graph with error propagation and sensitivity analysis. Combust Flame 157(9):1760–1770

61. Gustavsson J, Golovitchev VI (2003) Spray combustion simulation based on detailed chemistry approach for diesel fuel surrogate model. Technical report, SAE Technical Paper
62. Som S, Ramirez AI, Longman DE, Aggarwal SK (2011) Effect of nozzle orifice geometry on spray, combustion, and emission characteristics under diesel engine conditions. Fuel 90 (3):1267–1276
63. Som S, Longman DE, Luo Z, Plomer M, Lu T, Senecal PK, Pomraning E (2012) Simulating flame lift-off characteristics of diesel and biodiesel fuels using detailed chemical-kinetic mechanisms and large eddy simulation turbulence model. J Energy Res Technol 134 (3):032204
64. Niemeyer KE, Sung C-J (2014) Mechanism reduction for multicomponent surrogates: a case study using toluene reference fuels. Combust Flame 161(11):2752–2764
65. Davidson DF, Haylett DR, Hanson RK (2008) Development of an aerosol shock tube for kinetic studies of low-vapor-pressure fuels. Combust Flame 155(1):108–117
66. Narayanaswamy K, Pepiot P (under review) Simulation-driven formulation of transportation fuel surrogates. Combust Theory Model
67. Pintos M, Bravo R (1988) Maria Carmen Baluja, Maria Inmaculada Paz Andrade, Geneviève Roux-Desgranges, and Jean-Pierre E Grolier. Thermodynamics of alkanoate + alkane binary mixtures. concentration dependence of excess heat capacities and volumes. Can J Chem 66 (5):1179–1186
68. Ortega J, Alcalde R (1992) Determination and algebraic representation of volumes of mixing at 298.15 K of methyl n-alkanoates (from ethanoate to n-pentadecanoate) with n-pentadecane. Fluid Phase Equilib 71(1–2):49–62
69. José S (2001) Matos, José L Trenzado, Emilio González, and Rafael Alcalde. Volumetric properties and viscosities of the methyl butanoate + n-heptane + n-octane ternary system and its binary constituents in the temperature range from 283.15 to 313.15 K. Fluid Phase Equilib 186(1):207–234
70. Knothe G, Steidley KR (2005) Kinematic viscosity of biodiesel fuel components and related compounds. Influence of compound structure and comparison to petrodiesel fuel components. Fuel 84(9):1059–1065
71. Tsibanogiannis IN, Kalospiros NS, Tassios DP (1995) Prediction of normal boiling point temperature of medium/high molecular weight compounds. Ind Eng Chem Res 34(3):997–1002
72. Liu S, Cao C, Li Z (1998) Approach to estimation and prediction for normal boiling point (NBP) of alkanes based on a novel molecular distance-edge (MDE) vector, & #x03BB. J Chem Inf Comput Sci 38(3):387–394
73. Krishnasamy A, Ra Y, Reitz RD, Bunting B (2012) Combustion simulations of the fuels for advanced combustion engines in a homogeneous charge compression ignition engine. Int J Engine Res 191–208
74. Krishnasamy A, Reitz RD, Willems W, Kurtz E (2013) Surrogate diesel fuel models for low temperature combustion. SAE Technical Paper, 2013-01-1092
75. Anand K, Ra Y, Reitz RD, Bunting B (2011) Surrogate model development for fuels for advanced combustion engines. Energy & Fuels 25(4):1474–1484
76. Xue J, Grift TE, Hansen AC (2011) Effect of biodiesel on engine performances and emissions. Renew Sustain Energy Rev 15(2):1098–1116

Response Surface Methodology Based Multi-objective Optimization of the Performance-Emission Profile of a CI Engine Running on Ethanol in Blends with Diesel

Probir Kumar Bose, Vijay Narayan Bodkhe, Bishop Deb Barma and Rahul Banerjee

Abstract The present study is aimed at optimizing the effect of ethanol-diesel blends on the performance and emission characteristics of a single cylinder (indirect injection) four-stroke diesel engine at different loads. Hexane was used as a co-solvent for higher ethanol concentration while Diethyl ether (DEE) was added as an ignition improver. D-optimal was chosen as the Design of experiment methodology. Quadratic polynomial models were constructed for the desired emission-performance parameters based on experimental data through the Response Surface Methodology NOx, CO and HC were chosen as the emission output parameters while BSFC. Load and ethanol-hexane-DEE concentration in the diesel blend were chosen as the input parameters. Multi-objective optimization involving the objective of minimizing both the emission and BSFC simultaneously yielded an optimal input condition of 5% hexane and 15% DEE in blend with 40% ethanol and diesel at 95% full load operation with 15.3% absolute error in NOx, 17.1% in HC, 1.69% in CO and 3.4% in BSFC estimation with respect to actual experimental values at the calibrated test condition predicted through RSM model optimization.

Keywords Design of experiment · D-optimal · Desirability approach · RSM performance-emission trade-off · Multiobjective optimization

P.K. Bose (✉)
NSHM Knowledge Campus, Durgapur, India
e-mail: pkb32@yahoo.com

V.N. Bodkhe · R. Banerjee
Department of Mechanical Engineering, National Institute of Technology, Agartala, India

B.D. Barma
Department of Production Engineering, National Institute of Technology, Agartala, India

A.K. Agarwal et al. (eds.), *Biofuels*, Green Energy and Technology,
DOI 10.1007/978-981-10-3791-7_11

1 Introduction

The environmental effects like global warming and climate change, have greatly increased the interest of legislative agencies in making emission standards stricter for diesel engines. Diesel engines are widely used in off road and on road applications. There exist a sufficient number of alternatives to diesel which includes Butanol, Ethanol, Hydrogen, Biodiesel, Natural gas, propane [1]. Among these alternative fuels ethanol has emerged as a plausible on gasoline and diesel powertrains due to its low cost, simplicity in production, renewability, low toxicity, high octane [2, 3]. Ethanol can be made from agricultural yield such as corn potatoes, waste paper, wheat, brewery waste by fermenting sugars and food-waste. Research work published earlier [4] proved that the use of this renewable component i.e. ethanol in diesel provides a significant reduction in particulate emissions, with no considerable increase in other gaseous emissions. Huang et al. [5] in their study on a diesel engine fuelled with ethanol-diesel blends observed that the thermal efficiency of the engine when run on diesel ethanol blend were near to baseline diesel operation with a slight penalty of increment in fuel consumption. That said, there are problems associated with the direct use of ethanol by blending it with diesel, which include mainly phase separation and an overall decrease in cetane no. of the ethanol-diesel blend. Ethanol, when blended with diesel, is observed to separate after few hours of mixture formation due to the difference in chemical properties of ethanol and diesel. Phase separation of the blend can also be termed as non-homogeneous fuel. Non-homogeneous fuel disrupts the smooth operation of the engine as fuel injector cannot inject it (Non-homogeneous fuel) properly [6]. Phase separation can be avoided with the use of either Co-Solvent or Emulsifier [7]. Emulsifier helps to avoid phase separation but requires heating and blending of the fuel whereas with the addition of co-solvent phase separation can be avoided by mere stirred and mixing of the blend component properly [2]. Among the different co-solvents available, hexane has good miscibility with Ethanol [8]. Also, it has shown a positive impact on the performance and emission characteristics of the diesel engine when blended with diesel in the proportion of 4, 6 and 8% by volume. Almost at all concentration n-hexane and n-pentane, 3–6% rise in thermal efficiency was observed. At the same time, 5–6% decrease in NOx emission was also observed for the blend of n-hexane. NOx decrement was higher for a higher concentration of hexane, and this maximum value of NOx reduction was 7.528% associated with the 8% blend of n-hexane and diesel. The cetane number of ethanol is around 8, which it lowers the overall cetane of the blend. The decrement in the performance observed with Diesel-Ethanol Blends as used in four-cylinder direct injection engine have been seen to be distinctly improved by the addition of Cetane Improvers to the blends [9]. Though optimizing the baseline diesel injection timing can be an exploratory alternative to address the combustion and performance deteriorations, arising out of prolonged ignition delays, studies have clearly established that cetane improvers provide a more pragmatic solution to the iterations involved in optimising the injection timings during blend operation [9–11].

Among the Cetane improver, diethyl ether has been evolved as the more beneficial cetane improver [12]. The objectives of the present study were:

- To ascertain the minimum amount of Cetane no. improver and co-solvent required for the highest ethanol concentration in blend wirh diesel to maintain phase stability.
- To apply Design of experiment methodology to carry out experimentation in order to extract key traits of the emission-performance profile at different load settings.
- To develop and ascertain the robustness of polynomial models for predicting the brake specific fuel consumption and emission parameters (HC, CO, NOx,) of the engine for Ethanol Diesel Blend
- To find an optimum blend and load step of operation for the given engine to minimize brake specific fuel consumption and emission parameters simultaneously.

2 Methodology

2.1 Blend Stability Analysis

Series of experiment on the fuel blends were performed to ensure the stability of the fuel blend. Time for the phase separation of the blend was the prime factor against which fuel blend stability was verified. The experiments were performed in the chemical laboratory, where samples (10 ml each) of different blends of fuels were taken in the test tubes (15 ml each), kept in steady condition for certain duration of time and simultaneously observation were taken on the phase separation of the blends at intervals of 2, 6 and 12 h. According to the fuel composition, this experimental study was performed in two stages. Properties of fuels are given in Table 1 [13, 14].

Table 1 Properties of diesel, ethanol, hexane and diethyl ether [13, 14]

	Formula	Density at 200 (kg/m^3)	Viscosity (mm^2/s)	Lower heat value (MJ/kg)	Flash point	Cetane no.
Diesel	$C_{12}H_{23}$	833	4.5	42.612	78	48
Ethanol	C_2H_5OH	789	1.2	28.856	135	5
Hexane [2]	C_6H_{14}	654	0.458	44.752	−23.3	44
Diethyl Ether	$C_4H_{10}O$	712	0.22	33.892	−450	125

2.1.1 Stability of Ethanol-Diesel Blends

The aim of this study section was to verify the stability of ethanol-diesel blend after stirring and mixing for selected duration of time. Blends E10D90, E15D85, E20D80, E25D75, E30D70, E35D65, and E40D60 [where E xx = % vol of ethanol concentration in a given ethanol diesel blend] were observed immediately after 5 min, after 2, 6, 8 and 12 h. Table 2 shows the test results of the solubility and the physical stability of the Ethanol-Diesel blends. From the table, it can be seen that for all the blends, two different layers were formed. E10D90, which was not separated even after 12 h of the start of Test; E25D75 separated after 2 h while and E30D70 separated immediately even after stirring. The results show that the blends of ethanol greater than 25% vol with diesel were not stable and were all separated after 5 min.

2.1.2 Deciding Volume Percentage of Solvent

To maintain phase stability of ethanol-diesel blend, hexane was used as co-solvent. The aim of this analysis was to decide the minimum amount of co-solvent, which was to be added to the Ethanol-diesel blend in order to maintain phase stability. No Cetane Improver was added in this experiment. The blends were observed for a specified time duration for phase separation. Hexane was added in two different amount, i.e., 2 and 5% vol. for E10, E15, E20, E25, E30, E35, and E40 of ethanol concentrations in the blend. When ethanol was varied between 10 and 40%, the minimum Hexane required maintaining the stability of blend was found to be 5% as seen from Table 3.

Table 2 Phase separation duration in ethanol-diesel blend

Blend	Time			
	Instant (Up to 5 min) no stirring	After 2 h (Stirred)	After 6 h (Stirred)	After 12 h (Stirred)
E10D90	Homogeneous	Homogeneous	Homogeneous	Homogeneous
E15D85	Homogeneous	Homogeneous	Phase separation	–
E20D80	Homogeneous	Homogeneous	Phase separation	–
E25D75	Homogeneous	Phase separation	–	–
E30D70	Phase separation	–	–	–
E35D65	Phase separation	–	–	–
E40D60	Phase separation	–	–	–

Table 3 Effect of phase separation in the blend of ethanol and hexane with diesel

Blend	Time			
	Instant (Without stirring)	After 2 h (Stirred)	After 6 h (Stirred)	After 12 h (Stirred)
H2E15D83	Phase separation	Homogeneous	Homogeneous	Phase separation
H5E15D80	Phase separation	Homogeneous	Homogeneous	Homogeneous
H2E20D78	Phase separation	Homogeneous	Homogeneous	Phase separation
H5E20D75	Phase separation	Homogeneous	Homogeneous	Homogeneous
H2E25D73	Phase separation	Homogeneous	Phase separation	–
H5E25D70	Phase separation	Homogeneous	Homogeneous	Homogeneous
H2E30D68	Phase separation	Homogeneous	Phase separation	–
H5E30D65	Phase separation	Homogeneous	Homogeneous	Homogeneous
H2E35D63	Phase separation	Homogeneous	Phase separation	–
H5E35D60	Phase separation	Homogeneous	Homogeneous	Homogeneous
H2E40D58	Phase separation	Phase separation	–	–
H5E40D55	Phase separation	Homogeneous	Homogeneous	Homogeneous
H7E40D53	Phase separation	Homogeneous	Homogeneous	Homogeneous

2.1.3 Deciding Volume Percentage of Diethyl Ether

The next stage of the experimental investigation involved the investigation of the minimum quantity of cetane number improver need to be added in ethanol diesel blend. Owing to the higher cost and volatile nature of Diethyl ether it was imperative to keep its quantity as minimum as possible. This optimum quantity of diethyl ether has been mapped corresponding to meeting the minimum expectations of Cetane no. of blend according to ASTM D975 [15] (Table 4) [16]. Table 5 to this end, indicate the essential properties of compliance of the various ethanol-diesel blends tested with its corresponding minimum DEE addition and with 5% hexane as the required co-solvent calculated as per the methodology outlined in with the previous study of the authors [17].

2.2 The Design of Experiment (DoE) Paradigm

From Table 5, it can be seen that the possible combinations generated were high in number. Design of Experiment Methodology was adopted to reduce the number of experiments need to extract the key traits of the blends with regard 5 to its emission-performance profile. The advantage of using the design of experiment

Table 4 Compliance properties of conventional diesel fuels and various e-diesel products [3, 16]

Property	ASTM method	Units	No. 02 diesel requirement	Blend diesel requirement
Ethanol content	Nominal	vol%	–	–
ASTM D975 [4]				
Flash point	D93	°C, min	52	58
Kinematic viscosity 40 °C	D445	mm^2/s min mm^2/s, max	1.9 4.1	–
Cetane no.	D613	min	40	42
Cetane index	D975	min	40	–

methodology is to evaluate the performance of the engine over the entire range of variation of fuel blend and load with as a minimum number of experiments as possible. The concept of undertaking a design of experiment is to statistically plan the experimental design and then performing the designated experiments to get most information on the main and interactive effects of the participating controlling variables or input factors.

The research work done earlier focuses on the effect operating parameters on the performance and emission by varying one factor at a time. However, for the complete information on the effect of fuel composition and operating parameter on the performance and emission of diesel engine, an extensive multivariate study of the input parameters on the output holds a strong prerogative. In such cases, use of statistical techniques like the design of experiment helps to extract the maximum information about interactive effects of input factors on the responses with a minimum number of the experiment [18]. The design of experiment can be done by employing various statistical algorithms designed to this effect such as CCD, full factorial design. Box-Behnken, CCC, CCF, CCO, D-Optimal, Onion D-Optimal etc.

Among the methods stated above D-Optimal method has been extensively used where there is both involvement of process and mixture factors with minimum experiments as possible. Kitamura et al. [19] investigated about predictive accuracy of empirical engine models employing design of experiments methodology. Effect of a number of measurement points on the accuracy of models for different designs such as D-Optimal, Latin Hypercube Sampling (LHS) was discussed extensively in this literature. A higher level of accuracy was observed with the implementation of D-Optimal design than that with Latin Hypercube Sampling (LHS). El-Gendy et al. [20] optimized the transesterification of waste cooking oil by using D-Optimal design method based on RSM to find out the significance and interactive effects of catalyst concentration, mixing rate and reaction time on biodiesel production. Borhan et al. [21] undertook the optimization of Okara Soap formulation for Stratum Corneum application by using the D-Optimal design method of design of the experiment. Optimal design was applied to investigate the influence of the main composition. The presented study showed that optimization study of Okara soap

Table 5 Minimum values of DEE to meet regulatory limits of diesel blends

Sr No.	Volume of ethanol	Volume of diesel	Volume of hexane	Volume of diethyl ether	Calculated cetane no.	Kinematic viscosity
1	11	84	5	0	43.1	4.0
2	12	83	5	0	42.6	4.0
3	13	82	5	0	42.2	3.9
4	14	80	5	1	42.6	3.9
5	15	79	5	1	42.1	3.8
6	16	77	5	2	42.5	3.8
7	17	76	5	2	42.0	3.7
8	18	74	5	3	42.4	3.6
9	19	72	5	4	42.7	3.6
10	20	71	5	4	42.3	3.5
11	21	69	5	5	42.6	3.5
12	22	68	5	5	42.2	3.4
13	23	66	5	6	42.5	3.4
14	24	65	5	6	42.1	3.3
15	25	63	5	7	42.4	3.3
16	26	62	5	7	42.0	3.2
17	27	60	5	8	42.4	3.2
18	28	58	5	9	42.7	3.1
19	29	57	5	9	42.3	3.0
20	30	55	5	10	42.6	3.0
21	31	54	5	10	42.2	2.9
22	32	52	5	11	42.5	2.9
23	33	51	5	11	42.1	2.8
24	34	49	5	12	42.4	2.8
25	35	47	5	13	42.8	2.7
26	36	46	5	13	42.3	2.7
27	37	44	5	14	42.7	2.6
28	38	43	5	14	42.2	2.5
29	39	41	5	15	42.6	2.5
30	40	40	5	15	42.2	2.4

formulation for stratum corneum application could be done successfully with the application of D-Optimal Design by combining independent variables.

In the present study, the experiment was designed with the operating parameter of the engine (i.e. load) as process factors and the volumetric percentages of the components of the fuel blend as mixture factors. The fuel blend consists of Ethanol, Diesel, Hexane (Co-Solvent) and Cetane improver (Diethyl Ether). Factor load was varied at 5 levels from 2 kg (50% full load) to 4 kg (95% full load) at 0.5 kg increment intervals. The range of load investigated corresponded to the working range of the given engine below and beyond which baseline diesel operation was

inhibited due to engine stability issues. Ranges for the mixture factors were determined according to the constraints placed. The first constraint placed was the Cetane no of blend should not fall below the limit prescribed by the "ASTM D975 standard for the fuels and composition" [15]. As low Cetane no affects the performances of the engine [22], the second constraint placed on the factors was natural, the summation of volume percentages of components of blend should not exceed 100%.

$$\text{Volume Percentage}_{\text{Blend component}} = 100 = x_{ETH} + x_{DEE} + x_{HEX} + x_{D} \quad (1)$$

The objective of the experiment was to find the optimum composition of the blend and generate the model equation for the responses. From the total no of designs generated, the one with maximum value (73.7955017) of G-efficiency with 19 runs was selected as the design for carrying out experiments. G-efficiency has been defined as in [23]

where: G-efficiency $= 100 * \sqrt{\frac{f}{n}}/\sigma_m$.

It has been chosen as the index of efficiency for the present D-optimal design output as it contains constraints set by mixture variables. This measure being related to the G-optimality criterion invoked to minimize the maximum value of the standard error of the predicted responses during optimization. Now, according to the run order given in the design matrix (Table 6), experiments were performed, and values of the responses were noted corresponding to each designed experiment.

Table 6 Design matrix generated

Run order	Load	Hexane	Diethyl ether	Ethanol	Diesel
1	2	0.05	0.00	0.13	0.82
2	2	0.05	0.15	0.40	0.40
3	2	0.05	0.00	0.13	0.82
4	2	0.05	0.15	0.40	0.40
5	2	0.05	0.09	0.29	0.57
6	2.5	0.05	0.15	0.40	0.40
7	2.5	0.05	0.00	0.13	0.82
8	2.5	0.05	0.05	0.22	0.68
9	3.5	0.05	0.15	0.40	0.40
10	3.5	0.05	0.15	0.40	0.40
11	3.5	0.05	0.00	0.13	0.82
12	4	0.05	0.15	0.40	0.40
13	4	0.05	0.00	0.13	0.82
14	4	0.05	0.00	0.13	0.82
15	4	0.05	0.10	0.31	0.54
16	4	0.05	0.10	0.31	0.54
17	3	0.05	0.09	0.29	0.57
18	3	0.05	0.09	0.29	0.57
19	3	0.05	0.09	0.29	0.57

Where f stands for the number of design factors, n being the number of runs proposed in the design; σ_m denotes the maximum standard error of prediction across the generated candidate experiments.

2.3 The Experimental Setup

The engine test rig consisted of a diesel engine, calorimeter, Eddy current dynamometer, fuel tank, fuel flow measurement system, data acquisition system. The engine specification is given in Table 7 while the setup has been depicted in Fig. 1. The engine was loaded by Eddy current a Powermag dynamometer with the maximum loading capacity of 6 kg. The load was measured by load cell of 20 kg capacity and provided a precision of 0.02 kg increment. Load mentioned in kg was translated in corresponding to N-m scale via the following correlation provided by engine vendor:

$$\text{Load (N-m)} = \text{Load in (kg)} * 9.81 * 0.25.$$

The in-cylinder pressure sensor and crank angle encoder were synchronized onto the GUI based Engine post processing software. The data was averaged over a time span corresponding to 100 consecutive cycles at the constant engine speed of 1500 rpm (±2%) to avoid error due to cyclic variations. Determination of Specific fuel consumption was done using fuel burette of 30 ml volume. The time required for the drop in 0.3 ml of fuel in the fuel burette was observed and thereby specific fuel consumption for each blend was evaluated. The experiment was performed at the 30 °C ambient temperature. The cooling water temperature was recorded as 26 °C.

Table 7 Specification of test engine

Make/model	Kirloskar varsha
Type	Horizontal single cylinder four stroke indirect injection diesel engine
Combustion type	Pre-combustion chamber type
Cooling	Air
Displacement (swept volume)	0.381 L
Bore size	74 mm (0.074 m)
Stroke length	74 mm (0.074 m)
Swept volume	0.831 L
CR	20
Connecting length	200 mm (0.200 m)
Fuel	Diesel
Speed	1500–1800 RPM
HP	4 HP

Fig. 1 Experimental setup

2.4 Error Analysis

To ensure the repeatability of the experiment an uncertainty analysis was undertaken where the index of uncertainty due to inconsistency in observation at any designed experimental step and instrument accuracy were as per Eq. 2.

$$\Delta U = \sqrt{\left(\frac{\partial \mathrm{U}}{\partial \mathrm{X}_1}\Delta \mathrm{X}_1\right)^2 + \left(\frac{\partial \mathrm{U}}{\partial \mathrm{X}_2}\Delta \mathrm{X}_2\right)^2 + \cdots \left(\frac{\partial \mathrm{U}}{\partial \mathrm{X}_n}\Delta \mathrm{X}_n\right)^2} \tag{2}$$

The accuracy of the computed performance and emission parameters are calculated on the basis of the corresponding components of engine and emission analysis instrumentation, as declared by their respective manufacturers [24]. The root mean square method is used to carry out combined uncertainty analysis of the performance parameters by which total uncertainty U of a quantity Q has been estimated, depending on the independent variables x_1, x_2, x_3, x_n (i.e., Q = f[x_1, x_2, …x_n]) having individual errors Δx_1, Δx_2, …, Δx_n is given by Eq. (2) [25]. Brake power and Brake specific fuel consumption were analysed for the uncertainty using the combined uncertainty analysis method. Individual uncertainty of the all the instruments which were used to measure brake power and brake specific fuel consumption were considered. Uncertainty has been shown in terms of percentage in Tables 8 and 9 [17].

Table 8 Total percentage of uncertainty of computed performance parameters

Measurements	Accuracy	Percentage uncertainty
Engine speed	±1 rpm	±0.2
Temperatures	±10 C	±0.1
Nitrogen oxides	±20 ppm	±0.2
Hydrocarbon	±10 ppm	±0.2
Carbon monoxide	±0.02%	±1.0
Burette measurements	±0.3 CC	±1.5
Crank angle encoder	±0.50 CA	±0.2
Load	±1 N	±0.2

2.5 *Emission Analysis*

Exhaust gasses were sampled and measured by AVL Di-Gas 444 emission analyzer. Emission analyzer was used to mainly to measure the contents of oxides of nitrogen (ppm), Hydrocarbon (ppm) and carbon monoxide (%vol) in the exhaust. Average of 5 readings each sampled over a time span corresponding to 100 cycles for a given designed experiment at a given load step was computed and logged.

2.6 *RSM Technique: An Optimization Approach*

Silva et al. [26] applied response surface methodology for optimization of biodiesel production by transesterification of soybean oil with ethanol The biodiesel production process by transesterification of soybean oil with ethanol was optimized by the application of full factorial design and response surface methodology as part of an optimization procedure. The mutual effects of the molar ratio of alcohol, temperature, catalyst concentration and reaction time in relation to oil were investigated and optimized. Pandian et al. [23] did an investigation on the effect of injection system parameters on performance and emission characteristics of a twin cylinder compression ignition direct injection engine fuelled with Pongamia biodiesel–diesel blend using response surface methodology. The design of experiments (DoE) was used to design the experiments. Responses such as Brake Thermal Efficiency (BTE), Carbon monoxide (CO), Hydrocarbon (HC), Brake Specific Energy Consumption (BSEC), smoke opacity and Nitrogen Oxides (NOx) were well predicted by resultant models obtained by response surface methodology. Also, these models helped to identify significant Interactions between the input factors. Desirability approach of Response surface methodology was used. An injection timing of 21° BTDC, an injection pressure of 225 bar, and tip protrusion of 2.5 mm nozzle were found to be optimal values for the 7.5 kW engine using biodiesel-blended diesel fuel at 1500 rpm. Lee and Reitz [27] undertook a

Table 9 Total percentage of uncertainty of computed performance parameters [5, 22]

Computed performance parameter	Measured variables	Instrument involved in measurement	% Uncertainty of measuring instrument	Calculation	Total % uncertainty of computed parameters
B.P (Brake Power)	Load, RPM	Load sensor, Load indicator, Speed measuring unit	0.21 0.10 1.1	$\sqrt{[0.212 + 0.102 + 1.12]}$	1.12
BSFC	SFC (Liquid Fuel) BP	Burette measurements From BP measurement	1.5 1.01	$\sqrt{[1.52 + 1.122]}$	1.81

Response Surface Method Optimization of a High-Speed Direct-Injection Diesel Engine equipped with a common rail injection system. Response surface methodology was utilized to find out role of EGR and other parameters in reducing the emission footprint. The engine was test run @ 1757 rev/min, 45% load. Injection timing, Injection pressure, boost pressure and EGR rate were the variables for the optimization process. It was observed that RSM model based optimization is an effective tool for utilizing the interactive effects of combustion control techniques used during the investigation.

As in the previous case studies highlighted, the present study puts forward the necessity of optimization with the multiple responses of interest. For optimizing these multiple responses, techniques such as desirability approach, overlaying contour plots for each response and constrained optimization problems have been used widely [23].

In the present work, desirability approach based on response surface methodology was used for the optimization of operating (i.e. load) as well as mixture factors (blends components).

Desirability approach offers inherent benefits like availability in the software packages, its simplicity in use and flexibility in weighing and giving more importance to any individual response.

The optimization analysis was carried wherein each response was transformed into a dimensionless desirability value (d). The value of d suggests whether the response is acceptable or not. This value of d ranges between d = 0, which suggest response is absolutely unacceptable and d = 1 (highest value of d) suggesting it as the most desirable response. Contingent on the nature of the objectives to be handled, the goal of each response parameter can be set to be minimized, maximized or set a target range or an exact value. Based on the proposals set forth in the study of [28], Eqs. 3–6 indicate the methodology for calculating the desirability of the each response depending upon the goal of response.

When an objective is of minimum, $d_i = 1$ (as objective is minimum, so value becomes a set minimum value becomes unacceptable) when $Y_i \leq Low_i$; $d_i = 0$ when $Y_i \geq High$; and

$$d_i = \left(\frac{High_i - Y_i}{High_i - Low_i}\right)^{wt_i} \quad When\, Low_i < Y_i < High_i \tag{3}$$

When an objective is of maximum, $d_i = 0$ when $Y_i \leq Low_i$; $d_i = 1$ when $Y_i \geq High_i$ and

$$d_i = \left(\frac{Y_i - Low_i}{High_i - Low_i}\right)^{wt_i} \quad When\, Low_i < Y_i < High_i \tag{4}$$

When an objective is of target, $d_i = 0$, when $Y_i < Low_i$; $Y_i > High_i$

$$d_i = \left(\frac{Y_i - Low_i}{T_i - Low_i}\right)^{wt_{1i}} \quad When\, Low_i < Y_i < T_i \tag{5}$$

$$d_i = \left(\frac{Y_i - High_i}{T_i - High_i}\right)^{wt_{2i}} \quad When\, T_i < Y_i < High_i; \quad and \tag{6}$$

When an objective is within the range, $d_i = 1$ when $Low_i < Y_i < High_i$ and $d_i = 0$; otherwise.

In the above formulas, "i" suggests the response, "Y" the value of response, "Low" stands for the lower limit of the response, "High" stands for the upper limit of the response, "T" means the target value of the response, "wt" specifies the weight of the response. The weight field possesses potential of changing the shape of desirability function for each response. Lower/upper bound can be given more or less preference with the help of weights. Weight greater than 1 gives more preference to the objective whereas weights lower than 1 give less preference to the objective, in such manner weights can be varied in the range of 0.1–10. When the weight value is equal to one, the desirability function varies in a linear mode. To solve the problem of multiple response optimization, the desirability approach uses a technique by which all the responses are combined into a dimensionless measure of performance named as the Overall desirability function denoted by D varies between 0 and 1. Overall desirability function is calculated by the following Eq. 7 [23].

$$D = \left(\prod_{i=1}^{n} d_i^{r_i}\right)^{\frac{1}{\sum r_i}} \tag{7}$$

The desirability functions dk (where k = 1… m, responses) are generally used by the optimizing algorithm of the statistical packages to search for the possible

combination of input factor values which can predict a result in the given response specification as near to the target as possible for each response. The overall desirability function, f(ds) which is the sum of all dk is a measure of the best trade-off solution among the competing objectives that need to be satisfied simultaneously in a typical multiobjective optimization endeavour. Desirability function will only be able to find the optimum value if optimizer specification (Min, Target, Max) and the selected Desirability objective are given and chosen appropriately. Each response is generally compared with another response by allocating an importance (r) relative to the other. This importance r takes value from 1 to 5 where 1 stands for least important and 5 stands for most important. The best and most desirable function is generally identified by the function for which D value is larger. Individual desired function (d) that maximizes D helps to determine the optimal values of the input factors. The iteration that produces a minimum value of Log (D) [where D is the normalized distance to target] is selected as the best run for the objectives set.

3 Results and Discussion

3.1 Response Model Formulation

From variable importance plot i.e. from Fig. 2 the terms for which Variable Importance (VIP) values were greater than 0.8 have been deemed as a significant term for which the values of the coefficient (scaled and cantered) were taken from the coefficient analysis. Using the values of the constant and coefficients, the model equation for the responses were constructed based on a multi-regression analysis with quadratic order polynomial [23, 29] in order to capture any significant interaction effects of the input parameters evident from Fig. 2.

3.1.1 NOx Model Formulation

$$\begin{aligned} \mathrm{NOx} = {} & 30.605 - 2.72469 * \mathrm{L} * \mathrm{DEE} + 2.72634 * \mathrm{L} * \mathrm{DIE} - 2.72689 * \mathrm{L} \\ & * \mathrm{ETH} + 6.24731 * \mathrm{L} * \mathrm{L} - 3.35794 * \mathrm{L} - 0.878447 * \mathrm{DEE} + 0.873382 \\ & * \mathrm{DIE} - 0.870453 * \mathrm{ETH} \end{aligned} \tag{8}$$

where NOx (Fig. 3) is the amount of oxides of Nitrogen in exhaust gases (ppm), L is the load in kg, DEE is the diethyl ether (in volume percentage), ETH is the amount of ethanol (in volume percentage).

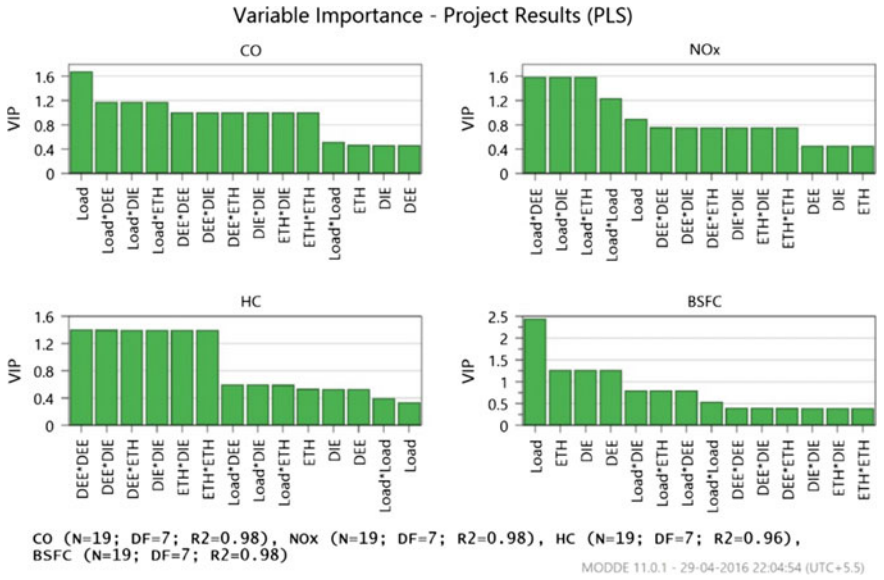

Fig. 2 VIP Plot for forming the model equation

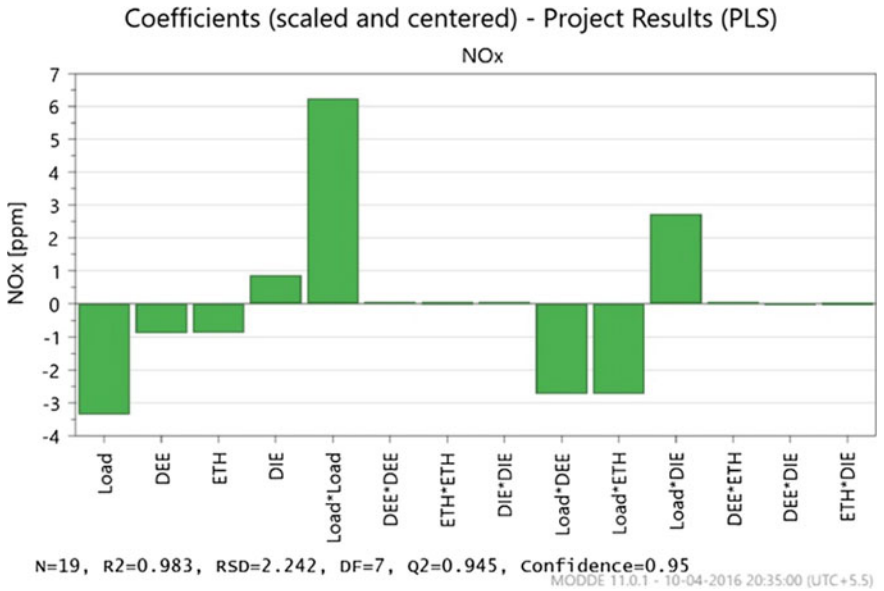

Fig. 3 Significance of the model terms coefficients in the NOx equation

3.1.2 HC Model Formulation

$$\begin{aligned} HC = {} & 73.6482 - 5.77758 * DEE * DEE + 5.74718 * DEE * DIE - 5.72781 * DEE * ETH \\ & - 5.7085 * DIE * DIE + 5.68463 * ETH * DIE - 5.65832 * ETH * ETH + 2.54231 * L * DEE \\ & - 2.53318 * L * DIE + 2.52773 * L * ETH - 1.79642 * ETH + 1.79379 * DIE \\ & - 1.78869 * DEE - 0.861918 * L * L + 1.64832 * L \end{aligned} \tag{9}$$

where HC (Fig. 4) is the amount of hydrocarbon in exhaust gases (ppm), L is the load in kg, DEE is the diethyl ether (in volume percentage), ETH is the amount of ethanol (in volume percentage).

3.1.3 CO Model Formulation

$$\begin{aligned} CO = {} & 0.0683459 - 0.00545963 * L + 0.00158234 * L * DEE \\ & - 0.00157988 * L * DIE + 0.00157828 * L * ETH \\ & - 0.00104385 * DEE * DEE + 0.00103776 * DEE * DIE - 0.00103393 * DEE * ETH \\ & - 0.00103067 * DIE * DIE + 0.00102631 * ETH * DIE \\ & - 0.00102166 * ETH * ETH + 0.000446938 * DEE + 0.000449426 * ETH \\ & - 0.000448573 * DIE - 0.00156091 * L * L \end{aligned} \tag{10}$$

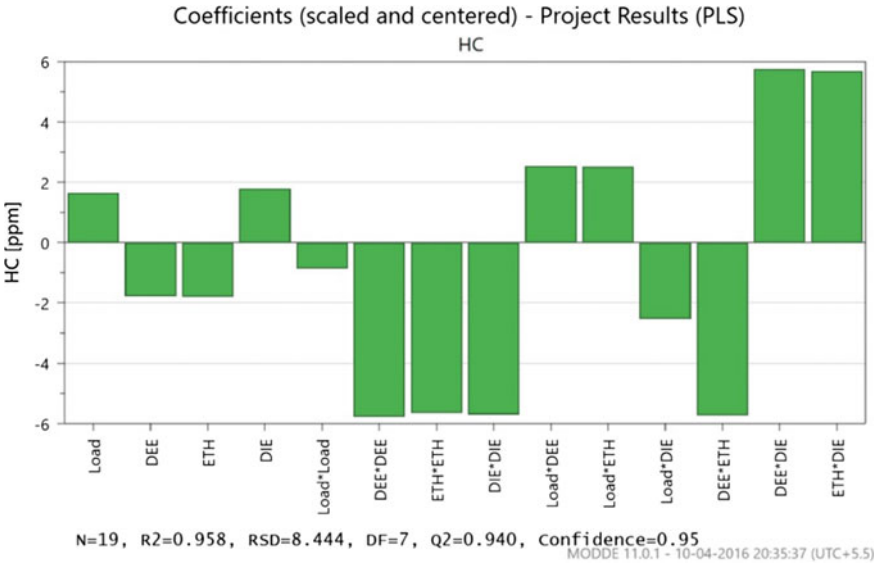

Fig. 4 Significance of the model terms coefficients in the HC equation

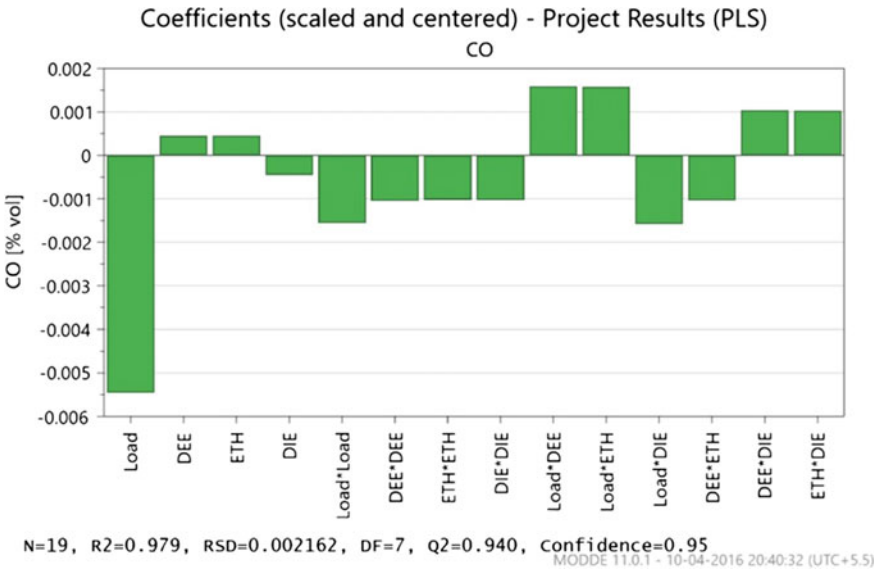

Fig. 5 Significance of the model terms coefficients in the CO equation

where CO (Fig. 5) is the amount of carbon monoxide in exhaust gases (in volume percentage), L is the load in kg, DEE is the diethyl ether (in volume percentage), and ETH is the amount of ethanol (in volume percentage).

3.1.4 BSFC Model Formulation

$$\begin{aligned}\mathrm{BSFC} = {} & 338.913 - 37.1354 * \mathrm{L} - 8.89047 * \mathrm{ETH} + 8.8661 * \mathrm{DIE} - 8.82065 * \mathrm{DEE} - 11.0562 * \mathrm{L} * \mathrm{L} \\ & - 3.70315 * \mathrm{DEE} * \mathrm{DEE} + 3.59351 * \mathrm{DEE} * \mathrm{DIE} - 3.53115 * \mathrm{DEE} * \mathrm{ETH} \\ & - 3.48268 * \mathrm{DIE} * \mathrm{DIE} + 3.41986 * \mathrm{ETH} * \mathrm{DIE} - 3.35691 * \mathrm{ETH} * \mathrm{ETH}\end{aligned} \tag{11}$$

where BSFC (Fig. 6) is the brake specific fuel consumption measured in (g/kwh), L is the load in kg, DEE is the diethyl ether (in volume percentage), and ETH is the amount of ethanol (in volume percentage).

3.2 *Evaluation of Fitness of RSM Models*

The partial least square method was chosen to fit the model to data. Now it's necessary to check whether the data was fitted well by the model. This can be verified by the summary of the fit plot.

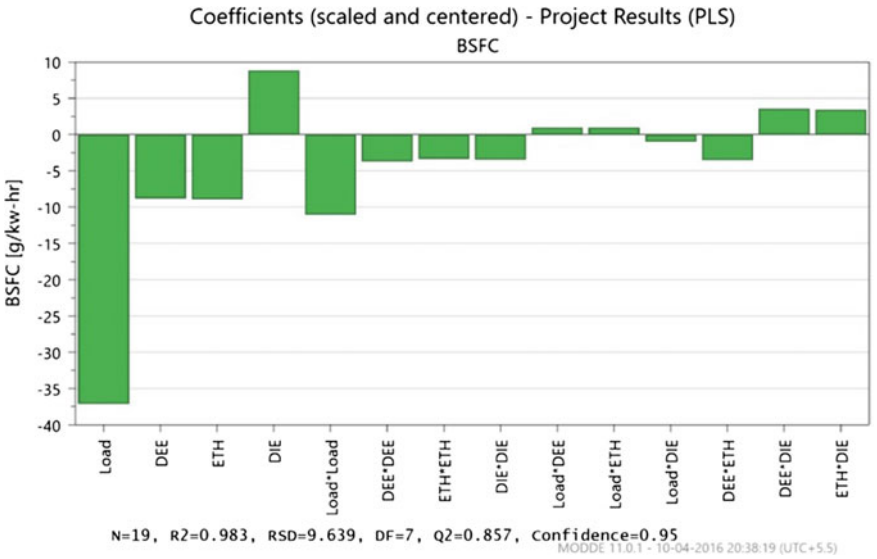

Fig. 6 Significance of the model terms coefficients in the BSFC equation

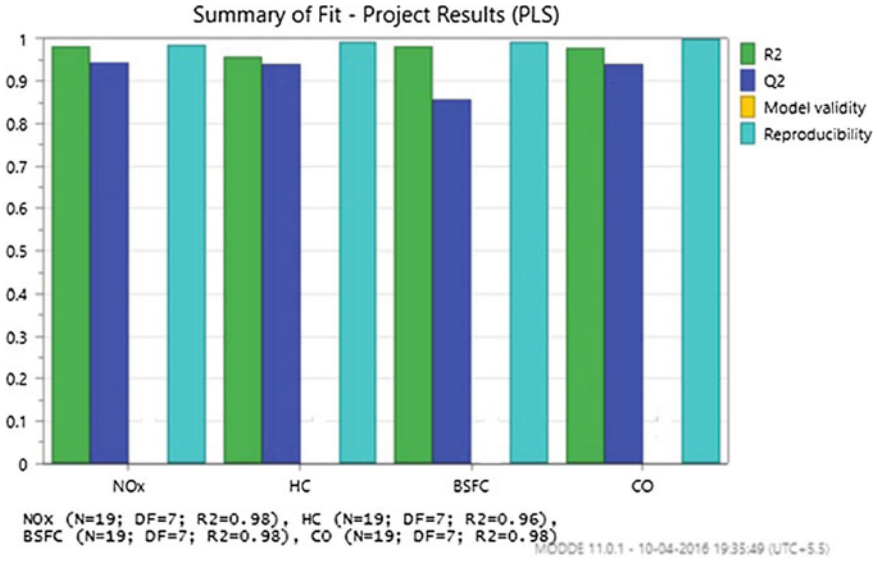

Fig. 7 Summary of fit plot for the model fitted to the experimental data

Observation: From the plot shown in Fig. 7, it can be observed that values of R2 Q2 are well above 0.5. So it can be said that models can be treated as significant as they overrule the null hypothesis at 95% confidence level of estimation.

3.2.1 Assessing Model Adequacy by Using Residual Plots Obtained for the Model

The residual plots were used to determine whether model meets the assumptions of analysis and in turn to check whether it is adequate or not. If the assumption were not met then the model may not fit the data during subsequent predictive iterations in the unexplored experimental domains and will require further investigations of recalibration after optimization.

Assumptions needed to be met were as the following

a. Residuals are normally distributed
b. Residuals are randomly distributed and have constant variance
c. Residuals are independent from one another.

Obtained Plots were as following, and they are discussed in the sub sequent section.

- Normal probability plot of residuals,
- Plot of residuals against fitted values, run order or other factors

From Figs. 8 and 9 it can be seen the normal probability plot of residuals is approximately following the straight line. So the model fulfills the assumption that residuals are normally distributed. As there is no point far away from the straight line, it indicates no presence of any outliers. The plot in the Figs. 10 and 11 shows the residuals versus the fitted values. No uneven spreading of the residuals across fitted values exist across all four responses; there exist no point, which is far away from

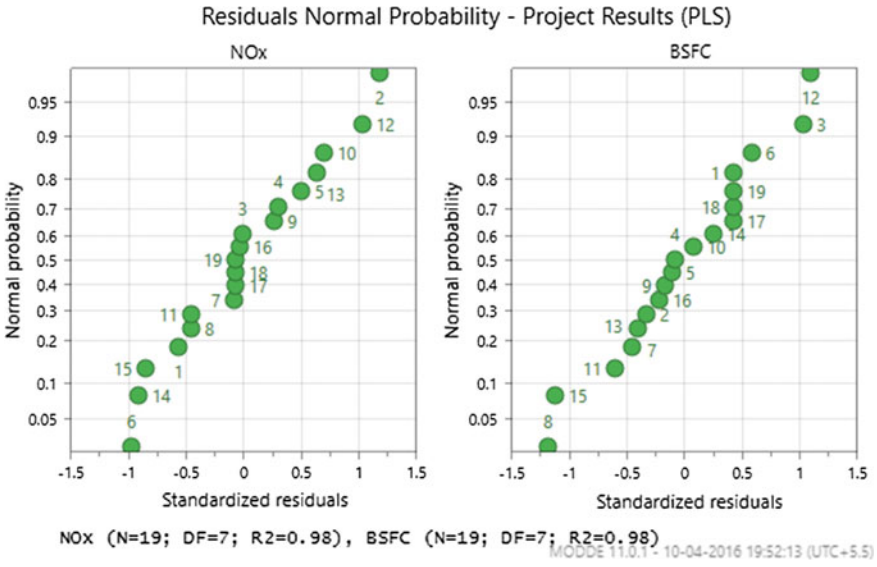

Fig. 8 Residuals versus normal probability plot for NOx and BSFC

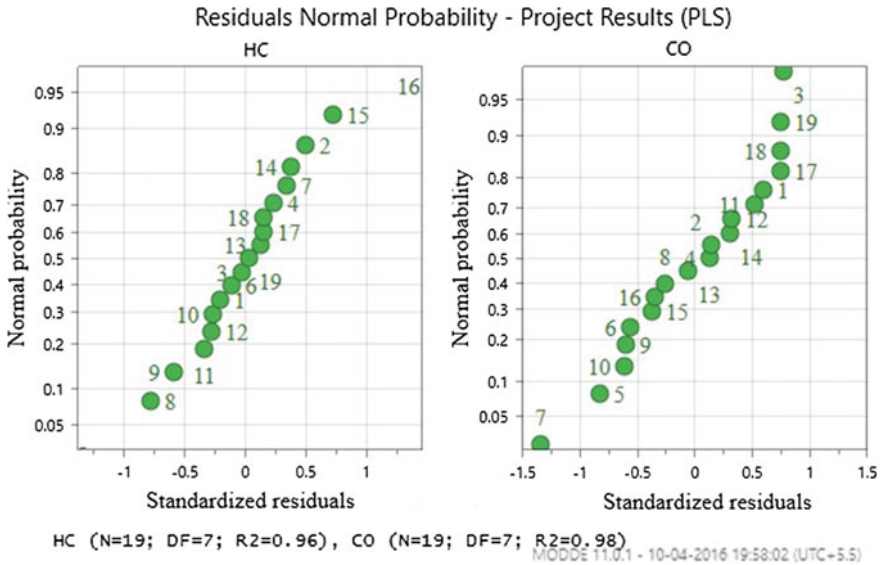

Fig. 9 Residuals versus normal probability plot for HC and CO

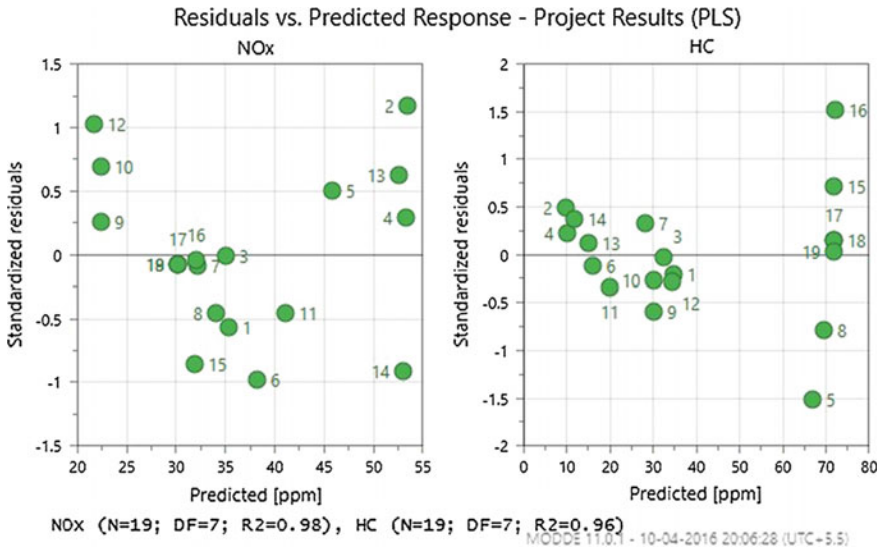

Fig. 10 Residual versus predicted response for NOx and HC

zero line. Points are falling on both sides of abscissa with no distinguishable patterns in the points. As the spreading of residuals across the fitted values is even, this indicates that model fulfills the assumption of the presence of constant variance.

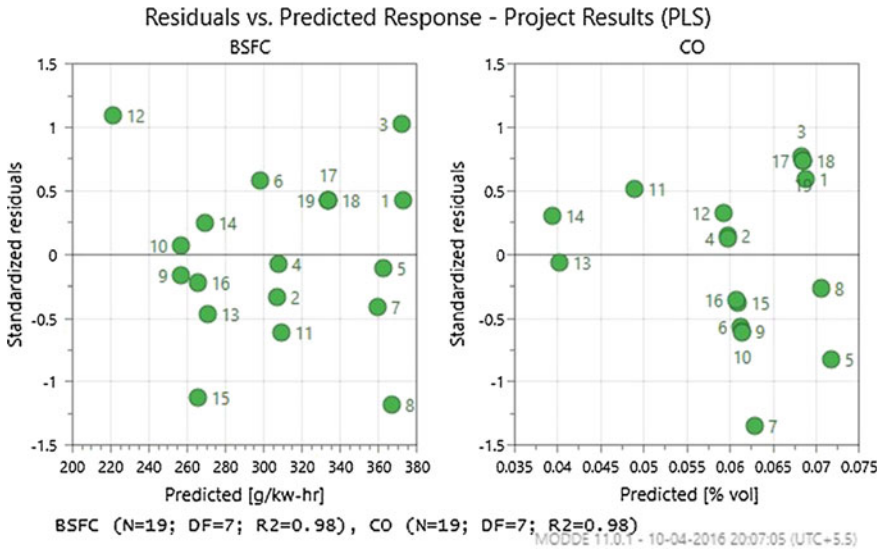

Fig. 11 Residual versus predicted response for BSFC and CO

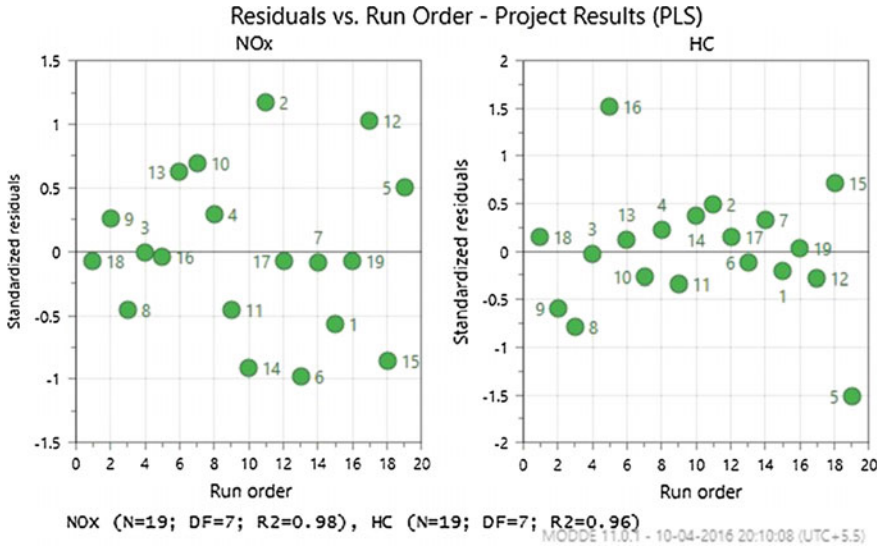

Fig. 12 Residual versus run order for NOx and HC

Observation of Residuals fall randomly around the centre line with no increasing or decreasing trend observed in the residuals. No cyclic or repeating pattern nor any sudden shift in the point is observed. The observations from Figs. 12 and 13 suggest that the residuals were independent from one another. Figures 14 and 15 show

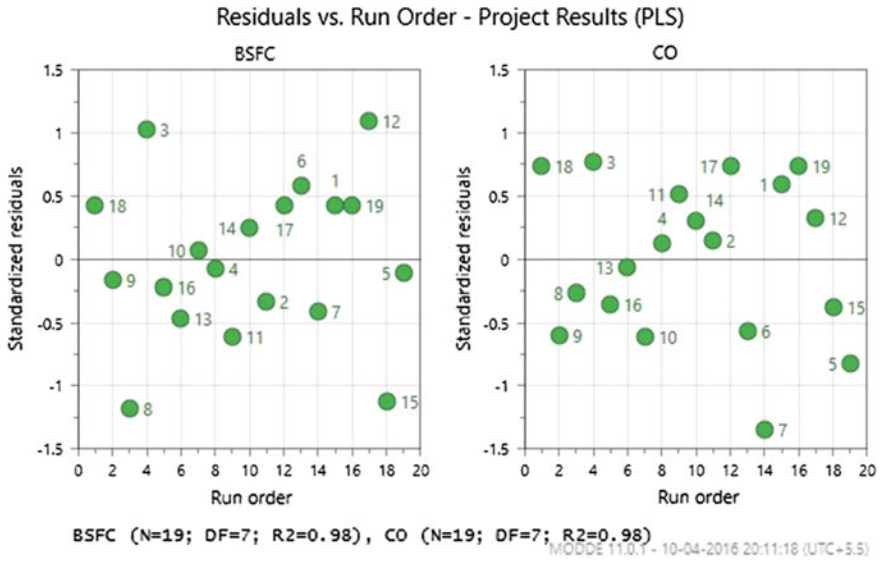

Fig. 13 Residual versus run order for BSFC and CO

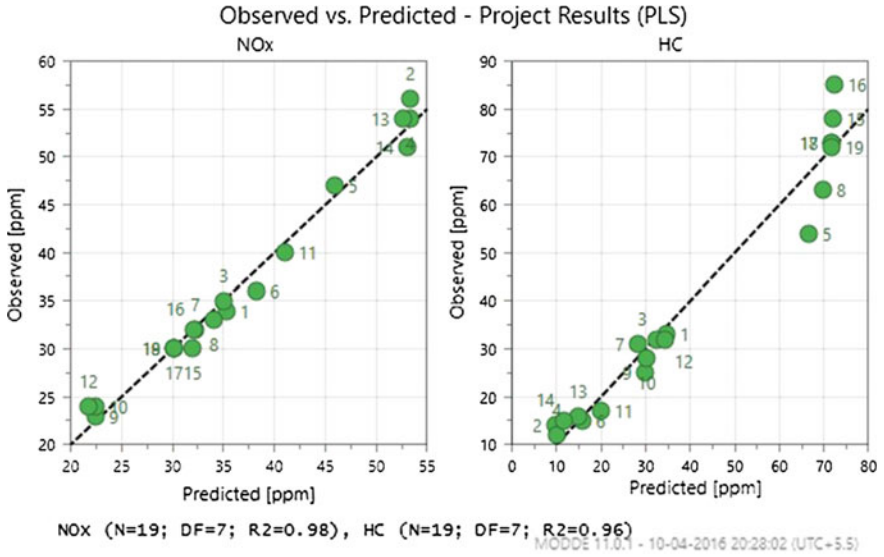

Fig. 14 Observed versus predicted for NOx and HC

points are close to a straight line, which in turn indicate good models. Theoretically, if a model is able to explain 100% of the variance, the fitted values would always equal the observed values and, therefore, all the data points would fall on the fitted regression line.

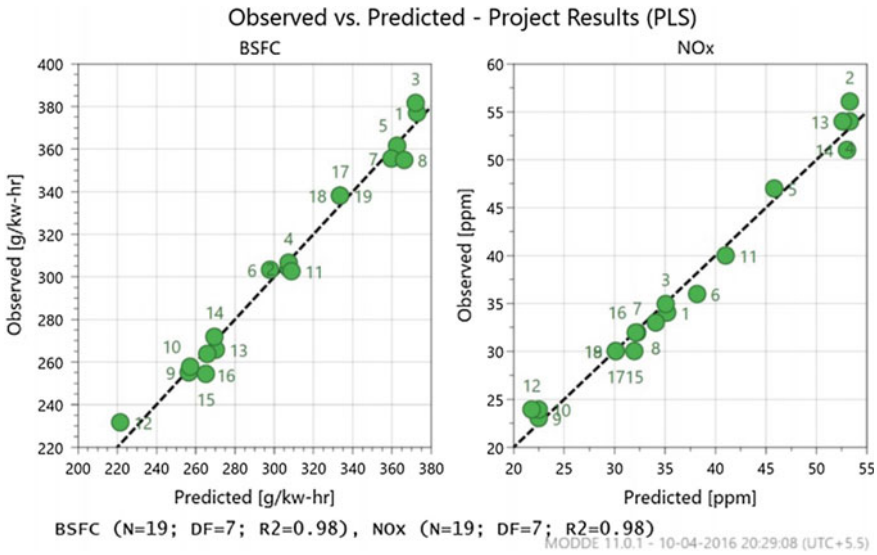

Fig. 15 Observed versus predicted plot for the responses BSFC and NOx

3.2.2 Assessing Model Adequacy by Further Goodness of Fit Measures

Once the models were found to satisfy the residual plot analysis, the developed models for each of the performance and emission responses were then evaluated again through an ANOVA analysis with respect to various goodness of fit measures such as R2 and adjusted R2 as detailed in Table 10 which indicated the robustness of the predicting ability of the developed RSM models when presented with unobserved data of the input parameters.

The ANOVA statistics for the NOx model shows a goodness of fit (R2) and goodness of prediction (Adjusted R2) as 0.983 and 0.956 respectively. The total variation as indicated by R2 and adjusted R2 values symbolise that the model or the equation for NOx fits the data appropriately. Results indicate that the developed RSM model for HC could not explain only 4.2% of the total variation. In addition, the corresponding adjusted R2 value for the HC model was acceptable at 0.892 considering the significant variations recorded in an experimental study for different

Table 10 Response surface model evaluation

Model	NOx	HC	CO	BSFC
Model degree	Quadratic	Quadratic	Quadratic	Quadratic
R2	0.983	0.958	0.979	0.983
Adj. R2	0.956	0.892	0.947	0.957
P value	0.000	0.001	0.000	0.000

blends. Also, p value for the model of HC was higher than other models but was still less than 0.05 to prove the model is still significant for predicting the values of response HC. For the response of CO concentration in exhaust, the value of determination coefficient (R2 = 0.979) and R2 adjusted was found to be 0.947 suggesting that only 2% of the variation could not be explained by the RSM CO model. The value of determination coefficient was high enough to consider the model as significant as reasoned in the study of [29]. For the response of brake specific fuel consumption, the value of determination coefficient (R2 = 0.983) suggested that the sample variation of 98.3% for BSFC attributed to the independent variables and only 0.017% of the total variation could not be explained by the model. The value of adjusted determination coefficient (Adjusted R2 = 0.957) was also seen to be high suggesting adequate robustness in the predictive ability of the model.

3.3 Optimization Results

Table 11 shows the results of the multiobjective optimization carried out based on the approach detailed in Sect. 2.6. NOx, CO, HC and BSFC being the output responses that needed to be minimized corresponding to the range of load steps outlined in the Table 11. The response factors being inherently contradictory in its traits of evolution in a typical diesel operation poses a multi-criteria investigation where no single optimum can satisfy the objectives of minimizing all response factors simultaneously. Thus, a trade-off solution is sought. The optimization endeavour was carried out at first keeping the load constant at a given point of interest incremented in equal epochs. At each given load step, all possible combination of the ethanol-hexane-DEE concentration were explored through the optimization iteration within the constraints of concentration of hexane and DEE in the blend set as per Sects. 2.1 and 2.2. Optimization exploration at each load step involved investigating the optimal set of constituents of a blend that yielded the best emission-emission (NOx vs. CO vs. HC) and emission-performance (BSFC vs. NOx–CO–HC and BSFC vs. NOx) trade-off footprint at the given load step. After investigation at the chosen load steps, the optimization iteration was allowed to run with the load step as an unconstrained factor (50–95% full load) in an effort to investigate the optimal load point of operation that provided the minimum BSFC–NOx–CO–HC trade-off footprint corresponding to a calibrated blend value of ethanol-hexane-DEE in diesel subject to the constraints as mentioned before.

For each load and with that particular strategy optimization was performed and best run (experiment no) was selected based on the minimum Log (D) value. This procedure was performed for different load steps and the obtained values of Log (D), and the optimum blend combination was then entered in the table.

The optimal trade-off point of operation was observed to be at 95% full load for a blend of 5% hexane, 15% Diethyl ether, 40% ethanol, and 40% Diesel yielding a

Table 11 Optimum combination of load and blend

Load	NOx	HC	CO	BSFC	Log D	HEX	DEE	ETH	DIESEL
2 kg (50% full load)	35	32	0.07	X	1.63	0.05	0.00	0.13	0.82
	35	X	0.07	X	1.74	0.05	0.00	0.13	0.82
	35	32	X	X	1.29	0.05	0.00	0.13	0.82
	53	8	0.06	306	1.68	0.05	0.15	0.40	0.40
	35	X	X	372	1.82	0.05	0.00	0.13	0.82
2.5 kg (60% full load)	32	28	0.06	X	1.46	0.05	0.00	0.13	0.82
	32	X	0.06	X	1.57	0.05	0.00	0.13	0.82
	32	28	X	X	1.12	0.05	0.00	0.13	0.82
	38	16	0.06	298	1.47	0.05	0.15	0.40	0.40
	38	X	X	298	1.50	0.05	0.15	0.40	0.40
3 kg (75% full load)	34	23	0.06	X	1.30	0.05	0.00	0.13	0.82
	34	X	0.06	X	1.43	0.05	0.00	0.13	0.82
	28	23	X	X	0.80	0.05	0.15	0.40	0.40
	28	23	0.06	281	1.34	0.05	0.15	0.40	0.40
	28	X	X	281	1.11	0.05	0.15	0.40	0.40
3.5 kg (85% full load)	41	20	0.05	X	1.30	0.05	0.00	0.13	0.82
	22	X	0.06	X	1.42	0.05	0.15	0.40	0.40
	22	29	X	X	0.82	0.05	0.15	0.40	0.40
	22	29	0.06	256	1.26	0.05	0.15	0.40	0.40
	22	X	X	256	0.61	0.05	0.15	0.40	0.40
4 kg (95% full load)	22	34	0.06	X	1.33	0.05	0.15	0.40	0.40
	22	X	0.06	X	1.35	0.05	0.15	0.40	0.40
	22	34	X	X	1.00	0.05	0.15	0.40	0.40
	22	34	0.06	221	1.21	0.05	0.15	0.40	0.40
	22	X	X	221	−0.60	0.05	0.15	0.40	0.40
Free mode at any load	22	34	0.06	221	1.20	0.05	0.15	0.40	0.40

Where, X denotes that the response was excluded during that particular optimisation stage

predicted value of 22 ppm NOx, 34 ppm HC, 0.06% vol. CO and a BSFC of 221 g/kw-at 1550 rpm.

3.4 Validation of Optimized Results

Validation of the optimized results was done by performing the experiment thrice at that factor setting which gave optimized results and after that these three readings

Table 12 Validation of test results

Exp no.	Load (kg)	HEX	DEE	ETH	Diesel	Response type	NOx (ppm)	HC (ppm)	CO (% vol.)	BSFC (g/kwh)
20	4	0.05	0.15	0.40	0.40	Actual	26	41	0.059	229
						Predicted	22	34	0.06	221
						% Absolute error	15.3	17.1	1.69	3.4

were averaged and compared with the readings predicted by the statistical software. Validation test results are given in Table 12.

4 Conclusion

The following were the conclusions arrived on performing the several tests in an IDI single cylinder engine by varying the process factor i.e. load and mixture factors i.e. Blend components.

1. Among tested quantities of Hexane, the maximum amount of hexane needed to maintain phase stability of ethanol-diesel blend with a concentration of ethanol ranging from E10 to E40 is 5% v/v.
2. Optimized results of NOx 22 ppm, HC 34 ppm, CO 0.06% vol. and BSFC 221 g/kwh can be obtained at the Load 4 speed 1550 rpm for a blend of 5% hexane, 15% Diethyl ether, 40% ethanol, and 40% Diesel with minimization criteria for the ethanol-diesel blend with the addition of co-solvent and cetane improver.
3. The D-optimal method of the design of experiment considerably reduced the time required by giving reduced no of experimental runs. It provided the potential of designing the experiment efficiently and found extremely helpful in the process. Also, statistical analysis helped to ascertain the significance of each model developed for predicting response parameters.
4. Multiobjective optimization based on RSM models provided an acceptable cost-effective estimation of the optimal blend of ethanol in diesel with its necessary co-solvent and cetane improver additives.

Acknowledgements The authors gratefully acknowledge the kind support of the AICTE (Govt. of India) grant under the RPS projects entitled "Development of an artificial intelligence model to simulate the performance and emission characteristics of a diesel engine operating in dual fuel mode with biodiesel and CNG under various EGR strategies" under Grant No: 8023/RID/RPS-4/(POLICY-III) (NER)/2011-12 and "An experimental study to explore the potential of biodiesel ethanol blend as an alternative fuel in diesel engine with hydrogen enrichment" under Grant No: 8023/BOR/RID/RPS(NER)-34/2010-11 which has made this study possible.

References

1. Folkson R (2014) Alternative fuels and advanced vehicle technologies for improved environmental performance: towards zero carbon transportation. Elsevier
2. Hansen AC, Zhang Q, Lyne PW (2005) Ethanol–diesel fuel blends—a review. Bioresour Technol 96(3):277–285
3. Ajav E, Akingbehin O (2002) A study of some fuel properties of local ethanol blended with diesel fuel. Agric Eng Int CIGR J
4. Lapuerta M, Armas O, Herreros JM (2008) Emissions from a diesel–bioethanol blend in an automotive diesel engine. Fuel 87(1):25–31
5. Huang J et al (2009) Experimental investigation on the performance and emissions of a diesel engine fuelled with ethanol–diesel blends. Appl Therm Eng 29(11):2484–2490
6. Yeom J, Park J, Chung S (2005) A study on the mixture formation process of diesel fuel spray in unsteady and evaporative field. J Mech Sci Technol 19(12):2253–2262
7. Kwanchareon P, Luengnaruemitchai A, Jai-In S (2007) Solubility of a diesel–biodiesel–ethanol blend, its fuel properties, and its emission characteristics from diesel engine. Fuel 86(7):1053–1061
8. Sadek PC (2002) HPLC solvent guide. Wiley-Interscience
9. Xing-cai L et al (2004) Effect of cetane number improver on heat release rate and emissions of high speed diesel engine fueled with ethanol–diesel blend fuel. Fuel 83(14):2013–2020
10. Ren Y et al (2008) Effects of the addition of ethanol and cetane number improver on the combustion and emission characteristics of a compression ignition engine. Proc Instit Mech Eng J Autom Eng 222(6):1077–1087
11. Yu W, Chen G, Zuohua H (2011) Influence of cetane number improver on performance and emissions of a common-rail diesel engine fueled with biodiesel-methanol blend. Front Energ 5(4):412–418
12. Sivaprakasam S (2014) Experimental investigation on combustion characteristics of DI diesel engine using diethyl ether fumigation with ethanol blended diesel. Int J Renew Energ Res 4 (4):872–878
13. He B-Q et al (2003) The effect of ethanol blended diesel fuels on emissions from a diesel engine. Atmos Environ 37(35):4965–4971
14. Balamurugan T, Nalini R (2014) Experimental investigation on the effect of alkanes blending on performance, combustion and emission characteristics of four-stroke diesel engine. Int J Ambient Energy 1–9
15. Testing, A.S.f. and Materials ASTM D975 (2011) Standard specification for diesel fuel oils. ASTM International West Conshohocken, PA
16. McCormick RL, Parish R (2001) Advanced petroleum based fuels program and renewable diesel program. NREL/MP 540–32674
17. Paul A et al (2013) An experimental investigation of performance-emission trade off of a CI engine fueled by diesel–compressed natural gas (CNG) combination and diesel–ethanol blends with CNG enrichment. Energy 55:787–802
18. Hirkude J, Padalkar A, Vedartham D (2014) Investigations on the effect of waste fried oil methyl ester blends and load on performance and smoke opacity of diesel engine using response surface methodology. Energy Procedia 54:606–614
19. Kitamura Y et al (2011) Investigation about predictive accuracy of empirical engine models using design of experiments. SAE Technical Paper
20. El-Gendy NS, Hamdy A, Abu S (2015) Amr, application of d-optimal design and RSM to optimize the transesterification of waste cooking oil using a biocatalyst derived from waste animal bones and novozym 435. Energy Sources Part A 37(11):1233–1251
21. Borhan FP, Abd Gani SS, Shamsuddin R (2014) The use of D-optimal mixture design in optimising okara soap formulation for stratum corneum application. Sci World J 2014:8

22. Liu S et al (2010) Effect of a cetane number (CN) improver on combustion and emission characteristics of a compression-ignition (CI) engine fueled with an ethanol–diesel blend. Energy Fuels 24(4):2449–2454
23. Pandian M, Sivapirakasam S, Udayakumar M (2011) Investigation on the effect of injection system parameters on performance and emission characteristics of a twin cylinder compression ignition direct injection engine fuelled with pongamia biodiesel–diesel blend using response surface methodology. Appl Energy 88(8):2663–2676
24. Kannan G, Anand R (2011) Experimental investigation on diesel engine with diestrol–water micro emulsions. Energy 36(3):1680–1687
25. Kumar Bose P, Banerjee R (2012) An experimental investigation on the role of hydrogen in the emission reduction and performance trade-off studies in an existing diesel engine operating in dual fuel mode under exhaust gas recirculation. J Energy Res Technol 134(1):012601–012601
26. Silva GF, Camargo FL, Ferreira AL (2011) Application of response surface methodology for optimization of biodiesel production by transesterification of soybean oil with ethanol. Fuel Process Technol 92(3):407–413
27. Lee T, Reitz RD (2003) Response surface method optimization of a high-speed direct-injection diesel engine equipped with a common rail injection system. J Eng Gas Turbines Power 125(2):541–546
28. Derringer G, Suich R (1980) Simultaneous optimization of several response variables. J Qual Technol 12(4):214–219
29. Khoobbakht G, Najafi G, Karimi M (2016) Optimization of operating factors and blended levels of diesel, biodiesel and ethanol fuels to minimize exhaust emissions of diesel engine using response surface methodology. Appl Therm Eng

Effect of Alcohol Blending on Performance of Kerosene Fuelled Four-Stroke Spark Ignition Genset

Mritunjay Shukla, Eshan Singh and Sunil Pathak

Abstract Environmental pollution from engine exhaust emission has attracted worldwide attention. Besides vehicular pollution, the significance of engine exhaust emission from stationary utility engines, particularly gensets for electrical energy applications, has also been realized. Gensets based on kerosene are widely in use in developing countries like India. To reduce the exhaust emission, from these small carbureted engines is challenging due to cost factor. In present work, an attempt has been made to reduce the exhaust emission of a portable genset by blending alcohols in kerosene. It was observed that blending alcohols in kerosene helps reducing Carbon Monoxide (CO) and Hydrocarbon (HC) emission and fuel consumption of the engine while Nitric Oxide (NO) emission increases. Further, the effect of varying carbureted jetsize on the performance and exhaust emission is also examined. A comparison of kerosene with base jetsize was done with the various combinations of fuels and jetsizes to achieve optimized emission and fuel economy. It was observed that by blending 10% n-butanol in kerosene and operating engine on a slightly richer side, emission from a kerosene operated genset can be reduced along with improvement in fuel economy without any engine hardware modification.

Keywords Kerosene gensets · Emission · Engine performance · Biofuels · SI engines

Abbreviations

CO	Carbon Monoxide
HC	Hydrocarbon
NO	Nitric Oxide

M. Shukla (✉) · E. Singh · S. Pathak
CSIR-Indian Institute of Petroleum, Dehradun 248005, India
e-mail: mshukla@iip.res.in

E. Singh
e-mail: eshan.singh@kaust.edu.sa

S. Pathak
e-mail: spathak@iip.res.in

A.K. Agarwal et al. (eds.), *Biofuels*, Green Energy and Technology,
DOI 10.1007/978-981-10-3791-7_12

K Kerosene
E10 K 10% Ethanol blended in Kerosene (v/v)
B10 K 10% n-Butanol blended in Kerosene (v/v)
RVP Ried-vapour Pressure

1 Introduction

In developing nations, kerosene is being used as fuel for portable gensets for electricity generation at domestic level due to frequent power cuts. India, for instance, being the biggest market to generator set, faces a demand-supply gap of 17% in Kerosene gensets [1]. More than 0.2 million engines or their application products are sold in the market every year. For domestic use, population of kerosene run gensets is large (more than 3 million) due to running cost advantage of these gensets over gasoline gensets and lower noise in comparison to diesel gensets [2]. Considering the environmental impact due to gensets, countries have come up with regulatory norms specific to kerosene based gensets, which ensures minimum harm to the environment. Central Pollution Control Board (CPCB), for instance, specifies the norms for India, laid out in the year 2000 [3]. The latest norms, revised in 2013, have been tabulated in Table 1.

Usually performing on richer mixture, kerosene based gensets emit higher unburned Hydrocarbon (HC) and Carbon monoxide (CO) emission [4]. Attempts have been made to reduce these, using catalytic converters in 2-stroke and 4-stroke kerosene driven gensets by leaning the exhaust using secondary air [4, 5] injected into the exhaust stream rather than the primary air inducted into the intake manifold. Similar studies were performed on SI engines with catalytic coating, resulting in improved emission [6]. Gensets have also been made to run on alternate fuels like LPG to reduce emission [7]. For small capacity gensets, it is a bit difficult to achieve emission reduction by simple design modifications, without significant cost increase. The progress in this direction has also been marred by insufficient cooperation between the engine and carburetor manufacturers [8]. A previous study has confirmed that kerosene internal combustion engines show higher thermal efficiency while working on leaner mixtures [9]. There have been prospects about

Table 1 CPCB emission norms on kerosene genset

Class	Displacement (CC)	CO (gm/kW-hr)	HC + NOx (gm/kW-hr)
1	Up to 99	≤ 250	≤ 12
2	>99 and up to 225	≤ 250	≤ 10
3	>225	≤ 250	≤ 8

kerosene levitating the burden off gasoline as an automotive fuel [10]. Tests on kerosene blended in gasoline on a variable compression ratio engine revealed a lower thermal and volumetric efficiency on increasing kerosene in blend [11].

Bio based fuels have garnered research interest across the globe, and various biofuels like alcohols, ethers, furans have been blended in gasoline as well as in diesel with positive reduction in CO and HC emission. Previous works on using blends of alcohols like methanol and ethanol in gasoline gensets have shown reduction in tailpipe emission of HC and CO [12, 13]. However, kerosene based gensets have been neglected in this regard. Hence, blending oxygenated biofuels in kerosene might be useful in providing a more environmentally viable option for gensets and other stationary engines.

Kerosene has a higher surface tension and viscosity compared to gasoline resulting in poorer fuel atomization and reduced combustion efficiency [14]. Kerosene has a higher rate of heat release compared to gasoline. It is also less volatile (boiling range 140–320 °C) requiring startup usually by gasoline. Comparative properties of kerosene with gasoline are given in Table 2. Huge difference in distillation pattern can be noted. Kerosene has a slightly higher density (0.8109) compared to gasoline (0.7453) and primarily composed of less volatile and high chain length compounds as compared to gasoline, and that is why it would require more air for stoichiometric mixture. Octane number of kerosene is 25, which is very low compared to gasoline. Since oxygenated fuels have higher octane rating, blending them in kerosene would enable use of higher compression ratio for such engines, which in turn would translate in higher thermal efficiency.

Engine emission studies on alcohol blends in kerosene engines or even kerosene combustion and emission in generator sets are scarce. Hereby in present work, an experimental investigation of performance and emission characteristics of 10% n-butanol blend in kerosene (v/v) and 10% ethanol blend in kerosene (v/v) has been carried out in a portable carbureted SI engine powered genset. Thereafter the effect of varying air-fuel ratio on tail pipe emission was also studied by varying main jetsize of carburetor. Finally, the optimized combination of blend and jetsize is recommended after the comparative study considering CO and HC + NO emission.

Table 2 Comparative properties of kerosene and gasoline

Properties	Kerosene	Gasoline
Density	0.8109	0.7453
Octane rating	25	88
Reid vapor pressure (RVP)	0.689	59.5
Lower heating value	43.1 MJ/kg	42.4 MJ/kg
Higher heating value	46.2 MJ/kg	46.6 MJ/kg
Water miscibility	Immiscible	Immiscible
T_{10}	179.1 °C	61.1 °C
T_{50}	208.2 °C	101.6 °C
T_{90}	248.9 °C	151.4 °C

2 Methodology

2.1 Nomenclature

Nomenclature followed in the results abbreviates the alternate fuel followed by its percentage in the blend followed by K for pure kerosene. For the current study, two blends are attributed with names E10 and B10 K referring to 10% ethanol +90% kerosene (v/v) and 10% butanol +90% kerosene (v/v) respectively. Ethanol (99.9% pure) and n-butanol (99.9% pure), supplied from Acros Organics, USA, and Commercially available kerosene, were used for the study. Blends of alcohols with kerosene were prepared by splash blending just prior to experiments. The important physico-chemical properties were analyzed as per their respective ASTM standards and are given in Table 3. Kerosene has very low octane rating and is prone to auto ignition and knocking. Blending alcohols help in this regard and provides better combustion of the blend. The boiling range of pure kerosene is also high and alcohol blends improve the front end volatility of the fuel, which can be observed by T_{10} values in the Table 3. E10 K provides more benefit in this regard. Tail end volatility is also improved with blended fuels. Air fuel ratio was adjusted by varying the size of carburetor main jet. Manufacturer recommended jet size is termed as jet size J(0) while one size larger jet is termed as J(−1), one size smaller jet size is termed as J(+1) in the paper which corresponds to air fuel equivalence ratio $\lambda = 1$, $\lambda = 0.9$ and $\lambda = 1.1$ respectively at engine idle load for kerosene fuel.

2.2 Experimental Setup

A single-cylinder, constant speed air-cooled carbureted spark ignition engine, coupled with 2.2 KVA AC brushless alternator was used for the study. A schematic diagram of the experimental set-up is given in Fig. 1. Details of the engine and electrical generator are listed in Table 4. A resistive load bank along with voltmeter, ammeter and frequency meter was used for loading the genset. The load bank was a single-phase load circuit consisting of a combination of stable resistive elements of appropriate rating, wired such that the total load current is adjustable to any value up to 125% of maximum value. Full throttle current of the genset under test was

Table 3 Physico-chemical properties of fuels

Sample	K	B10 K	E10 K
Density at 15 °C, g/cc	0.8109	0.8099	0.8069
Flash point °C	43	36	9
Calorific value (MJ/kg)	46.2	44.4665	44.8875
T_{10}	179.1 °C	135	95.5
T_{50}	208.2 °C	204.7	200.6
T_{90}	248.9 °C	248.3	244.9

Fig. 1 Experimental setup

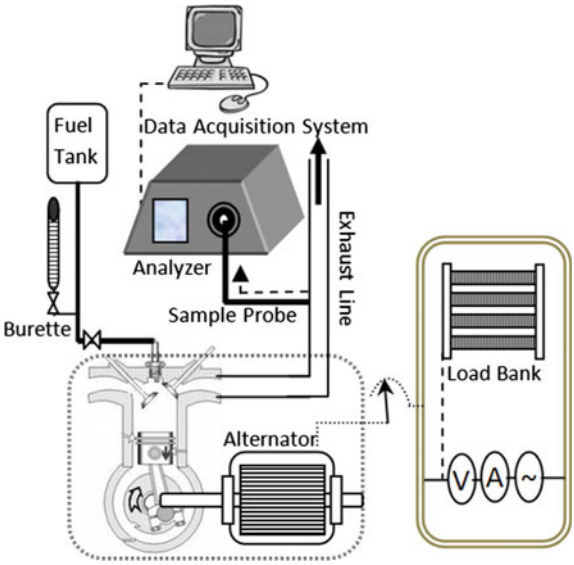

Table 4 Specifications of test engines

Engine type	4-stroke, forced air cooled, side valve engine
No. of cylinder	1
Bore X stroke (mm)	73 X 61
Displacement (cc)	256
Comp ratio	5.1:1
Rated O/P (HP/HR)	4.0/3000
Fuel con. at rated load (l/hr)	2.4 Petrol
Lube oil sump capacity	950 ml
Rated AC O/P	2200 VA
Max. AC output	2400 VA
Voltage	220 V
Current	10 A
Frequency	50 Hz

measured with accuracy of ±0.1 Amp. The resistive elements used were capable of withstanding continuous energization at 150% of the rated voltage of the genset without overheating. Voltmeter and ammeter were AC RMS meters, direct acting digital type conforming to BIS 1248 (part 4), and accuracy class 1. The range of frequency meter was 45–65 Hz.

Engine output was measured in terms of electrical power by measuring output current and voltage at constant frequency (50 Hz). K type thermocouples were used to monitor the temperature of engine oil and exhaust gases. Volumetric fuel consumption was recorded for each load point. Portable automotive emission analyzer (Horiba MEXA-584L) was used to measure engine tail pipe emission levels of CO, HC and NO emission along with air/fuel equivalence ratio. HC emission were measured in terms of propane equivalent.

The exhaust sampling arrangement consists of an extension pipe fitted with an exhaust sample probe connected to the outlet of the normal exhaust system. In order to prevent condensation, exhaust sample probe was kept close to the muffler in a suitable location which could yield a well-mixed homogeneous representative sample of the exhaust.

2.3 Test Procedure

The engine was run to reach steady state conditions till the engine oil temperature reached 75 °C to ensure steady state operation. Engine load was varied by increasing current demand. Concentrations of carbon monoxide (CO), hydrocarbon (HC), nitrogen monoxide (NO) along with fuel consumption were recorded with respect to change in load for three partial engine loads of 753, 1228 and 1650 W which approximately corresponds to 35, 55 and 75% of full engine load. Metering of emission was done, considering a weight factor of 0.2–35% load, 0.5–55% load and 0.3–75% load to obtain a single cumulative value of emission for comparison with baseline kerosene emission to attain a conclusive optimum combination of jet size and fuel.

First, the test was carried out for all the three test fuels for carburetor main jet size of 880 microns which is the manufacturer's optimized jet size for kerosene fuel and corresponds to a stoichiometric mixture ($\lambda = 1$) at idling engine loads, termed as J(0). Once the emission results from the three test fuels were recorded, attempts were made to reduce the emission with a combination of fuel and jet size. Hence, the effect of varying main jet size on engine exhaust emission and fuel consumption was studied for E10 K and B10 K fuel. By using two different jet sizes, air fuel equivalence ratio was varied. The three jet sizes J(−1), J(0) and J(+1) correspond to slightly rich ($\lambda = 0.9$), stoichiometric ($\lambda = 1.0$) and slightly lean ($\lambda = 1.1$) mixture respectively for kerosene fuel at engine idling loads only. For actual kerosene engine operation, however, kerosene fueled engines are operated on the rich side for appropriate performance [4], actual air fuel ratios tend to decrease with an increase in engine loads. Values of air fuel equivalence ratio for the three fuels at all the test conditions are presented in Figs. 2a, b and c.

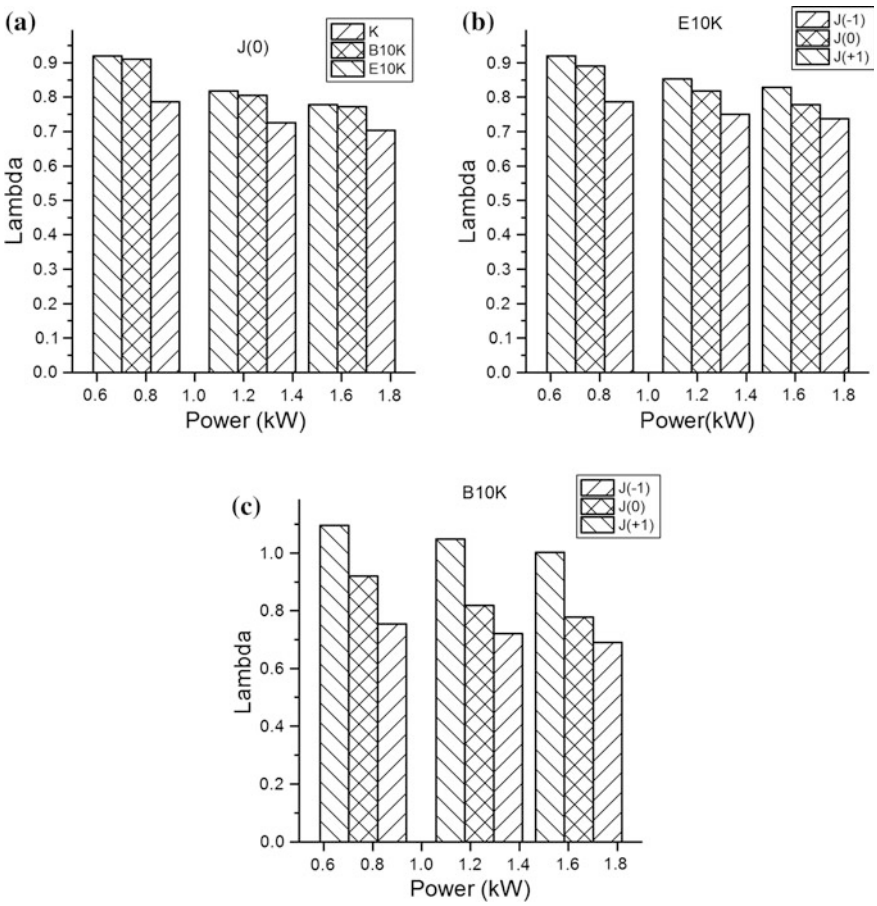

Fig. 2 Variation of air-fuel equivalence ratio with power **a** with different fuels at J(0) **b** with E10 K for different jet sizes **c** with B10 K for different jet sizes

3 Results and Discussion

Figure 3 represents comparative CO emission for the three test fuel corresponding to standard jet size. CO is a toxic by-product of combustion, resulting due to incomplete combustion of fuel. Leaning of mixture due to oxygenated fuel blends should lead to better combustion and thereby reducing the CO level. CO emission decrease in case of E10 and B10 K fuels, which can be attributed to better combustion due to the presence of oxygenated molecules. 21–41% reduction of CO emission is observed for B10 K fuels. E10 K fuel offers more reduction in CO emission, which varies from 23 to 48% at various loads. This is due to higher oxygen content for Ethanol (47.82%) compared to Butanol (21.62%). Alcohols have been thought of as partially oxydised fuels in previous literatures, and

presence of oxygen molecule certainly helps in leaning of the mixture (considering the jet size is kept constant and fuel flow is maintained). This leads to more complete combustion and hence the CO formation is reduced, in accordance with oxygen content in the molecule. Ethanol contains more oxygen than butanol on mass basis. Heby E10 K fuel offers more oxygen than B10 K fuel for oxidation of CO leading to better reduction of CO emission.

Figure 4 shows HC emission levels in engine exhaust for kerosene, E10 K and B10 K fuels. HC emission occur due to highly varied reasons. It may be due to incomplete oxidation of fuel that might have escaped combustion, slipping of liquid fuel into the crankcase, flame quenching and many other reasons. HC emission also reduce in case of both the blended fuels by 48–77%. However, it is difficult to deduct that which of the both oxygenates offers more reduction. Blending of ethanol and n-butanol in kerosene improves its evaporation, as it is evident from distillation properties of E10 and B10 K fuel. This facilitates formation of homogenous mixture. Faster flame propagation with alcohol blends insures completion of combustion of charge before expansion process cools the gases and quenches the flame reaction which in turn leads to less amount of unburned HC emission.

As, both the alcohols offer higher flame speeds than kerosene, which ensures smaller time for highly compressed HC to move into crevice volume. Hereby, for E10 K and B10 K fuels better mixture formation and flame propagation ensures lesser emission of hydrocarbons from engine tailpipe.

NOx is very harmful emission contributing to the greenhouse effect, acid rains and global warming. NOx is a collective term for harmful gases Nitric Oxide (NO), Nitrogen Dioxide (NO_2) and other Nitrogen-Oxygen compounds formed during

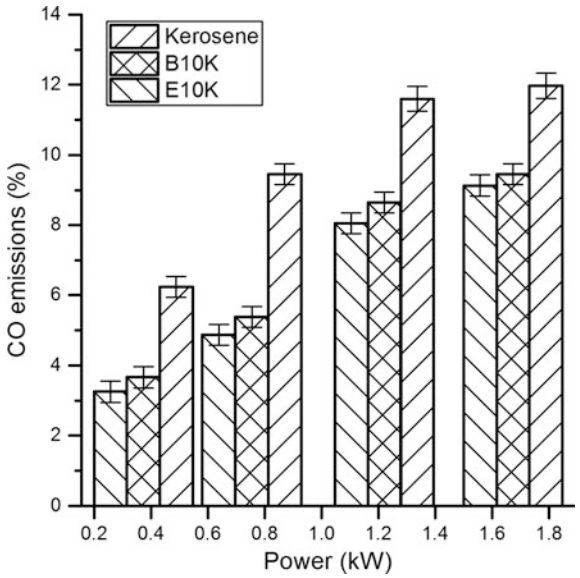

Fig. 3 CO emission comparison

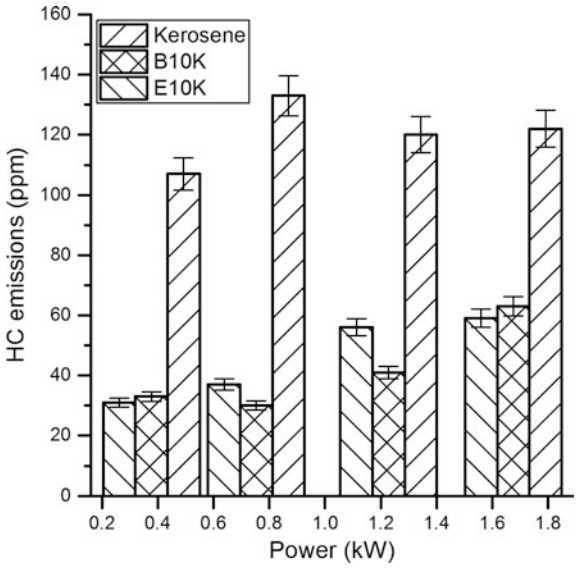

Fig. 4 HC emission comparison

combustion of fuel due to reaction to Nitrogen and Oxygen at high temperature and pressure. NO comprises of 90–95% of the NOx, while NO_2 makes up the rest [17]. NO emission tend to increase with in-cylinder temperature. Comparative emission of NO for the three fuels on standard jet size has been presented in Fig. 5. It can be observed that NO emission rise significantly in case of E10 and B10 K fuel as compared to kerosene. This rise is more than 100% at higher loads with both the

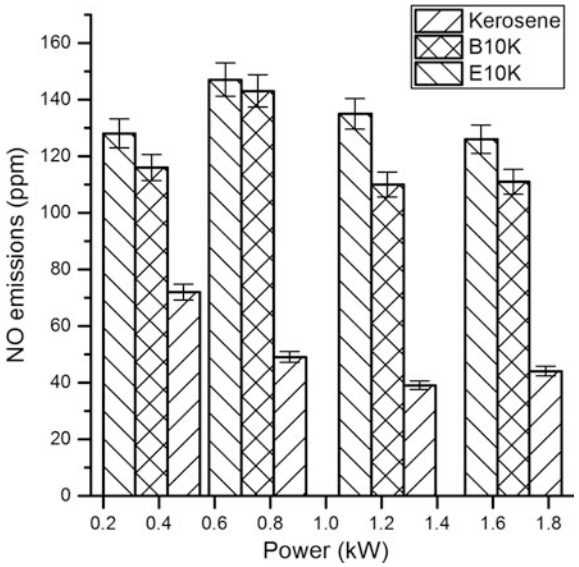

Fig. 5 NO emissions comparison

alcohol blended test fuels. This is due to sudden rise in combustion chamber temperatures as alcohols tend to burn quickly due to higher flame speed.

Brake specific fuel consumption for all the three fuels is plotted in Fig. 6. BSFC of E10 and B10 K are less than that of kerosene. Despite the fact that the calorific values of ethanol and butanol is lower than of kerosene, BSFC tends to improve for alcohol blended fuels. Alcohols are oxygenated fuels. Here blending alcohols in kerosene enhances oxygen availability for attaining better combustion of hydrocarbons. Kerosene operated generator-sets operate on richer mixtures therefore by alcohol additions in kerosene complete combustion can be attained leading to better fuel efficiency. Reduction in unburned hydrocarbon emission confirms the fact. This result is in accordance with previous works on alcohol blended gasoline fuel [15, 16]. The results stated above have been considering Jet size corresponding to $\lambda = 1$.

Figures 7a, b represent variations of CO emission for E10 and B10 K fuel with different jet sizes. For all three loads, CO emission increases with J(−1) and decreases for J(+1). For J(−1) the CO rises from 24–95%, while CO decreases by 4–21% for J(+1) with E10 K fuel. B10 K fuel shows a trend similar to E10 K. With jet size J(−1) there is a nominal rise in CO level of B10 K fuel. However, reduction in CO emission with jet size J(+1) is more prominent. This increase in CO for J(−1) with both alcohol blended fuels is caused due to incomplete combustion for richer mixtures. With J(+1) due to leaning effect, CO reduces.

Figures 8a, b represents variation of HC emission with varying jet sizes for E10 and B10 K fuel. With E10 K fuel, HC emission are higher in case of J(−1) as compared to J(0) for all loads. Jet size J(+1) provides the lowest HC emission with a decrease of 30–46% compared to J(0). Similar results are observed for B10 K fuel,

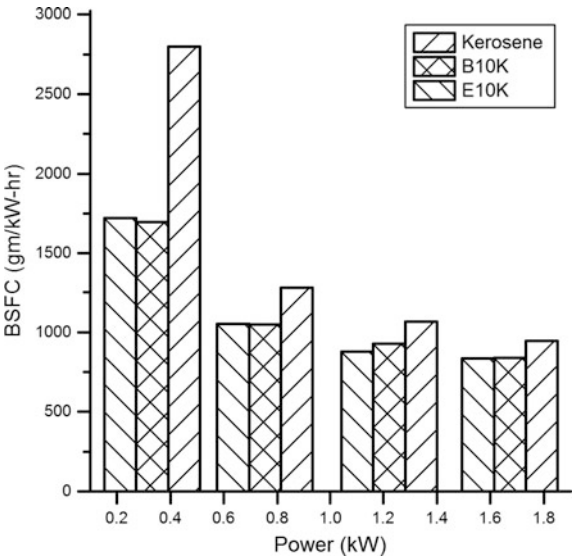

Fig. 6 BSFC comparison

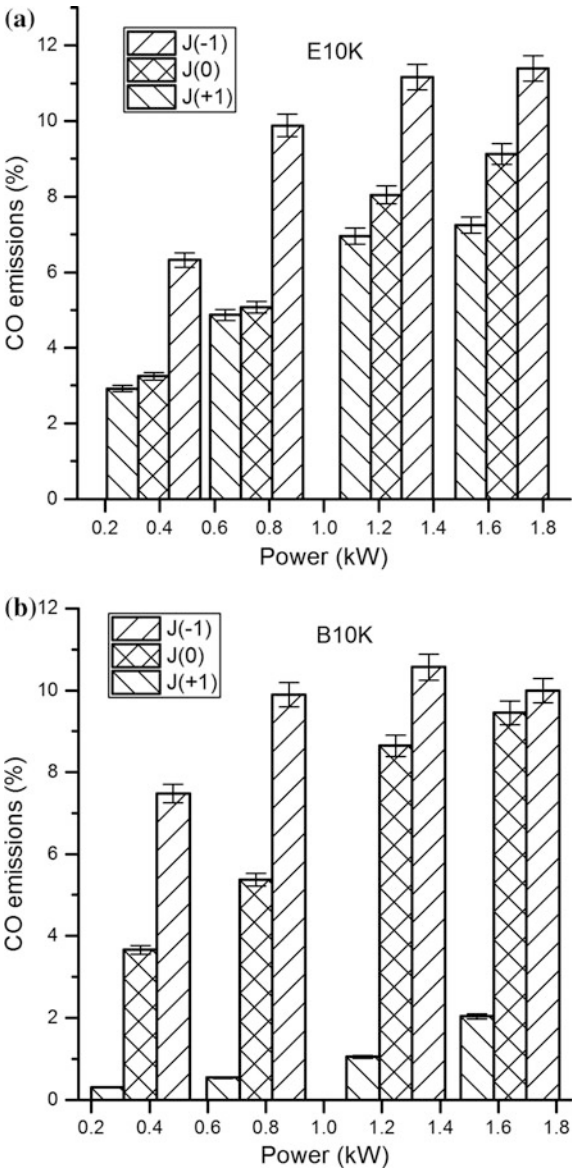

Fig. 7 Comparison of CO emissions for different jet sizes in **a** E10 K **b** B10 K

where HC emission rise for J(−1) and show a decreasing trend for J(+1). A decrease of 60–78% is attained using jet size J(+1). With richer mixtures, HC emission rise due to incomplete combustion caused from availability of less air. While in case of J(+1), mixture leans slightly providing more air available for better combustion of fuel. Also, ethanol has more oxygen content than butanol; Due to which leaning is more effective in decreasing emission of HC in case of B10 K fuel than E10 K.

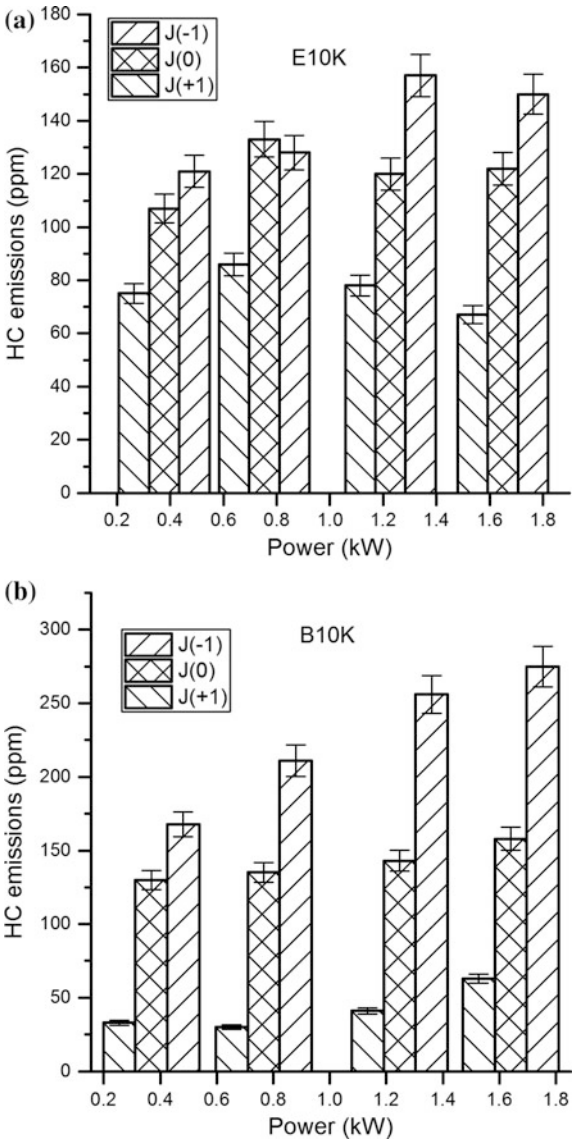

Fig. 8 Comparison of HC emissions for different jet sizes in **a** E10 K **b** B10 K

Variation of NO emission is shown in Figs. 9a, b for E10 K fuel and B10 K fuel respectively for different jet sizes. A decrease in NO emission is observed for jet size J(−1) ranging from 43 to 68%. With J(+1), there is a sudden increase in NO emission. Similar trends are showcased by B10 K, where the increase in NO emission for J(+1) is even higher.

Variation of BSFC for different jet sizes in case of E10 and B10 K fuel is represented in Figs. 10a, b. Jet size J(−1) has higher value of BSFC compared to

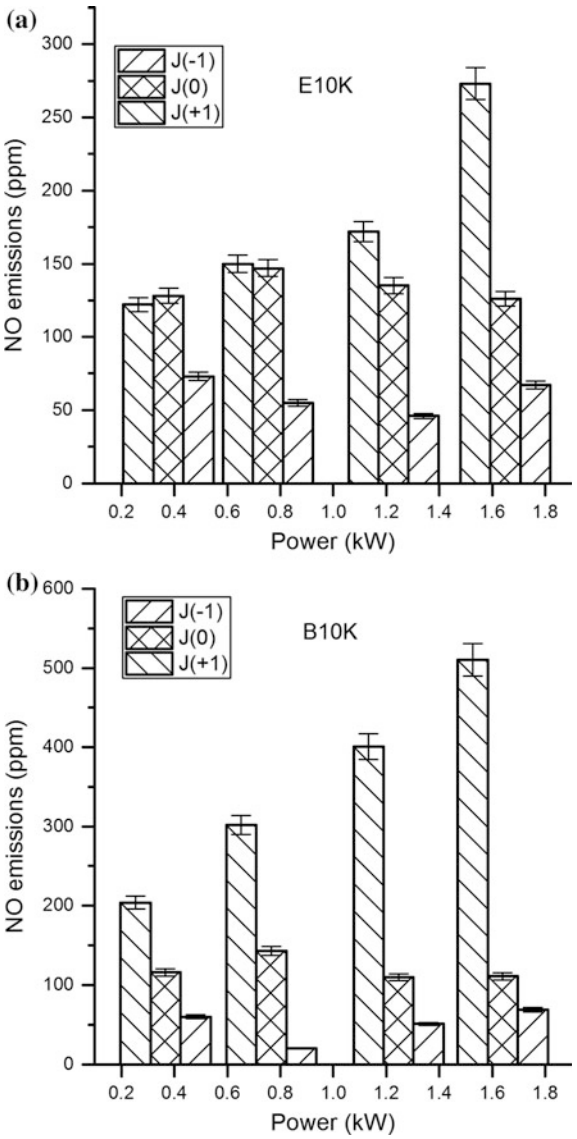

Fig. 9 Comparison of NO emissions for different jet sizes in **a** E10 K **b** B10 K

the other two jet sizes for all loads. There is an increase of 7–20%. With J(+1), the value of BSFC decreases from 2–11% in case of E10 K. For B10 K, BSFC decreases by 2–27% in J(+1) with respect to initial jet size J(0), while an increase of 3–17% is observed for J(–1).

It can be observed that leaning the mixture with jet size J(+1) for both E10 and B10 K fuels NO emission level rises drastically, which tend to supersede the benefits of reduction in HC and CO emission and fuel economy. With jet size J(−1)

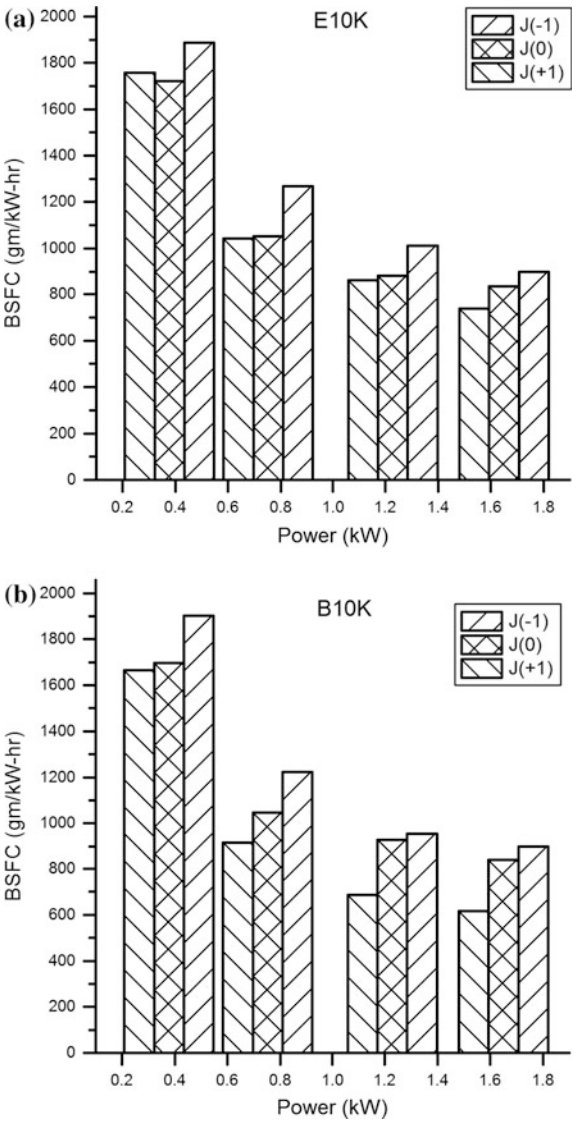

Fig. 10 Comparison of BSFC for different jet sizes in **a** E10 K **b** B10 K

corresponding to even richer mixture, NO emission levels can be reduced significantly at cost of increase emission of CO, HC and BSFC.

Due to trade off between HC and NO emission, it is not possible to reduce both by means of only adjusting air-fuel ratio. Hence, in order to reach an optimized solution, the cumulative metered emission level for HC, NO and CO were calculated by giving weights to part load points for all fuel and jet size combinations. Weightage scheme is defined in methodology. HC and NO emission are clubbed together in order to attain a better comparison with emission standards. Figure 11

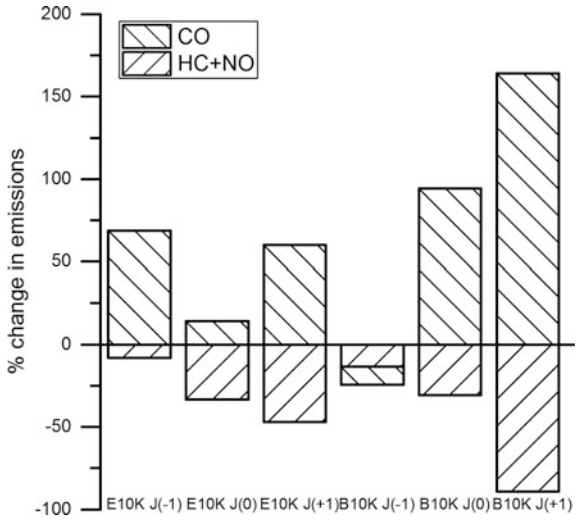

Fig. 11 Emission difference from baseline kerosene J(0)

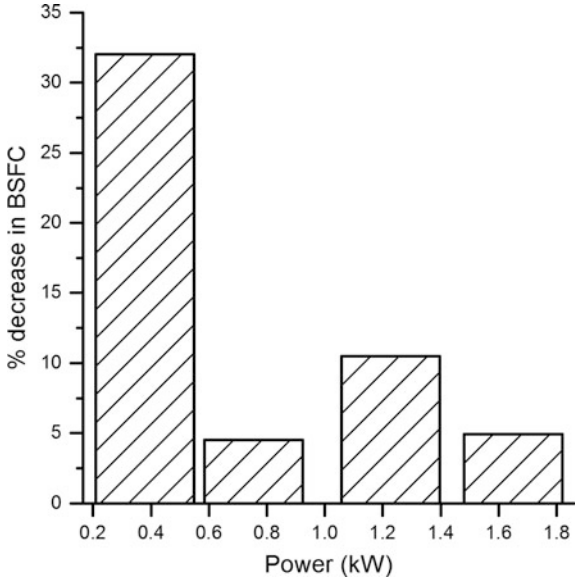

Fig. 12 Change in BSFC for B10 K J(−1)

represents the percentage change of two regulated emission with respect to Kerosene at standard jet size J(0) compared to all the combinations of test fuels and jet sizes. It can be observed that B10 K fuel with J(−1) shows a decrease in overall emission compared to baseline kerosene. Percentage change in fuel consumption at different loads for B10 K fuel with J(−1) is shown in Fig. 12. Fuel consumption is

lower for B10 K at J(−1). It is observed that in a kerosene run genset, optimized level of emission and fuel economy can be achieved with B10 K fuel operating at jet size J(−1).

4 Conclusion

Comparative evaluation of engine performance and emission of 10% blend of n-butanol and ethanol in kerosene (v/v) was carried out in a SI genset. It was observed that, on blending 10% ethanol and n-butanol in kerosene (v/v), fuel consumption decreases. Decrease in emission of CO and HC emission concentration was observed. However NO emission rises significantly. To achieve optimized fuel consumption, along with engine tail pipe emission from E10 and B10 K fuels, engine test were also carried out at different air fuel ratios using three different main jet size of carburetter. When leaning the fuels slightly, HC and CO emission decrease while NO emission increases dramatically. With slightly richer mixture of B10 K fuel, a decrease was observed in overall emission level. Using this configuration also yielded lower fuel consumption. Hence, by blending 10% n-butanol in kerosene and operating engine on a slightly richer side, emission from a kerosene operated genset can be reduced along with improvement in fuel economy without any engine hardware modification.

References

1. EIA US Energy Information Administration (2013) full report
2. Pathak S, Aigal AK, Sharma ML, Narayan L, Saxena M (2004) Reduction of exhaust emission in a kerosene operated genset for electrical energy applications. SAE Technical Paper 2005-26-026, 2005. doi:10.4271/2005-26-026
3. www.cpcb.org.in
4. Pundir B (2004) Emission reduction in small SI engine generator sets. SAE Technical Paper 2004-01-1089. doi:10.4271/2004-01-1089
5. Pundir B, Lachiram B, Malhotra R (2001) Catalytic emission control for portable SI engine generator sets. SAE Technical Paper 2001-28-0047
6. Krishna MVSM, Kishor K, Ramana Reddy CV (2006) Studies on emission of catalytic coated spark ignition engine with adulterated gasoline. J Environ Sci Engg 48(2):97–102
7. Pathak S, Aigal A, Sharma M, Narayan L et al. (2005) Reduction of exhaust emission in a kerosene operated genset for electrical ENERGY applications. SAE Technical Paper 2005-26-026. doi:10.4271/2005-26-026
8. Clark W (1917) Burning Kerosene In Tractor Engines. SAE Technical Paper 170031. doi:10.4271/170031
9. Sanchez TDAF (2008) Experimental study of a kerosene fuelled internal combustion engine. Thesis, EPFL, Instituto superior Tecnico
10. Lucke C (1916) Kerosene versus gasoline in automobile engines. SAE Technical Paper 160022. doi:10.4271/160022

11. Seshaiah N (2010) Efficiency and exhaust gas analysis of variable compression ratio spark ignition engine fuelled with alternative fuels. Int J Energy Environ 1(5):861–870
12. Misron N, Rizuan S, Vaithilingam A, Mailah NF, Tsuyoshi H, Hiroaki Y, Yoshihito S (2011) Performance improvement of a portable electric generator using an optimized bio-fuel ratio in a single cylinder two-stroke engine. Energies 4:1937–1949. doi:10.3390/en411937
13. Yasar A (2010) Effect of alcohol-gasoline blends on exhaust and noise emission in small scaled generators. Metalurgija 49(4):335–338
14. Kerosene Base Fuels in Small Gasoline Engines U.S. Army/CR91/A90-210 (1991)
15. Yucesu HS, Sozen A, Topgul T, Arcaclioglu E (2007) Comparative study of mathematical and experimental analysis of spark ignition engine performance used ethanol-gasoline blend fuel. Appl Therm Eng 27(2007):358–368
16. Gravalos I, Moshou D, Gialamas T, Xyradakis P, Kateris D, Tsiropoulos Z (2011) Performance and emission characteristics of spark ignited engine fuelled with ethanol and methanol gasoline blends. Alternative Fuels. Dr. Maximino Manzanera (Ed.), ISBN: 978-953-307-372-9, InTech. doi:10.5772/23176
17. Chan LK (2005) Reduction of nitrogen oxides (NOx) using liquefied petroleum gas (LPG) In Spark Ignition (Si) Engine. Dissertation, University of Southern Queensland